Imperial College London

Faculty of Medicine
Department of Surgery & Cancer
Division of Cancer

RSK4 targeting: A new therapeutic strategy against drug resistance and metastasis in non-small cell lung cancer

Stelios Chrysostomou

A thesis submitted for the degree of Doctor of Philosophy

Principal supervisor: Dr Olivier Pardo
Co-supervisor: Professor Michael Seckl
Co-supervisor: Dr Filippo Prischi

Declaration of Originality

I declare that unless otherwise stated, this thesis is the result of my own work.

Stelios Chrysostomou

Copyright Declaration

Abstract

Lung cancer is the commonest cause of cancer death worldwide with a five-year survival rate of less than five percent for metastatic tumours. Non-small cell lung cancer (NSCLC) accounts for 80% of lung cancer cases of which adenocarcinoma prevails. Patients almost invariably develop metastatic drug-resistant disease and this is responsible for our failure to provide curative therapy. Hence, a better understanding of the mechanisms underlying these biological processes is urgently required to improve clinical outcome.

The p90 (90 kDa) Ribosomal Protein S6 Kinases (RSKs) are downstream effectors of the RAS/MAPK cascade. RSKs are highly conserved serine/threonine protein kinases implicated in diverse cellular processes, including cell survival, proliferation, migration and invasion. There are four human isoforms (RSK1-4), which are uniquely characterised by the presence of two non-identical N- and C-terminal kinase domains. RSK isoforms are 73%-80% identical at the protein level and this has been thought to suggest overlapping functions.

However, through functional genomic kinome screens, we show that RSK4, contrary to RSK1, promotes both drug resistance and metastasis in lung cancer. RSK4 is overexpressed in the majority of NSCLC biopsies and this correlates with poor overall survival in lung adenocarcinoma patients. Genetic silencing of RSK4 sensitises lung cancer cells to chemotherapy and prevents their migration and invasiveness *in vitro* and *in vivo*. This is associated with downregulation of the anti-apoptotic proteins c-IAP1 and c-IAP2, and induction of mesenchymal-epithelial transition (MET), respectively. A small-molecule inhibitor screen identified several floxacins as potent allosteric inhibitors of RSK4 activation. Trovafloxacin reproduced all biological and molecular effects of RSK4 silencing *in vitro* and *in vivo* and it is predicted to bind a novel allosteric site as revealed by our RSK4 N-terminal kinase domain crystal structure and mathematical Markov Transient Analysis.

Taken together, our data implicate RSK4 as a promising novel therapeutic target in lung cancer.

Acknowledgements

I would like to thank my supervisors Olivier Pardo and Michael Seckl first, for giving me the opportunity to undertake my PhD studies in their lab and second, for their constant guidance and supervision throughout the project. I also thank my co-supervisor Filippo Prischi (University of Essex, Colchester, UK) whose structural biology work has been instrumental in further understanding the biophysical properties of RSK4.

This work would not have been possible without the significant contribution from our collaborators. I would like to acknowledge:

- Rajat Roy, Leandro Castellano, Silvia Ottaviani and Joel Abrahams (Imperial College London, London, UK) for the xenograft (trovafloxacin) experiment.
- Francesco Mauri (Imperial College London, London, UK) for his histopathology work.
- Yulan Wang (Wuhan Institute of Physics and Mathematics, Wuhan, China) for the xenograft (RSK4 CRISPR) experiments.
- David Hancock, Christopher Moore, Miriam Molina Arcas and Julian Downward (The Francis Crick Institute, London, UK) for the KP-driven GEM experiment.
- Mark Skehel (MRC Laboratory of Molecular Biology, Cambridge, UK) for the LC-MS/MS of our tandem affinity purification.
- Howard Desmond and Paul Huang (The Institute of Cancer Research, London, UK) for the global proteomics and phosphoproteomics.
- Stephen Rothery (FILM, Imperial College London, UK) for his invaluable insights into confocal microscopy and especially his macro script (FIJI Image-J) that was used to analyse our 3D collagen invasion assays.

I want to express my gratitude and appreciation to Rajat Roy for his invaluable contribution, encouragement and supervision. I also thank members of the Cellular Regulatory Networks (Lung) Lab: Marina Georgiou, Yueyang Huang, Yakinthi Chrisochoidou and Lucksamon Thamlikitkul for the countless fruitful scientific (or not) discussions. This thesis has also been supported by the work of Master students: Devmini Moonamale, Thanasis Tsalikis, Desislava Kuzeva, Alice Ormrod, Filippos Konstandinidis, Yuewei Tao, Alex Power, Zhuyan Su and Mirko De Iacobis.

Last but not least, I want to express my deepest gratitude to my family and friends for their patience, kindness and support. Thank you so very much to my parents Loizos and Anna, my brothers George and Panayiotis as well as Salomi, Tonia, Emmelia-Anna, Maximos-Loizos, Annabel, Mireille, Christos and all my friends for enduring this journey with me.

“Cancer ultimately kills the host.
Hence, it does not evolve to survive,
which bears the question:
why does cancer arise then?
Perhaps because it can!”

- Stelios Chrysostomou -

Table of Contents

List of Figures

List of Supplementary Figures

List of Supplementary Tables

Abbreviations

RSKs: gene/protein*	Full name
RPS6KA1/RSK1	Ribosomal protein S6 kinase alpha-1/p90 (90 kDa) ribosomal protein S6 kinase 1
RPS6KA3/RSK2	Ribosomal protein S6 kinase alpha-3/p90 (90 kDa) ribosomal protein S6 kinase 2
RPS6KA2/RSK3	Ribosomal protein S6 kinase alpha-2/p90 (90 kDa) ribosomal protein S6 kinase 3
RPS6KA6/RSK4	Ribosomal protein S6 kinase alpha-6/p90 (90 kDa) ribosomal protein S6 kinase 4
RPS6KA5/MSK1	Ribosomal protein S6 kinase alpha-5/Mitogen- and stress-activated protein kinase 1
RPS6KA4/MSK2	Ribosomal protein S6 kinase alpha-4/Mitogen- and stress-activated protein kinase 2
RPS6KB1/S6K1	Ribosomal protein S6 kinase beta-1/p70 (70 kDa) ribosomal protein S6 kinase 1
RPS6KB2/S6K2	Ribosomal protein S6 kinase beta-2/p70 (70 kDa) ribosomal protein S6 kinase 2

***** Based on GeneCards® Human Gene Database and UniProtKB Swiss-Prot database

Gene/Protein*	Full name
ABCB1/MDR1 (P-glycoprotein)	Multidrug resistance protein 1
ABCC2/MRP2	Multidrug resistance protein 2
AGC	Protein kinase A, G, and C
AKT1/PKB	AKT Serine/Threonine Kinase 1/Protein Kinase B
ALK	Anaplastic lymphoma kinase
ANTXR1/TEM8	Anthrax toxin receptor 1/tumour endothelium marker 8
APAF1	Apoptotic peptidase activating factor 1
aPKC	Atypical protein kinase C
AR	Androgen receptor
ARF	ADP-ribosylation factor
ARID1A	AAT-rich interactive domain-containing protein 1A
ATM	Ataxia-telangiectasia mutated
ATR	Ataxia telangiectasia and RAD3-related
ATXN1/SCA1	Ataxin-1/Spinocerebellar ataxia 1
BBC3/PUMA	BCL2 Binding Component 3/P53-Upregulated Modulator Of Apoptosis
BCL-2	B-cell lymphoma-2
BIRC1/NAIP	Baculoviral IAP Repeat-Containing Protein 1/Neuronal apoptosis-inhibitory protein
BIRC2/c-IAP1	Baculoviral IAP Repeat-Containing Protein 2/cellular-Inhibitor of Apoptosis 1
BIRC3/c-IAP2	Baculoviral IAP Repeat-Containing Protein 3/cellular-Inhibitor of Apoptosis 2
BIRC4/XIAP	Baculoviral IAP Repeat-Containing Protein 4/X-linked Inhibitor of Apoptosis
BIRC5/Survivin	Baculoviral IAP Repeat-Containing Protein 5/Survivin
BIRC6/BRUCE/Apolllon	Baculoviral IAP Repeat-Containing Protein 6/BRUCE/Apolllon
BIRC7/ML-IAP (Livin)	Baculoviral IAP Repeat-Containing Protein 7/Melanoma Inhibitor of Apoptosis
BIRC8/ILP2	Baculoviral IAP Repeat-Containing Protein 8/Inhibitor of Apoptosis-like protein 2
BYSL	Bystin
CAMK	Ca^{2+}/calmodulin-dependent protein kinase
CAPN2	Calpain-2
CAPNS1/CAPN4	Calpain-4
CCAR2	Cell-cycle and apoptosis regulator protein 2
CD34	Hematopoietic progenitor cell antigen CD34
CD44	Cluster of differentiation 44
CDC42	Cell division cycle 42
CDH1/E-cadherin	Epithelial cadherin
CDH2/N-cadherin	Neural cadherin
CDK5	Cyclin-dependent-like kinase 5
CDK6	Cyclin-dependent-like kinase 6
CDKN1A/$p21^{Cip1/WAF1}$	Cyclin-dependent kinase inhibitor 1A
CHGA/Chromogranin A	Chromogranin A
CK	Cytokeratin
CRB	Crumbs
CREB	cAMP responsive element-binding protein
CSNK1A1/CK1	Casein kinase I isoform alpha
CTNND1	catenin delta-1 (p120-catenin)
CXCR4	Chemokine (C-X-C Motif) Receptor 4
DAPK	Death-associated protein kinase
DDB1	DNA damage-binding protein 1

DDB2	DNA damage-binding protein 2
DDX1	DEAD-Box Helicase 1
DDX5	DEAD-Box Helicase 5 (RNA helicase p68)
DISC	Death-inducing signalling complex
DKC1	Dyskerin
DLG1	Discs large
DNA-PKcs	DNA-dependent protein kinase catalytic subunit
DNMT3B	DNA (cytosine-5)-methyltransferase 3B
DUSP	Dual specificity phosphatase
EGF	Epidermal growth factor
EGFR/ERBB1/HER-1	Epidermal growth factor receptor
EIF2B1/eIF2B	Eukaryotic Translation Initiation Factor 2B
ERBB2/ HER-2/NEU	Receptor tyrosine-protein kinase erbB-2
ERBB3/ HER-3	Receptor tyrosine-protein kinase erbB-3
ERBB4/ HER-4	Receptor tyrosine-protein kinase erbB-4
ESR1/ER	Estrogen receptor
FADD	Fas-associated death domain protein
FADS1	Fatty acid desaturase-1
FADS2	Fatty acid desaturase-2
FAS (APO-1 or CD95)	Fas cell surface death receptor
FGFR	Fibroblast growth factor receptor
FLT1/VEGFR1	Vascular endothelial growth factor receptor 1
FNTA/FTase	Farnesyltransferase
FTH1	Ferritin heavy chain
G6PD	Glucose-6-phosphate dehydrogenase
GDP	Guanosine diphosphate
GIGYF1	GRB10-interacting GYF protein 1
GOLGA7/GCP16	Golgin subfamily A member 7/Golgi Complex-Associated Protein Of 16kDa
GPC3	Glypican-3
GRB2	Growth factor receptor-bound protein 2
GSK3B/ GSK3β	Glycogen Synthase Kinase 3 Beta
GTP	Guanosine triphosphate
GTPase	Guanosine triphospatase
HDAC1	Histone deacetylase 1
HDAC2	Histone deacetylase 2
HDAC8	Histone deacetylase 8
HGF	Hepatocyte growth factor
HIPK2	Homeodomain interacting protein kinase 2
HNRNP	Heterogeneous nuclear ribonucleoprotein
HPRT	Hypoxanthine-guanine phosphoribosyltransferase
HRAS/GTPase HRas	**H**arvey **ra**t **s**arcoma viral oncogene homolog
HSPB1/HSP27	Heat shock protein beta-1/Heat shock protein 27
ICMT	Isoprenylcysteine carboxylmethyltransferase/ Protein-S-isoprenylcysteine O-methyltransferase
IDS	Iduronate-2-sulfatase
IGF1	Insulin-like growth factor 1
KDM1A (LSD1)	Lysine-Specific Histone Demethylase 1A
KDR/VEGFR2	Vascular endothelial growth factor receptor 2
KMT5A/SET8	N-Lysine Methyltransferase SET8
KRAS/GTPase KRas	**K**irsten **ra**t **s**arcoma viral oncogene homolog

KRT14	Keratin, type I cytoskeletal 14
KRT5	Keratin, type II cytoskeletal 5
KRT6A/B	Keratin, type II cytoskeletal 6A/B
KSR1	Kinase suppressor of RAS 1
LASP1	LIM and SH3 protein 1
LGL1	Lethal giant larvae
MAP2	Microtubule-associated protein-2
MAP2K1/MEK1	Dual Specificity Mitogen-Activated Protein Kinase Kinase 1
MAP2K2/MEK2	Dual Specificity Mitogen-Activated Protein Kinase Kinase 2
MAPK	Mitogen-activated protein kinase
MAPK1/ERK2	Mitogen-activated protein kinase 1/Extracellular signal-regulated kinase 2
MAPK14/p38	Mitogen-activated protein kinase 14/p38 α,β,γ,δ
MAPK3/ERK1	Mitogen-activated protein kinase 3/Extracellular signal-regulated kinase 1
MAPK7/ERK5	Mitogen-activated protein kinase 7/Extracellular signal-regulated kinase 5
MAPK8/JNK	Mitogen-activated protein kinase 8/c-Jun N-terminal kinases (JNK1,2,3)
MARK	Microtubule affinity-regulating kinase
MCL1	Myeloid Cell Leukemia 1
MDM2	Mouse double-minute 2
MET/HGFR	Mesenchymal-epithelial transition factor/Hepatocyte growth factor receptor
MLKL	Mixed lineage kinase domain-like protein
MMP-14/MT1-MMP	Matrix metalloproteinase 14
MMP-9	Matrix metalloproteinase 9
MRE11A	Double-strand break repair protein
mTOR	Mammalian target of rapamycin
mTORC1	Mammalian target of rapamycin complex 1
MYC/C-Myc	Myc proto-oncogene protein
NES	Nestin
NF1	Neurofibromin 1
NFKBIA/IκBα	NFKB Inhibitor Alpha
NFKBIB/IκBβ	NFKB Inhibitor Beta
NRAS/GTPase NRas	**N**euroblastoma **RAS** viral oncogene homolog
NRG	Neuregulin
PAK	p21-activated kinase
PALS	Proteins associated with Lin seven
PAR3	Partition defective 3
PAR6	Partition defective 6
PARP-1	Poly(ADP-Ribose) Polymerase 1
PATJ	Protein-associated with tight junction
PDE6D/PDED (PDEδ)	Phosphodiesterase 6D
PDGFR	Platelet-derived growth factor receptor
PDPK1/PDK1	3'-phosphoinositide-dependent protein kinase 1
PGF/PlGF	Placental growth factor
PGGT1B/GGTase I	Protein Geranylgeranyltransferase Type I Subunit Beta/ Geranlygeranyltransferase I
PIK3CA/PI3K	Phosphoinositide 3-kinase
PLK1	Polo-like kinase 1
PMAIP1/NOXA	Phorbol-12-Myristate-13-Acetate-Induced Protein 1
PML	Promyelocytic leukemia protein
POLD1	DNA polymerases delta 1
POLD2	DNA polymerases delta 2
PP2A	Protein phosphatase 2A

PPP1CA/PP1	Serine/threonine-protein phosphatase PP1-alpha catalytic subunit/ Protein phosphatase type 1
PRKAA1/AMPK	Adenosine monophosphate-activated protein kinase
PRKACA/PKA	cAMP-dependent protein kinase catalytic subunit alpha/Protein kinase A
PRKCA/PKC	Protein kinase C alpha type/ Protein kinase C
PRKDC/DNA-PKcs	DNA-dependent protein kinase catalytic subunit
PRKX	Protein kinase X-linked
PRMT1	Protein arginine N-methyltransferase 1
PRPF38A	Pre-mRNA-splicing factor 38A
RAB	Ras-like proteins in brain
RAC1	Rac Family Small GTPase 1/Ras-related C3 botulinum toxin substrate 1
RAC1	Rac Family Small GTPase 1
RAN	Ras-like nuclear
RAS	Rat sarcoma
RB1/Rb	Retinoblastoma-associated protein
RbAp46	Retinoblastoma-binding protein P46
RCE1	RAS-converting CAAX endopeptidase 1/CAAX prenyl protease 2
RHO	Ras homologous
RHOA	Ras Homolog Family Member A
RIPK3	Receptor Interacting Serine/Threonine Kinase 3
RRP8	Ribosomal RNA-processing protein 8
SAA3	Serum amyloid A3
SCGB1A1/CC10	Secretoglobin1a1/Clara cell secretory protein
SCRIB	Scribble Planar Cell Polarity Protein
SFTPC/SPC	Pulmonary surfactant-associated protein C/surfactant protein C
SIRT1	Sirtuin 1
SMAC/DIABLO	Second mitochondria-derived activator of caspase/Diablo IAP-binding mitochondrial protein
SMARCA4/BRG1	Brahma related gene-1
SOS1	Son-of-sevenless homologue 1
SOS2	Son-of-sevenless homologue 2
SPRY	Sprouty
SQSTM1 (p68)	Sequestosome-1
SRF	Serum response factor
SRSF10	Serine/arginine-rich splicing factor 10
SYP/Synaptophysin	Synaptophysin
TAF4	Transcription initiation factor TFIID subunit 4
TGFA	Transforming growth factor alpha
TGFB	Transforming growth factor beta
TIAM1	T Cell Lymphoma Invasion And Metastasis 1
TNFRSF10A/TRAILR1 (DR4)	TNF-related apoptosis-inducing ligand receptor 1
TNFRSF10B/TRAILR2 (DR5)	TNF-related apoptosis-inducing ligand receptor 2
TNFRSF1A/TNFR1	TNF receptor superfamily member 1A/Tumour Necrosis Factor Receptor 1
TNPO2	Transportin-2
TP53/p53	Cellular tumour antigen p53
TP63/p63	Tumour protein 63
TSC1/Hamartin	Tuberus sclerosis complex 1
TSC2/Tuberin	Tuberus sclerosis complex 2

TTBK2	Tau tubulin kinase 2
TTF1/Nkx2.1	Transcription termination factor 1/Thyroid transcription factor
UBE2G2	Ubiquitin-conjugating enzyme E2 G2
VASP	Vasodilator Stimulated Phosphoprotein
VEGF	Vascular endothelial growth factor
XPC	Xeroderma pigmentosum C
ZDHHC9	Zinc Finger DHHC-Type Containing 9/Palmitoyltransferase ZDHHC9

***** Based on GeneCards® Human Gene Database and UniProtKB Swiss-Prot database

Abbreviation	Full name
AAH	Atypical adenomatous hyperplasia
ABC	ATP-binding cassette
ACD	Accidental cell death
AD	Acidic domain
AIS	Adenocarcinoma *in situ*
AT2	Alveolar type II
BAC	Bronchioalveolar carcinoma
BADJ	Bronchioalveolar duct junction
BASCs	Bronchioalveolar stem cells
BH	BCL-2 homology
bHLH	basic helix-loop-helix
BIR	Baculoviral IAP repeat
CAFs	Cancer-associated fibroblasts
CARD	Caspase recruitment domain
cDNA	Complementary DNA
CHM	Choroideremia
CLL	Chronic lymphocytic leukemia
Co-IP	Co-Immunoprecipitation
COSMIC	Catalogue of somatic mutations in Cancer
CRD	Cysteine rich domain
CSCs	Cancer stem cells
CTKD	C-terminal kinase domain
DBD	DNA-binding domain
DDR	DNA damage response
DED	Death effector domain
DEF	Docking site for ERK and FXFP
DFN3	X-linked deafness type 3
DNA	Deoxyribonucleic acid
DPCs	Double positive cells
dsDNA	Double-stranded DNA
EC	Endothelial cell
ECM	Extracellular matrix
EMA	European Medicines Agency
EMT	Epithelial-mesenchymal transition
EPC	Endothelial progenitor cell
ER	Endoplasmic reticulum
EV	Empty vector
FDA	Food and Drug Administration
FFPE	Formalin-fixed paraffin-embedded
FMK	Fluoromethylketone
FNA	Fine-needle aspirations
FOX	Forkhead box
GAP	GTPase activating protein
GEF	Guanine nucleotide exchange factor
GEM	Genetically engineered mouse
HPC	Haematopoietic progenitor cell
IARC	International Agency for Research on Cancer

IEG	Immediate-early gene
IFN	Interferon
IHC	Immunohistochemistry
IMAC	Immobilised metal affinity chromatography
IP injection	Intraperitoneal injection
KIM	Kinase interaction motif
KO	Knockout
LCC	Large cell carcinoma
LC-MS/MS	Liquid chromatography tandem mass spectrometry
LCNEC	Large cell neuroendocrine carcinoma
LUAD	Lung adenocarcinoma
LUSC	Lung squamous cell carcinoma
m/z	Mass-to-charge ratio
MET	Mesenchymal-epithelial transition
MIA	Minimally invasive adenocarcinoma
Micro-CT	Micro-computerised tomography
MOMP	Mitochondrial outer membrane permeabilisation
mRNA	Messenger RNA
MRX	X-linked mental retardation
NCDs	Non-communicable diseases
NECs	Neuroendocrine cells
NER	Nucleotide excision repair
NES	Nuclear export signal
NETs	Neutrophil extracellular traps
NK	Natural killer
NLS	Nuclear localisation signal
NSCLC	Non-small cell lung cancer
NT	Non-targeting
NTKD	N-terminal kinase domain
o/n	Overnight
OD	Oligomerisation domain
ORF	Open reading frame
OS	Overall survival
PA	Protective antigen
PAGE	Polyacrylamide gel electrophoresis
PCD	Programmed cell death
PCR	Polymerase chain reaction
PFS	Progression-free survival
pfu	Plaque-forming unit
PHE	Public Health England
PK	Pharmacokinetic
PRD	Proline-rich domain
RBD	RAS binding domain
RCC	Renal cell carcinoma
RCD	Regulated cell death
REM	RAS exchange motif
RING	Really interesting new gene
RNA	Ribonucleic acid
ROS	Reactive oxygen species
RR	Response rate

RT	Room temperature
RTK	Receptor tyrosine kinase
SCID	Severe combined immunodeficient
SCLC	Small cell lung cancer
SCX	Strong cation-exchange
SH2	Src homology 2
shRNA	Short hairpin RNA
siRNA	Small interfering RNA
SLL	Small lymphocytic lymphoma
SRP	Surveillance Research Program
SWI/SNF	SWItch/Sucrose Non-Fermentable
TAD	Transactivation domain
TEM	Transendothelial migration
TET	Tetramerisation domain
TKI	Tyrosine kinase inhibitor
TMA	Tissue microarray
TMT	Tandem Mass Tag
WHO	World Health Organization

Reagents	Full name
ATP	Adenosine triphosphate
BPB	Bromophenol blue
BSA	Bovine serum albumin
CDDP	Cisplatin
CHX	Cycloheximide
DDI	Distilled deionised water
DMEM	Dulbecco's modified Eagle's medium
DMSO	Dimethyl sulfoxide
dNTP	Deoxyribonucleotide triphosphate
DTT	Dithiothreitol
ECL	Enhanced chemiluminescence
EDTA	Ethylenediaminetetraacetic acid
FCS	Foetal calf serum
H&E	Haematoxylin and eosin
HEPES	4-(2-hydroxyethyl)-1-piperazineethanesulfonic acid
LB	Lysogeny broth
NBF	Neutral buffered formalin
PBS	Phosphate-buffered saline
PFA	Paraformaldehyde
PVDF	Polyvinylidene difluoride
RIPA	Radioimmunoprecipitation assay buffer
RPMI	Roswell Park Memorial Institute
SDS	Sodium dodecyl sulphate
SOC	**S**uper **O**ptimal broth with **C**atabolite repression
TBS	Tris-buffered saline
TCEP	Tris(2-carboxyethyl)phosphine hydrochloride

Chemical Formula	Full name
C_2H_5OH (EtOH)	Ethanol
CH_2O_2	Formic acid
CH_3CN	Acetonitrile (ACN)
CO_2	Carbon dioxide
Cu	Copper
H_2O_2	Hydrogen peroxide
H_3NO	Hydroxylamine
HCl	Hydrochloric acid
KH_2PO_4	Monopotassium phosphate (MKP)
MgCl	Magnesium chloride
Na_3VO_4	Sodium orthovanadate
NaCl	Sodium chloride
NaF	Sodium fluoride
TiO_2	Titanium dioxide

1. Introduction

1.1 Cancer in perspective

According to the World Health Organization (WHO), non-communicable diseases (NCDs), primarily cardiovascular diseases, cancers, chronic respiratory diseases and diabetes, are responsible for the majority of global deaths[1]. Cancer is expected to dominate the list and become the leading cause of death worldwide as it already ranks as the first or second leading cause of death before 70 years age in 91 of 172 countries. Based on GLOBOCAN, an International Agency for Research on Cancer (IARC) project, in the year 2002 there were 10.9 million new cancer cases and 6.7 million cancer related deaths (Parkin et al., 2005). These numbers have risen to about 14.1 million new cases and 8.2 million deaths in 2012 (Torre et al., 2015), while for the year 2018, it is estimated that 18.1 million new cases and 9.6 million deaths have occurred **(Figure 1a)** (Bray et al., 2018). In the UK, cancer is the leading cause of death, surpassing heart diseases and dementia (Public Health England (PHE), 2017), with 359,960 new cases of cancer reported in 2015 and 161,849 cancer deaths[2]. The global cancer burden as measured by *incidence*[3], *mortality*[4] and *prevalence*[5] rates, has been rapidly growing and this is mainly attributed to population growth and aging (i.e. greater longevity), lack of awareness and resources, late diagnosis and exposure to common risk factors for cancer, namely tobacco use, unhealthy dietary patterns and physical inactivity; several of which are associated with socioeconomic status (Clegg et al., 2009).

1.2 What is cancer?

Siddhartha Mukherjee, an oncologist and author, in his 2010 book, *The Emperor of All Maladies: A Biography of Cancer* (Mukherjee, 2010), described cancer as a "distorted version of our normal selves". In more scientific terms, cells that evade physiological constraints and engage in abnormal growth and division rates. The word

[1] World Health Organization. (n.d.) *Global Health Observatory (GHO) data*. Available from: https://www.who.int/gho/database/en/ [Accessed 16th July 2019].
[2] Cancer Research UK. (2018) *Cancer in the UK*. Available from: https://www.cancerresearchuk.org/sites/default/files/state_of_the_nation_apr_2018_v2_0.pdf [Accessed 18th July 2019].
[3] Incidence: Absolute number of new cases occurring per year.
[4] Mortality: Number of deaths occurring per year.
[5] Prevalence: Number of people (alive) with cancer at a particular point in time.

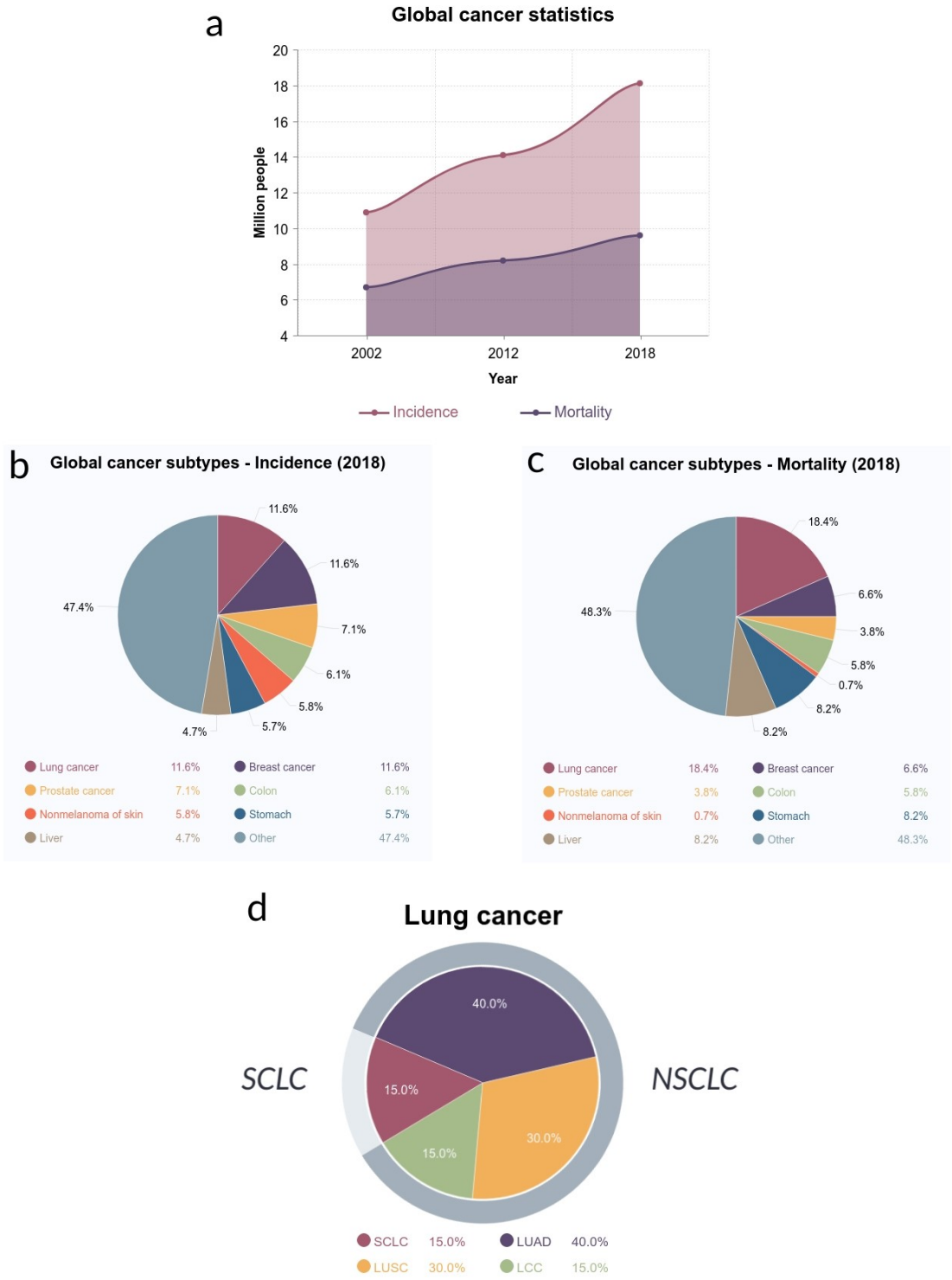

Figure 1| Global cancer statistics. (a) According to GLOBOCAN estimates, in 2002 there were 10.9 million new cancer cases and 6.7 million cancer deaths. In 2012, incidence rates have increased by 29% (14.1 million new cancer cases) and mortality rates by 22% (8.2 million cancer deaths). In the year 2018, incidence rates are estimated to have increased by 28% (18.1 million new cancer cases), and mortality rates by 17% (9.6 million cancer deaths). **(b, c)** Based on 2018 estimates (in both sexes), lung cancer was the most commonly diagnosed cancer (11.6%) and the principal cancer killer worldwide (18.4%); followed by breast cancer (11.6%) and prostate cancer (7.1%), which are estimated to account for 6.6% and 3.8% of worldwide cancer deaths, respectively. (Incidence rates; colon: 6.1%; nonmelanoma of skin: 5.8%; stomach: 5.7%; liver: 4.7%; other: 47.4%; Mortality rates; colon: 5.8%; nonmelanoma of skin: 0.7%; stomach: 8.2%; liver: 8.2%; other: 48.3). **(d)** Lung cancer is broadly classified into non-small cell lung cancer (NSCLC; 85% total) and small cell lung cancer (SCLC; 15%). NSCLC is histologically divided into lung adenocarcinoma (LUAD; 40%), which is the commonest type; lung squamous cell carcinoma (LUSC; 30%) and large cell carcinoma (LCC; 15%) (Bray et al., 2018; Torre et al., 2015; Parkin et al., 2005). Figure created with visme.co.

"cancer" used in a medical context can be traced back to 400 BC when the "Father of Medicine", Hippocrates (460-370 BC), used the Greek word for "crab", *karkinos (carcinos; carcinoma)* to describe the appearance of the cut surface of a solid malignant tumour that was reminiscent of a crab (i.e. the tumour) and its legs (i.e. the blood vessels surrounding the tumour). During the 2nd century AD, another prominent Greek physician and surgeon, Claudius Galen (130-200 AD), used the term "onkos" (oncos), a Greek word for mass or swelling, to describe all tumours. This word would also intersect with medical terminology, giving rise to the modern word of *oncology*, the practice of preventing, diagnosing and treating cancer. Cancer is certainly not a "modern" disease, rather it is an "ancient" one with the first descriptions of cancer appearing in the Edwin Smith Papyrus, discovered in Egypt and dating back to 2500 BC[6].

We now know that cancer is not a single disease, rather it is many distinct diseases with their unique and complex epigenetic (i.e. DNA modifications that do not change DNA sequence), genetic (DNA), transcriptomic (RNA) and proteomic (protein) profiles. There are over 30 trillion cells in the human body, each with a genome of three billion DNA base pairs. The protein-coding part of our genome (i.e. exome) gives rise to around 22,000 protein-coding genes, which constitute less than two percent of the genome. Cancer is a clonal disease that arises from abnormal changes in our genes (i.e. DNA mutations) in a single somatic cell. Most mutations have no effect on the fitness of the cell, and are referred to as *passenger mutations*; however, occasionally a mutation may confer a proliferative or survival advantage to the cell. These are called *driver mutations*. It is now estimated that, on average, 1 to 10 driver coding substitution mutations (or point mutations; where a single nucleotide base is changed) are required for cancer to emerge (Martincorena et al., 2018). This results in cells that show deregulated and uncontrolled proliferation, resistance to death cues and enhanced invasive and metastatic potential. Cancer cells become tumorigenic and ultimately malignant, a phenotype that allows them to disseminate throughout the body (a phenomenon referred to as metastasis), through the acquisition of certain fundamental traits or hallmarks as described by D. Hanahan and R.A. Weinberg. These include

[6] American Cancer Society. (n.d.) *Early History of Cancer*. Available from: https://www.cancer.org/cancer/cancer-basics/history-of-cancer/what-is-cancer.html [Accessed 17th July 2019].

sustained proliferative signalling, resistance to cell death, induction of angiogenesis (i.e. formation of new blood vessels), evasion of growth suppressors, activation of invasion and metastasis, replicative immortality, reprograming of cellular energy metabolism (i.e. switch to aerobic glycolysis) and evasion of immune destruction (Hanahan & Weinberg, 2011). Another dimension of complexity, is the recruitment of a diverse, ostensibly normal repertoire of cells that surrounds tumours, including cancer-associated fibroblasts (CAFs) and immune cells, which participate in the construction of a tumour microenvironment that reflects the extensive heterogeneity detected between tumours (i.e. inter-tumour heterogeneity) or within tumours (i.e. intra-tumour heterogeneity). Tumour progression is further supported by genomic instability at the mutational and chromosomal level which renders cancers more heterogeneous and genetically diverse, a phenotype that fuels drug resistance. This and the various cells of origin involved, explain why over 100 different types of cancer exist, each characterised by extreme heterogeneity, a fact that fuels current efforts into precision medicine and personalised therapy. Cancer is indeed a distorted version of our normal selves, which exploits existing physiological processes in an abnormal and uncontrolled manner. Hence, in order to beat this disease and target these abnormal cells, we need to first understand the biological mechanisms of normal cells.

1.3 Lung cancer

1.3.1 Statistics

Lung cancer is the principal cancer killer worldwide. In both sexes combined, it is the most commonly diagnosed cancer and the primary cause of cancer death globally, accounting for 2 million new cases (18.1 million total cases) and 1.7 million deaths (9.6 million total cases) in 2018 **(Figure 1b, c)** (Bray et al., 2018). In males, lung cancer remains the most frequent cancer and the leading cause of cancer death, followed by prostate and colorectal cancer for incidence rates and liver and stomach cancer for mortality rates. Among females, breast cancer dominates both incidence and mortality rates, followed by colorectal and lung cancer for incidence rates and lung and colorectal cancer for mortality rates (Bray et al., 2018). In the UK, lung cancer is the 3rd most common cancer in both sexes combined (preceded by prostate [2nd] and breast cancer [3rd]),

and the 2nd most common cancer in males (preceded by prostate cancer [1st]) or females (preceded by breast cancer [1st]), accounting for 25,000 and 22,300 new cases in 2016, respectively[7]. In terms of mortality rates, lung cancer accounts for the majority of cancer deaths in the UK in both sexes combined or individually, accounting for 19,300 deaths in males and 16,300 deaths in females in 2016[7]. Notably, in western countries, greater than 80% of lung cancers are attributed to active smoking or involuntary exposure to tobacco smoke. Lung cancer exhibits amongst the highest prevalence of somatic mutations in human cancers and this is due to the chronic mutagenic exposure to tobacco smoke (Alexandrov et al., 2013). Excluding age, the biggest cancer risk factor, tobacco smoking represents one of the main cancer risk factors and the number one risk factor for lung cancer. Global cancer incidence and mortality rates, among other factors, are linked to smoking prevalence; nevertheless, there is a 20-fold variation in lung cancer rates when stratified by region, an observation that reflects the corresponding evolution of smoking prevalence (Bray et al., 2018). While low- and middle-income countries are generally at early stages of their tobacco epidemic (i.e. increasing smoking prevalence), high-income countries are towards later stages (i.e. stabilising or decreasing smoking prevalence). Therefore, these differences are expected to translate into corresponding changes in smoking-related death rates[8]. Early stage diagnosis in lung cancer is rare (around 16% of cases) and while lung cancer five-year survival rate for localised tumours (i.e. within the lungs) is 56%, the five-year survival rate for distant tumours (i.e. metastasised to other organs) is five percent (Surveillance Research Program (SRP), 2019). This is attributed to the aggressiveness of this cancer, late stage diagnosis, metastatic dissemination and the onset of drug resistance disease. Hence, a better understanding of the mechanisms underlying these biological processes is urgently required to improve clinical outcome.

1.3.2 Types of lung cancer – cell of origin

Lung cancer is broadly categorised into two main histopathological groups, namely non-small cell lung cancer (NSCLC), which is the commonest type (80%-85% of the cases), and small cell lung cancer (SCLC), which

[7] Cancer Research UK. (n.d.) *Lung cancer statistics*. Available from: https://www.cancerresearchuk.org/health-professional/cancer-statistics/statistics-by-cancer-type/lung-cancer#heading-Zero [Accessed 18th July 2019].
[8] The Tobacco Atlas. (2018) *Prevalence*. Available from: https://tobaccoatlas.org/topic/prevalence/ [Accessed 18th July 2019].

accounts for about 15%-20% of lung cancer cases **(Figure 1d)** (Mengoli et al., 2018). SCLC is believed to derive predominantly from neuroendocrine cells (NECs) in the midlevel bronchioles of the lung (Karachaliou et al., 2016; Sutherland et al., 2011) and is almost always caused by smoking (Khuder, 2001). Microscopically, SCLC cells appear much smaller compared to NSCLC cells. NSCLC is further subdivided into lung adenocarcinoma (LUAD), lung squamous cell carcinoma (LUSC) and large cell carcinoma (LCC), of which LUAD is the commonest type and accounts for 40% of lung cancer cases, while LUSC and LCC account for 30% and 15%, respectively **(Figure 1d)** (Dela Cruz, Tanoue & Matthay, 2011). While LUADs are seen in smokers, it is also the most common type of lung cancer diagnosed in people who never smoked (Khuder, 2001), while women are more likely to develop this particular type than men (Jemal et al., 2018). LUSC on the other hand, is more common in men than women (Jemal et al., 2018) and is usually caused by smoking (Khuder, 2001). This subtype is thought to arise from tracheal KRT5^{+}, KRT14^{+}, p63^{+} basal cell progenitors (Sutherland & Berns, 2010). LCC can appear in any part of the lung and unlike LUAD and LUSC, it tends to grow and spread rapidly. A subtype of LCC, large cell neuroendocrine carcinoma (LCNEC) (Fasano et al., 2015), shares some characteristics with SCLC and constitutes one of the four major types of lung neuroendocrine tumours (Rekhtman, 2010).

LUAD, was initially reported to derive from cells located at the bronchioalveolar duct junction (BADJ), the region where the airways terminate and form alveoli (Sutherland & Berns, 2010; Jackson et al., 2001). Clara cells, the secretory bronchiolar epithelial club cells lining the airways, and AT2 cells, the surfactant-producing epithelial cells in alveoli, are widely believed to be the precursors of adenocarcinomas. Double positive cells (DPCs), cells comprised of both the Clara cell marker CC10 (*SCGB1A1* gene) and AT2 marker surfactant protein C (SPC, *SFTPC* gene), were reported in the junction of bronchiolar and alveolar epithelium in the respiratory bronchioles within adenomatous lesions of *Kras*^{G12D}-driven mouse lung tumours (Jackson et al., 2001). DPCs were subsequently shown to express two key skin and hematopoietic stem cell markers, namely CD34 and SCA1 (Blanpain et al., 2004; Morrison & Weissman, 1994). These cells displayed self-renewal abilities and multipotency and gave rise to both Clara- and AT2 (alveolar type II)-like cells when grown *in vitro* in Matrigel (Kim et al., 2005). Thus, DPCs were termed bronchioalveolar stem cells (BASCs). Even though the stem cell

property of BASCs for the bronchiolar and alveolar regions has come under scrutiny (Rawlins et al., 2009), they still represent a credible cell population from which lung adenocarcinomas might arise. Subsequent studies have provided conflicting evidence as to whether *KRAS*-driven lung adenocarcinomas predominantly arise from AT2 or Clara cells (Rowbotham & Kim, 2014). A compelling report by Mainardi and colleague's, where a resident $Kras^{G12V}$ oncoprotein was coexpressed with the bacterial surrogate marker β-Geo, elegantly showed that only SPC^{+} AT2 cells were able to yield malignant adenocarcinomas in a *Kras*-driven genetically engineered mouse (GEM) model (Mainardi et al., 2014). Yet, Cho and colleagues, using fluorescence-activated cell sorting fractionation in a $Kras^{G12D}$-driven lung adenocarcinoma, indicated that only the bronchiolar $CC10^{+}$ Clara cells could give rise to lung adenocarcinomas (Cho et al., 2011). Collectively, lung adenocarcinomas might be initiated from multiple cell types within the bronchioalveolar vicinity depending on developmental and genetic factors (Sutherland et al., 2014).

1.4 Lung adenocarcinoma

1.4.1 Histological/Morphological classification

Currently, lung adenocarcinoma broadly follows a stepwise progression, in which a premalignant lesion, known as atypical adenomatous hyperplasia (AAH), progresses to a small (≤3 cm), solitary pre-invasive lesion, known as adenocarcinoma *in situ* (AIS) (formerly known as bronchioalveolar carcinoma [BAC]), leading to a small (≤3 cm), solitary adenocarcinoma with ≤0.5 cm invasion, known as minimally invasive adenocarcinoma (MIA) and subsequently leading to invasive adenocarcinoma (Travis et al., 2011). Most cases of AIS and MIA are non-mucinous and rarely mucinous (i.e. contain intracytoplasmic mucin), a feature that might be predictive for targeted therapy (Wislez et al., 2010). Histologic subtyping of invasive adenocarcinomas includes lepidic predominant pattern: type II pneumocytes and Clara cells lining the surface of intact alveolar walls; acinar predominant pattern: oval-shaped malignant glands invading the fibrous stroma; papillary predominant pattern: cuboidal malignant cells supported by fibrovascular cores; micropapillary predominant pattern: glandular cells growing in small papillary clusters in the absence of fibrovascular cores; and solid predominant pattern: malignant cells with no lepidic, acinar, or papillary patterns, characterised with abundant

intracytoplasmic mucin and vesicular nuclei (Travis et al., 2011). Lung adenocarcinomas are highly heterogeneous tumours with variable prognoses, therefore pathological classification is not only important for patient stratification prior to therapy, but may also serve as a predictive tool for patient survival (Russell et al., 2011).

1.4.2 Molecular classification

Various studies comparing cytomorphology versus immunohistochemistry methods in differentiating/diagnosing NSCLC subtypes, have shown that both strategies are essential in stratifying lung cancer patients with greater accuracy. Further, since the lung represents an organ common for cancer metastases, aside from histomorphological classification, defining cancer or subtype specific molecular markers (i.e. biomarkers) is key in determining the origin of cancer cells from other organs. For instance, p63, a member of the p53 family and an important transcription factor for the development of epithelial cells, is a key immunochemical marker (but not exclusive) for LUSC. The authors of a tissue microarray study of 408 primary lung tumour cases showed p63 expression in 96.9% of LUSC cores (n=123), most with a strong positive nuclear signal (Au et al., 2004), while Khayyata and colleagues in fine-needle aspiration (FNA) specimens, indicated p63 and KRT5/6 dual expression in 75% LUSC cases and none in LUAD cases (Khayyata et al., 2009), an important observation for distinguishing these two subtypes. On the other hand, thyroid transcription factor (TTF-1), also known as Nkx2.1, is a sensitive marker for pulmonary and thyroid adenocarcinomas (Stenhouse et al., 2004). TTF-1 is a master regulatory, tissue-specific transcription factor (Guazzi et al., 1990) that plays a key role in early differentiation and development of the lung. It is expressed in terminal respiratory unit cells from foetal through adult stages (Yatabe, Mitsudomi & Takahashi, 2002) and regulates the expression of Clara cell marker CC10 (Zhang, Whitsett & Stripp, 1997), and surfactant protein A (Bruno et al., 1995), B (Yan, Sever & Whitsett, 1995), and C (Kelly et al., 1996). TTF-1 expression has been clinically important in distinguishing primary lung adenocarcinomas from those originating from different organs. Moldvay and colleagues compared the expression of TTF-1 between surgically resected primary peripheral bronchial adenocarcinomas and metastatic lung adenocarcinomas of different origins (e.g. colon and breast), showing

immunopositivity in 92% (N=50) of primary samples while only in four percent (N=50) of metastatic samples (Moldvay et al., 2004). Further, a meta-analysis study into the impact of TTF-1 expression on NSCLC survival, indicated that TTF-1 overexpression is associated with a favourable prognosis for NSCLC patients (Qian et al., 2015). While LCC and SCLC represent two poorly differentiated lung cancer subtypes, the latter manifests neuroendocrine differentiation, with synaptophysin and chromogranin being key SCLC markers (Taneja & Sharma, 2004).

1.5 Oncogene addiction – the "Achilles heel" of (certain) tumours

Tumourigenesis is driven by progressive accumulation of multiple gain-of-function (i.e. activating) mutations in oncogenes (tumour promoters) and loss-of-function (i.e. inactivating) mutations in tumour suppressors. Nevertheless, *oncogene addiction,* a term first coined by Bernard Weinstein, highlights the dependency of certain tumour cells on a single activated oncogenic pathway or protein (Weinstein & Joe, 2008). For instance, inactivation of the MYC oncogene culminates in significant and sustained tumour regression in various cancers (Felsher, 2010; Felsher & Bishop, 1999). Abrogating the function of these oncogenic drivers (i.e. oncoproteins) creates an imbalance between the rates of pro-apoptotic and pro-survival signals, a concept known as *oncogenic shock*. According to this model, pro-apoptotic signals exceed pro-survival signals, which dissipate rapidly, thereby commiting the malignant cell to apoptotic death (Sharma et al., 2006). These concepts have been the rationale for molecular targeted therapies in cancer.

1.6 Receptor tyrosine kinases – onset of targeted therapies

Receptor tyrosine kinases (RTKs) share a similar structure, an extracellular ligand binding domain (i.e. ectodomain), a single transmembrane helix and an intracellular protein tyrosine kinase (TK) domain with C-terminal regulatory regions. Growth factors, hormones and cytokines (i.e. ligands) elicit complex signalling pathways by binding transmembrane receptors on their extracellular regions, which induces receptor dimerisation and initiation of a cascade of events intracellularly through their cytoplasmic TK domains. There are 58 known human RTKs within 20 subfamilies, of which many have emerged as master regulators of

essential cellular processes, namely the epidermal growth factor receptor (EGFR), fibroblast growth factor receptor (FGFR), vascular endothelial growth factor receptor (VEGFR) and platelet-derived growth factor receptor (PDGFR) (Lemmon & Schlessinger, 2010). Although their activity is tightly regulated in normal cells, constitutive and aberrant activation of RTKs and their downstream signalling components through activating mutations, gene amplifications and protein overexpression, contribute significantly in perpetuating tumourigenesis. As such, RTKs have been extensively implicated in the pathophysiology of human cancers. Hence, RTKs have become an attractive therapeutic target, with EGFR being the first receptor proposed for targeted cancer therapy.

1.7 The ERBB/HER family of receptor tyrosine kinases – 1st and 2nd generation inhibitors

EGFR (ERBB1), the first discovered RTK (Carpenter, King & Cohen, 1978) and member of the ERBB family (HER-2/NEU, ERBB2; HER-3, ERBB3; HER-4, ERBB4), triggers downstream signalling pathways that control cell survival, growth and proliferation **(Figure 2a)** (Scaltriti & Baselga, 2006). It is frequently expressed in epithelial tumours and extensively altered in NSCLCs by activating mutations, gene amplification and protein overexpression (Hirsch et al., 2003). EGFR is overexpressed in 40% to 80% NSCLCs, while up to 50% of adenocarcinomas in Asian populations and 10% to 15% in Caucasians, are driven by activating EGFR mutations (Midha, Dearden & McCormack, 2015). The two most common somatic EGFR mutations are exon 19 in-frame deletions (60%) and missense substitutions (point mutations) in codon 858 (exon 21; 35%), where leucine is replaced by arginine (L858R) resulting in receptor constitutive activation (Chan & Hughes, 2015; Rosell et al., 2009). These mutations are present in the TK domain of EGFR and are significantly more frequent in adenocarcinomas versus other lung cancer subtypes, in females versus males, in never smokers than ever smokers and in East Asian patients (Shigematsu et al., 2005). NSCLCs with the aforementioned activating EGFR mutations are highly sensitive to small molecule ATP-competitive inhibitors of the EGFR TK domain, such as the first generation reversible inhibitors gefitinib (Iressa) and erlotinib (Tarceva) and second generation irreversible inhibitor afatinib (Gilotrif) (Paez et al., 2004; Lynch et al., 2004). Longer survival following treatment with erlotinib or gefitinib was seen in NSCLC patients with EGFR exon 19 deletions compared to

those with the L858R mutation (Jackman et al., 2006). A meta-analysis of randomised trials indicated significant improvement in response rate (RR) and progression-free survival (PFS) in patients with EGFR activating mutations treated with EGFR TK inhibitors (TKIs) as compared with first-line chemotherapy (Lee et al., 2015). Thus, front-line EGFR TKI therapy is the standard of care for NSCLC patients with EGFR sensitising mutations.

1.8 Emergence of resistance – 3rd (and 4th) generation inhibitors

Nevertheless, in most patients the disease progresses 9 to 12 months post-treatment, who eventually acquire resistance. Following results from the IMPRESS trial, continued administration of gefitinib plus chemotherapy in patients with acquired resistance to first-line EGFR TKI, is not recommended. Therefore, prior to the development of third generation EGFR TKIs, platinum-based chemotherapy remained the standard of care for this setting (Soria et al., 2015). Approximately 40% to 60% of the resistance cases are mediated through the secondary EGFR exon 20 T790M missense mutation ("gatekeeper" mutation), which alters the configuration of the kinase domain thereby enhancing its affinity for ATP relative to its affinity for EGFR TKIs (Yu et al., 2013). T790M mutations may be acquired during/following exposure to EGFR TKIs (i.e. acquired mutations) or can exist at a low frequency as resistant clones within tumour cells and become more dominant following targeted treatment (i.e. *de novo* mutations). In a meta-analysis study, advanced NSCLC patients with a *de novo* T790M mutation prior to EGFR TKI treatment (erlotinib or gefitinib) performed worst compared to advanced NSCLC patients who acquired a T790M mutation post-EGFR TKI treatment (erlotinib or gefitinib) (Liu et al., 2017). Osimertinib (Tagrisso; AZD9291), a third-generation irreversible EGFR TKI, targets EGFR primary activating mutations as well as the T790M mutation while sparing wild-type EGFR activity. During a phase I/II clinical trial (AURA), this small molecule produced greater RRs and PFS in EGFR T790M-positive patients compared to EGFR T790M-negative patients who had disease progression following first-line EGFR TKI therapy (Janne et al., 2015). It has also shown greater efficacy in a phase III clinical trial (AURA3) comparing osimertinib to platinum-based therapy plus pemetrexed in T790M-positive NSCLC patients who had disease progression following first-

line EGFR TKI therapy (Mok et al., 2017). Thus, osimertinib was approved as a therapeutic treatment for these patients by the FDA, EMA, and in Japan. However, whether osimertinib provides greater overall survival (OS)

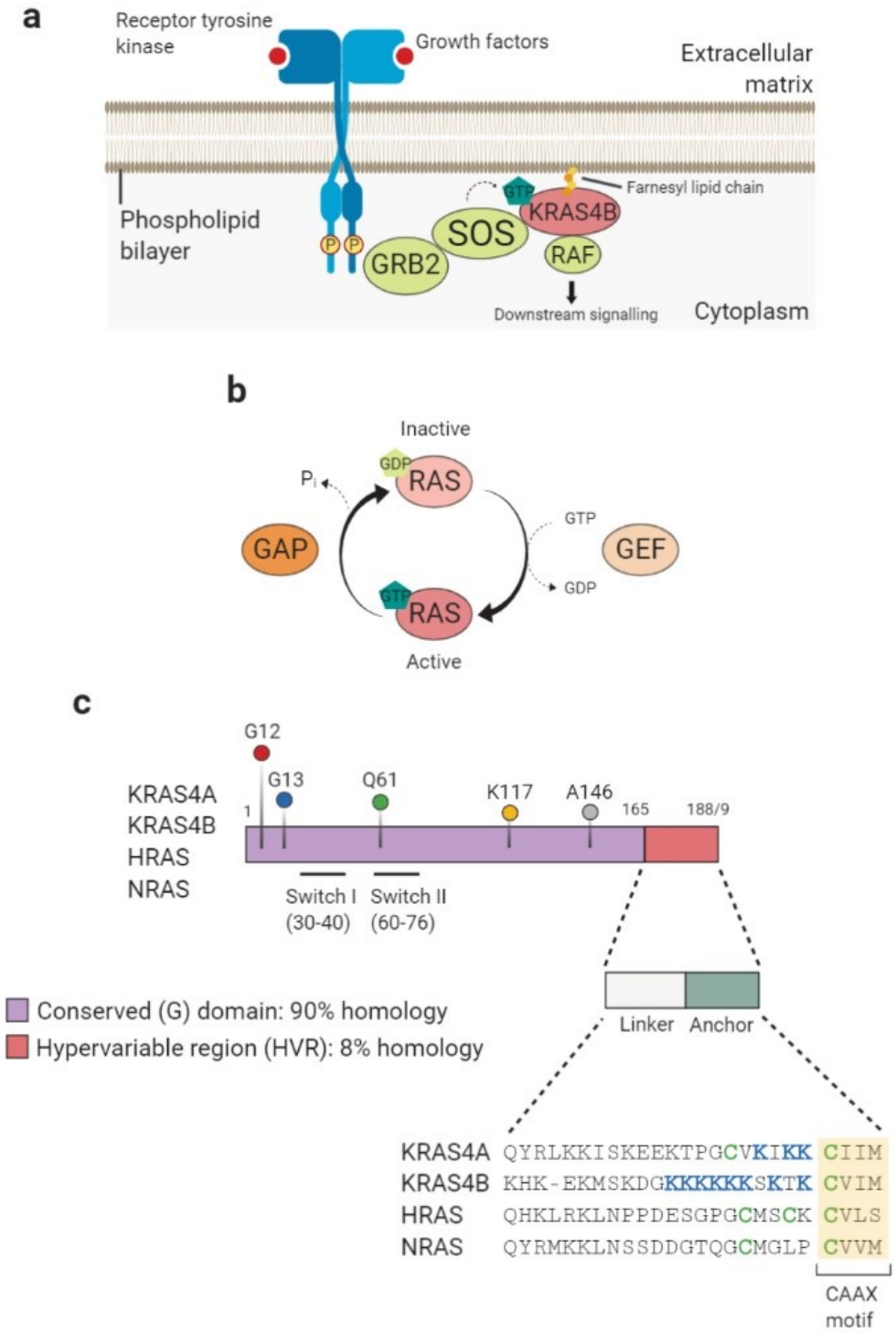

Figure 2| RAS activation and structure. (a, b) Receptor tyrosine kinases (RTKs; e.g. EGFR, PDGFR), cytokine receptors (not shown) or heterotrimeric G-proteins (not shown) initiate RAS signalling activation. Growth factor binding (e.g. EGF, TGFα) on EGFR extracellular domain causes receptor dimerisation, which promotes autophosphorylation on tyrosine residues within the intracellular domain. GRB2 docks (via its SH2 domain) on the phosphotyrosine residues of EGFR and recruits SOS to the plasma membrane (via its SH3 domains).

RAS is attached to the inner side of the plasma membrane via a farnesyl lipid chain (i.e. KRAS4B). RAS cycles between a GTP-bound (active) and GDP-bound (inactive) state. The guanine nucleotide exchange factor (GEF) SOS catalyses the exchange of GDP for GTP to activate RAS (RAS-GTP). GTP-bound RAS phosphorylates and activates RAF to initiate downstream signalling. GTPase activating proteins (GAPs; e.g. neurofibromin) enhance GTP hydrolysis, which causes the release of γ-phosphate, inactivation of RAS (RAS-GDP) and attenuation of downstream signalling. **(c)** There are three RAS isoforms, KRAS (KRAS4A and KRAS4B splice variants), HRAS and NRAS (21 kDa; 188/9 aa) (See **Figure 3**), which share a highly conserved N-terminal catalytic domain, also called the G domain (1-165 aa). Within the G domain are switch I (30-40 aa) and switch II (60-76 aa) regions, which interact with and activate RAS downstream effector proteins (e.g. RAF). The majority of RAS mutations occur at one of three hotspots: G12, G13 and Q61, while K117 and A146 are less frequent mutations (See **Figure 4**). All mutations constitutively activate RAS by decreasing the rate of intrinsic or GAP-mediated hydrolysis and/or enhancing the rate of intrinsic nucleotide exchange. The C-terminal hypervariable region (HVR) is the most diverse region in RAS proteins (only 8% homology). This domain contains the cysteine-aliphatic-aliphatic-terminal amino acid motif (CAAX) motif, which undergoes several post-translational modifications and is crucial for RAS membrane localisation. Farnesyl lipids are attached to the cysteine residue (green shaded) of the CAAX motif, while palmitoyl lipids are attached to cysteine residues adjacent to the CAAX motif (HRAS is anchored by two palmitoyl lipids). KRAS4B is not palmitoylated; however, the presence of a positively charged lysine (K) rich region (blue shaded) enhances its association with the negatively charged phospholipid heads of the plasma membrane (Ryan & Corcoran, 2018; Simanshu, Nissley & McCormick, 2017). Figure created with biorender.com.

as a first-line treatment compared to first-line treatment with first- or second-generation EGFR TKIs followed by second-line osimertinib treatment, remains to be discovered. Not surprisingly, resistance to third-generation EGFR TKIs has also been reported, the most frequent being the EGFR C797S mutation (Thress et al., 2015). A fourth-generation allosteric, non-ATP competitive EGFR inhibitor overcoming both T790M and C797S resistance is under preclinical development (Wang, Song & Liu, 2017).

1.9 Small molecules Vs monoclonal antibodies

An alternative approach for the molecular targeting of EGFR and downstream signalling involves the use of monoclonal antibodies (mAbs). Unlike small molecules, therapeutic mAbs are large proteins (typically 150 kDa) that interfere with receptor extracellular domain. ERBB-targeted mAbs block receptor function via several putative mechanisms, including inhibition of receptor homo- and hetero-dimerisation (pertuzumab; Omnitarg: ERBB2/HER2 inhibitor) (Franklin et al., 2004), inhibition of receptor shedding[9] (trastuzumab; Herceptin: ERBB2/HER2 inhibitor) (Molina et al., 2001), or hindering ligand-receptor interaction and triggering receptor internalisation (cetuximab; Erbitux: ERBB1/HER1/EGFR1 inhibitor) (Harding & Burtness, 2005). Small molecule inhibitors and mAbs have markedly different mechanisms of action, biological activities and pharmacokinetic properties. For instance, while mAbs are unable to cross the plasma membrane therefore targeting only cell-surface or secreted molecules, small molecule inhibitors can target intracellular proteins regardless of their

[9] Receptor shedding: The proteolytic cleavage of a cell-membrane receptor's extracellular domain (ectodomain) from the cell surface (ScienceDirect).

subcellular localisation. Further, unlike small molecules, mAbs can directly elicit immune effector mechanisms such as antibody-dependent cellular cytotoxicity, which might account for their synergistic effects when used in combination with chemotherapy (Imai & Takaoka, 2006). Dual molecular targeting with both anti-EGFR mAbs and EGFR TKIs suggested that utilising the non-redundant properties of distinct EGFR inhibitors may potentiate EGFR signalling inhibition (Huang et al., 2004). Nevertheless, both strategies individually or in combination represent indispensable tools for oncogenic driver-targeted cancer therapies.

1.10 EGFR-independent mechanisms of resistance

Resistance to EGFR inhibitors may also arise through EGFR-independent mechanisms, the most prominent being activation of phosphatidylinositol 3-kinase (PI3K)/AKT/mTOR (mammalian target of rapamycin) pathway via amplification of the proto-oncogene mesenchymal-epithelial transition factor (MET) (5%-20%) (Bean et al., 2007). MET amplification permits the transmission of the same signalling pathway downstream of EGFR in the presence of EGFR TKIs by phosphorylating ERBB3/HER3 and promoting PI3K/AKT/mTOR pathway (Engelman et al., 2007). Although moderate MET amplifications could coexist with the T790M mutation in gefitinib-refractory autopsy tumour samples, clinically relevant MET amplifications (≥ 4-fold MET gene copy number gain) were almost mutually exclusive with T790M mutations (Suda et al., 2010). Combination treatments with MET small molecule inhibitors (e.g. tivantinib, tepotinib), mAbs (e.g. onartuzumab) or antibodies against its ligand HGF (hepatocyte growth factor), and EGFR TKIs are undergoing clinical trials in humans (Wang et al., 2019). In a phase II clinical trial, NSCLC patients with acquired resistance to first-line EGFR TKI (T790M –ve) and MET gene amplification (gene copy number ≥ 5-fold), had a PFS five times longer when received tepotinib and gefitinib combination compared to the chemotherapy only arm (pemetrexed + cisplatin/carboplatin) (Soo et al., 2015). The emergence of secondary and tertiary EGFR mutations or activation of EGFR-independent pathways in a subset of neoplastic cells within the tumour cell population manifests the significant dependency of these cells on oncogenic drivers and therefore the need for the development or combination of novel molecular targeted therapies to overcome resistance.

1.11 RAS superfamily – RAS, RHO, RAB, RAN and ARF

The human RAS superfamily represents a group of over 150 members of small guanosine triphospatases (GTPases). GTPases are low molecular weight (20-40 kDa) GDP/GTP-binding proteins (G proteins), which act as binary molecular switches by cycling between active guanosine triphosphate (GTP)-bound and inactive guanosine diphosphate (GDP)-bound states (i.e. GTPase activity). Based on structural, sequence and functional similarities, this superfamily has been traditionally divided into five major branches, namely RAS, RHO, RAB, RAN and ARF (Colicelli, 2004). Despite extensive sequence conservation, these families control different cellular processes. While the RHO (Ras homologous) family (RHOA, RAC1, CDC42) is implicated in the regulation of cell movement, cell shape and cell polarity by controlling actin reorganisation (Etienne-Manneville & Hall, 2002), the RAB (Ras-like proteins in brain) family orchestrates intracellular vesicular transport and trafficking of proteins in the endocytic and secretory pathways (Zerial & McBride, 2001). Similar to the RAB proteins, the ARF (ADP-ribosylation factor) family regulates organelle structure and membrane trafficking (Donaldson & Jackson, 2011), while the most abundant small GTPases in the cell, the RAN (Ras-like nuclear) family of proteins, are involved in the nuclear and cytoplasmic transport of proteins and RNA (Weis, 2003).

1.12 RAS subfamily – KRAS, HRAS and NRAS

The Rat sarcoma (RAS) proto-oncogenes – HRAS, NRAS and two splice variants of KRAS, KRAS4A and KRAS4B[10] - are the founding members of the RAS superfamily and despite their high degree of homology (85% overall amino acid sequence identity) and common activators and effectors, RAS proteins transduce extracellular signals through distinct intracellular networks that control cell survival, cell proliferation, differentiation and cell motility/invasion. RAS isoforms are ubiquitously expressed in mammalian cells, however early knockout mice studies have shown that while HRAS and NRAS are nonessential for normal mouse development, embryos with KRAS homozygous mutation die between E12 and E14 with severe foetal liver defects (Johnson

[10] Alternative splicing of exon four allows the expression of two KRAS proteins, differing only in their carboxyl-terminal residues. Throughout this work, KRAS refers to the predominant and ubiquitously expressed KRAS4B variant.

et al., 1997). This might reflect the more ubiquitous expression of KRAS and its participation in cell growth and differentiation pathways.

1.13 KRAS, HRAS, NRAS – structure and membrane localisation

RAS genes encode a 21 kDa monomeric GTPase, which cycles between GTP-bound active and GDP-bound inactive states, a process tightly regulated by guanine nucleotide exchange factors (GEFs) and GTPase activating proteins (GAPs), respectively **(Figure 2b)**. RAS isoforms possess a highly conserved (90% amino acid sequence identity) N-terminal catalytic domain (1-165 aa), also known as the G domain, which is involved in GTP binding and hydrolysis **(Figure 2c)**. Switch I and switch II regions within the G domain change conformation during GDP-GTP cycling and constitute key determinants during RAS interaction with downstream effectors (Ryan & Corcoran, 2018). However, the carboxyl-terminal sequence, also known as the hypervariable region (HVR) (166-188/9 aa), differs markedly between RAS isoforms and probably accounts for their distinct subcellular localisations and signal outputs **(Figure 2c)**. All RAS isoforms terminate with a C-terminal CAAX tetrapeptide motif (C=Cysteine, A=aliphatic amino acid, X=any amino acid) that is activated through post-translational modifications and is indispensable for membrane-targeting and subcellular localisation **(Figure 2c)** (Hancock, 2003). RAS proteins are synthesised as cytosolic precursors and can elicit downstream signalling only if attached to the plasma membrane, a process that involves three sequential post-translational modifications within the CAAX tetrapeptide. First, RAS proteins are prenylated[11] by farnesylation, a process catalysed by a farnesyltransferase enzyme, whereby a farnesyl isoprenoid lipid is attached to the cysteine residue of the CAAX motif. The farnesylated CAAX sequence is then targeted to the cytosolic surface of the endoplasmic reticulum (ER) where the RAS-converting CAAX endopeptidase 1 (RCE1), an intrinsic ER membrane protein, cleaves the –AAX tripeptide. This cleavage is followed by carboxymethylation of the α-carboxyl group of the now farnesylated cysteine, by isoprenylcysteine carboxylmethyltransferase (ICMT) and S-adenosylmethionine (SAM). Unlike HRAS and NRAS, KRAS exits the ER and traffics to the plasma membrane

[11] Prenylation: Covalent attachment of 15-carbon (farnesyl) or 20-carbon (geranylgeranyl) isoprenoid lipids to a free thiol of a cysteine residue (of proteins) by the enzymes farnesyltransferase (FTase) and geranlygeranyltransferase I (GGTase I), respectively (ScienceDirect).

bypassing the classical secretory pathway through the Golgi. RAS trafficking between membranes requires additional lipid modifications, which HRAS and NRAS acquire at the Golgi apparatus, where they are palmitoylated[12] by a palmitoyltransferase encoded by the human genes *ZDHHC9* and *GCP16* (Swarthout et al., 2005). Since KRAS does not shuttle through the Golgi, it is not palmitoylated; however, the presence of a positively charged polybasic (K, lysine rich) domain adjacent to its CAAX motif, facilitates KRAS-membrane association via electrostatic interaction with the negatively charged phospholipid heads of the plasma membrane **(Figure 2c)** (Hancock, Cadwallader & Marshall, 1991). Lastly, the chaperone protein phosphodiesterase-δ (PDEδ) facilitates RAS localisation on the plasma membrane where it transduces extracellular signals to intracellular downstream pathways (Ryan & Corcoran, 2018; Wang & Casey, 2016; Hancock, 2003).

1.14 RAS – upstream signalling

Multiple receptors have been shown to trigger RAS signalling, such as RTKs (Satoh et al., 1993), cytokine receptors (Chang et al., 2003) and heterotrimeric G-proteins (Gutkind, 1998). EGFR, one of the best characterised RAS receptors, has at least seven known ligands, including EGF, transforming growth factor alpha (TGFα), amphiregulin and betacellulin (Scaltriti & Baselga, 2006). In the absence of ligands, almost all RTKs exist as monomeric transmembrane receptors. EGF binding on two separate binding surfaces, the β-helix domains I and III (L domains) of EGFR, promotes a conformational change in the extracellular region of the receptor (i.e. 130° rotation of domains I and II), thereby exposing the dimerization arm of cysteine-rich domain II and allowing for receptor homo- or hetero-dimerisation. Contrary to most RTKs, EGFR dimerisation is exclusively receptor mediated, whereby the domain II of a receptor monomer interacts with the domain II of another monomer that has also been ligand-induced (Burgess et al., 2003). Ligand-induced EGFR dimers are autophosphorylated (in *trans*) on tyrosine residues within the cytoplasmic domain. Tyrosine phosphorylation

[12] Palmitoylation: Covalent attachment of 16-carbon palmitic acid (fatty acid) to a cysteine residue (S-palmitoylation) of proteins via thio-ester linkage (ScienceDirect).

activates downstream signalling pathways, of which the best studied include the PI3K/AKT/mTOR and the RAS/RAF/MEK/ERK pathways (Ono & Kuwano, 2006).

The phosphotyrosine residues on EGFR serve as docking sites for the adaptor protein growth factor receptor-bound protein 2 (GRB2) **(Figure 2a)**. GRB2 interacts directly with the phosphotyrosine-containing sequence of the receptor via its single Src homology 2 (SH2) domain. The two SH3 domains of GRB2 recruit SOS1 (son-of-sevenless homologue 1), a well-known GEF and RAS activator, to the cell membrane by binding to its proline-rich C-terminal tail (Rozakis-Adcock et al., 1993). SOS1 and SOS2 specificity for RAS is dictated by the presence of a CDC25 homology domain and a RAS exchange motif (REM) on these proteins (Bos, Rehmann & Wittinghofer, 2007). RAS intrinsic GEF activity requires SOS and GRB2 interaction, which is indispensable for coupling EGFR and its cytoplasmic protein tyrosine kinase to the RAS/RAF/MEK/ERK signalling pathway (Aronheim et al., 1994). Once at the plasma membrane, SOS interacts with KRAS, which is also attached to the inner side of the membrane via a single farnesyl lipid chain, to induce a conformational change and the exchange of GDP for GTP, the rate-limiting step for RAS protein activation (Simanshu, Nissley & McCormick, 2017; Downward, 2003). In the GTP-bound state, KRAS switch I and switch II regions change conformation, thereby enhancing its affinity for downstream effector proteins, of which the best characterised are the RAF (Rapidly Accelerated Fibrosarcoma) kinases. KRAS recruits RAF family members to the plasma membrane to initiate downstream signalling. However, this state is transient and KRAS inactivation occurs by GTP hydrolysis, a process catalysed by GTPase activating proteins (GAPs), such as neurofibromin 1 (NF1). Since the rate of intrinsic GTP hydrolysis of RAS proteins is very slow, efficient GTP hydrolysis requires interaction with a GAP (Bos, Rehmann & Wittinghofer, 2007). Ultimately, GTP hydrolysis and the release of the γ-phosphate causes the dissociation of effector proteins from KRAS and thereby attenuation of downstream signalling.

1.15 Therapeutic targeting of RAS signalling in cancer

Oncogenic, gain-of-function RAS mutations typically occur in hot spots that interfere with normal RAS regulation and function, such as the GDP-GTP molecular switch **(Figure 2c)**. These mutations alter the

homeostatic balance between GDP and GTP binding, by either enhancing GTP-loading or reducing the rate of GTP hydrolysis; thereby, favouring a constitutively active, GTP-bound state, which permits aberrant downstream signalling without EGFR activation. RAS mutations[13] are found in approximately 25% of all human cancers, rendering RAS genes the most frequently mutated oncogene family in cancer **(Figure 3)**. The mutation frequency is highest in three of the four most lethal cancers: pancreatic ductal adenocarcinoma (PDAC) (97.7%), colorectal carcinoma (CRC) (52.2%) and lung adenocarcinoma (LUAD) (32.1%) **(Figure 3)**. KRAS represents the most commonly mutated RAS isoform, accounting for the majority of RAS mutations (85%), followed by NRAS (11%) and the infrequently mutated HRAS (4%) **(Figure 3)** (Haigis, 2017).

The majority of mutations are missense substitutions (>90%) and mostly occur (>95%) at one of three mutational hotspots: G12, G13 and Q61, of which the former represents the most prominent KRAS mutation **(Figure 2c & Figure 4)**. These mutations cluster around the nucleotide-binding pocket and contribute towards KRAS oncogenic activity by either decreasing the rate of intrinsic or GAP-mediated hydrolysis and/or enhancing the rate of intrinsic nucleotide exchange. The replacement of glycine at codons 12 or 13 with virtually any amino acid (except proline), is thought to cause a steric clash with GAP's arginine side chain (Arg-789) thereby preventing it from entering the GTPase site and blocking GTP hydrolysis (Scheffzek et al., 1997). While both codon 12 and 13 mutants decrease GAP-induced hydrolysis rate, codon 13 mutants also increase intrinsic nucleotide exchange. Glutamine-61 (Q61) within switch II domain **(Figure 2c)** is important for the conformational changes that occur during the transition between structural states. It is thought that Q61 stabilises the transition state of RAS during the hydrolysis reaction, thus codon 61 mutants display the lowest hydrolysis rates among all KRAS mutants (Haigis, 2017; Hunter et al., 2015). In NSCLC, the two most common KRAS mutations, G12C and G12V **(Figure 4c)**, result from the same type of substitution, a G to T transversion (G12C: GGT → TGT; G12V: GGT → GTT). The G.C → T.A transversions causing the G12C mutations are associated with bulky DNA adduct formation generated by exposure to polycyclic hydrocarbons found in

[13] COSMIC database: https://cancer.sanger.ac.uk/cosmic/gene/analysis?ln=KRAS
COSMIC database: https://cancer.sanger.ac.uk/cosmic/gene/analysis?ln=NRAS
COSMIC database: https://cancer.sanger.ac.uk/cosmic/gene/analysis?ln=HRAS

tobacco smoke. This mutational signature (signature 4) is probably an imprint of tobacco smoking and is the most prevalent signature in lung adenocarcinomas (Alexandrov et al., 2013).

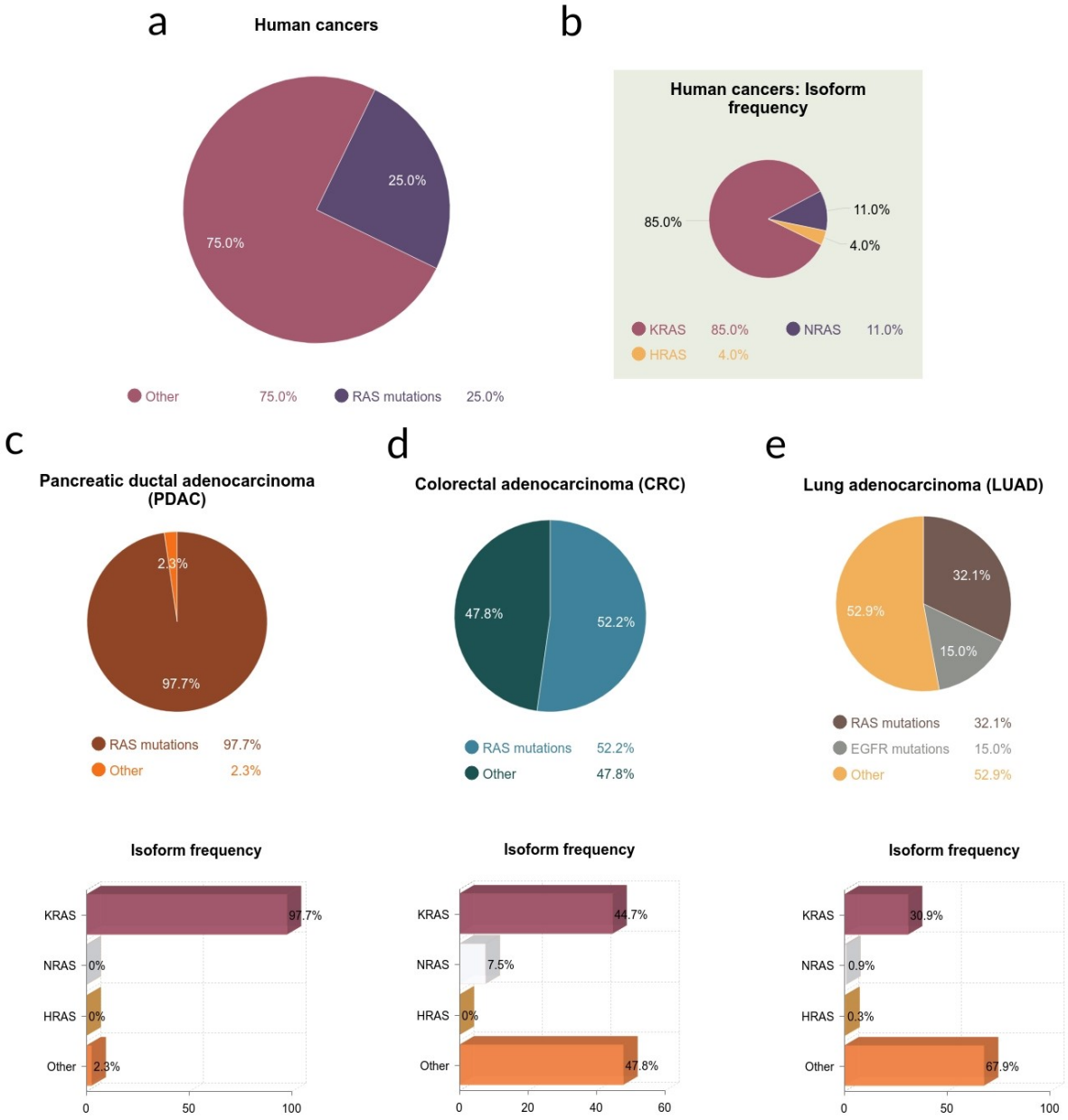

Figure 3| Frequency of RAS mutations in human cancers. (a) RAS mutations account for a quarter (25%) of all molecular alterations in human cancers. **(b)** KRAS is the most commonly mutated RAS isoform accounting for 85% of all RAS mutations, followed by NRAS (11%) and the least mutated isoform, HRAS (4%). Three of the most heavily RAS mutated cancers are pancreatic ductal adenocarcinoma (PDAC), colorectal adenocarcinoma (CRC) and lung adenocarcinoma (LUAD). **(c)** Almost all PDACs harbour RAS mutations (97.7%) on KRAS isoform (97.7%). **(d)** In CRC, RAS mutations account for more than half of all molecular alterations (52.2%). KRAS is the predominantly mutated isoform (44.7%), followed by NRAS (7.5%). **(e)** The two most common molecular alterations in LUAD are RAS mutations (32.1%) and EGFR mutations (including gene amplification/protein overexpression; 15%), which are almost always mutually exclusive. Similar to PDACs and CRCs, KRAS is also the predominantly mutated isoform accounting for 30.9%, followed by NRAS (0.9%) and HRAS (0.3%). Other frequent LUAD alterations include ALK (anaplastic lymphoma kinase) translocations, MET (mesenchymal epithelial transition factor receptor) amplification, and ROS1 rearrangements. Data based on COSMIC (catalogue of somatic mutations in Cancer) and (Cox et al., 2014). Figure created with visme.co.

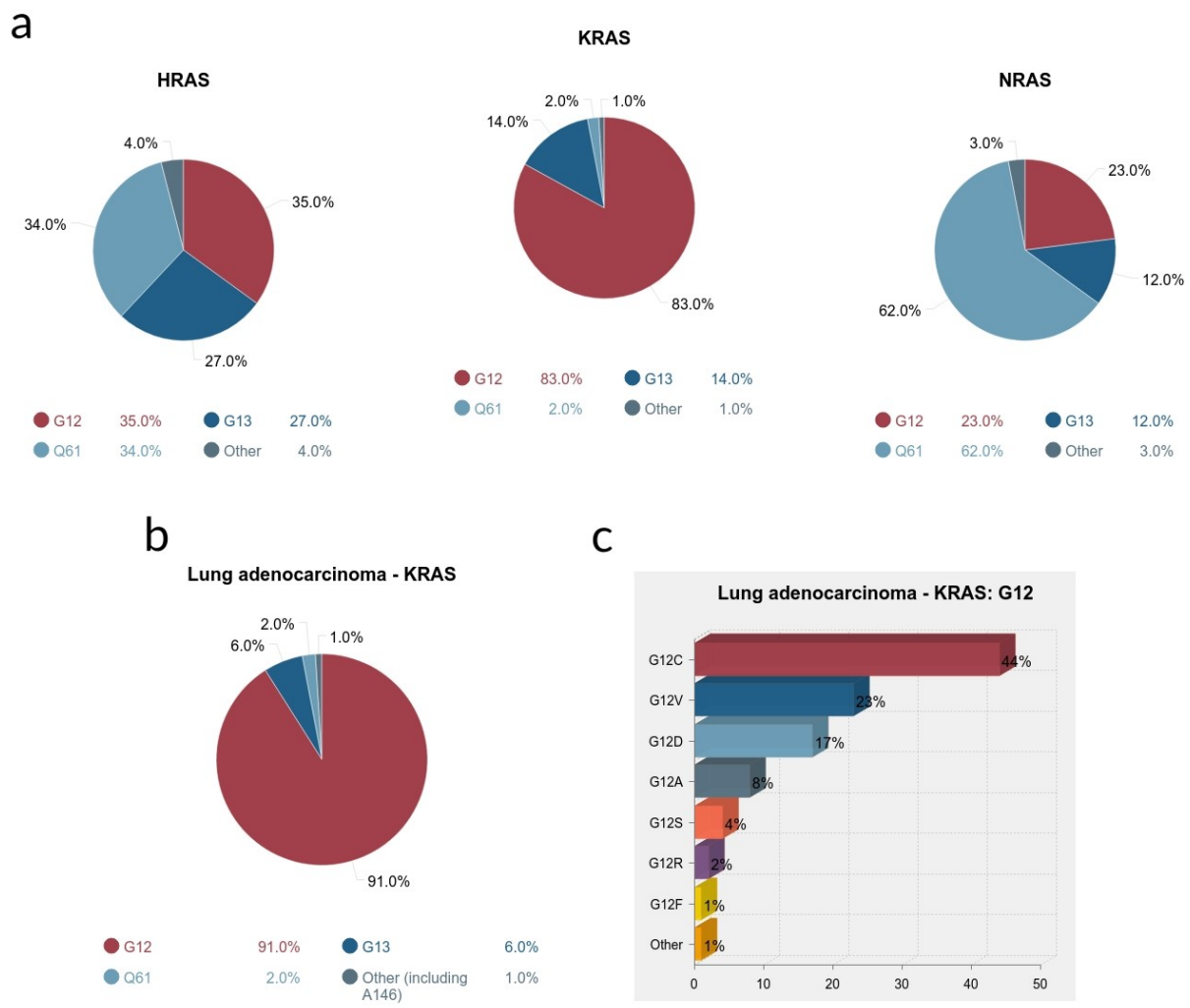

Figure 4| Types and frequency of RAS mutations in human cancers. (a) The majority of HRAS mutations occur almost uniformly at codons 12 (G12: 35%), 13 (G13: 27%), and 61 (Q61: 34%). G12 mutations are the predominant KRAS mutations accounting for 83%, followed by mutations at codon 13 (G13: 14%) and the least mutated codon 61 (Q61: 2%). Conversely, the majority of NRAS mutations occur at codon 61 (Q61: 62%), followed by codon 12 (G12: 23%) and 13 (G13: 12%). **(b)** Codon 12 (G12: 91%) is the most commonly affected site in KRAS mutant lung adenocarcinomas (LUADs), followed by mutations in codons 13 (G13: 6%) and 61 (Q61: 2%). (Other, including A146 mutations, account for 1%). **(c)** The most frequent point mutation subtype in KRAS mutant LUADs is G12C (44%), followed by G12V (23%), G12D (17%), G12A (8%), G12S (4%), G12R (2%), G12F (1%) and other (1%). Data based on COSMIC and (Cox et al., 2014). Figure created with visme.co.

Aberrant RAS activation is an indispensable driver of tumour initiation and maintenance and is linked to poor prognosis and resistance to therapy. RAS mutations are resistant to EGFR-targeted therapy and are mostly mutually exclusive to EGFR gene mutations (Jamal-Hanjani et al., 2017); hence, therapeutic targeting of RAS has attracted great scientific interest over the last decades. Despite numerous targeted drug development efforts, RAS oncoproteins were considered undruggable targets, due to the high picomolar binding affinity of RAS for GTP and the lack of drug-binding pockets outside the nucleotide-binding pocket; thus, rendering GTP-competitive inhibitors ineffective (Goody, Frech & Wittinghofer, 1991). These challenges, prompted

researchers to develop alternative strategies to abrogate RAS signalling, including renewed efforts for direct RAS inhibition (pan-RAS and allele-specific inhibitors), inhibition of RAS membrane association, and inhibition of RAS effectors or downstream pathway components (Ryan & Corcoran, 2018).

Initial efforts focused on inhibiting RAS prenylation (farnesylation or geranylgeranylation), which is critical for RAS localisation to the plasma membrane. Several potent farnesyltransferase inhibitors (FTIs), including tipifarnib and lonafarnib, were developed and despite their efficacy in preclinical HRAS driven cancer models, limited clinical efficacy was observed in KRAS driven cancers (Berndt, Hamilton & Sebti, 2011). This most likely reflects poor patient selection and the lack of understanding of isoform-specific lipid post-translational modifications. In fact, unlike HRAS, NRAS and KRAS isoforms are prenylated in the absence of a farnesyltransferase enzyme (FTase) by geranlygeranyltransferase I (GGTase I); thus, while FTIs can effectively block HRAS farnesyltransferase-dependent plasma membrane localisation, they are ineffective against NRAS and KRAS (Whyte et al., 1997). Tipifarnib is currently used in several clinical trials in HRAS mutant urothelial carcinoma (NCT02535650) and advanced squamous NSCLC patients (NCT03496766), while dual FTase and GGTase I inhibition is being explored in NRAS and KRAS cancers. Considering PDEδ is a critical mediator of RAS translocation from Golgi or ER to the plasma membrane, inhibition of RAS-PDEδ interaction with deltarasin, which binds to the prenyl-binding pocket of PDEδ, caused the retention of RAS on endomembranes and suppressed proliferation of human KRAS-driven PDAC cells *in vitro* and *in vivo* (Zimmermann et al., 2013). Nevertheless, the aforementioned strategies do not discriminate between wild-type (WT) and mutant RAS proteins and they might also inhibit several other proteins of which their physiological role depends on prenylation and plasma membrane localisation. Therefore, selective targeting of mutant RAS isoforms utilising allele-specific therapeutic strategies, could abrogate oncogenic RAS signalling while also sparing the physiological function of WT RAS. The KRAS-G12C mutant protein, unlike KRAS-G12D and KRAS-G12V mutants, displays the unique characteristic of cycling between the GDP-bound and the GTP-bound states. As a result, several groups sought to target an allosteric pocket underneath the switch II loop region (S-IIP), which is only accessible during the GDP-bound state. These efforts led to the development of potent and selective KRAS-

G12C inhibitors (ARS-853 and ARS-1620), which covalently bind the cysteine residue and lock RAS in an inactive conformation. While these inhibitors are paving the way for a new generation of allele-specific inhibitors with enormous therapeutic potential, their usefulness is restricted to a subset of KRAS mutant cancers – predominantly LUADs, since the majority of PDACs and CRCs are driven by G12D and G12V KRAS mutations. Pan-RAS inhibition (e.g. RAS-IN-3144) or genetic inhibition with anti-sense oligonucleotides (e.g. AZD4785: NCT03101839) have shown promising results *in vitro* and *in vivo* by targeting multiple RAS mutations (Ryan & Corcoran, 2018). However, despite significant achievements in targeting RAS directly or indirectly, downstream signalling persists in the absence of this master regulator, reflecting the significant crosstalk that exists between parallel pathways and adaptive feedback through WT RAS isoforms. Targeting RAS effectors or downstream pathway components of the RAF/MEK/ERK signalling cascade has therefore been perceived as an attractive therapeutic intervention of what is arguably one of the most significant and complex signalling networks driving cancer growth.

1.16 Signalling downstream of RAS – The RAF/MEK/ERK pathway

There are four well-characterised mitogen-activated protein kinase (MAPK) pathways in mammalian cells, which consist of three protein kinases: a MAPK kinase kinase (MAPKKK), a MAPK kinase (MAPKK) and a MAPK, and activate each other, in part, by phosphorylation. The terminal and executioner serine/threonine MAPKs of these pathways are ERK1/2, p38 (α, β, γ, δ), JNK (1, 2, 3) (c-Jun N-terminal kinases) and ERK5 (MAPK7). Notably, while the ERK1/2 pathway is mainly initiated by growth factor stimulation, the others are also activated downstream of cellular stress and stimulation by cytokines (Roberts & Der, 2007). The RAS/RAF/MEK/ERK pathway, probably one of the best characterised signal transduction pathways, controls key cellular processes such as cell proliferation, differentiation, survival and growth (Roberts & Der, 2007). This pathway has been the subject of extensive research due to its central physiological and pathophysiological roles. Mutations or overexpression in signalling components of this cascade have been reported in various human cancers and diseases (Roberts & Der, 2007). In fact, more than 30% of all human cancers manifest constitutive activation of the 44 kDa (ERK1; MAPK3) and 42 kDa (ERK2; MAPK1) mitogen-activated protein

(MAP) kinases (Hoshino et al., 1999). Extracellular signal-regulated kinases 1 and 2 (ERK1/2) lie downstream of this pathway and are activated in response to binding of growth factors, neurotransmitters, chemokines, and polypeptide hormones to an upstream RTK **(Figure 5)** (Chen, Sarnecki & Blenis, 1992).

RAS effectors include RAF proteins, PI3K (activates AKTs), GEF TIAM1 (activates RAC1 pathway) and RALGDS (activates RALA and RALB). RAF kinases are the best characterised RAS effectors and constitute a family of serine/threonine kinases, which includes RAF-1 (aka CRAF), BRAF and ARAF, of which the former is the best characterised. Plasma membrane localised and GTP-bound RAS (RAS-GTP), recruits RAF kinases to the membrane by binding with high affinity to their RAS binding domain (RBD) and cysteine rich domain (CRD) through its switch I and II regions **(Figure 5)**. RAS-GTP promotes the formation of RAF homodimers or heterodimers and interferes with the 14-3-3 [14] dimer that holds RAF in an inactive state, thereby exposing two phosphorylation sites necessary for initiating RAF activation. RAF-1 activation by phosphorylation is a highly complex process that involves a series of dephosphorylation and phosphorylation events on negatively and positively regulatory sites, respectively **(Figure 5)** (Wellbrock, Karasarides & Marais, 2004). Activated RAF kinases act as MAPK kinase kinases (MAPKKKs or MAP3Ks) and constitute the first step of the three-tiered RAF (MAPKKK)/MEK (MAPKK)/ERK (MAPK) cascade.

Signalling specificity and efficiency within the MAPK pathway is partly dependent on specialised docking motifs (D-domains) present upstream or downstream of the phosphoacceptor site of multiple MAPK pathway kinases (e.g. MAPKKs) and substrates. RAF kinases phosphorylate and activate the dual-specificity protein kinases MEK1 (MAP2K1) and MEK2 (MAP2K2), the main downstream substrates of RAF **(Figure 5)**. Activation of MEK1 and MEK2 requires major conformational rearrangements to allow for correct ATP and substrate alignment. This is achieved firstly, by RAF binding on MEK1 and MEK2 D-domains (domain of versatile docking (DVD)) at the C-terminus of these kinases, and secondly, by phosphorylation of Ser218/Ser222 (MEK1) and Ser222/Ser226 (MEK2) within the activation loop of their kinase catalytic domains **(Figure 5)** (Caunt et al.,

[14] 14-3-3: Dimeric phosphoserine/threonine-binding adaptor/scaffold proteins involved in signal transduction and checkpoint control.

2015). Various *in vitro* studies have shown that BRAF can bind and phosphorylate MEK kinases more efficiently than ARAF and CRAF, rendering it the main MEK activator (Pritchard et al., 1995).

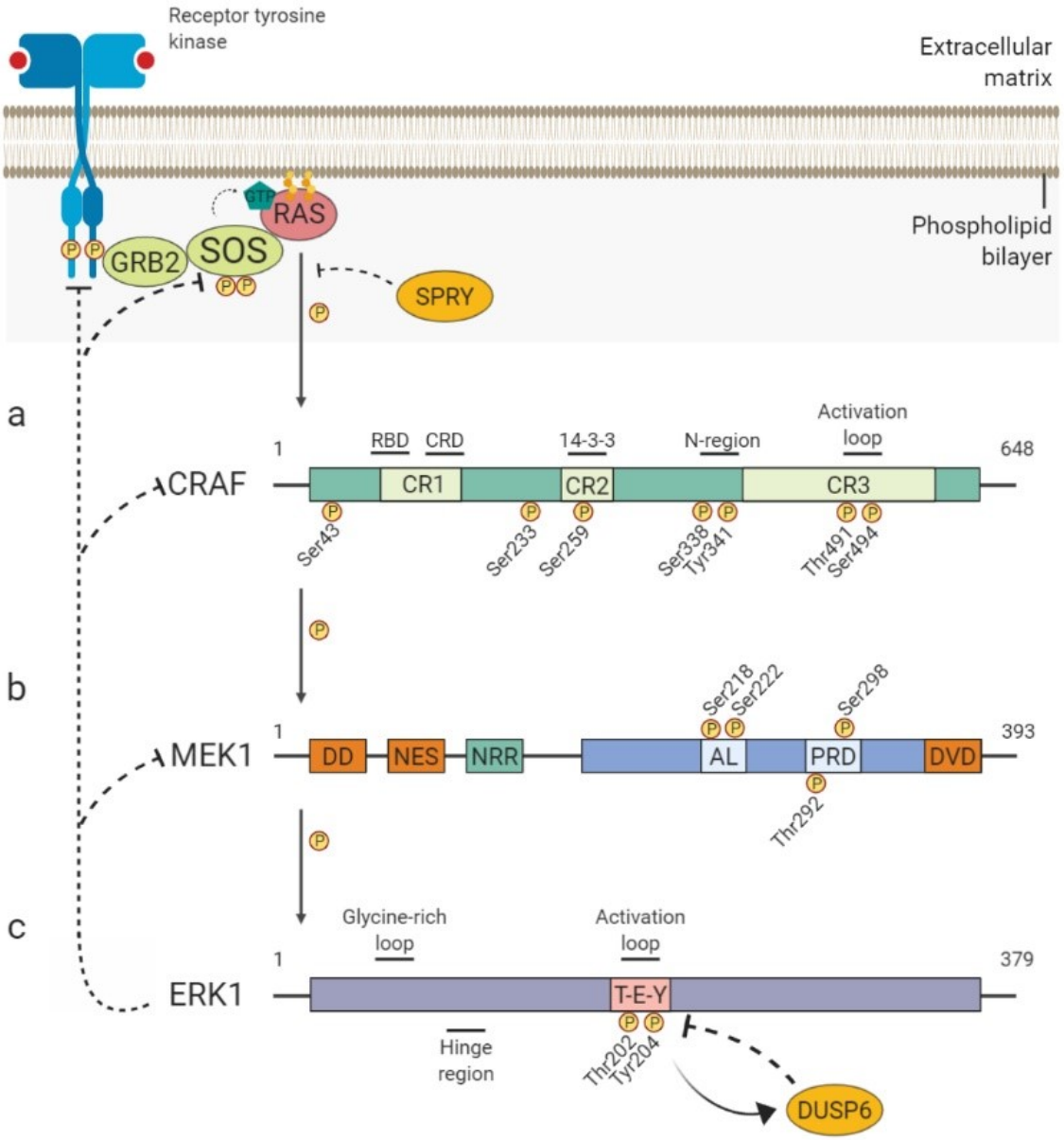

Figure 5| RAF/MEK/ERK pathway and feedback loops. (a) RAS signalling pathway is initiated in response to growth factor stimulation (See **Figure 2**). Activated RAS binds to the RAS binding domain (RBD) and cysteine rich domain (CRD) within the conserved region 1 (CR1) of RAF (structure of CRAF; 73 kDa; 648 aa). Phosphorylation of Ser259 (by PKA or AKT (PKB)) within the conserved region 2 (CR2) creates a docking site for 14-3-3 proteins, which interfere with RAS binding. Phosphorylation of Ser43 and Ser233 by PKA also blocks RAS binding. RAS-GTP and PP2A (protein phosphatase 2A) dephosphorylate Ser259 to displace 14-3-3 proteins and promote the formation of RAF dimers. Phosphorylation of Ser338/Tyr341 within the negatively charged N-region (by SRC) and Thr491/Ser494 (possibly by autophosphorylation) within the activation loop of conserved region 3 (CR3) are essential for full CRAF activation. **(b)** Activation of MEK1/2 (structure of MEK1; 43 kDa; 393 aa) requires binding of CRAF on the C-terminal docking domain (domain of versatile docking (DVD)) and phosphorylation of Ser218/Ser222 within the activation loop (AL). Ser298 within the proline-rich domain (PRD) is phosphorylated by p21-activated kinase (PAK). NES; nuclear export sequence. NRR; negative regulatory region (this region is mutated in cancer). **(c)** Activated MEK1 interacts with ERK1/2 (structure of ERK1; 43 kDa; 379 aa) through its N-terminal docking domain (DD) and phosphorylates Thr202/Tyr204 (**T**-E-**Y** motif) in the activation loop. Glycine-rich loop is the ATP-phosphate-binding loop. Hinge region is involved in kinase activation. ERK1/2-mediated negative feedback loops control the fine-tuning of the pathway. ERK1/2

negatively regulate the pathway by phosphorylation of EGFR (e.g. Thr669), phosphorylation of SOS directly or through RSKs (See **Figure 9**), phosphorylation of CRAF on several residues, including Ser43, and phosphorylation of MEK1 on Thr292 in the PRD. RAF/MEK/ERK pathway is also regulated by dual-specificity phosphatases (DUSP) and Sprouty (SPRY). DUSP6 dephosphorylates and inactivates ERK1/2 in the cytoplasm, while ERK1/2 induce the transcriptional activation of DUSPs. SPRY blocks protein interactions of GRB2 with SOS and RAF with RAS (Caunt et al., 2015; Lito, Rosen & Solit, 2013; Wellbrock, Karasarides & Marais, 2004). Figure created with biorender.com.

Further, although RAF kinases are the best-studied MEK activators, a number of other MAPK kinase kinases (MAPKKK; MAP3Ks) promote MEK activation, such as MEKK3 (activates ERK5 pathway) and mixed-lineage kinases (MLK1-4) (activate p38 and JNK pathways). MEK1 (45-kDa) and MEK2 (46-kDa) are 85% identical at the protein level and were first identified as ERK1 and ERK2 activators (Gomez & Cohen, 1991). Once active, MEK1/2 bind ERK1/2 through their N-terminal docking domain (DD) and phosphorylate conserved tyrosine and threonine residues within the Thr-Glu-Tyr (T-E-Y) motif of their activation loop (Thr202/Tyr204 in ERK1) **(Figure 5)**. Evolutionary conserved ERK1 and ERK2 are important executioner kinases of the MAPK pathway, and unlike RAF and MEK isoforms, these highly homologous (84% identical) kinases, as of now, do not display obvious functional, tissue-specific or subcellular localisation differences. More than 200 phosphorylation substrates and interacting partners of ERK1/2 have been described to date. Active ERK is released from MEK and can either phosphorylate cytosolic kinases and cytoskeletal proteins or translocate to the nucleus and phosphorylate transcription factors and nuclear kinases. In general, ERK1/2 kinases phosphorylate serine/threonine residues followed by a proline residue (S/T-**P**). Further, efficient binding and phosphorylation by ERK is dictated by two well-defined substrate docking domains: the D-domain and the DEF domain (docking site for ERK and FXFP). D-domains are characterised by the presence of positively charged amino acids, hydrophobic residues and/or a conserved L-X-L motif (Leu-X-Leu). DEF domains consist of the Phe-X-Phe-Pro motif and unlike D-domains, they typically lie C-terminal to the phosphoacceptor site and are only recognised by ERK1/2 (Sharrocks, Yang & Galanis, 2000).

The efficiency and maintenance of the pathway is, at least in part, dependent on scaffold proteins, which stabilise and coordinate interactions between kinases and substrates in each step and insulate the pathway against signal inputs from parallel pathways. For instance, the kinase suppressor of RAS 1 (KSR1) assembles around RAF, MEK1/2 and ERK1/2 to increase signal transmission and regulate the subcellular localisation of

the pathway (Ebisuya, Kondoh & Nishida, 2005). In non-malignant tissues, the fine-tuning of the pathway is further controlled by several homeostatic negative feedback signals **(Figure 5)**. ERK1 and ERK2 phosphorylate: RTKs, such as EGFR, to inhibit downstream signalling; SOS at multiple sites, causing its dissociation from GRB2 and thereby inhibition of RAS activation; BRAF and CRAF (preventing their binding to RAS-GTP) to inhibit MEK phosphorylation and activation; and MEK1 to inhibit ERK1/2 phosphorylation and activation **(Figure 5)**. In turn, dual-specificity phosphatases (DUSPs) dephosphorylate the pT-E-pY motif and directly inactivate ERK1/2, while Sprouty (SPRY) inhibits ERK1/2 indirectly by blocking protein interactions of GRB2 with SOS and RAF with RAS **(Figure 5)** (Ramos, 2008). Despite their critical role in fine-tuning the pathway, such feedback loops allow for adaptations to therapeutic interventions and have been implicated in the resistance of MEK inhibitors (Little, Smith & Cook, 2013).

1.17 Targeting the RAF/MEK/ERK pathway

The RAF/MEK/ERK and PI3K/AKT/mTOR cascades display extensive crosstalk and have been widely associated with RAS-driven oncogenesis (Fruman et al., 2017; Ryan et al., 2015), therefore prompting extensive therapeutic development efforts. Expression of a mutant BRAF (V600E), but not a mutant PIK3CA (H1047R), in the mouse pancreas was able to phenocopy a KRAS G12D mutation, suggesting intact RAF signalling downstream of RAS is a requisite for KRAS-driven oncogenesis in PDACs (Collisson et al., 2012). In lung cancer mouse models, CRAF, but not BRAF, is essential for KRAS-driven non-small cell lung carcinoma (Blasco et al., 2011).

While ARAF and CRAF kinases are rarely mutated in human cancer, BRAF mutations are frequent. In fact, BRAF is an important oncogene that is mutationally activated in seven percent of human cancers and around 30% to 60% of melanomas, the majority of which harbour the BRAF V600E constitutively active mutant. This mutant, unlike the WT RAF, can potently activate downstream pathways in the absence of RAF dimerisation. The second-generation small molecule inhibitors vemurafenib and dabrafenib are ATP-competitive inhibitors of BRAF V600E and have shown greater PFS and OS compared to chemotherapy alone in patients with

metastatic melanoma (Jang & Atkins, 2013). Vemurafenib and dabrafenib are both approved for the treatment of BRAF V600E melanoma. While ARAF and CRAF activation mechanism is very similar, BRAF does not share some of the conserved phosphorylation sites and displays crucial differences in its structure and regulation. The most prominent difference lies within the negatively-charged regulatory region (N-region) of RAF kinases, where ARAF and CRAF share a conserved tyrosine residue, Tyr302 and Tyr341, respectively. However, in B-RAF's N-region this is replaced by an aspartic acid (Asp448), resulting in a constant negative charge, which is an important feature for kinase activation. Further, within the same region, BRAF displays a constitutively phosphorylated site (Ser445). Therefore, BRAF exhibits elevated basal activity levels and unlike ARAF and CRAF, does not require further inputs from SRC kinases for its activation (Wellbrock, Karasarides & Marais, 2004). These differences might account for the frequent BRAF mutations as opposed to the infrequent ARAF and CRAF mutations. In other words, single amino-acid changes are sufficient to hyperactivate BRAF and confer a competitive advantage to cancer cells. Nevertheless, resistance to RAF inhibitors does develop and several mechanisms of resistance have been proposed, all of which reactivate ERK signalling in the presence of drug. RAF dimerisation-dependent mechanisms include NRAS activating mutations (NRAS Q61), CRAF overexpression or expression of alternatively BRAF spliced variants (p61), which retain their kinase activity in a RAS-independent manner. On the other hand, resistance to RAF inhibitors may be acquired in a RAF dimerisation-independent manner either through MEK activating mutations or activation of MEK through parallel pathways (e.g. COT/MAP3K8, MAPK kinase kinase). Paradoxically, BRAF inhibitors promote ERK signalling activation in RAS mutant cells and cancers, rendering them ineffective in RAS-driven cancers (Lito, Rosen & Solit, 2013).

MEK inhibitors (MEKis) remain an attractive therapeutic intervention for ERK signalling targeting and have usually been favoured over BRAF inhibitors in the clinical setting. This is because most compounds are not ATP-competitive inhibitors, rather they bind to a hydrophobic pocket adjacent to the ATP-binding site and allosterically inhibit MEK1/2 activity. Second, considering that MEK1/2 are the only known BRAF substrates, MEKis can be effective in a variety of BRAF V600 mutant cancers. Lastly, MEKis do not display the paradoxical

activation of ERK signalling in RAS-driven tumours (Little, Smith & Cook, 2013). Several MEK1/2 inhibitors are under (phase I-III) clinical trials (e.g. Selumetinib: NCT01933932), while Trametinib, a small molecule allosteric inhibitor of MEK1/2, is currently approved for the treatment of unresectable or metastatic melanoma with BRAF V600 mutations. Similar to BRAF inhibitors (BRAFis), resistance has also been reported to allosteric MEKis. Since MEKis block ERK1/2 signalling, they relieve ERK-dependent negative feedback loops acting upstream of the pathway **(Figure 5)**, thereby resulting in RAF activation and MEK phosphorylation. Newer generation MEKis, like trametinib, mitigate this by interfering with MEK phosphorylation by RAF, resulting in reduction of rebound pathway activation (Caunt et al., 2015). Additional mechanisms of acquired resistance to MEKis include amplification of upstream mutant proteins such as KRAS G13D and BRAF V600E and the emergence of MEK mutations that augment MEK intrinsic activation and hamper drug binding (Little, Smith & Cook, 2013). The inevitable appearance of resistance to BRAF or MEK inhibitors, has prompted researchers to clinically assess the efficacy of combined BRAF (dabrafenib) and MEK (trametinib) inhibition in metastatic melanoma patients with BRAF V600 mutations (Flaherty et al., 2012). As a result, combined BRAF-MEK inhibition is the standard-of-care for this setting, with three FDA-approved combination therapies: dabrafenib + trametinib, vemurafenib + cobimetinib (MEKi) and encorafenib (BRAFi) + binimetinib (MEKi). While resistance to MEKis via BRAF V600E amplification can be overcome through combination therapies, resistance through KRAS mutation or amplification is more challenging due to RAS involvement in multiple parallel pathways, such as PI3K. Further, despite their demonstrated potential in BRAF V600 cancers, MEKis have failed to improve PFS and RRs when compared with the standard-of-care treatment in KRAS-mutant NSCLC patients (Blumenschein et al., 2015).

Due to the high incidence of resistance to BRAF and MEK inhibitors and the appearance of resistance mechanisms that involve the reactivation of ERK1/2 in the presence of upstream inhibitors, direct blockade of ERK function/activity is emerging as a novel approach to overcome the current limitations of these compounds. Further, while reactivation of ERK alone is sufficient to overcome MEK inhibition, it is unlikely that reactivation of a single ERK substrate will be able to compensate for ERK loss. Multiple ERK inhibitors are in

clinical trials, including the first-in-class ATP-competitive inhibitor ulixertinib, currently undergoing a Phase II trial for the treatment of advanced solid tumours with MAPK mutations (NCT03698994). MK-8353, an allosteric and ATP-competitive ERK inhibitor is tested in combination with a MEKi (selumetinib) in a Phase I trial for the treatment of advanced/metastatic solid tumours (NCT03745989). Similar to BRAF and MEK inhibitors, acquired resistance to ERK1/2 inhibitors appears in preclinical models (Jha et al., 2016). Resistance is a prominent phenomenon in targeted therapy and this reflects the complexity of these pathways which are characterised by the presence of multiple parallel networks that are interconnected with regulatory (positive and negative) feedback loops. Further, the ability of cancer cells to adapt to such therapeutic interventions by pathway rewiring and dependency on novel proteins or pathways, demonstrates the need for combining MAPK inhibitors with parallel pathway inhibitors such as PI3K, AKT and mTOR, or targeting downstream pathway components that are crucial for the survival of cancer cells.

1.18 Ribosomal protein S6 (rpS6) – a ribosomal S6 kinase (RSK) family substrate

Ribosomal protein S6 (rpS6) is a 28 kDa protein and one of the 33 proteins that make up the mammalian 40S (small) ribosomal subunit. The critical role rpS6 plays as a ribosomal protein was manifested by multiple studies. For instance, rpS6 deficient mouse hepatocytes were unable to synthesise the 40S ribosomal subunit and failed to proliferate (Volarevic et al., 2000), while $rps6^{wt/del}$ mouse embryos died at E8.5 (Panic et al., 2006). Since its discovery in 1974 (Gressner & Wool, 1974), there was substantial scientific interest in elucidating the mechanisms of rpS6 phosphorylation, owing to its involvement in central cellular processes, such as protein synthesis (Meyuhas, 2008). Erikson and Maller in 1985 (Erikson & Maller, 1985) purified, from unfertilised *Xenopus laevis* eggs, an intracellular kinase activity able to specifically phosphorylate rpS6 on serine residues. This kinase was later referred to as ribosomal S6 kinase (S6K). Subsequently, biochemical purification of *X. laevis* egg extracts gave rise to two ribosomal S6 kinases (S6KI and S6KII) of 85-90 kDa, and led to the cloning of cDNAs encoding highly homologous proteins later renamed p90 (90 kDa) RSKs or RSKs (Jones et al., 1988). Soon after it became evident that RSKs are phosphorylated and activated by insulin-stimulated microtubule-

associated protein-2 (MAP2) kinase (later renamed to ERK2), for the first time linking the activation of a RSK to the RAF/MEK/ERK pathway (Sturgill et al., 1988).

Ribosomal S6 kinase (RSK) family is comprised of two subfamilies, the p90 (90 kDa) RSKs (RSK1-4) and the p70 (70 kDa) RSKs, also known as S6 kinases (S6Ks: S6K1 and S6K2). The 90 kDa RSK family and their structural homologs, the mitogen- and stress-activated protein kinases 1 and 2 (MSK1 and MSK2) (Romeo, Zhang & Roux, 2012), are downstream effectors of the RAS/RAF/MEK/ERK pathway and are directly phosphorylated and activated by ERK1/2 **(Figure 6)**. Despite their structural similarities, MSKs have diverse biological functions and while RSKs are activated by ERK1/2, MSKs are activated by both the ERK1/2 and p38 MAPK pathways **(Figure 6)** (Vermeulen et al., 2009). Insulin-like growth factor 1 (IGF1) receptor, the best studied activator of S6Ks, converges on the PI3K/AKT/mTOR pathway to activate the serine/threonine protein kinase mTORC1 (mammalian target of rapamycin complex 1), which directly phosphorylates and activates S6Ks (Magnuson, Ekim & Fingar, 2012).

S6K1 and S6K2 are the predominant rps6 kinases, phosphorylating this substrate on five conserved serine residues (Ser235, Ser236, Ser240, Ser244 and Ser247). RSK1-4 are also able to phosphorylate rpS6 on Ser235 and Ser236 (Ser235/236), albeit at a lesser extent. This was evident when phosphorylation of rpS6 Ser235/236 could still be detected in S6K1 and S6K2 deficient cells or in cells treated with an mTOR inhibitor (rapamycin), while MEK1/2 inhibitors (U0126, PD184352) abolished this signal, suggesting rpS6 is receiving inputs from the ERK1/2 pathway (Meyuhas, 2008). The phosphorylation consensus sequences of RSKs and S6Ks are very similar, **Arg/Lys**-X-**Arg**-X-X-pSer/Thr and **Arg**-X-**Arg**-X-X-pSer/Thr, respectively, which might account for their common substrates. RSKs have a stronger preference for the -3 arginine residue over the -5 arginine (arginine also preferred over lysine residues), while they have the propensity to phosphorylate serine rather than threonine residues (Romeo, Zhang & Roux, 2012). Protein kinase A (PKA) and casein kinase 1 (CK1) have also been shown to phosphorylate rpS6 on Ser235/236 residues, while rpS6 is primarily dephosphorylated by the serine/threonine protein phosphatase type 1 (PP1) phosphatase (Meyuhas, 2008).

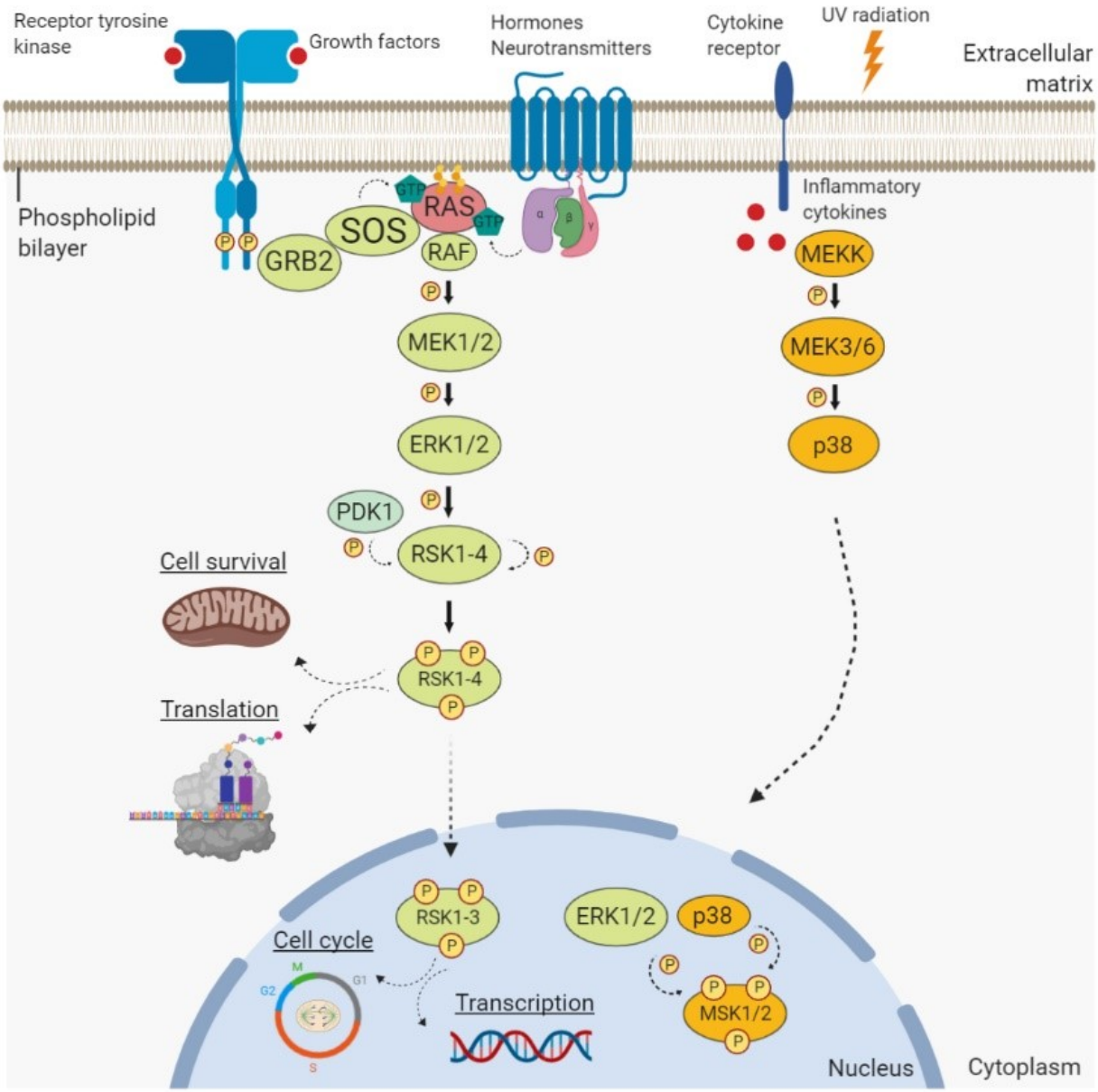

Figure 6| p90 (90 kDa) ribosomal S6 kinases (RSKs) & mitogen- and stress-activated kinases (MSKs). RSKs (RSK1-4) and their structural homologs MSK1 and MSK2 are downstream effectors of the RAS/RAF/MEK/ERK pathway **(Figure 2 & Figure 5)** and are directly phosphorylated and activated by ERK1/2 (See **Figure 8** for RSK activation). ERK1/2 is a key RAS downstream effector activated in response to growth factor, hormone or neurotransmitter binding to an upstream receptor. Activation of MSKs also occurs via the p38 pathway, which is initiated by MEK kinases (MEKKs) in response to physical and chemical stresses. MEKKs phosphorylate MEK3/6, which in turn phosphorylate p38 in the conserved Thr-Gly-Tyr (TGY) motif within the activation loop. Unlike RSKs (RSK1-3), PDK1 is not required for MSK activation. Activated MSKs phosphorylate nuclear substrates, while activated RSKs can either phosphorylate cytoplasmic (RSK1-4) or nuclear substrates (RSK1-3). RSK1 and RSK2 were shown to phosphorylate several substrates involved in cell cycle, transcription, translation, cell survival and cell migration/invasion (not shown) (Lara, Seckl & Pardo, 2013; Anjum & Blenis, 2008). Figure created with biorender.com.

1.19 p90 (90 kDa) RSK family – structure and activation mechanism

RSKs are highly conserved serine/threonine protein kinases implicated in diverse cellular processes, including cell survival, proliferation, migration and invasion. Four isoforms exist in humans (RSK1 to 4), of which RSK1

and RSK2 are the most studied isoforms in cancer. RSKs are 73%-80% identical (protein level), and are uniquely characterised by the presence of two non-identical kinase catalytic domains at their N- and C-terminals **(Figure 7)** (Lara, Seckl & Pardo, 2013). It is believed that, during evolution, genes coding for two distinct protein kinases were fused generating a single protein kinase with two distinct kinase catalytic domains. Thus, while the N-terminal kinase domain (NTKD, or D1) of RSKs belongs to the AGC (protein kinase A, G, and C) family (includes PKA, PKC and AKT (PKB)), the C-terminal kinase domain (CTKD) belongs to the CAMK (Ca^{2+}/calmodulin-dependent protein kinase) family (includes AMPK, MARK and DAPK) (Romeo, Zhang & Roux, 2012). While S6Ks share about 40% amino acid identity with the NTKD of RSKs and MSKs, they lack the CTKD. RSK kinase domains are connected via a linker region, which contains crucial phosphorylation sites for RSK activation, known as the *turn motif* and the *hydrophobic motif* **(Figure 7)**. Downstream of the CTKD, all RSKs contain an ERK1/2 D-domain (docking motif), characterised by the consensus **Leu**-Ala-Gln-**Arg**-**Arg** (resembles a kinase interaction motif (KIM) consensus sequence (MacKenzie et al., 2000)), where only the Leu and Arg residues are necessary for docking and activation by ERK1/2 **(Figure 7)** (Roux, Richards & Blenis, 2003).

All RSKs isoforms share six evolutionary conserved phosphorylation sites (Ser221, Thr359, Ser363, Ser380, Thr573 and Ser732 in human RSK1; Ser232, Thr368, Ser372, Ser389, Thr581 and Ser742 in human RSK4) that are responsive to mitogenic stimulation, while four of those (see underlined) are indispensable for RSK activation **(Figure 7)** (Roux & Blenis, 2004). In response to growth factors, peptide hormones, neurotransmitters and other stimuli, the RAS/MAPK cascade leads to ERK1/2 activation, which dock on the D-domain of RSKs and directly phosphorylate Thr573 (RSK1 amino acid numbering), a proline-directed (pro-directed) phosphorylation site within the CTKD activation loop **(Figure 8)**. Stimulated CTKD phosphorylates Ser380 within the hydrophobic motif of the linker region to create a docking site for 3'-phosphoinositide-dependent kinase 1 (PDK1). PDK1, a constitutively active AGC kinase master regulator (Mora et al., 2004), phosphorylates Ser221 in the activation loop of the NTKD, fully activating the kinase **(Figure 8)** (Anjum & Blenis, 2008).

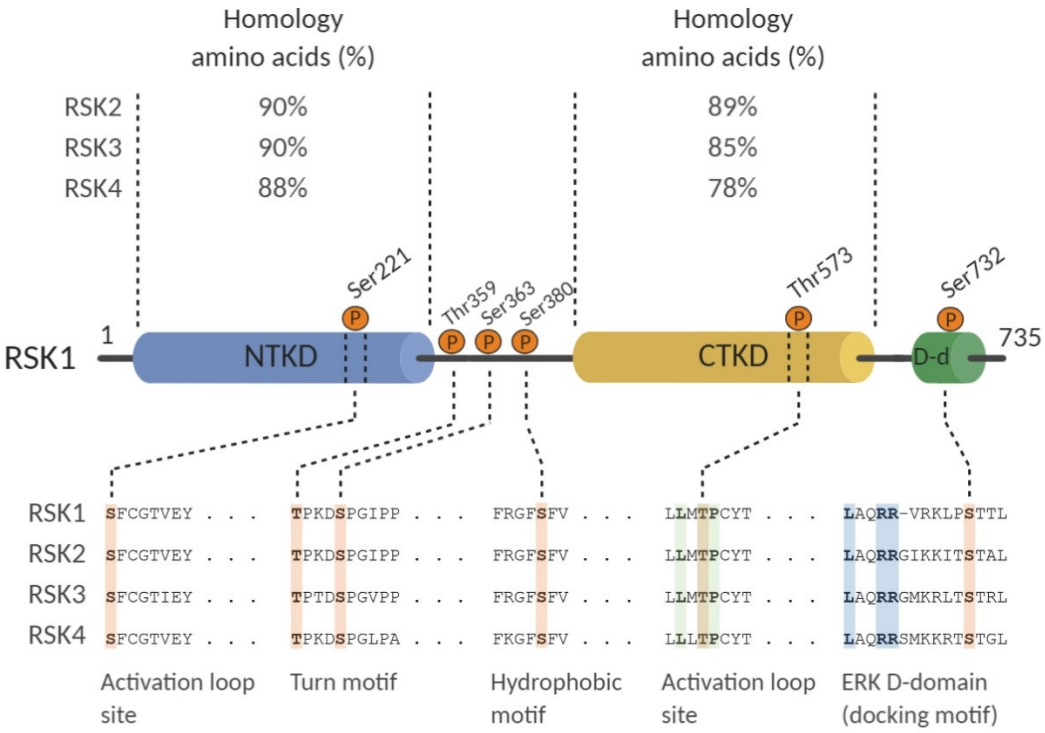

Figure 7| RSK1 domain structure. p90 (90 kDa) ribosomal S6 kinases (RSKs) are characterised by the presence of two functional, non-identical phosphotransferase domains; the N-terminal kinase domain (NTKD) and C-terminal kinase domain (CTKD), which contain the activation loop sites Ser221 (RSK1) and Thr573 (RSK1), respectively. Thr573 lies within the conserved L-X-**T**-P sequence (green shaded). These highly homologous domains (78%-90%) are connected by a linker region, which contains the turn motif (RSK1: Thr359 and Ser363) and hydrophobic motif (RSK1: Ser380) sites. RSKs contain a carboxyl-terminal ERK (extracellular signal-regulated kinase) D-domain (D-d) characterised by the conserved **L**-X-X-**R**-**R** motif (blue shaded). ERK1/2 C-terminal docking is required to initiate kinase activation. Activation of RSKs correlates with increased phosphorylation at the six highly conserved (orange) highlighted sites (Lara, Seckl & Pardo, 2013). Figure created with biorender.com.

While RSK1-3 require PDK1 for their activation, RSK4 maintains high basal activity independently of PDK1. Activated RSKs phosphorylate downstream cytosolic (RSK1-4) and nuclear (RSK1-3) substrates (Dummler et al., 2005). Interestingly, a study by Richards and colleagues (Richards et al., 2001) has postulated a mechanism by which cytosolic RSK1, upon mitogen stimulation and prior to nuclear translocation, transiently associates with the plasma membrane where it receives additional MEK/ERK-independent signals necessary for its full activation. While the phosphotransferase activity of a C-terminal truncated RSK1 mutant, which precludes ERK1/2 binding, is completely abolished; when myristoylated[15], it can reach similar levels of activation to its WT myristoylated counterpart. Indeed human RSK1 Ser363, a potential ERK-targeted phosphorylation site critical to RSK phosphotransferase activity, is not phosphorylated in the C-terminal truncated RSK1 mutant, although when myristoylated, it is activated at a level equivalent to WT myristoylated RSK1 (Richards et al.,

[15] Myristoylation: A lipid post-translational modification catalysed by *N*-myristoyltransferase (NMT) and involves the addition of a myristic acid typically to an N-terminal glycine. Myristoylated proteins are targeted to the plasma membrane (ScienceDirect).

2001). Therefore, it is possible that ERK1/2 do not directly activate this site, but are instead required to recruit RSK1 to the plasma membrane where it receives additional inputs. Dissociation of ERK1/2 from RSKs is mediated through RSK (NTKD) autophosphorylation on Ser732 adjacent to the docking motif **(Figure 8)** (Roux, Richards & Blenis, 2003). Lastly, although the sole known function of the CTKD is the activation of the NTKD via autophosphorylation, the possibility that the CTKD could also phosphorylate downstream substrates should not be excluded.

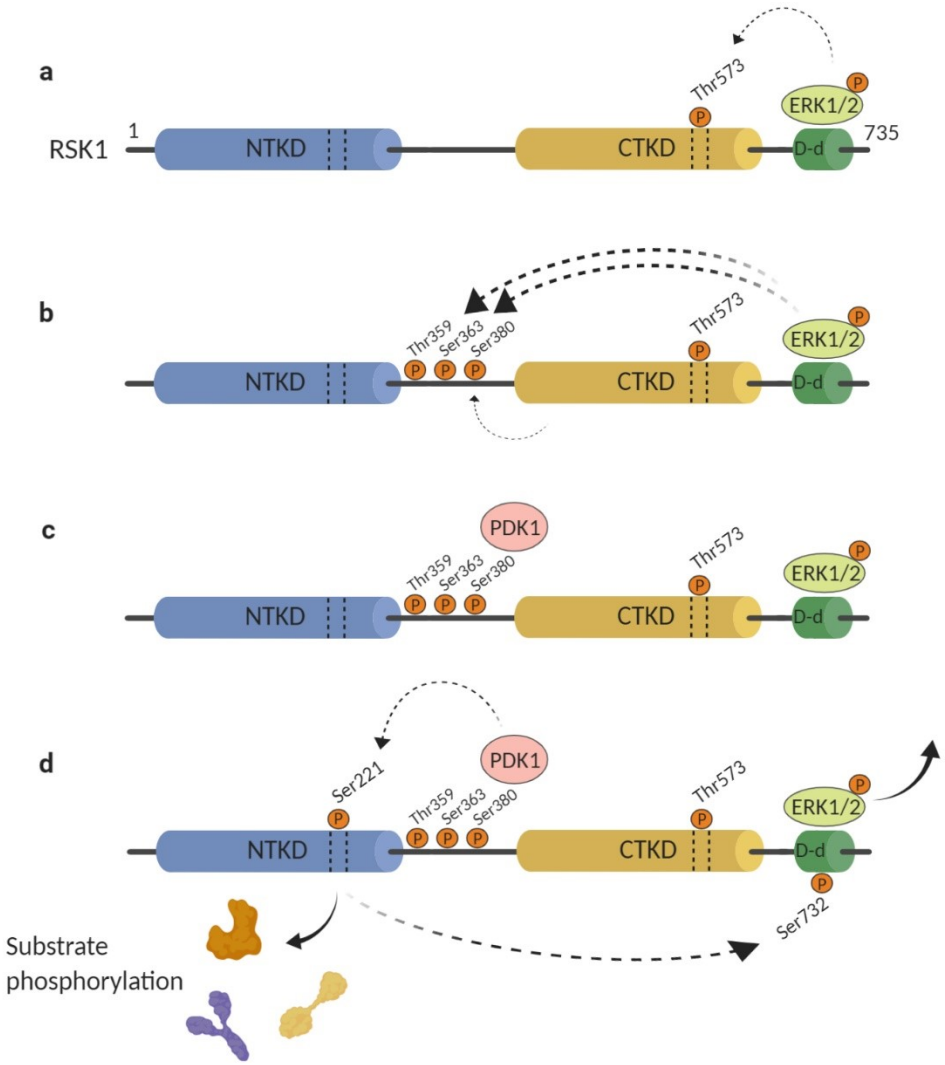

Figure 8| RSK1 model of activation. **(a)** Following mitogenic stimulation, phosphorylated extracellular signal-regulated kinases 1 and 2 (ERK1/2) dock at the D-domain (D-d) and phosphorylate Thr573 (RSK4: Thr581) at the C-terminal kinase domain (CTKD) activation loop. **(b)** Activated CTKD phosphorylates Ser380 (RSK4: Ser389) at the hydrophobic motif (linker region). The possibility that other kinases might also phosphorylate this site should not be excluded. ERK1/2 might also be involved in the phosphorylation of Thr359 (RSK4: Thr368) and Ser363 (RSK4: Ser372). **(c)** CTKD phosphorylation creates a docking site for constitutively active Ser/Thr kinase 3'-phosphoinositide-dependent kinase-1 (PDK1), which **(d)** phosphorylates Ser221 (RSK4: Ser232) at the N-terminal kinase domain (NTKD) activation loop to fully activate the kinase. PDK1 is not required for RSK4 activation. Activated RSKs phosphorylate downstream substrates in the cytoplasm (RSK1-4) or nucleus (RSK1-3). NTKD phosphorylates Ser732 (RSK4: Ser742) at the D-domain, which may result in ERK1/2 dissociation and attenuation of RSK activation (Anjum & Blenis, 2008). Figure created with biorender.com.

1.20 RSK biological functions – protein synthesis, transcriptional regulation, cell survival, migration and invasion

In addition to rpS6 phosphorylation, RSKs were shown to promote protein synthesis via several different mechanisms. RSK1, phosphorylates tuberus sclerosis complex 2 (TSC2) (Ser1798), which encodes tuberin, and along with tuberus sclerosis complex 1 (TSC1; encodes hamartin), inhibit mTOR signalling. RSK1 phosphorylation, relieves the inhibitory function of the tuberin/hamartin complex, thereby promoting S6K1 signalling through mTOR (Roux et al., 2004). Another mechanism by which the RAS/MAPK pathway converges on the PI3K/AKT/mTOR cascade, involves RSK1 and RSK2 phosphorylation of Raptor (Ser719, Ser721, Ser722), an mTORC1 associated protein. This phosphorylation promotes mTORC1 kinase activity and thereby protein synthesis (Carriere et al., 2008). Components of both the RAS/MAPK and PI3K/AKT/mTOR pathways were also shown to regulate protein synthesis by mutually phosphorylating glycogen synthase kinase-3β (GSK3β). RSK2 and S6K phosphorylate GSK3β on Ser9 to inhibit its activity and thereby relieve the inhibition of eukaryotic initiation factor (eIF) 2B (Sutherland, Leighton & Cohen, 1993).

RSKs play a prominent role in transcriptional regulation, especially phosphorylating immediate-early gene (IEG) response transcription factors (TFs). For instance, RSK1 was shown to directly phosphorylate serum response factor (SRF) (Ser103) (Rivera et al., 1993), c-Fos (Ser362) (Chen, Abate & Blenis, 1993) and estrogen receptor α (ERα) (Ser167) (Joel et al., 1998), while RSK2 indirectly regulates c-Fos transcription by phosphorylating and activating both the cAMP responsive element-binding protein (CREB) (Ser133) (De Cesare et al., 1998) and ELK-1 (Bruning et al., 2000). RSK1 is also involved in the regulation of the NF-κB pathway by phosphorylating and promoting the proteasomal degradation of NF-κB inhibitors, IκBα (Ser32) and IκBβ (Ser19 and Ser23) (Xu et al., 2006; Schouten et al., 1997).

Considering that RSKs regulate several master regulator transcription factors, it is not surprising that they are involved in the regulation of crucial cellular processes such as cell survival, cell cycle and proliferation, as well as migration and invasion. RSK1 promotes the NF-κB pathway, thereby increasing NF-κB-dependent cell survival (Xu et al., 2006; Schouten et al., 1997), while both RSK1 and RSK2 promote cell survival through CREB-

dependent transcription (Bonni et al., 1999; Xing, Ginty & Greenberg, 1996). Interestingly, RSK1 phosphorylates the pro-apoptotic BCL-2 family member BAD (Ser112 and Ser155), which promotes BAD binding to 14-3-3 proteins rather than BAD/BCL-XL heterodimerisation, therefore decreasing BAD's pro-apoptotic activity and promoting cell survival (Tan et al., 2000). Several lines of evidence highlight the involvement of RSK in cell cycle progression and proliferation. RSKs were previously shown to phosphorylate or promote the transcription of c-Fos (De Cesare et al., 1998; Chen, Abate & Blenis, 1993), which activates cyclin D1, resulting in G1-S phase progression. Further, RSK1 and RSK2 promote G1 phase progression by phosphorylating $p27^{Kip1}$ (cyclin E/CDK2 inhibitor) on Thr198, which promotes its binding to 14-3-3 proteins and cytoplasmic sequestration (Fujita, Sato & Tsuruo, 2003). RSK role in cell migration and invasion has been conflicting. While Doehn and colleagues implicate RSK1 and RSK2 as the principal ERK effectors of a pro-motile and invasive gene program in epithelial cells (Doehn et al., 2009), an siRNA screen in lung adenocarcinoma cells indicates that RSK1 depletion enhances migration and invasion *in vitro* and *in vivo* in a zebrafish model (Lara et al., 2011). RSK1 and RSK2 pro-migratory role was shown to be mediated by phosphorylation of Filamin A on Ser2152 in melanoma cells (Woo et al., 2004), while RSK1 anti-migratory effects could be, at least in part, attributed to VASP Thr278 phosphorylation, which correlates with inhibition of lamellipodia formation and cell migration (Lara et al., 2011).

1.21 RSK4 – functional characterisation

Ribosomal protein S6 kinase 4 (RSK4; *RPS6KA6*) was initially discovered by Yntema and colleagues in 1999, who mapped its gene to the mental retardation (MRX) critical region on chromosome Xq21 (Yntema et al., 1999). Noteworthy, large deletions in this chromosomal region are often associated with X-linked deafness type 3 (DFN3), choroideremia (CHM) and mental retardation (MRX) (May et al., 1995; Bach et al., 1992; Cremers et al., 1989). Similarly, the gene encoding RSK2, RPS6KA3, is also located on the X chromosome (Xp22.13), and mutations in this gene are associated with the Coffin-Lowry syndrome, which is characterised by severe psychomotor retardation (Trivier et al., 1996). Whether RSK4 is implicated in X-linked mental retardation remains to be elucidated. RSK4 is ubiquitously expressed during murine embryogenesis (Kohn et

al., 2003) and is predominantly expressed in the brain, cerebellum, heart, kidney and skeletal muscle in adult mouse tissues, while expression in the lungs is undetectable (Dummler et al., 2005). Contrary to RSK4, RSK1-3 are expressed in most mouse tissues, including lung tissues (Zeniou et al., 2002). Myers and colleagues (Myers et al., 2004), studying the mouse orthologue of human RSK4, indicated that RSK4 overexpression disrupts, rather than mediates RTK signals. RSK4 deletion mutants indicated this is dependent on the first 96 amino acids of the N-terminal region of this protein (Δ1-96RSK4); while this construct was still able to phosphorylate rpS6, indicating no disruption of its kinase activity. Interestingly, this region is not conserved in other RSK isoforms.

Sun and colleagues (Sun et al., 2013) demonstrated expression of RSK4 in multiple human tissues with the highest levels being in liver, kidney, pancreas, testis, prostate and placenta, and almost undetectable expression in lung tissues. Contrary to RSK1-3, RSK4 is predominantly cytoplasmic, in serum-starved or growth factor-stimulated conditions, suggesting RSK4 might exclusively phosphorylate cytosolic substrates. Furthermore, it manifests growth factor-independent constitutive activity due to constitutive phosphorylation of Ser232 (within NTKD), Ser372 and Ser389 (within linker region), which showed similar phosphorylation levels in serum-starved and growth factor-stimulated cells, indicating that low basal ERK activity is sufficient for inducing significant RSK4 activity (Dummler et al., 2005). In the same study, Dummler and colleagues (Dummler et al., 2005) showed that a point mutation of the PDK1 docking site (Ser389) did not significantly affect phosphorylation of Ser232, which is required for RSK4 activation. The lack of PDK1 requirement for RSK4 activation was further verified genetically in embryonic stem (ES) cells lacking the PDK1 gene. Considering the lack of PDK1 requirement for Ser232 phosphorylation and RSK4 activation and that ERK contributes towards only 30%-50% of endogenous RSK4 activity, it is possible that RSK4 might depend on autophosphorylation from the CTKD for its full activation. Indeed, a CTKD catalytically inactive RSK4 mutant had reduced Ser232 phosphorylation levels in PDK1-deficient ES cells (Dummler et al., 2005). Collectively, it is evident that RSK4 emerges as a distinct RSK family member, and subtle differences in its structure, localisation or activation might confer this isoform different cellular roles.

1.22 RSK4, an X-linked gene

The role of X-linked genes has been well demonstrated in cancer. Like autosomal genes, genomic rearrangements, mutations and gain or losses of chromosomes lead to loss of function of tumour suppressors or gain of function of oncogenes. However, unlike autosomal genes, X-linked genes represent a unique characteristic within the chromosomal repertoire. In mammals, while male cells have one X chromosome, females have two; thus, early during female embryonic stem cell differentiation, random X chromosome inactivation takes place. Therefore, genetic events that cause cancer will produce differential effects when they occur in autosomes compared to X-chromosomes. For example, gain of function mutations which result in oncogene activation will be dominant in autosomal genes; however, they might be silent in an X-linked gene if it occurs on the inactivated allele. Most importantly though, loss of function mutations in tumour suppressors will be recessive in autosomes, but can be dominant in X-linked genes if the other allele has already been inactivated. This gives rise to the loss of heterozygosity concept and manifests the importance of X-linked genes and particularly those that are tumour suppressors in cancer (Spatz, Borg & Feunteun, 2004).

1.23 RSK4 in breast cancer

RSK4, as an X-linked gene has also sparked great scientific interest since its discovery (Yntema et al., 1999). A study by Thakur and colleagues (Thakur et al., 2005) has used cDNA microarray analysis to compare X-linked gene expression profiles of MMTV-*c-myc* transgenic mammary tumour (MT) or MMTV-*c-myc*/MT-*tgf-α* double transgenic mouse mammary tumour (DT) to the lactating mammary gland. More than a hundred genes were modulated by ±2 fold change in MT and DT samples, including genes involved in chromatin remodelling (e.g. *Hdac8*) and translational control (e.g. *Dkc1* and *Rps6ka6*; RSK4). Genes involved in ribosomal biogenesis, like *Rps6ka6* and *Dkc1*, were upregulated, manifesting the importance of elevated protein synthesis in cancer progression (White-Gilbertson, Kurtz & Voelkel-Johnson, 2009). The same group in a later study (Thakur et al., 2007) showed upregulation in the mRNA levels of X-linked genes (e.g. RbAp46 and RSK4) in breast cancer cell lines compared to benign breast cancer cells; an observation further validated with immunostaining in breast cancer biopsies. Interestingly, by assessing the activation status of X-chromosome in a panel of human breast

carcinoma samples, human breast cancer cell lines, and normal mammary tissues, the authors showed expression of two highly polymorphic markers (i.e. *IDS*, *G6PD*) from two alleles, indicating the presence of two active X-chromosomes. Hence, the activation status of X-chromosomes may influence expression levels of X-linked genes such as RSK4. However, another study by Liu and colleagues (Liu et al., 2011) indicated reduced RSK4 mRNA levels in breast cancer compared to normal and benign tissues. This might be due to variability between different breast cancer cell lines or differences between murine and human cancer tissues.

Phenotypic effects of RSK4 modulation in breast cancer were later assessed by Thakur and colleagues (Thakur et al., 2008). Although RSK4 was previously shown to be upregulated in transgenic mammary tumours (Thakur et al., 2005), breast cancer cell lines and breast cancer biopsies (Thakur et al., 2007), RSK4 overexpression was associated with decreased MDA-MB-231 cell proliferation and accumulation in G0-G1 phase. This effect was paralleled with increased expression of p21, pRb, and RbAp46 tumour suppressor proteins. RSK4 overexpression reduced colony formation in soft agar and reduced tumour growth *in vivo*. Further, it suppressed *in vitro* and *in vivo* migration and invasion of breast cancer cells, an effect, at least in part, mediated by upregulation of claudin-2 and downregulation of CXCR4. RSK4 was also implicated as a transcriptional target of c-MYC (Thakur et al., 2008). T47D breast cancer cells transfected with MycER (Myc-estrogen receptor fusion protein) and treated with 4-hydroxytamoxifen showed increased RSK4 mRNA and protein levels compared to untreated or empty vector control cells. Subsequent *in vivo* studies, where severe combined immunodeficient (SCID) mice injected with RSK4-overexpressing MDA-MB-231 cells, showed reduction in tumour growth (Jiang et al., 2017; Yang et al., 2012b). The reverse approach by Zhu and colleagues (Zhu et al., 2015), where stable shRNA-mediated RSK4 silencing in MCF7 cells promoted proliferation, migration and invasion *in vitro* and *in vivo*, validated these findings. The aforementioned studies provide evidence for RSK4 tumour suppressive properties and thus its requirement for the physiological maintenance of normal breast cells. Conversely, Serra and colleagues (Serra et al., 2013) suggested the requirement for a combined use of PI3K and RSK3/4 inhibitors in breast cancer patients with activated RSKs due to RSK3/4-mediated resistance to PI3K inhibitors through

inhibition of apoptosis and upregulation of protein translation. Hence, there are conflicting reports about the biological function of RSK4 in breast cancer tumourigenesis.

1.24 RSK4 and epigenetic modifications – oesophagus adenocarcinoma, breast, endometrial and ovarian cancers

Several studies have sought to uncover the relationship between epigenetic modifications and RSK4 expression status. In breast cancer, RSK4 mRNA expression was significantly decreased compared to normal tissues, an effect associated with increased promoter hypermethylation in cancer samples (Li et al., 2014). Li and colleagues suggested estradiol treatment in ER+ breast cancer cells decreases RSK4 protein and mRNA levels by stimulating DNMT3B-induced RSK4 methylation, an effect accompanied with upregulation of cell proliferation and invasion (Li et al., 2019). In endometrial cancer cell lines and tissues, Dewdney and colleagues (Dewdney et al., 2011), using combined bisulfite restriction analysis and bisulfite sequencing, showed frequent *RPS6KA6* (RSK4) hypermethylation, and reduced RSK4 mRNA expression. The correlation of epigenetic modifications and RSK4 silencing was further validated in 5-azacytidine-treated endometrial cancer cell lines (SKUT1B, RL952, and ANC3A), where RSK4 transcript levels increased 8 to > 1,200 fold. A similar study by Niskakoski and colleagues (Niskakoski et al., 2014) also indicated frequent epigenetic inactivation (by DNA methylation) of several genes, including *RPS6KA6*, in non-serous ovarian carcinomas compared to serous tumours. The discrepancies between ovarian subtypes might be explained by different tissues used for reference and different methylation analysis methods. Mostly though, RSK4 mRNA levels were significantly decreased in malignant ovarian tumours as compared to benign or normal ovarian tissues. Further corroborating these results, RSK4 mRNA and protein levels were decreased in malignant ovarian tumours compared to normal or benign tissue counterparts (Arechavaleta-Velasco et al., 2016). *RPS6KA6* was also hypermethylated in oesophagus adenocarcinoma, as compared to corresponding normal tissues (Xi & Zhang, 2017). Collectively, these studies postulate that RSK4 inactivation by DNA methylation is a frequent event in cancer, which might be associated with tumour development and progression.

1.25 RSK4 in senescence – colorectal and renal cancer

A large RNAi screen by Berns and colleagues (Berns et al., 2004) identified new modulators of p53-dependent proliferation arrest. Utilising a modified primary human BJ fibroblast cell system, the authors showed that shRNA against RSK4, bypassed p53- and $p19^{ARF}$-dependent proliferation arrest, as well as p53-dependent G1 cell-cycle arrest, following exposure to ionising radiation (IR). Further, knockdown of RSK4 resulted in downregulation of $p21^{Cip1/WAF1}$, a critical p53 downstream target. This screen raised the possibility that the genes identified, including RSK4, may act as tumour suppressors regulating cell arrest and senescence. This study prompted Vicente and colleagues (Lopez-Vicente et al., 2009) to investigate the role of RSK4 in the senescence of cancer cells. RSK4 was significantly downregulated in colon and renal carcinoma and colon adenoma tissues compared to their normal counterparts. Retroviral infection of RSK4 in colon carcinoma cell lines, with absent endogenous RSK4 expression, upregulated senescence related proteins p21 and Rb, an effect also accompanied with senescent morphological characteristics and an increase in SA-b-gal activity (Tabor, Bocci & Larsson, 2013). In addition, RSK4 mRNA and protein levels were increased in replicative-induced IMR90 (normal fibroblasts) senescent cells, while RSK4 mRNA was also increased in stress-induced HCT-116 senescent cells. Corroborating these data in a follow-up study (Lopez-Vicente et al., 2011), RSK4 shRNA bypassed stress-induced (H_2O_2 and CDDP treatment (Toussaint, Medrano & von Zglinicki, 2000)), and oncogene-induced ($KRAS^{V12}$ or $BRAF^{E600}$ overexpression) senescence in immortalised human diploid fibroblasts (TIG3). The importance of RSK4 in suppressing cancer development was also proposed in colorectal carcinoma. RSK4 mRNA levels were downregulated in colon carcinomas as compared to normal tissues (LLeonart et al., 2006), while low RSK4 expression correlated with poor overall survival in colorectal cancer patients (Cai et al., 2014). *In vitro*, RSK4 overexpression in HCT-116 and SW480 colorectal cancer cell lines, inhibited cell growth in an MTT assay and invasion through a Matrigel-coated transwell chamber (Ye et al., 2018). Taken together, these studies implicate RSK4 in the regulation of senescence and suggest that downregulation of this kinase could be an important event during cell transformation.

1.26 RSK4 in renal, melanoma and lung cancers – contradicting evidence

While the aforementioned studies suggest that RSK4 acts in a tumour suppressive manner, a few reports contradict these findings. Bender and Ullrich 2012 (Bender & Ullrich, 2012) employed cDNA microarray analysis in selected melanoma and renal cancer cell lines in an attempt to correlate sunitinib resistance and transcriptional alterations. PRKX, TTBK2 and RSK4 were exclusively upregulated in the sunitinib-resistant cell lines (similar profiles between melanoma and renal cell lines) and selected for further validation. Downregulation of these protein kinases increased sunitinib sensitisation (i.e. increased sunitinib-mediated apoptosis) and sunitinib inhibition of cancer cell migration. The potential oncogenic activity of RSK4 was further proposed by a study from Fan and colleagues (Fan et al., 2013) in renal cell carcinoma (RCC). Using tissue microarrays (TMAs) this group showed RSK4 overexpression in RCC compared to normal adjacent tissues, an observation which could predict poor prognosis in RCC patients. Further, RSK4 overexpressing ACHN cells invaded significantly more through a matrigel, an effect accompanied with upregulation of CD44 and MMP-9, two key proteins associated with tumour invasion (Yu & Stamenkovic, 2000; Yu & Stamenkovic, 1999). Conversely, RSK4 shRNA-silencing in GRC-1 cells significantly reduced migration and invasion and decreased CD44 and MMP-9 protein expression. In lung cancer, RSK4 siRNA-silencing in A549 lung adenocarcinoma cells significantly impaired migration in a time-lapse motility assay and invasion through a collagen matrix (Lara et al., 2011). Collectively, the above studies propose a tumour promoting role for RSK4, rendering this kinase an attractive therapeutic target for these cancers.

1.27 RSK inhibitors

Since RSK activity is typically closely correlated with ERK1/2 activity, the use of MEK1/2 (e.g. U0126) or ERK1/2 (e.g. SCH772984) specific inhibitors has been useful in studying RSK biological functions and role in cancer **(Figure 9)**. However, considering that RSKs might receive additional positive or negative signals from parallel pathways, the development of direct RSK inhibitors has been crucial in elucidating RSK exclusive functions. Several classes of pan-RSK small-molecule inhibitors exist to date. These include SL-0101 and BI-D1870, two reversible, ATP-competitive inhibitors that target the NTKD, and FMK (fluoromethylketone), an irreversible

inhibitor of the CTKD **(Figure 9)**. The flavonol rhamnoside SL-0101 was isolated from the tropical plant *Fosteronia refracta*, and was the first RSK inhibitor to be identified (Smith et al., 2005). It was shown to inhibit the RSK2 NTKD at *in vitro* half-maximal inhibitory concentration (IC_{50}) of 89 nM (with 10 µM ATP); however, in intact cells the half-maximal effective concentration (EC_{50}) of SL-0101 was 50 µM, indicating poor activity *in vivo* and raising the possibility of potential off-target effects (Smith et al., 2005). Indeed, in a panel of 70-80 protein kinases SL-0101 significantly inhibited the activity of PIM1, PIM3 and Aurora B, albeit at a lower potency compared to RSK1/2 inhibition (Bain et al., 2007). Further, while SL-0101 treatment inhibited the proliferation of breast cancer cells (Smith et al., 2005), it promotes the invasion of lung adenocarcinoma cells (Chrysostomou et al., Unpublished), phenocopying the results of RSK1 downregulation in the same setting (Lara et al., 2011). The dihydropteridinone BI-D1870 is a highly potent pan-RSK inhibitor with *in vitro* IC_{50} of 5 nM for RSK1 and 10 nM for RSK2 with 10 µM ATP (inhibits RSK3/4 with similar potency) **(Figure 9)** (Sapkota et al., 2007). Nevertheless, when tested in a panel of protein kinases, BI-D1870 significantly inhibited the activity of Aurora B, MST2, MELK and GSK3β (Bain et al., 2007). Noteworthy, BI-D1870 was highly potent against PLK1 (polo-like kinase 1), reducing its activity by 83% at 0.1 µM (Sapkota et al., 2007). Unlike SL-0101 and BI-D1870, the pyrrolopyrimidine FMK is an irreversible RSK1, 2 and 4 inhibitor that covalently binds to a cysteine residue within the ATP-binding pocket of the CTKD (Cohen et al., 2005). Although RSK3 has a cysteine residue within the conserved glycine-rich loop of the CTKD, unlike RSK1, 2 and 4, it lacks a threonine gatekeeper (threonine is replaced by methionine in RSK3) which is required to form a covalent bond with the inhibitor. FMK inhibits RSK2 at *in vitro* IC_{50} of 15 nM with 100 µM ATP, and EC_{50} of 200 nM (Cohen et al., 2005). Similarly, in a panel of protein kinases, FMK also inhibited the activity of S6K1, Src, Lck, Yes and Eph-A2 (Bain et al., 2007). Another drawback of this compound is that it inhibits the activation of RSKs and therefore it is ineffective at inhibiting an already active kinase.

Despite their high degree of sequence homology and overlapping functions, several isoform specific substrates have been described for RSKs, which might account for their differing biological functions (Lara, Seckl & Pardo, 2013). While RSK1 and RSK2 are generally thought to promote tumourigenesis, RSK3 and RSK4 are thought to

act in a tumour suppressive manner. Consistent with this notion, RSK1 and RSK2 expression and/or activation is increased in several cancer types, including melanoma, leukemia, breast cancer and prostate cancer, while reduced expression of RSK3 and RSK4 has been observed in colorectal cancer, breast cancer and ovarian cancer (Houles & Roux, 2018). Nevertheless, additional reports have shown that while RSK1 siRNA enhances the migration and invasion of lung adenocarcinoma cells (Lara et al., 2011), RSK4 siRNA hampers these processes, an effect at least in part, mediated by modulation of epithelial-mesenchymal transition (EMT) **(Figure 13)**. Here, we show that RSK1 siRNA increases resistance of lung adenocarcinoma cells to chemotherapeutic drugs cisplatin and paclitaxel, while RSK4 siRNA sensitises lung adenocarcinoma cells to these agents by impinging on the EMT and apoptosis programmes **(Chapter 3, p.118)**. Indeed, RSK3 and RSK4 have been implicated in promoting resistance to PI3K inhibitors in breast cancer, proposing the combined use of PI3K and RSK3 and/or RSK4 inhibitors (Serra et al., 2013). Collectively, it is unlikely that a single pan-RSK inhibitor will be effective or beneficial in a pan-cancer setting, highlighting the need for the development of isoform-selective inhibitors.

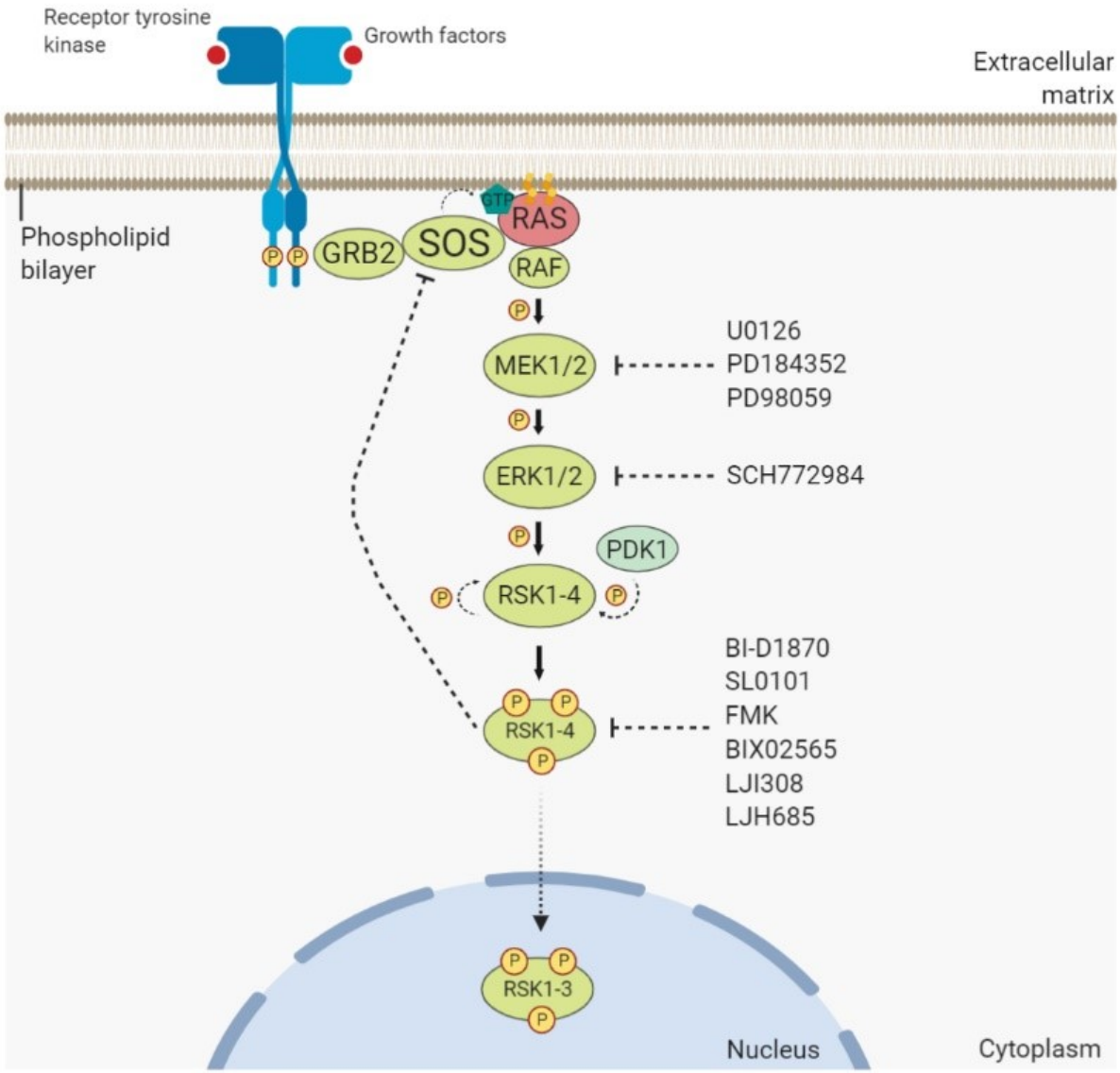

Figure 9| MEK/ERK/RSK inhibitors. Following activation of the RAS/MAPK pathway, RSKs are directly phosphorylated and activated by ERK1/2 (RSK1-4) and PDK1 (RSK1-3) (See **Figure 2, Figure 5 & Figure 6**). Activated RSKs can either phosphorylate cytoplasmic (RSK1-4) or nuclear substrates (RSK1-3). RSK activation can be blocked (indirectly) by MEK1/2 (U0126, PD184352, PD98059) or ERK1/2 (SCH772984) inhibitors. Direct RSK inhibitors include the NTKD inhibitors BI-D1870 and SL0101, which are reversible (pan-RSK) ATP-competitive inhibitors, and the CTKD inhibitor FMK (fluoromethylketone), which is irreversible and blocks the activation of RSKs (RSK1-3). LJI308 and LJH685 are difluorophenylpyridine derivatives of BI-D1870 and inhibit all RSKs at the 4-13 nM range. BIX02565 is a novel RSK inhibitor that was reported to potently inhibit RSK2 (IC_{50}= 1.1 nM). RSK2 (and RSK1) phosphorylate SOS on Ser1134 and Ser1161, via a negative feedback loop to attenuate MAPK activation (Houles & Roux, 2018). Figure created with biorender.com.

1.28 Cellular and molecular mechanisms of epithelial-mesenchymal transition

Epithelial or endothelial cells possess the inherent plasticity of cellular and molecular reprogramming, which enables them to adopt a mesenchymal phenotype, a process known as epithelial-mesenchymal transition (EMT). The resulting mesenchymal cells can revert back to an epithelial state through the reverse process known as mesenchymal-epithelial transition (MET). The EMT/MET balance plays crucial roles during specific stages of embryonic development where a series of cell differentiation and cell fate specification events take place (type I EMT), participates in tissue regeneration and wound healing in adults (type II EMT), while it pathologically contributes to organ fibrosis (type II EMT), cancer progression and CSC properties (type III EMT). EMT is undoubtedly a cornerstone of tumour invasiveness and metastasis in epithelial cancers (i.e. carcinomas), which constitute more than 70% of human cancers worldwide (Thiery et al., 2009). In surgically resected NSCLC tissues (LUAD & LUSC), the expression of EGFR and EMT biomarkers (N-cadherin and vimentin) was significantly higher in peripheral tumour cells compared to centrally located cells, a characteristic that related to poor prognosis (Mahmood et al., 2017).

Cuboidal-shaped epithelial cells display apical (top) and basal (bottom) polarity. They are tethered to the basement membrane (BM) through interactions with hemidesmosomes and α6β4 integrins, and establish close contacts with neighbouring epithelial cells with the help of lateral adherens junctions[16], tight junctions[17], gap junctions and desmosomes. This orderly organisation, which is crucial for the integrity of epithelia, is maintained by the expression of molecules associated with the epithelial state and apical-basal cell polarity, such as epithelial cadherin (E-cadherin; CDH1), claudins, occludins, α6β4 integrin and cytokeratin intermediate filaments. Conversely, spindle-shaped mesenchymal cells are loosely and individually organised with minimal cell-cell junctions, and display front-rear polarity, which contributes to directional migration. Similarly, this

[16] **Adherens junctions:** Important for the structural integrity of epithelia by mediating cell-cell adhesions through homophilic interactions between (single-pass) transmembrane E-cadherin molecules. Intracellularly, E-cadherin interacts with and regulates the actin cytoskeleton by binding to p120-catenin, α-catenin and β-catenin (Hartsock & Nelson, 2008).

[17] **Tight junctions:** Present at the apical end of epithelial cells, they regulate permeability between cells through the transmembrane proteins (four membrane-spanning domains) claudin and occludin. Claudin and occludin interact with cytoskeletal proteins and adherens junctions through the cytosolic scaffold proteins zonula occludens ZO-1,-2 and -3 (Hartsock & Nelson, 2008).

disorganised phenotype is maintained by the expression of molecules associated with the mesenchymal state, including neural cadherin (N-cadherin; CDH2), vimentin, fibronectin, α5β1 integrin, and matrix metalloproteinases (MMPs), which are involved in the degradation of the underlying basement membrane and extracellular matrix (ECM) proteins (Lamouille, Xu & Derynck, 2014). EMT involves extensive morphological reorganisation and gene expression reprogramming, a process orchestrated by key EMT-inducing TFs, which suppress epithelial gene expression while concomitantly activating the mesenchymal gene repertoire.

1.29 Gene expression changes – disassembly of cell-cell junctions, loss of cell polarity, cytoskeletal rearrangements and ECM remodelling

EMT is initiated with the destruction of lateral cell-cell junctions (adherens junctions[16], tight junctions[17], gap junctions and desmosomes) and apical-basal cell polarity. The dissolution of adherens and tight junctions is accompanied by the cleavage and degradation of E-cadherin and downregulation of occludin and claudin expression, respectively (Huang, Guilford & Thiery, 2012). Loss of E-cadherin is a key event during EMT, which results in the disruption of epithelial (or endothelial) cell-cell junctions. This event is associated with acquisition of mesenchymal adhesions mediated by upregulation of N-cadherin, a phenomenon known as "cadherin switch". N-cadherin homophilic interactions are weaker than their E-cadherin counterparts and are important during mesenchymal cell migration (Theveneau & Mayor, 2012). The loss of apical-basal cell polarity and acquisition of front-rear polarity is mediated by the disruption (and relocalisation) of the Scribble (SCRIB, LGL, DLG), PAR (PAR3, PAR6, aPKC) and Crumbs (Crumbs [CRB], PALS1, PATJ) complexes[18] and subsequent reorganisation of cortical actin cytoskeleton into actin stress fibres. The cells become more contractile and motile, by forming lamellipodia (sheet-like protrusions) and filopodia (spike-like protrusions at the edge of lamellipodia), and more invasive by forming invadopodia, which along with MMPs (e.g. MT1-MMP) proteolytically degrade the ECM to initiate metastasis (Ridley, 2011). The RHO GTPase, RHOA, mainly localises at the rear of the cell and promotes the formation of actin stress fibres, cell retraction and adhesion

[18] See Abbreviations section.

disassembly. The RHO GTPases, CDC42 and RAC1, are localised at the front edge of the cell (along with the Scribble, PAR and PATJ of Crumbs complex) where they promote lamellipodia, filopodia and invadopodia formation (Ridley, 2011). Further cytoskeletal alterations involve the replacement of cytokeratin (type I and II) intermediate filaments with vimentin equivalents (type III) by repression of cytokeratin and concomitant activation of vimentin expression, respectively. While cytokeratins are crucial for maintaining epithelial cell attachment to the basal lamina by binding to the intracellular component of hemidesmosomes, they might also be involved in targeting E-cadherin to the membrane (Toivola et al., 2005). On the other hand, vimentin intermediate filaments encourage a mesenchymal cell shape which disrupts desmosomal contacts, and promote cell motility possibly by interacting with motor proteins (Mendez, Kojima & Goldman, 2010). The last step of EMT and the first step of the invasion-metastasis cascade involves the remodelling and degradation of ECM, which enables cell invasion into surrounding tissues. Cells undergoing EMT no longer interact with the laminin and collagen type IV-rich basement membrane, instead they communicate with a fibronectin and collagen type I-rich ECM. Integrins are key mediators of cell interactions with ECM proteins. Therefore, the expression of α6β4 integrins, which mediate the interaction of epithelial cells with the basement membrane (through hemidesmosomes, cytokeratins and laminin), is repressed. Concomitantly, the expression of α1β1 and α2β1 integrins, which facilitate the disruption of E-cadherin complexes through interactions with collagen type I (Koenig et al., 2006), and α5β1 integrin, which promotes cell migration by increasing adhesion of cells to fibronectin (Mise et al., 2012), is promoted. Integrin gene expression changes correlate with upregulation of several MMPs, such as MT1-MMP, MMP-2, MMP-3 and MMP-9, which promote ECM degradation and invasion. MMPs can also directly initiate EMT by proteolytically shedding the extracellular domain of E-cadherin thereby causing its dissociation from intracellular β-catenin, which promotes transcriptional repression of this epithelial marker (See Transcription Factor interplay during EMT) (Zheng et al., 2009).

1.30 Transcription factor interplay during EMT

The alterations in the gene expression programme that promotes a mesenchymal phenotype while repressing the epithelial state are orchestrated by master regulator TFs, namely basic helix-loop-helix (bHLH) TFs TWIST1

and TWIST2, zinc-finger E-box binding homeobox TFs ZEB1 and ZEB2, and the SNAIL family members, zinc-finger TFs SNAIL1 (SNAI1) and SNAIL2 (SNAI2; SLUG). Novel TFs regulating EMT include forkhead box (FOX) (e.g. FOXA1, FOXO3A) and GATA family (GATA4 and GATA6) factors. These TFs are initiated at early stages during EMT and their activity, stability and subcellular localisation is tightly controlled transcriptionally and post-translationally by complex nuclear and cytoplasmic machineries (Dongre & Weinberg, 2019; Lamouille, Xu & Derynck, 2014).

The functional loss of E-cadherin through transcriptional repression represents not only one of the hallmarks of EMT, but it has also been implicated in the resistance to kinase inhibitors in several cancer types (Singh & Settleman, 2010). SNAIL1 was the first TF found to directly bind three E-box DNA sequences within the CDH1 promoter (which encodes E-cadherin) through its C-terminal zinc-finger domain, and represses E-cadherin transcription by recruiting SIN3A/histone deacetylase 1 (HDAC1)/HDAC2 complex and histone demethylase LSD1 (Lamouille, Xu & Derynck, 2014; Batlle et al., 2000). Providing an additional role for MMPs, Zheng and colleagues indicated that downstream of TGF-β1 signalling, MMP-3 or MMP-9 cleave the extracellular domain of E-cadherin, which results in the dissociation of intracellular β-catenin (Zheng et al., 2009). In turn, β-catenin translocates to the nucleus where it is thought to promote SLUG expression. Similar to SNAIL1, SLUG is also a potent transcriptional repressor of E-cadherin (Bolos et al., 2003). Following the initial observations of SNAIL1, TWIST1 and ZEB1 were also shown to bind E-cadherin promoter and repress its expression by recruiting methyltransferase SET8 and the SWI/SNF chromatin-remodelling protein BRG1, respectively (Yang et al., 2012a; Sanchez-Tillo et al., 2010). Interestingly, TWIST1/SET8 interaction promotes dual epigenetic modifications by repressing E-cadherin expression, while concomitantly promoting N-cadherin transcription through the H4K20 monomethylation activity of SET8 (Yang et al., 2012a). Further, ZEB1 was also shown to suppress E-cadherin transcription by recruiting the histone deacetylace SIRT1 to the proximal promoter of CDH1, where it deacetylates histone H3 and reduces RNA polymerase II enrichment at the promoter (Byles et al., 2012).

The remarkable power of these master regulators is manifested by their capacity to co-ordinately suppress epithelial genes (E-cadherin, claudins, occludin, desmosomal and hemidesmosomal proteins) while also promote the induction of mesenchymal genes (N-cadherin, vimentin, fibronectin and MMPs), and often directing both roles simultaneously. While all the aforementioned TFs have the capacity to induce EMT, several lines of evidence suggests SNAIL1 exerts a more prominent role in promoting EMT in primary tumours, while bHLH and ZEB factors are crucial in maintaining the migratory phenotype once EMT is initiated (Peinado, Olmeda & Cano, 2007). Further, while the epigenetic machinery is central in mediating and/or enhancing the effects of EMT TFs, their own activity is tightly regulated by the epithelia status, either post-transcriptionally through several non-coding miRNAs (e.g. miR-34, miR-101, miR-200), or post-translationally by phosphorylation, sumoylation and ubiquitination. This tight regulation is essential in maintaining a balance between the epithelial and mesenchymal phenotypes (De Craene & Berx, 2013). Last but not least, alternative splicing (e.g. exon skipping and exon inclusion) constitutes another mode of regulation of EMT. For instance, CD44, a cell surface glycoprotein involved in cell adhesion, migration and invasion, undergoes extensive alternative splicing, which generates diverse protein isoforms in mesenchymal cells that are crucial EMT regulators in many cancer subtypes (Brown et al., 2011).

1.31 Cellular and molecular insights into tumour metastasis

The ability of primary tumour cells to colonise distant metastatic sites and form secondary tumours involves a highly complex and multistep process portrayed by the invasion-metastasis cascade. Early-stage primary carcinomas initially display robust responses towards therapeutic interventions. However, inevitably metastatic resistant clones arise, which are almost invariably incurable. In fact, about 90% of cancer-related deaths are attributed to metastatic disease and not primary tumours. Hence, understanding the pathways that initiate and/or drive this process is of utmost importance.

While the acquisition of a series of somatic gene mutations in oncogenes and tumour suppressors has been well implicated in the initiation of tumourigenesis, the identification of recurrent mutations in metastasised

cells or associated with metastatic dissemination, has failed. It is possible that metastasis might not be driven by genetic determinants, rather it could be largely driven by the EMT programme. For instance, in a mutant Kras and p53 driven PDAC mouse model, the potent EMT activator Zeb1 was crucial for invasion and metastatic dissemination, while its depletion suppressed stemness and colonisation (Krebs et al., 2017). Another study elegantly showed that coexpression of SLUG and SOX9 TFs was sufficient to convert luminal cells into mammary stem cells and could promote the metastatic dissemination abilities of human breast cancer cells (Guo et al., 2012).

1.32 The invasion-metastasis cascade

Carcinoma cells become metastatic following acquisition of certain traits that equip them with the ability to colonise distant niches. These cells may hijack the EMT programme which endows them with migratory and invasive properties and the ability to degrade the ECM. The invasion-metastasis cascade entails a multistep process by which primary tumour cells (1) invade into nearby surrounding tissues, (2) intravasate into the circulatory system as individual or clusters of circulating tumour cells (CTCs), (3) transit and survive through the hostile bloodstream environment, (4) arrest at distant sites, (5) extravasate into the tissue parenchyma, (6) colonise the new microenvironment by initially forming micrometastases and ultimately (7) proliferate to form clinically detectable macroscopic metastases (Lambert, Pattabiraman & Weinberg, 2017). Importantly, this process is extraordinarily inefficient mainly due to the inhospitable environments of the haematogenous transit and the new tissue microenvironment that lacks the familiar growth factors, ECM components and stromal cells of the primary site. Therefore, only a small fraction of cells are able to form macroscopic metastases.

1.33 Single cell Vs collective migration and invasion

Local invasion entails the degradation of the underlying BM. Carcinoma cells derail the tightly controlled regulation of MMP activity to enhance their function and initiate BM and ECM degradation. Carcinomas can migrate and invade either as individual CTCs, referred to as “single-cell (or individual) migration”, or in cell

clusters, strands or sheets, referred to as “collective migration”. While lymphomas, leukaemias and sarcomas disseminate mostly as single cells, epithelial cancers principally disseminate via collective migration (Friedl & Wolf, 2003). Based on the cell type, protease production, integrin engagement and cytoskeletal architecture, single-cell migration is further distinguished into *amoeboid* and *mesenchymal* migration. Cells that undergo amoeboid migration lack mature focal contacts, therefore are able to migrate at 10-30-fold higher velocities compared to cells that employ mesenchymal migration (Friedl, Borgmann & Brocker, 2001). Instead, amoeboid movement is generated by cortical filamentous actin in an integrin- and stress fibre-independent manner. Further, while cells that undergo mesenchymal migration exhibit proteolytic activity and are able to degrade their way through ECM, amoeboid-type migrating cells use physical mechanisms to circumnavigate in a protease-independent manner (Friedl & Wolf, 2003). On the other hand, most epithelial tumours, like carcinomas of the lung and breast, migrate and invade collectively as a group of CTCs (i.e. collective migration), while maintaining cell-cell contacts. To maintain these contacts, cells continue to express key epithelial markers like E-cadherin, an observation that questions the role of EMT during metastatic cell dissemination. However, some reports propose that ‘partial’ or ‘hybrid’ EMT occurs during this step, which sustains the cohesion between these multicellular networks, while concomitantly ensuring expression of mesenchymal markers (Schliekelman et al., 2015). Yet other reports postulate that the leading carcinoma cells of these cohorts display more prominent EMT features compared to the trailing epithelial-like cells. These mesenchymal leading cells exhibit enhanced expression of MMPs and anterior, actin-rich protrusions, which engage and cluster β1 integrins for forward movement (Friedl et al., 2012). Another interesting study indicates that the leading cells are always stromal fibroblasts, which generate tracks within the ECM, sufficient for the collective invasion of trailing epithelial-like carcinoma cells (Gaggioli et al., 2007).

1.34 Intravasation, haematogenous survival, arrest and extravasation

Following the loss of BM barrier, invading cells enter a “reactive” stromal compartment where they encounter a diverse cell population including endothelial cells, cancer-associated fibroblasts (CAFs), cancer-associated adipocytes, tumour-associated macrophages and immune cells. These stromal cells secrete potent EMT

stimulators and can further enhance the aggressiveness of invading cells; for instance, secretion of interleukin-6 (IL-6) by cancer-associated adipocytes stimulates breast cancer cell invasion (Dirat et al., 2011), while CAFs secrete an array of growth factors, such as EGF, transforming growth factor beta (TGFβ) and vascular endothelial growth factor (VEGF), which can induce and/or maintain EMT (Dongre & Weinberg, 2019). Once, at the stromal compartment, carcinoma cells can intravasate into the vasculature (or lymphatics) by penetrating through the microvessel barriers of pericytes and endothelial cells (ECs). Although, lymphatic spread is a frequent phenomenon, dissemination through the blood circulation represents the major mechanism by which carcinoma cells metastasise (De Palma, Biziato & Petrova, 2017). The property of tumour cells to stimulate the formation of new blood vessels via the process of *neo-angiogenesis*[19], strongly enhances their invasive and metastatic abilities. Under oxygen- (i.e. hypoxic) and nutrient-deprived conditions, carcinoma cells, secrete VEGFA which stimulates VEGF receptor 2 (VEGFR2) expressed on ECs and initiate angiogenesis. Several antiangiogenic inhibitors are currently FDA approved in cancer, including Avastin (bevacizumab)[20], a VEGFA monoclonal antibody inhibitor (Weis & Cheresh, 2011). Once in the circulation, metastatic cells are challenged by a harsh environment of physical stresses and clearance by natural killer (NK) cells. Platelets and neutrophils support disseminating tumour cells by protecting them from both physical and immune cell destruction. While tumour cells are coated by platelets shortly after intravasation, they might also become entangled by neutrophil extracellular traps (NETs) (used to capture pathogens), both of which protect them against the shear stress and turbulence encountered within blood vessels. Further, both cell types have shown immunosuppressive properties, for instance by secreting soluble factors, such as PDGF and TGFβ (in the case of platelets), which inhibit NK cell activity (Lambert, Pattabiraman & Weinberg, 2017). Arrest of disseminating cells may occur via physical trapping, due to vascular architecture and size restrictions of the blood vessels, or via predetermined mechanisms which favour specific ligand-receptor interactions (Brown &

[19] Judah Folkman pioneered the field of tumour angiogenesis.

[20] Approved in combination with Tecentriq (atezolizumab), carboplatin and paclitaxel as a first-line treatment for metastatic NSCLC patients with no ALK (anaplastic lymphoma kinase) translocations or EGFR mutations. Available from: https://www.drugs.com/history/avastin.html [Accessed 06th Sep 2019].

Ruoslahti, 2004). Once arrested at a distant site, CTCs, extravasate from the vasculature and enter into the parenchyma of tissues by a process called transendothelial migration (TEM). Several mechanisms have been reported to take place during this process, including the recruitment of $CCR2^{+}$ inflammatory monocytes (Qian et al., 2011), and the cancer cell-stimulated ATP release from platelets, which enhances endothelial wall permeability (Schumacher et al., 2013).

1.35 Micrometastasis formation and metastatic colonisation

Within the parenchyma of distant tissues, extravasated carcinoma cells are faced with the final and most lethal step of the invasion-metastasis cascade. In order to form micrometastases (0.2-2 mm), they must survive and thrive within a foreign environment devoid of the familiar, tumour-permissive ECM components, stromal cells, growth factors, cytokines and metabolic components that were present at the primary tumour site. This process is highly inefficient, with in vivo experiments suggesting only 0.01% of cells succeed (Chambers, Groom & MacDonald, 2002). Once adjusted to their new environment, surviving cells within micrometastatic colonies proliferate to form clinically detectable macrometastases (>2 mm), a process referred to as colonisation. It is possible for micrometastatic clusters to enter into a dormant state that may persist for weeks, months or years, before receiving the signals required to form macroscopic tumours (Luzzi et al., 1998). Interestingly, dormant disseminated cells may reside within tissue-specific stem cell niches (e.g. hematopoietic stem cell niche in bone metastases) (Shiozawa et al., 2011).

Following Steven Paget's pivotal "seed and soil" hypothesis, whereby a receptive, tumour-permissive microenvironment is required for disseminating cells to form metastases, rather than passively arrested at distant sites as a result of anatomical constraints of the vasculature (James Ewing's theory); an abundance of breakthroughs have led to the evolution of the "metastatic niche model" (Psaila & Lyden, 2009). This model proposes the requirement of a suitable microenvironment (pre-metastatic niche), which can sustain the foreign cancer cells and assist them in growing and proliferating into macroscopic tumours (micrometastatic to macrometastatic transition). Bone represents the commonest metastatic site, probably due to the plethora

of bone marrow-derived cytokines, chemokines and growth factors; while lung, liver and brain metastases are also very frequent, all of which are common sites of lung cancer metastasis (Langley & Fidler, 2011). The pre-metastatic niche is created in response to primary tumour-secreted TGFβ, VEGFA and placental growth factor (PlGF), stimulating the release of serum amyloid A3 (SAA3) and inflammatory S100 chemokines in pre-metastatic sites, which in turn recruit haematopoietic progenitor cells (HPCs) from the bone marrow. HPCs secrete several factors including MMPs, TGFβ, VEGFR1 and tumour necrosis factor alpha (TNFα), while activated fibroblasts secrete fibronectin, thereby preparing the metastatic niche for disseminating carcinoma cells (Psaila & Lyden, 2009). Within their new microenvironment, cancer cells recruit endothelial progenitor cells (EPCs) to stimulate angiogenesis, which is elemental for the progression to macrometastases, while the presence of inflammatory cells and inflammatory cytokines and chemokines in the metastatic niche is also required (Mantovani et al., 2008). For instance, lymphocyte and leukocyte trafficking is strongly associated with blood vessel formation by stimulating the release of pro-angiogenic factors in VEGF-independent fashion (Noonan et al., 2008).

While the EMT and stem-cell programs are key determinants of metastatic colonisation, reversion of EMT (i.e. MET) accompanied with re-acquisition of key epithelial markers including E-cadherin and β-catenin and reorganisation into hierarchical cell structures similar to those in the primary tumour, may also be fundamental for establishing macrometastases. In fact, tumour dormancy following extravasation, may be initiated due to the inability of disseminating cells to revert back into an epithelial-like phenotype and proliferate (Tsai et al., 2012).

1.36 Molecular mechanisms of cell death

Cell death, the loss of cellular integrity in response to the degeneration of fundamental cellular functions (e.g. ATP production), is broadly categorised into accidental cell death (ACD) and regulated cell death (RCD). While ACD occurs in an uncontrollable practically instantaneous fashion in response to extreme and unexpected mechanical (e.g. shear forces), physical (e.g. high temperatures) or chemical (extreme pH) cues, RCD relies on

a tightly controlled and precise molecular machinery. This fundamental difference implies that by definition ACD is virtually untargetable, whereas RCD may be manipulated (enhanced or diminished) by pharmacological interventions. RCD may also operate under two distinct scenarios. RCD can originate in the absence of exogenous perturbations, during which it regulates physiological developmental programs, a form of cell death also known as programmed cell death (PCD), or result in response to unsustainable extracellular or intracellular perturbations (Galluzzi et al., 2018).

Based on molecular and macroscopic morphological characteristics and diverse initiating stimuli, cell death manifests in multiple subroutines: apoptosis (intrinsic or extrinsic), anoikis (variant of intrinsic apoptosis; characterised by the loss of integrin-dependent anchorage), autophagy-dependent cell death, autosis (variant of autophagy-dependent cell death; mediated by Na^+/K^+-ATPase pump), lysosome-dependent cell death, necroptosis (requires RIPK3 and its substrate MLKL), pyroptosis (highly inflammatory form of cell death), ferroptosis (iron-dependent cell death), alkaliptosis (pH-dependent cell death), oxeiptosis (ROS-induced caspase-independent cell death), parthanatos (PARP1-dependent cell death), entotic cell death (cell-in-cell internalisation), netotic cell death (e.g. neutrophil cell death during NET extrusion), mitotic catastrophe and immunogenic cell death (Tang et al., 2019).

1.37 Apoptosis

Apoptosis involves the tightly controlled demolition of cellular architecture in response to extracellular (extrinsic apoptosis) or intracellular (intrinsic apoptosis) microenvironment perturbations, culminating not only in cell death but also elimination of cellular debris by phagocytes to avoid immunological responses and disruption of neighbouring cells. Extrinsic and intrinsic pathways are distinguished by their requirement for BCL-2 (B-cell lymphoma-2) family members and engagement of distinct caspases for their execution. While both pathways converge on caspase activation, the extrinsic pathway, unlike the intrinsic one, does not require BCL-2 family members for caspase activation. Nonetheless, in some cells these pathways can intersect (Taylor, Cullen & Martin, 2008).

Caspases, the executioners of apoptosis, are cysteine aspartic acid-specific proteases, which target major cytoskeletal constituents, including actin and actin-associated proteins (e.g. filamin and myosin), tubulin and microtubule-associated proteins (e.g. dynein and tau) and intermediate filaments such as keratins and vimentin. The effects of caspases are contributing towards the retraction and rounding of the apoptotic cell as well as plasma membrane blebbing (i.e. formation of circular bulges or protrusions), a distinctive feature of apoptosis (Taylor, Cullen & Martin, 2008). Caspases exist in cells as inert precursor enzymes (i.e. pro-caspases or zymogens) and require proteolytic processing for their activation. Mammalian apoptotic caspases are divided into the *initiator caspases*: caspase-2, caspase-8, caspase-9 and caspase-10, which can activate themselves or other caspases, and *effector caspases*: caspase-3, caspase-6 and caspase-7, which target substrates for cleavage during apoptosis. All caspases are characterised by the presence of an N-terminal pro-peptide which is followed by a large (p20) and small (p10) subunit. While effector caspases contain a small pro-peptide motif, initiator caspases harbour extended N-terminal regions known as the death effector domain (DED) and the caspase recruitment domain (CARD), which are crucial for their interaction with other caspases and complexes. Initiator caspases mediate an aspartic-acid directed proteolytic cleavage between the p20 and p10 subunits of effector caspases, which results in caspase dimerisation and activation (Riedl & Shi, 2004).

The activation of caspases is countered by two classes of apoptosis inhibitors: 1) anti-apoptotic BCL-2 and 2) inhibitor of apoptosis (IAP) family members. While anti-apoptotic BCL-2 members inhibit apoptosis by blocking cytochrome c release through the mitochondria (discussed later), IAPs bind caspases directly to inhibit their activity (Riedl & Shi, 2004). The BCL-2 family members (10-40 kDa) are classically grouped into three subfamilies based on their structure/activity. The anti-apoptotic (pro-survival) BCL-like subfamily is characterised by the presence of four BCL-2 homology (BH) domains (BH1-4) and is comprised of BCL-2, BCL-XL (BCL2L1), BCL-W (BCL2L2), BCL-B (BCL2L10), BCL-RAMBO (BCL2L13), BCL-G (BCL2L14), BCL2A1 and MCL1. The pro-apoptotic BAX-like subfamily lacks the BH4 domain and incudes BAX (21 kDa), BAX (24 kDa) and BOK. The third subfamily constitutes a structurally diverse group of pro-apoptotic proteins that harbour only the

BH3 domain, also known as BH3-only proteins, and includes BIK, BIM, BID, BAD, PUMA (p53 upregulated modulator of apoptosis), NOXA, HRK (DP5), BMF and MULE (E3 ligase). Most BCL-2 family members contain a C-terminal transmembrane domain, which is crucial for mitochondrial membrane localisation (Youle & Strasser, 2008). Not surprisingly, tumour cells acquire resistance to apoptosis by upregulation (e.g. gene amplification, protein overexpression) of BCL-2 anti-apoptotic family members or inactivation (downregulation or mutation) of BCL-2 pro-apoptotic family members. Multiple strategies have sought to target the activity and/or function of anti-apoptotic BCL-2 proteins, most notably BH3 or BH4 mimetics and small molecule inhibitors, which bind directly and block anti-apoptotic BCL-2 members to restore apoptosis (discussed later) (Thomas et al., 2013). Venetoclax (venclexta) is the first-in-class BCL-2 inhibitor approved for the treatment of chronic lymphocytic leukemia (CLL) or small lymphocytic lymphoma (SLL)[21].

IAPs constitute a family of conserved proteins originally identified in the baculovirus genome. Eight mammalian IAPs have been characterised to date, namely: XIAP (X-linked IAP; *BIRC4*), cellular-IAP1 (c-IAP1; *BIRC2*), c-IAP2 (*BIRC3*), Survivin (*BIRC5*), NAIP (neuronal apoptosis-inhibitory protein; *BIRC1*), BRUCE/Apollon (*BIRC6*), ILP2 (IAP-like protein 2; *BIRC8*) and ML-IAP/Livin (melanoma IAP; *BIRC7*) (Riedl & Shi, 2004). IAPs are classified by the presence of one or more zinc-binding domains, also known as baculoviral IAP repeat (BIR) domains. XIAP, c-IAP1 and c-IAP2 share all three BIR domains (BIR1, BIR2, BIR3), which serve different functions, and a C-terminal RING domain, which equips them with an E3 ubiquitin ligase activity (Yang et al., 2000). c-IAPs also possess a caspase recruitment domain (CARD), the function of which is as of yet unknown. XIAP can directly bind and inhibit the effector caspase-3 and -7 and initiator caspase-9. The linker region between BIR1 and BIR2, which is conserved between cIAPs, specifically targets caspase-3 and -7, and inhibits their catalytic activity by blocking substrate entry, while the BIR3 domain of XIAP specifically binds and inhibits processed caspase-9 by preventing its dimerisation. The presence of an E3 ubiquitin ligase domain also allows IAPs to target caspases as well as themselves for proteasomal degradation (Fulda & Vucic, 2012). In turn,

[21] Available from: https://www.fda.gov/drugs/resources-information-approved-drugs/fda-approves-venetoclax-cll-and-sll [Accessed 09th Sep 2019].

second mitochondria-derived activator of caspase/diablo IAP-binding mitochondrial protein (SMAC/DIABLO), binds IAPs on BIR3 domain via its N-terminal tetrapeptide motif and antagonises their function, thereby promoting apoptosis. Considering the expression and/or function of IAPs is heavily deregulated in cancer, therapeutic targeting of these proteins, most notably with SMAC mimetics (IAP antagonists), has been very attractive (Fulda & Vucic, 2012). For instance, LCL161, a SMAC mimetic, is undergoing a Phase II clinical trial for the treatment of refractory multiple myeloma (NCT01955434).

1.38 Extrinsic Vs intrinsic apoptosis

The extrinsic signalling (or death receptor) pathway is initiated in response to extracellular microenvironment perturbations and is mainly driven by transmembrane death receptors: TNF receptor superfamily member 1A (TNFRSF1A; TNFR1), TNF-related apoptosis-inducing ligand receptor 1 (TRAILR1 or DR4), TRAILR2 (or DR5) and Fas cell surface death receptor (FAS or APO-1 or CD95). Extracellular ligand binding (e.g. TNFα, FasL) on death receptors promotes the recruitment of Fas-associated death domain protein (FADD), which in turn drives death-inducing signalling complex (DISC) assembly by aggregating several molecules of caspase-8 (or caspase-10) and c-FLIP. Caspase-8 initiates apoptosis by proteolytic cleavage and activation of effector caspases-3 and -7 (Galluzzi et al., 2018).

Intrinsic (or mitochondrial) apoptosis is initiated mostly by intracellular microenvironment perturbations, including ER stress, DNA damage and reactive oxygen species (ROS) accumulation. The most critical step during intrinsic apoptosis involves the irreversible process of mitochondrial outer membrane permeabilisation (MOMP), which is tightly controlled by both anti-apoptotic and pro-apoptotic BCL-2 family members. Pro-apoptotic BH3-only proteins (e.g. PUMA, NOXA and BAD), in response to apoptosis-promoting signals that persist long enough to relieve the inhibitory signals from anti-apoptotic BCL-2 family members (e.g. BCL-2, BCL-XL), promote the assembly of BAK-BAX (or BOK) oligomers across outer mitochondrial membranes, which culminates in the cytoplasmic efflux of cytochrome c and SMAC/DIABLO. Cytosolic cytochrome c binds to apoptotic peptidase activating factor 1 (APAF1) in an ATP or deoxy ATP-dependent manner to form a large

protein complex known as the apoptosome, which recruits and activates the initiator caspase-9. Caspase-9 initiates apoptosis by proteolytic cleavage and activation of effector caspases-3 and -7 (Galluzzi et al., 2018). The extrinsic pathway can intersect with the mitochondrial pathway by caspase-8-driven proteolytic cleavage of the pro-apoptotic BH3-only protein BID. The truncated version of BID can promote MOMP and cytochrome c release, which results in apoptosome formation (Li et al., 1998).

1.39 p53: "The guardian of the genome"

Cellular tumour antigen p53 is a critical tumour suppressor activated in response to cellular stress including (but not limited to) DNA damage, oncogene activation and hypoxia. Once active it converges on hundreds of genes involved in DNA damage repair, cell cycle arrest, apoptosis, senescence and metabolism. As a result of this multimodal control of genome integrity, p53 has been termed "the guardian of the genome". Consistent with its central role in suppressing tumour development and progression, *TP53* (the gene that encodes p53) is the most frequently mutated gene (point mutations and deletions/small insertions) in a TCGA Pan-Cancer cohort (Kandoth et al., 2013).

1.40 p53 structure

TP53 encodes a 53 kDa (393 aa), DNA binding protein that controls transcription, a function that depends on several well-characterised domains **(Figure 10a)**. The p53 protein contains two tandem transactivation domains (TAD1 & TAD2) at the N-terminus, which are required for DNA damage-induced apoptosis and cell-cycle arrest but are dispensable for cellular senescence (Brady et al., 2011). TADs are directly followed by a proline-rich domain (PRD) that is characterised by the presence of five SH3-domain binding motif (P-X-X-P) repeats, and contributes towards transcription activation (Walker & Levine, 1996). Centrally located is the DNA-binding domain (DBD), which specifically binds dsDNA on target genes that contain two half site canonical

p53 binding (decameric) motifs: 5'- R – R – R – **C** – W – W – **G** – Y – Y – Y – 3'[22], which may be separated by up to 13 base pairs (el-Deiry et al., 1992). The DBD is the most heavily mutated p53 site **(Figure 10a)**.

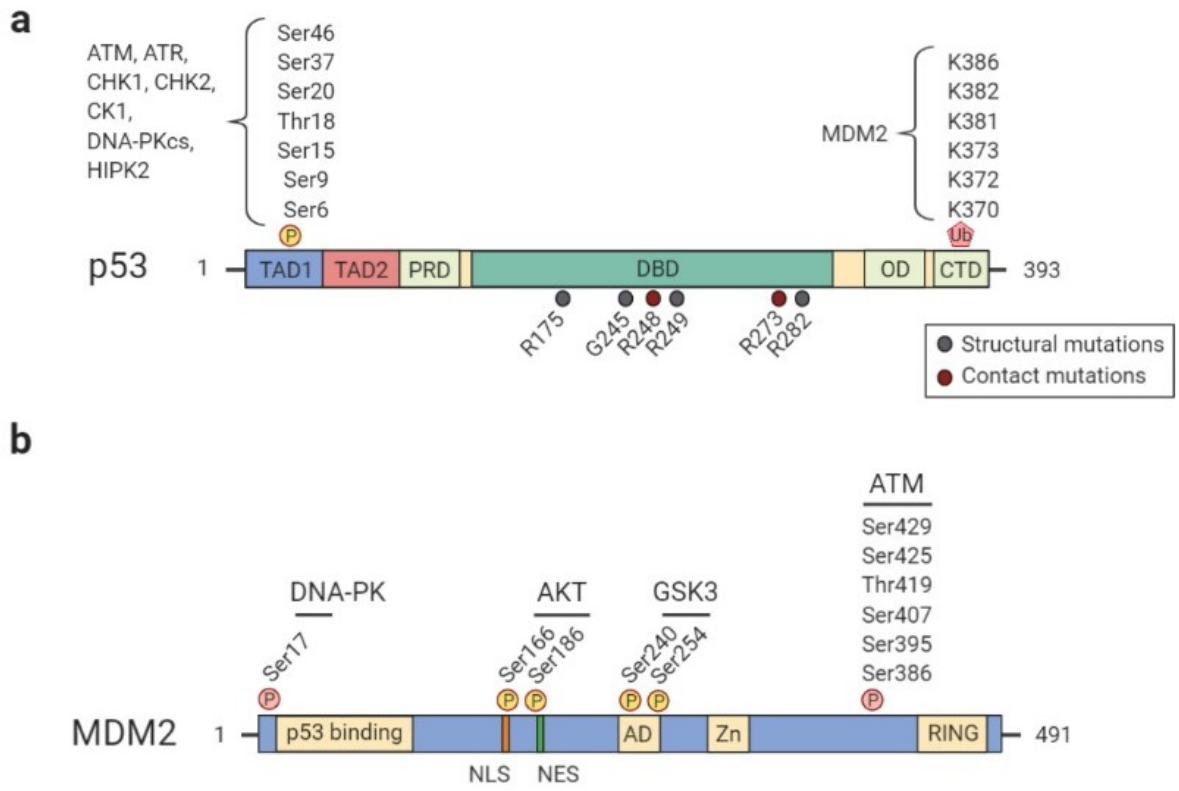

Figure 10| Structure and post-translational regulation of p53 and MDM2. (a) p53 (53 kDa; 393 aa) is post-translationally modified by phosphorylation, and lysine ubiquitination, acetylation (not shown) and methylation (not shown). Phosphorylation principally takes place within the two tandem N-terminal transactivation domains (TAD1 & TAD2; 1-62 aa), which are phosphorylated by (and not limited to) ATM (Ser9, Ser15, Ser46), ATR (Ser15), CHK1 (Ser20), CHK2 (Ser20), CK1 (Thr18), DNA-PKcs (DNA-dependent protein kinase catalytic subunit; Ser9, Ser15, Thr18, Ser37) and HIPK2 (homeodomain interacting protein kinase 2; Ser46). In general, these phosphorylation events stabilise p53 by blocking its interaction with MDM2. TADs are followed by a proline-rich domain (PRD; 63-94 aa) with few well-characterised modifications (not shown). The core DNA binding domain (DBD; 95-292 aa) is the most heavily mutated p53 domain in cancer, usually at one of six hotspots: Arg175(H/L), Gly245(S), Arg248(Q/W), Arg249(S), Arg273(H/C) and Arg282(Q/W). The 'contact' mutations (Arg248(Q/W) and Arg273(H/C)) disrupt DNA-protein binding without altering p53 conformation, while the 'structural' mutations (Arg175(H/L), Gly245(S), Arg249(S) and Arg282(Q/W)) alter the conformation of the DNA binding surface; both of which inhibit p53 transactivation. Adjacent to DBD lies the oligomerisation domain (OD), also called tetramerisation domain (TET), which is involved in p53 tetramer formation and activation. The carboxyl-terminal region (CTD) is enriched in basic residues and subjected to lysine acetylation (e.g. by p300; not shown), methylation (e.g. by SETD7&8; not shown) and ubiquitination by the E3 ubiquitin ligase MDM2 (K370, K372, K373, K381, K382, K386). **(b)** MDM2 (55 kDa; 491 aa), interacts with p53 TADs through its amino-terminal p53 binding domain, a prerequisite for ubiquitin-dependent p53 degradation. The nuclear localisation signal (NLS) and nuclear export signal (NES) sequences are critical for the nucleocytoplasmic transport of MDM2 and p53 (not shown). The central acidic domain (AD) interacts with the RING (really interesting new gene) domain and stimulates its E3 ubiquitin ligase activity. MDM2 is also subjected to several post-translational modifications, for simplicity the figure indicates a few examples of phosphorylation modifications. Shown in yellow are phosphorylation sites that are reported to enhance MDM2-mediated inhibition of p53, while shown in red are phosphorylation sites that are reported to inhibit MDM2-mediated inhibition of p53. For instance, AKT phosphorylation on Ser166 or Ser186 stabilise MDM2, while DNA-PK phosphorylation on Ser17 block MDM2-p53 protein-protein interaction. Zn, zinc finger domain. (Hafner et al., 2019; Wade, Li & Wahl, 2013). Figure created with biorender.com.

[22] R: Purine (A or G); W: Weak (A or T); Y: Pyrimidine (C or T). NB: these motifs may be present at different orientations (e.g. head-to-head or tail-to-tail).

Around 95% of p53 mutations occur within the DBD, while 40% of those occur in one of six p53 hotspots: Arg175(H/L), Gly245(S), Arg248(Q/W), Arg249(S), Arg273(H/C) and Arg282(Q/W). These mutations have been classified as "contact" (Arg248(Q/W) and Arg273(H/C)) or "structural" (Arg175(H/L), Gly245(S), Arg249(S) and Arg282(Q/W)), depending on whether they are involved in direct DNA contacts without affecting p53 conformation (i.e. DNA-contact mutations), or alter the conformation of the DNA-binding surface (i.e. structural mutations) (Muller & Vousden, 2014); all of which block p53-DNA interaction thereby diminishing p53 transactivation. Under non-stressed conditions p53 predominantly exists in an inefficient monomeric state. In fact, p53 binds to its target genes with greater efficiency and affinity as a tetramer (i.e. dimer of primary dimers). Tetramerisation is orchestrated by the oligomerisation domain (OD) or tetramerisation domain (TET), which lies adjacent to the DBD **(Figure 10a)**. C-terminaly located is the carboxyl-terminal domain (CTD) also known as basic domain (rich in basic residues). Although CTD is required for p53-DNA binding and transcription, its precise role has been challenging to elucidate. Noteworthy, this site is heavily post-translationally modified by lysine *acetylation* (e.g. by p300) and *methylation* (e.g. by SETD7 and SETD8) (Hafner et al., 2019).

1.41 p53-MDM2 interaction

p53 expression and/or activity is tightly controlled by post-translational modifications, notably *phosphorylation* (mostly within TADs; e.g. by ATM/ATR) and lysine *acetylation*, *ubiquitination* (by MDM2) and *methylation* (mostly within the C-terminus) (Hafner et al., 2019). In fact, over 300 distinct post-translational modifications were identified by mass spectrometry, some of which have been well characterised and are critical for p53 regulation (Bode & Dong, 2004). In non-stressed conditions, p53 levels are maintained low by the oncogenic E3 ubiquitin ligases (Mouse Double Minute) MDM2 and MDM4 (also known as MDMX or HDMX), two of the most potent negative regulators of p53. MDM2 (55 kDa; 491 aa) and MDM4 (55 kDa; 490 aa) share an amino-terminal p53-binding pocket, which is a critical structural feature for interaction with p53 **(Figure 10b)**. This region is followed by a centrally located acidic domain (AD) that upon phosphorylation attenuates MDM2 function and promotes p53 activation. MDM2 and MDM4 harbour self- and p53-specific E3

ubiquitin ligase activity that depends on a carboxyl-terminal RING (Really Interesting New Gene) finger domain **(Figure 10b)** (Wade, Li & Wahl, 2013). MDM2 mainly regulates p53 stability by promoting ubiquitin-depended p53 degradation by both cytoplasmic and nuclear 26S proteasomes, while MDM4 regulates p53 activity. A prerequisite for this mechanism entails direct MDM2 (or MDM4)-p53 interaction, which has been deciphered by crystallographic data and biochemical analysis. This association is confined between a small hydrophobic pocket within the amino-terminal p53 binding domain of MDM2 and an amphipathic peptide within the amino-terminal TAD of p53 (Moll & Petrenko, 2003), which is sufficient to directly block the transcriptional activity of p53 (Oliner et al., 1993). p53 ubiquitination takes place in the nucleus. Initially, MDM2 oligomers mediate p53 monoubiquitination at C-terminal lysine residues (K370, K372, K373, K381, K382, K386), which is followed by polyubiquitination mediated by MDM2 (E3-type ligase activity) in a complex with CREB-binding protein (CBP)/p300 (E4-type ligase activity). p53 is then directed for degradation by nuclear or cytoplasmic 26S proteasomes. Importantly, MDM2 (and MDM4 albeit less responsive) is a p53-target gene, therefore forming an autoregulatory feedback loop, whereby p53 drives MDM2 expression, which in turn inhibits p53 activity, thereby maintaining low p53 levels under non-stressed conditions (Moll & Petrenko, 2003). While p53 is mutationally deactivated in the majority of cancers, MDM2 gene amplification is a frequent phenomenon in many tumours (Forslund et al., 2008). MDM2 and MDM4 gene or protein alterations are more frequent in p53 WT well-differentiated liposarcomas, cutaneous melanoma and breast cancer (Wade, Li & Wahl, 2013). Small molecules that antagonise MDM2-p53 protein-protein interaction have been developed, most notably nutlin 3a, a *cis*-imidazoline analog that binds MDM2 N-terminal hydrophobic cleft and prevents p53 degradation. RG7112, a nutlin 3a derivative, has shown promising results in reactivating the p53 pathway in leukemia and liposarcoma patients, although it correlated with adverse events (Andreeff et al., 2016; Ray-Coquard et al., 2012).

1.42 p53 activation and response

Genotoxic stress triggers the initiation of DNA damage response (DDR) pathway. DNA double-strand breaks (DSBs) trigger the activation of kinase ataxia-telangiectasia mutated (ATM), which phosphorylates and

activates CHK2 kinase (Thr68); while stalled DNA replication forks recruit and activate the kinase ataxia telangiectasia and RAD3-related (ATR)[23], which phosphorylates and activates CHK1 kinase (Ser317, Ser345) (Marechal & Zou, 2013). p53 is a substrate for both CHK1 (Ser20) and CHK2 (Ser20) kinases, as well as ATM (Ser9, Ser15, Ser46) and ATR (Ser15), which typically phosphorylate p53 on TAD serine residues **(Figure 10a)**. These phosphorylation events stabilise p53 by disrupting its interaction with MDM2. ATM and ATR further phosphorylate and inhibit MDM2 directly, possibly by disrupting its oligomerisation **(Figure 10b)** (Bieging, Mello & Attardi, 2014). Similar to acute DNA damage, hyperproliferative signals activate p53 by disrupting MDM2-p53 interaction. E2F transcription factors drive the expression of tumour suppressor ARF (or p14/p19; encoded by *CDKN2A*), which antagonises the E3 ligase activity of MDM2, and/or sequesters MDM2 in the nucleus (Nag et al., 2013). In response to DNA damage, activated p53 drives the transcription of cyclin-dependent kinase inhibitor 1A (*CDKN1A*; encodes $p21^{Cip1/WAF1}$) and triggers G1/S and G2/M cell-cycle arrest, thereby allowing cells to repair their DNA before division. p53 impinges on the DNA damage response, for instance by driving the expression of the *XPC* (xeroderma pigmentosum C) and *DDB2* (DNA damage-binding protein 2) genes, which are involved in nucleotide excision repair (NER). In the event where cells fail to repair damaged DNA, p53 can promote both extrinsic and intrinsic apoptotic pathways by inducing the expression of death receptors FAS and TNFRSF10A (TRAILR1), and BCL-2 family members BBC3 (PUMA), PMAIP1 (NOXA) and BAX, respectively. APAF1, the protein that forms the apoptosome (with cytochrome c), is also a p53 target gene (Fischer, 2017).

1.43 Drug resistance

Anticancer therapies almost invariably fail due to the acquisition of drug resistance, which is driven, at least in part, by intratumoural heterogeneity (Dagogo-Jack & Shaw, 2018). TRACERx (Tracking Non-Small-Cell Lung Cancer Evolution through Therapy), a study that exome-sequenced multiple neoplastic regions of 100 early stage NSCLC tumours resected before therapy, indicated extensive intratumoural heterogeneity for both

[23] ATM is primarily activated in response to DSBs, whereas ATR is activated in response to a broad spectrum of DNA damage events, including DSBs, single-strand breaks (SSBs) and DNA replication stress

somatic mutations and copy-number alterations (Jamal-Hanjani et al., 2017). In this study, targetable driver mutations or amplifications (e.g. EGFR, MET, BRAF) were almost always clonal (i.e. present in all cancer cells) and arose early (i.e. before genome doubling) during NSCLC evolution. Therefore, these mutations are associated with tumour initiation (rather than tumour maintenance), and reflect the initially robust responses when molecularly targeted (Jamal-Hanjani et al., 2017). Nonetheless, more than 75% of tumours in the TRACERx study carried sub-clonal (i.e. present in a subset of neoplastic cells) driver alterations (e.g. NF1, PIK3CA, NOTCH) and occurred late during NSCLC evolution (Jamal-Hanjani et al., 2017). Importantly, these mutations were often not specific to NSCLC and were involved in DNA damage response and repair and chromatin modification. These mutations are associated with tumour maintenance and are thought to give rise to resistant sub-clones.

In parallel to genetic heterogeneity, non-genetic determinants, namely epigenetic modifications (e.g. histone modification and DNA methylation) and tumour microenvironment also contribute to overall tumour heterogeneity. These three facets of heterogeneity impinge on stemness, the stem-cell like properties of a subset of cancer cells, which is involved in tumour progression and resistance to therapy (Kreso & Dick, 2014). Cancer stem cells (CSCs), a small subpopulation of cells within the tumour microenvironment, possess the unique property of seeding new tumours and have been shown to emerge as a result of epithelial-mesenchymal transition (EMT) (Shibue & Weinberg, 2017). Further, cells that have undergone EMT acquire resistance to several drugs and chemotherapeutic agents by regulating genes associated with cell survival, thereby resisting apoptosis and senescence (Shibue & Weinberg, 2017).

Importantly, the mechanisms by which cancer cells acquire resistance to molecular targeted therapies and chemotherapeutic (i.e. cytotoxic) agents largely overlap[24]. In general, the amount of drug that reaches the tumour is influenced by several pharmacokinetic (PK) factors including drug absorption and distribution, as

[24] This section will outline a few examples of chemotherapeutic resistance mechanisms. Various resistance mechanisms against targeted therapies such as EGFR, RAF and MEK inhibitors have been described throughout this work.

well as drug metabolism and elimination (not discussed here). The efficacy of anticancer drugs may be limited due to poor cellular drug influx and/or excessive drug efflux; lack of drug activation; induction of pro-survival signals and resistance to apoptosis; mutation, gene amplification and protein overexpression of the drug target or dependence of the cell on parallel pathways for survival and growth (Holohan et al., 2013).

The ATP-binding cassette (ABC) transporters, which constitute a family of 49 transmembrane transporter proteins, have been heavily implicated in chemotherapeutic resistance against taxanes, topoisomerase inhibitors and targeted compounds by promoting drug efflux. For instance, multidrug resistance protein 1 (MDR1 or P-glycoprotein) overexpression is associated with resistance to topoisomerase II inhibitors (e.g. etoposide and doxorubicin) and microtubule inhibitors (e.g. paclitaxel) in several cancer types including lung cancer, breast cancer and lymphoma (Szakacs et al., 2006). Drug inactivation or lack of drug activation constitutes another resistance mechanism that affects both chemotherapeutic and targeted agents. For example, the thiol glutathione inactivates platinum-based drugs (e.g. cisplatin) by several mechanisms, such as serving as a redox regulator or copper (Cu) chelator, or facilitating drug efflux as a cofactor with multidrug resistance protein 2 (MRP2) (Chen & Kuo, 2010).

While the functional role of EMT has been largely characterised *in vitro*, by manipulating the expression and/or activity of key EMT TFs (TWIST, ZEB, SNAIL), the *in vivo* functional contribution of EMT during invasion and metastasis, remains unclear. Several lines of evidence argue that EMT is dispensable for metastasis but instead contributes to chemoresistance. Deletion of TWIST or SNAIL TFs in a PDAC mouse model did not prevent systemic dissemination or metastasis, but increased cancer cell proliferation and expression of nucleotide transporters, and sensitised mice to gemcitabine treatment (Zheng et al., 2015). In an elegant study, Fischer and colleagues using a lineage-tracing system to monitor EMT in a spontaneous breast-to-lung metastasis mouse model, demonstrated that most lung metastases consisted of non-EMT epithelial-like tumour cells, while inhibition of EMT by miR-200 overexpression did not impact lung metastasis. Interestingly, cancer cells that underwent EMT were resistant to cyclophosphamide treatment *in vitro* and *in vivo*, due to reduced cell proliferation, increased apoptotic resistance and upregulation of drug metabolising genes (Fischer et al.,

2015). Hence targeting components or mediators of the EMT programme represents an attractive anti-cancer strategy, which can tackle both metastasis and chemoresistance.

1.44 Aims of this study

Here, we aim to address an area of unmet therapeutic need and identify a novel strategy for the treatment of lung cancer. In particular we will:

1) Test the therapeutic potential of RSK4 targeting *in vitro* and *in vivo* (Chapter 3)

2) Identify prospective substrates and interactors of RSK1 and RSK4 (Chapter 4)

3) Elucidate the underlying mechanisms of p53 regulation by RSK family members (Chapter 5)

2. Materials & Methods

2.1 Mammalian cell culture

Cells were maintained at 37 °C in a humidified environment with 10% CO_2, 20% O_2, and grown in DMEM (Dulbecco's modified Eagle's medium) (Sigma Life Sciences, MO, USA) supplemented with 10% foetal calf serum (FCS), 100 units/mL penicillin, 100 µg/mL streptomycin, 2 mM L-glutamine (Sigma Life Sciences, MO, USA). CRISPR/Cas9-mediated RSK4 knockout (KO) A549 cell lines were previously generated in our lab (Rajat Roy, personal communication) (See CRISPR/Cas9-mediated RSK4 knockout). Stably-expressing cell lines HEK293A-EV, HEK293A-RSK1 and HEK293A-RSK4 were grown as described above and supplemented with 1 µg/mL puromycin (Sigma Life Sciences, MO, USA) to maintain selection (See Stably-expressing cell lines). *Kras*$^{LSL\text{-}G12D/+}$;*p53*$^{flox/flox}$ (KP) NSCLC mouse cells were kindly provided by J. Downward Lab (The Francis Crick Institute, London, UK). Urinary bladder cancer cell lines T24, TCCSUP and J82 were maintained at 37 °C in a humidified environment with 5% CO_2, 20% O_2, and grown in RPMI-1640 (Roswell Park Memorial Institute) (Sigma Life Sciences, MO, USA) supplemented with 10% foetal calf serum (FCS), 100 units/mL penicillin, 100 µg/mL streptomycin, 2 mM L-glutamine (Sigma Life Sciences, MO, USA). Unless otherwise stated the A549 cell line has been the primary cell line used throughout this study **(Table S 1)**.

2.2 CRISPR/Cas9-mediated RSK4 knockout

CRISPR/Cas9-mediated RSK4 knockout (KO) A549 cell lines were generated as described previously (Ran FA et al., 2013). The backbone vector pX458, pSpCas9(BB)-2A-GFP was a gift from Feng Zhang (Addgene plasmid #48139). Two guide RNA sequences were designed to target RSK4 gene (5'-CCCTATTACTCATCATGTTAAGG-3' on Exon 3 and 5'-TGGGCAGCTCTATGCAATGAAGG-3' on Exon 4). Forward and reverse oligonucleotides for each were annealed and phosphorylated using T4 DNA Ligase Reaction Buffer and T4 Polynucleotide Kinase (New England Biolabs, MA, USA) at 37°C for 30 min followed by 95°C for 5 min. pX458 was digested using BbsI (Thermo Scientific™, Thermo Fisher Scientific, MA, USA) at 37°C for 2 h, and gel purification was performed using a QIAquick Gel Extraction Kit (QIAGEN, Hilden, Germany). The ligation reactions of pX458 and the annealed oligonucleotides were performed at room temperature for 4 h using the T4 DNA ligase Kit (New

England Biolabs, MA, USA). Ligated products were purified using PlasmidSafe exonuclease (Cambio, Cambridge, UK) at 37℃ for 30 min. The plasmids were transformed into Stbl3 competent cells, and amplified using the PureLink® HiPure Plasmid Filter Maxiprep Kit (Invitrogen™, Thermo Fisher Scientific, MA, USA). Each plasmid was transfected into A549 cells by electroporation using amaxa Nucleofector II (Lonza, Basel, Switzerland) according to the manufacturer's protocol. The transfectants were selected using puromycin prior to isolation of clones by serial dilutions. Cell lines were tested for knockdown of RSK4 by western blotting and two clones were selected for further experiments. Hereafter referred to as cr421 (partial RSK4 KO) and cr437 (complete RSK4 KO).

2.3 EGF stimulation

Cells were serum-starved overnight (o/n) with 0.5% FCS and stimulated with 100 ng/mL EGF (epidermal growth factor) for 15 min in a 37 °C, 10% CO_2 incubator. RAS/MAPK pathway activation was confirmed by assessing phospho-p44/42 MAPK (Erk1/2) (Thr202/Tyr204) levels (by Western blotting) (Zhou et al., 2015; Tomshine et al., 2009).

2.4 Drug treatments

2.4.1 Cisplatin

Cisplatin (300.05 g/mol) (Sigma Life Sciences, MO, USA) was freshly prepared in DMSO (Dimethyl sulfoxide) at 200 mM stock concentration for crystal violet staining assays (See Crystal violet staining). For animal experiments, 5 mg/kg cisplatin was freshly prepared prior treatment (25 mg cisplatin dissolved in 250 µL DMSO; 30 µL DMSO+cisplatin diluted in 2970 µL PBS (phosphate-buffered saline)) (See Xenograft mouse model experiments & *Kras*$^{LSL\text{-}G12D/+}$/*p53*$^{flox/flox}$ (KP) driven genetically-engineered mouse model).

2.4.2 Paclitaxel (Taxol)

Taxol (853.906 g/mol) (Sigma Life Sciences, MO, USA) was dissolved in DMSO at 5 mM stock concentration and stored in -80 °C (See Crystal violet staining).

2.4.3 Trovafloxacin, Levofloxacin, Ciprofloxacin

Trovafloxacin (512.46 g/mol) (Tocris Bioscience, Bristol, UK) and levofloxacin (361.37 g/mol) (Sigma Life Sciences, MO, USA) were freshly prepared in DMSO, and ciprofloxacin (331.34 g/mol) (Sigma Life Sciences, MO, USA) in 0.1 M HCl (Hydrochloric acid). For western blotting, A549 and KP cells (3 x 10^5) were mixed with two-fold serially diluted trovafloxacin (0-15 µM) or ciprofloxacin (0-15 µM) or two-fold serially diluted levofloxacin (0-100 µM) before seeded into 6-well plates. Lysates were prepared for Western blotting 24 h post-treatment (See Western blotting). For cell motility and 3D collagen invasion assays, A549 cells (3 x 10^5) were mixed with 0 (i.e. 10 µM DMSO control), 5 or 10 µM trovafloxacin before seeded into 6-well plates (See Cell motility assay). For crystal violet assay, A549 cells (3 x 10^5) were mixed with two-fold serially diluted trovafloxacin or ciprofloxacin (0-30 µM) before seeded into 6-well plates (See Crystal violet staining). For animal experiments, 175 mg/kg trovafloxacin was freshly prepared prior treatment (90 mg trovafloxacin dissolved in 4.5 mL Milli-Q water) (See Xenograft mouse model experiments & *Kras*$^{LSL\text{-}G12D/+}$/*p53*$^{flox/flox}$ (KP) driven genetically-engineered mouse model).

2.4.4 BI-D1870

BI-D1870 (RSK Inhibitor II; 782.83 g/mol) (Calbiochem, Sigma Life Sciences, MO, USA) was dissolved in DMSO at 20 mM stock concentration and stored in -80 °C (See ATP-competitive pan-RSK inhibition).

2.4.5 Cycloheximide (CHX)

CHX (281.35 g/mol) (Sigma Life Sciences, MO, USA) was dissolved in DMSO at 50 mM stock concentration and stored in -20 °C (See Cycloheximide assay).

2.5 Small interfering RNA (siRNA) transient transfection

Cells of 40-60% confluency were transfected using Lipofectamine™ RNAiMAX Transfection Reagent (Invitrogen™, Thermo Fisher Scientific, MA, USA) as per the manufacturer's protocol. Transfection mixes were prepared in Opti-MEM Reduced Serum Medium (phenol red$^-$, HEPES$^+$, L-Glutamine$^+$) (Gibco^R Life Technologies, NY, USA). NT2 (non-targeting) scramble siRNA (Dharmacon Inc., CO, USA) was used as negative control. Unless

otherwise stated, siRNAs were used at a final concentration of 20 nM. Assays were performed 48-72 h post-transfection, as appropriate **(Table S 2 & Table S 3)**.

2.6 ATP-competitive pan-RSK inhibition: BI-D1870

For pan-RSK inhibition, 2.5 x 10^5 cells seeded in 6-well plates were serum-starved o/n with 0.5% FCS, stimulated with ± 100 ng/mL EGF for 15 min and treated with ± 10 µM BI-D1870 (See Drug treatments; BI-D1870) for 30 min (Sapkota et al., 2007) in a 37 °C, 10% CO_2 incubator (See EGF stimulation), before protein extraction and SDS-PAGE (See Western blotting).

2.7 Bacterial transformation

Plasmids were transformed into competent bacterial cells by heat shock. Briefly, 1 – 5 µL plasmid DNA was mixed into 20 – 50 µL of competent cells and incubated at 4 °C for 30 min. Each transformation tube was heat-shocked at 42 °C for 30 – 45 s, mixed with 250 µL SOC (Super Optimal broth with Catabolite repression) media and incubated in a 37 °C shaking incubator for 1 h. Bacteria were plated onto a 10 cm LB (lysogeny broth) agar plate containing the appropriate antibiotic (100 µg/mL ampicillin or 50 µg/mL kanamycin) and incubated at 37 °C o/n. Individual colonies were grown in 5 mL LB media with antibiotics for 4-6 h (pre-culture) before being transferred into 250 mL LB media with antibiotics and incubated in a 37 °C shaking incubator o/n. Cultures were pelleted by centrifugation and plasmids purified using PureLink® HiPure Plasmid Filter Maxiprep Kit (Invitrogen™, Thermo Fisher Scientific, MA, USA).

2.8 Expression vectors

GFP-p53 plasmid was purchased from Addgene (plasmid #12091). pCMV3-Myc-RPS6KA6 plasmid was purchased from Sino Biological (Catalogue number: HG10147-NM). FLAG-HA-HA tagged RSK1 and RSK4 were constructed by PCR (polymerase chain reaction) cloning. RSK4 transcript variant I (NM_014496.5) ORF (open reading frame) **(Table S 4 & Table S 5)** was PCR-amplified using RSK4-GFP as template (pLPS-3'EGFP backbone; Arizona State University plasmid repository, AZ, USA), and primers introducing a 5' XhoI (New England Biolabs,

MA, USA) restriction site prior to the start codon and a 3' EcoRI (New England Biolabs, MA, USA) restriction site after the stop codon **(Table S 6)**. RSK4 transcript variant II (NM_001330512.1) ORF was PCR-amplified from A549 cDNA, and primers introducing a 5' XhoI restriction site prior to the start codon and a 3' EcoRI restriction site after the stop codon. RSK1 transcript variant I (NM_002953.4) ORF was PCR-amplified using RSK1-pBABE as template (kindly provided by Blenis Lab, Weill Cornell Medicine, NY, USA), and primers introducing a 5' XhoI restriction site prior to the start codon and a 3' EcoRI restriction site after the stop codon. Double digested PCR products (XhoI/EcoRI) were cloned into a pLPC vector containing a FLAG-HA-HA tag (FH2) at the N-terminus, kindly provided by deLange Lab (The Rockefeller University, NY, USA), and transformed into One Shot® TOP10 Chemically Competent *E.coli* cells (Invitrogen™, Thermo Fisher Scientific, MA, USA) (See Bacterial transformation). Vectors were purified using PureLink® HiPure Plasmid Filter Maxiprep Kit (Invitrogen™, Thermo Fisher Scientific, MA, USA) and confirmed by full-length sequencing with overlapping primers (Genewiz, NJ, USA). RSK4 variant I plasmid hereafter referred to as RSK4-I FH2. RSK4 variant II plasmid hereafter referred to as RSK4-II FH2. RSK1 plasmid hereafter referred to as RSK1 FH2.

2.9 Stably-expressing cell lines

HEK293A cells were transfected with 2 µg pLPC-N'-FH2 empty vector (EV), RSK1 FH2 or RSK4-I FH2 (See cDNA transient transfection). At 48 h post-transfection, cells were treated with the selection antibiotic Puromycin (1 µg/mL) (Sigma Life Sciences, MO, USA), and media were replenished every 2-3 days until no more cell death occurred and only Puromycin-resistant cells (i.e. construct bearing cells) were selected. Untransfected cells and no antibiotic treated cells were used as controls. Resulting cell lines hereafter referred to as HEK293A-EV, HEK293A-RSK1 and HEK293A-RSK4 **(Table S 1)**.

2.10 *In vitro* site-directed mutagenesis

To generate kinase active (KA) and kinase dead (KD) RSK1 and RSK4 mutants, RSK1 FH2 and RSK4-I FH2 plasmids (See Expression vectors), were subjected to *in vitro* site-directed mutagenesis using the QuikChange II Site-Directed Mutagenesis Kit (Agilent Technologies, CA, USA). KA (RSK1: S221E; RSK4: S232E) and KD (RSK1:

S221A; RSK4: S232A) mutations were introduced by PCR amplification with primers synthesised to contain the desired mutation **(Table S 7)**. PCR thermal-cycling conditions were 95 °C for 30 s followed by 16 cycles of 95 °C for 30 s, 55 °C for 1 min and 68 °C for 11 min (1 min/kb of plasmid length). Following temperature cycling, reactions were *Dpn I* digested (1 µL of 10 U/µL enzyme) at 37 °C for 1 h to digest the parental, non-mutated dsDNA, and transformed into XL1-Blue supercompetent cells (Agilent Technologies, CA, USA) as previously described (See Bacterial transformation). Vectors were purified using PureLink® HiPure Plasmid Filter Maxiprep Kit (Invitrogen™, Thermo Fisher Scientific, MA, USA) and confirmed by full-length sequencing with overlapping primers (Genewiz, NJ, USA). RSK1 KA and KD mutant plasmids hereafter referred to as RSK1 S221E and RSK1 S221A, respectively. RSK4 KA and KD mutant plasmids hereafter referred to as RSK4 S232E and RSK4 S232A, respectively.

2.11 cDNA transient transfection

Cells of 60-80% confluency were transfected using Lipofectamine® 3000 Transfection Reagent (Invitrogen™, Thermo Fisher Scientific, MA, USA) as per the manufacturer's protocol. Transfection mixes were prepared in Opti-MEM Reduced Serum Medium (phenol red^{-}, HEPES^{+}, L-Glutamine^{+}) (Gibco^{R}, Life Technologies, NY, USA). Empty vector (EV) controls and expression vectors (See Expression vectors) were transfected at 2500 ng per 6-well plate. Media were changed 4-6 h post-transfection to reduce toxicity. Assays were performed 24-48 h post-transfection, as appropriate.

2.12 Preparation of cell lysates

Cells were washed twice with ice-cold PBS and lysed in ice-cold RIPA buffer (radioimmunoprecipitation assay buffer) (0.15 M NaCl, 50 mM Tris-HCl [pH 7.4], 0.1% SDS [sodium dodecyl sulfate], 1% Na-deoxycholate, 2 mM EDTA [pH 8.0], 2% Triton-X100) (added fresh: 2 mM DTT [dithiothreitol], 10 mM NaF, 1 mM Na_3VO_4, 10 mM β-glycerophosphate, 1X cOmplete™, Mini, EDTA-free protease inhibitor cocktail) (Sigma Life Sciences, MO, USA). Lysates were incubated on ice (on plates) for 10 min prior to scraping, and either sonicated or vortexed (2-3 times within 10 min) to shear DNA. Lysates were cleared by centrifugation (13,000 x g for 25 min) (protein

concentration was measured [See Bio-Rad protein assay]), and heated for 5-10 min at 100 °C in Laemmli sample buffer (0.02% bromophenol blue (BPB), 50% Glycerol, 10% SDS, 200 mM Tris-HCl [pH 6.8]) (added fresh: 200 mM DTT) prior to loading equal amounts (30-50 µg) (See Western blotting) or storing in -20 °C.

2.13 Bio-Rad protein assay

Protein concentrations were determined using the Bio-Rad Protein Assay Dye Reagent Concentrate (Bio-Rad Laboratories, Inc., CA, USA). Dye was prepared by diluting one part Dye Reagent Concentrate with five parts distilled, deionised (DDI) water. Cell lysates (2 µL) were mixed with 498 µL Dye. Bovine serum albumin (BSA) protein standards ranging from 0-20 µg/µL (five dilutions) were prepared in the same buffer supplemented with 2 µL RIPA buffer (cell lysis buffer). Protein solutions were loaded in duplicates (100 µL/well) in a 96-well microtiter plate and absorbance was read at 595 nm using the Sunrise™ microplate reader (Tecan, Männedorf, Switzerland). A standard curve was prepared and protein concentrations were determined from the resulting 'y=mx + c' equation.

2.14 Western blotting

Proteins were resolved by 8-15% SDS-PAGE (polyacrylamide gel electrophoresis) and electroblotted onto an Immobilon-P PVDF (polyvinylidene difluoride; activated in MeOH) (Merck Millipore, MA, USA) or nitrocellulose membrane (Thermo Scientific™, Thermo Fisher Scientific, MA, USA) using the Genie® electrophoretic transfer apparatus (Research Products International Corp., IL, USA). Transfer was confirmed by Ponceau S staining (Sigma Life Sciences, MO, USA). Membranes were blocked in 5% non-fat dried milk powder in 0.05% Tween-20 (polysorbate surfactant) in PBS for 1 h and immunoblotted with the appropriate primary (o/n) and secondary antibodies (1 h) **(Table S 8 & Table S 9)**. Membranes were washed three times with PBST (0.05% Tween-20) for 10 min before each incubation step and prior to developing. Blots were developed using Pierce™ ECL (enhanced chemiluminescence) western blotting substrate or SuperSignal™ west dura extended duration substrate (Thermo Scientific™, Thermo Fisher Scientific, MA, USA) for 1 min. Imaging was performed on X-ray autoradiography films (Jet X-Ray, London, UK) in a darkroom or using the FUSION SOLO chemi-imager

system (Analis, Suarlée, Belgium). Protein levels were quantified by densitometry using ImageJ software and normalised to loading control.

2.15 E-PAGE

RSK1 and RSK4 basal expression (protein) levels were assessed on a lung cancer cell line panel and other cancer cell lines from the NCI-60 human cancer cell line panel **(Table S 10 & Table S 11)**, using the E-PAGE™ 48 Protein Electrophoresis System (Invitrogen™, Thermo Fisher Scientific, MA, USA). Lysates were processed as previously described (See Preparation of cell lysates), prepared in 2.5 µL E-PAGE™ Loading Buffer 1 (4X) and 1 µL NuPAGE® Sample Reducing Agent (10X), and made up to 15 µL with DDI water. Wells were firstly loaded with 5 µL DDI water prior to running up to 20 µg protein (maximum) per lane of the E-PAGE™ 48 well 8% gel (20 µL total well volume). Gels were run on the Mother E-Base™ electrophoresis apparatus under program EP for 30 min (maximum). Gels were then electroblotted onto a membrane and incubated with the appropriate primary and secondary antibodies as previously described (See Western blotting).

2.16 RNA extraction

Total RNA was extracted from cells using the PureLink® RNA Mini Kit (Invitrogen™, Thermo Fisher Scientific, MA, USA) at room temperature (RT) as per the manufacturer's protocol. Briefly, cells were PBS washed and lysed in Lysis Buffer with 1% 2-mercaptoethanol (to inactivate enzymatic activity of intracellular RNases). Lysates were vortexed until the cell pellet was dispersed and were then loaded into a clean homogenisation tube and centrifuged at 13,000 x g for 2 min. To each volume of cell homogenate 70% EtOH (ethanol) was added and vortexed to mix thoroughly and disperse any visible precipitate. Sample was loaded onto the spin cartridge (with the collection tube) and centrifuged at 13,000 x g for 15 s to bind RNA to membrane. Flow-through was discarded. Membrane-bound RNA was washed three times (once with Wash Buffer I and twice with Wash Buffer II) and eluted in RNase-free water in a recovery tube. RNA concentration was quantified using the NanoDrop™ (Thermo Scientific™, Thermo Fisher Scientific, MA, USA) spectrophotometer and ND-

1000 Software. Purified RNA was stored in -80 °C or used for downstream applications (See cDNA conversion and Real-Time qRT-PCR).

2.17 cDNA conversion

Total RNA was reverse transcribed with random primers using the High Capacity cDNA Reverse Transcription Kit (Applied Biosystems™, Thermo Fisher Scientific, MA, USA) as per the manufacturer's protocol. Up to 1 µg RNA was cDNA converted per 20 µL reverse transcription reaction. PCR thermal-cycling conditions were 25 °C for 10 min, 37 °C for 120 min and 85 °C for 5 min. cDNA was stored in 4 °C (short-term) or -20 °C (long term) or used for downstream applications (See Real-Time qRT-PCR).

2.18 Real-Time qRT-PCR

For detection and quantification of gene transcripts, cDNAs (~ 12.5 – 25 ng) were amplified using 2X Fast SYBR Green Master Mix (Applied Biosystems™, Thermo Fisher Scientific, MA, USA) (SYBR Green I Dye, AmpliTaq Fast DNA Polymerase, Uracil-DNA Glycosylase, ROX dye Passive Reference, dNTPs and optimised buffer components) and 250-500 nM forward and reverse primers **(Table S 12)**. Samples were loaded into MicroAmp™ Fast Optical 96-Well Reaction Plates and run on the 7900HT Fast RT-PCR System (Applied Biosystems™, Thermo Fisher Scientific, MA, USA). PCR thermal-cycling conditions were 95 °C for 20 s (AmpliTaq Fast DNA Polymerase activation) and followed by 40 cycles of 95 °C for 1 s (denaturation) and 60 °C for 20 s (annealing/extension). Primer efficiency was tested with standard curves and an additional cycle of 95 °C for 15 s, 60 °C for 15 s and 95 °C for 15 s was performed to obtain dissociation curves for each primer pair. Data were recorded using the Sequence Detection System (SDS version 2.4; Applied Biosystems, MA, USA). All data were analysed using the $\Delta\Delta C_t$ method, where threshold cycle (*Ct*) represents the intersection between the amplification curve and a threshold line (i.e. the relative measure of the concentration of target in the PCR reaction). All mRNA levels were normalised to housekeeping gene mRNA levels (i.e. ***HPRT***; Hypoxanthine-guanine phosphoribosyltransferase).

2.19 Cycloheximide (CHX) assay

To ensure uniform knockdown efficiency between different cycloheximide time-points, 7 x 10^5 A549 cells were initially seeded in 10 cm dishes prior to NT, RSK1 or RSK4 siRNA transfection (See siRNA transient transfection). 24 h post-transfection, cells were re-plated in 60 mm plates (one 60 mm plate/cycloheximide time-point) and allowed to adhere o/n. To assess p53 protein stability, cells were treated with 50 µM (~ 15 µg/mL) CHX (See Drug treatments; Cycloheximide) and protein was extracted at 0 (DMSO control), 2.5, 5, 10, 15, 20, 30, 60 and 90 min post-CHX treatment (Anwar, Norris & Fujita, 2011).

2.20 Co-Immunoprecipitation (Co-IP)

Up to 3 µg Anti-FLAG® (M2) antibody produced in mouse (Sigma, F1804) or anti-FLAG® antibody produced in rabbit (Sigma, F7425) were conjugated to Protein G (Invitrogen, Cat.: 10004D) and Protein A (Invitrogen, Cat.: 10002D) magnetic beads, respectively (~ 35 µL beads in 1 mL 3% BSA/1% Triton X-100 in PBS incubated at 4 °C under rotary agitation o/n). Antibody-conjugated beads were washed three times with 1% Triton X-100 PBS. For RSK1-p53 and RSK4-p53 interactions, HEK293A-EV, HEK293A-RSK1, HEK293A-RSK4 stable cells (See Stably-expressing cell lines) were transiently transfected with 20 µg GFP-p53 (Addgene, plasmid #12091) in 15 cm dishes (4 x 10^6 cells/dish). Media were changed 4-6 h post-transfection to reduce toxicity. Cells were lysed 48 h post-transfection in IP lysis buffer (50 mM HEPES [pH 7.4], 150 mM NaCl, 2 mM EDTA [pH 8.0], 1% Triton X-100, 10% Glycerol) (added fresh: 10 mM NaF, 1 mM Na_3VO_4, 10 mM β-glycerophosphate, and 1X cOmplete™, Mini, EDTA-free protease inhibitor cocktail) (Sigma Life Sciences, MO, USA). For RSK1-RSK4 interaction, HEK293A-EV and HEK293A-RSK1 stable cells (See Stably-expressing cell lines) were transiently transfected with 20 µg Myc-RSK4 (Sino Biological, Cat.: HG10147-NM) in 15 cm dishes and processed as described above. Whole cell lysate (input) was prepared before up to 3 mg of lysate was incubated with antibody-conjugated beads at 4 °C under rotary agitation for 4 h. Beads were then washed three times with IP lysis buffer (see above) to remove unbound protein. Bound proteins were eluted from the beads with 2X Laemmli sample buffer (~ 25 µL) and analysed by SDS-PAGE (See Western blotting).

2.21 FLAG® HA Tandem Affinity Purification (TAP): Isolation of RSK1 and RSK4 complexes

FLAG®-HA dual-tagged fusion proteins RSK1, RSK4 variant I and RSK4 variant II were isolated from whole HEK293A cell lysates using the FLAG® HA Tandem Affinity Purification (TAP) technology (Ye et al., 2004b; Ye et al., 2004a; Rigaut et al., 1999). RSK1 FH2, RSK4-I FH2 and RSK4-II FH2 previously cloned in tandem-linked FLAG®-HA constructs (See Expression vectors) and pLPC-N'-FH2 empty vector (EV), were transiently transfected (20 µg) in HEK293A cells in 15 cm dishes (4 x 10^6 cells/dish). Media were changed 4-6 h post-transfection to reduce toxicity. 24 h post-transfection, cells were serum-starved o/n with 0.5% FCS and stimulated with 100 ng/mL EGF for 15 min (See EGF stimulation). Cells were lysed 48 h post-transfection in IP lysis buffer (50 mM HEPES [pH 7.4], 150 mM NaCl, 2 mM EDTA [pH 8.0], 1% Triton X-100, 10% Glycerol) (added fresh: 10 mM NaF, 1 mM Na_3VO_4, 10 mM β-glycerophosphate, and 1X cOmplete™, Mini, EDTA-free protease inhibitor cocktail) (Sigma Life Sciences, MO, USA). Up to 5 µg Anti-FLAG® (M2) antibody produced in mouse (Sigma, F1804) was conjugated to Protein G (Invitrogen, Cat.: 10004D) magnetic beads (~ 60 µL beads in 1 mL 3% BSA/1% Triton X-100 in PBS incubated at 4 °C under rotary agitation o/n). Antibody-conjugated beads were washed three times with 1% Triton X-100 PBS. Whole cell lysate (input) was prepared before up to 5 mg of lysate was incubated with antibody-conjugated beads at 4 °C under rotary agitation o/n. Beads were then washed three times with IP lysis buffer (see above) to remove unbound protein. Tandem tagged FLAG®-HA proteins were competitively eluted from Anti-FLAG® beads (1st elution) by incubating beads with 500 µg 3XFLAG® peptide (prepared in Tris-buffered saline [TBS]) (Sigma, F4799) in TBS (+phosphatase/protease inhibitors) at 4 °C under rotary agitation for 2 h. Eluate was incubated with Pierce™ Anti-HA magnetic beads (50 µL/condition) (Thermo Scientific™, Cat.: 88836) at 4 °C under rotary agitation for 2 h. Beads were then washed three times with IP lysis buffer (see above) to remove unbound protein. Bound proteins were eluted from the beads (2nd elution) with 2X Laemmli sample buffer (~ 25 µL), denatured and separated by SDS-PAGE (See Western blotting).

2.22 FLAG® HA Tandem Affinity Purification (TAP): Liquid chromatography tandem mass spectrometry (LC-MS/MS)

Gel lanes were then excised into 32 1-2 mm gel slices per condition and prepared for mass spectrometric analysis (Mark Skehel, MRC Laboratory of Molecular Biology, Cambridge, UK) using the JANUS® automated liquid handling system (PerkinElmer, Beaconsfield, UK). Excised protein gels were placed in 96-well clear V-bottom microplates (Corning Inc., NY, USA), reduced with 10 mM DTT (1 h at 56 °C) and alkylated with 55 mM iodoacetamide (1 h at RT). Following alkylation, proteins were digested with 6 ng/µL trypsin (Promega, Southampton, UK) o/n at 37 °C. The resulting peptides were extracted in 2% v/v formic acid (CH_2O_2), 2% v/v acetonitrile (CH_3CN; ACN). Digests were analysed by nano-scale capillary liquid chromatography tandem mass spectrometry (LC-MS/MS) using an UltiMate U3000 HPLC (high performance liquid chromatography) (Thermo Scientific™, Thermo Fisher Scientific, MA, USA) to deliver a flow of approximately 300 nL/min. An Acclaim™ PepMap™ 100 C18, 5 µm, 100 µm x 20 mm nanoViper™ (Thermo Scientific™, Thermo Fisher Scientific, MA, USA), trapped the peptides prior to separation on an Acclaim™ PepMap™ 100 C18, 3 µm, 75 µm x 250 mm nanoViper™ (Thermo Scientific™, Thermo Fisher Scientific, MA, USA). Peptides were eluted with a 60 min gradient of acetonitrile (2% to 80%). The analytical column outlet was directly interfaced via a nano-flow electrospray ionisation source, with a hybrid quadrupole orbitrap mass spectrometer (Q-Exactive™ Plus Hybrid Quadrupole-Orbitrap) (Thermo Scientific™, Thermo Fisher Scientific, MA, USA).

2.23 FLAG® HA Tandem Affinity Purification (TAP): LC-MS/MS data analysis

Data dependent analysis was carried out using a resolution of 30,000 for the full MS spectrum, followed by ten MS/MS spectra. MS spectra were collected over a m/z (mass-to-charge ratio) range of 300–2000. MS/MS scans were collected using a threshold energy of 27 for higher energy collisional dissociation (HCD). LC-MS/MS data were then searched against the human protein database UniProtKB/Swiss-Prot (148,327 entries; 2016 database) using the Mascot search engine programme version 2.4.1 (Matrix Science, London, UK) (Perkins et al., 1999). Database search parameters were set with a precursor tolerance of 10 ppm (parts per million) and a fragment ion mass tolerance of 0.15 Da. One missed enzyme cleavage was allowed and variable

modifications for oxidized methionine, carbamidomethyl cysteine, pyroglutamic acid, phosphorylated serine, threonine and tyrosine. MS/MS data were validated using the Scaffold programme, version 4.8.4 (Proteome Software Inc., OR, USA). Peptide identifications were accepted if they could be established at greater than 50% probability by the Peptide Prophet algorithm with Scaffold delta-mass correction (Peptide false discovery rate [FDR]: 11.4%) (Keller et al., 2002). Protein identifications were accepted if they could be established at greater than 50% probability and contained at least 2 identified peptides (Protein FDR: 1.6%). Protein probabilities were assigned by the Protein Prophet algorithm (Nesvizhskii et al., 2003). Proteins that contained similar peptides and could not be differentiated based on MS/MS analysis alone were grouped to satisfy the principles of parsimony. All data were additionally interrogated manually. Resulting data were then used to build directed functional networks in Cytoscape using the Reactome FI (functional interaction) plugin (Wu, Feng & Stein, 2010). Modules were then isolated based on network connectivity and gene ontology (GO) enrichment analysis (FDR: <5%, *P*-value ≤5%) (Olivier Pardo, Imperial College London, London, UK).

2.24 Global proteomics and phosphoproteomics: Liquid chromatography tandem mass spectrometry (LC-MS/MS)

A549 cell total proteome and phosphoproteome were profiled downstream of RSK1 or RSK4 silencing (Howard Desmond, Paul Huang, The Institute of Cancer Research, London, UK). Cells transiently transfected with NT2 (non-targeting), RSK1 or RSK4 siRNA (two separate siRNA pools for each target: Dharmacon and Qiagen pools) (See siRNA transient transfection) **(Table S 2 & Table S 3)** were lysed in 8 M urea (Sigma Life Sciences, MO, USA) to denature proteins and protein concentration was measured by BCA protein assay kit (Thermo Scientific™, Thermo Fisher Scientific, MA, USA). A total of 100 µg protein per condition was then incubated with 10 mM TCEP (1 h at 56 °C) to reduce disulphide bonds and alkylated with 100 mM iodoacetamide (40 min at RT). Samples were adjusted to 2 M urea, 100 mM tetraethylammonium bicarbonate and proteins were digested with 6 ng/µL trypsin (Promega, Southampton, UK) o/n at 37 °C. Peptides were then desalted on a Sep-Pak C18 Plus Short Cartridge (Waters Corporation, MA, USA) and dried in a SpeedVac concentrator (Thermo Scientific™, Thermo Fisher Scientific, MA, USA). Each sample was resuspended in 100 µL of 100 mM

tetraethylammonium bicarbonate buffer and labelled with Tandem Mass Tag™ (TMT™) 10-plex Isobaric Mass Tag Labelling Reagents (Thermo Scientific™, Thermo Fisher Scientific, MA, USA) as per the manufacturer's protocol. Briefly, TMT label reagents were equilibrated to RT and dissolved in 42 µL of LC-MS grade anhydrous acetonitrile (Thermo Scientific™, Thermo Fisher Scientific, MA, USA). Each TMT label reagent was added to one sample (100 µg protein digest/condition) and incubated for 1 h at RT. Reactions were quenched with 5% (w/w) hydroxylamine (H_3NO) for 15 min at RT before equal amounts were combined and desalted on a Sep-Pak C18 Plus Short Cartridge (Waters Corporation, MA, USA). Following desalting, 20% of the pooled, labelled sample was dried in a SpeedVac concentrator for total proteome analysis, while the remaining 80% was dried for phosphopeptide enrichment by immobilised metal affinity chromatography (IMAC), as previously described (Vyse et al., 2018; Erdjument-Bromage, Huang & Neubert, 2018; Tan et al., 2017), for the phosphoproteome analysis. Total proteome samples were dissolved in 100 µL of Buffer A (5 mM KH_2PO_4 in 20% ACN, pH 2.7) and fractionated by strong cation-exchange (SCX) chromatography on 2.1 x 100 mm, 5 µm, 200A PolySULFOA column (PolyLC Inc., MD, USA) using a 30 min linear gradient (0-40%) of Buffer B (5 mM KH_2PO_4, 0.5 M NaCl in 20% ACN, pH 2.7) at a flow rate of 200 µL/min. Twelve fractions were collected, desalted by Bond Elut C18 OMIX tips (Agilent Technologies, CA, USA) and dried in a SpeedVac concentrator. IMAC-enriched and total proteome samples were analysed by LC-MS/MS using an UltiMate™ 3000 RSLCnano system coupled to Q-Exactive™ Plus Hybrid Quadrupole-Orbitrap™ Mass Spectrometer (Thermo Scientific™, Thermo Fisher Scientific, MA, USA). Peptides were separated on an Acclaim™ PepMap™ 100 C18, 3 µm, 75 µm x 50 cm column over 90 min for total proteome and 120 min for phosphoproteome.

2.25 Global proteomics and phosphoproteomics: LC-MS/MS data analysis

The acquired LC-MS/MS data were processed by MaxQuant (version 1.6.2.6.) and searched against the human protein database UniProtKB/Swiss-Prot (42,148 sequences, downloaded on 09/02/2017) using the Andromeda search engine (Cox et al., 2011) with the following parameters: MS-2 reporter ion quantification with reporter ion mass tolerance of 0.003 Da; maximum 2 miscleavages; fixed modifications: carbamidomethylation of cysteines, TMT label on lysin and peptide N-terminus; variable modifications:

deamidation of glutamine and asparagine, oxidation of methionine; calibration search peptide tolerance of 20 ppm; main search peptide tolerance of 4.5 ppm; 1% FDR threshold on peptide and protein level. Results were further Log2 transformed and each sample was median-centred in Perseus (version 1.5.6.0) (Tyanova et al., 2016). Final sample-reference ratios were calculated in Microsoft Office Excel 2013. Resulting data were then used to build directed functional networks in Cytoscape using the Reactome FI (functional interaction) plugin (Wu, Feng & Stein, 2010). Modules were then isolated based on network connectivity and gene ontology (GO) enrichment analysis (FDR: <5%, *P*-value ≤5%) (Olivier Pardo, Imperial College London, London, UK).

2.26 *In vitro* kinase assay

Recombinant human (full length) RSK4 (rRSK4) (i.e. the kinase) was kindly provided by Dr Filippo Prischi (University of Essex, Colchester, UK). Recombinant human (full length) RSK1 (rRSK1) (i.e. the kinase) and MDM2 (rMDM2) (i.e. the substrate) were purchased from Abcam (Cambridge, UK) (rRSK1: ab159427; rMDM2: ab82080). Increasing concentrations of rMDM2 (0.25 µg, 0.50 µg and 1.0 µg) were incubated with 1.0 µg of rRSK1 or 1.0 µg of rRSK4 in the presence of Kinase Buffer (KB) (50 mM HEPES, 10 mM $MgCl_2$, 10 mM β-glycerophosphate, 1 mM DTT) supplemented with 2 mM fresh ATP, for 15 min at RT. Kinase alone or substrate alone controls were also run in parallel. All conditions were mixed with Laemmli sample buffer and analysed by SDS-PAGE (See Western blotting).

2.27 Cell motility assay (time-lapse migration)

A549 cells were seeded in 6-well plates and transfected with RSK4 siRNA, RSK4 cDNA, or treated with trovafloxacin (See Drug treatments; Trovafloxacin, Levofloxacin, Ciprofloxacin) as previously described. The following day, cells were trypsinised and re-plated into black clear flat bottom 96-well imaging plates (BD Biosciences, NJ, USA) at a density of 1 x 10^3/well. Cells were allowed to adhere o/n in a 37 °C, 10% CO_2 incubator. Time-lapse brightfield imaging was performed for 18 h (1 image/10 min) in a 37 °C, 10% CO_2 environment, using the Zeiss Axiovert 100 Inverted Widefield Microscope (MRC, Imperial College, London, UK) driven by Metamorph software package (Molecular Devices, Chicago, IL, USA). Brightfield images were taken

at three sites per well (5 wells/condition). Cells were manually tracked (5 cells/3 sites/5 wells; n=75/condition) using FIJI Image-J's manual tracking plugin. Migration speed (arbitrary units) and X/Y tracking (arbitrary units) were analysed using "Cell Migration analysis.R" script written in RStudio 0.99.89 by Dr Olivier Pardo (Division of Cancer, Imperial College London, London, UK; o.pardo@imperial.ac.uk) (Lara et al., 2011).

2.28 3D collagen invasion assay

A549 cells were seeded in 6-well plates and treated with trovafloxacin as previously described (See Drug treatments; Trovafloxacin, Levofloxacin, Ciprofloxacin). The following day, cells were trypsinised and re-plated into black clear flat bottom 96-well imaging plates (BD Biosciences, NJ, USA) at a density of 12 x 10^3/well. Cells were allowed to adhere o/n in a 37 °C, 10% CO_2 incubator. Media were aspirated and replaced with 100 µL type-I rat-tail collagen (Gibco™, Thermo Fisher Scientific, MA, USA) supplemented with 5X DMEM (20%) and FCS (0.01%), and incubated for 1 h (37 °C, 10% CO_2) until collagen polymerised. Subsequently, 50 µL complete DMEM (Sigma Life Sciences, MO, USA) supplemented with epidermal growth factor (EGF; 1 µg/mL) was added per well to encourage invasion of cells upwards through the polymerised collagen matrix. Cells were incubated (37 °C, 10% CO_2) for 48 h prior fixing with 4% paraformaldehyde (PFA) supplemented with 1.25 µM sytox green fluorescent nuclear stain (Invitrogen™, Thermo Fisher Scientific, MA, USA). Using the Zeiss AxioObserver Inverted Widefield Microscope (FILM, Imperial College London, UK) with VivaTome Spinning Disc system and EC Plan-Neofluar 10x/0.30 Ph 1 Objective, 131 stacks of 500 µm were taken at 7 sites per well. Images were deconvoluted using Huygens deconvolution software (FILM, Imperial College London, UK) and analysed using FIJI Image-J's 3D object counter plugin and macro script written by Stephen Rothery (FILM, Imperial College London, UK). The Z distances were normalised to the median, averaged per condition, and normalised to control (Lara et al., 2011).

2.29 Crystal violet staining (cell viability)

A549 cells were seeded in 6-well plates and transfected with RSK4 siRNA, RSK4 cDNA, or treated with trovafloxacin or ciprofloxacin (See Drug treatments; Trovafloxacin, Levofloxacin, Ciprofloxacin) as previously

described. For cDNA transfections, media were changed 4-6 h post-transfection to reduce toxicity. The following day, cells were trypsinised and re-plated into flat bottom 96-well plates at a density of 2-3 x 10^3/well and allowed to adhere o/n in a 37 °C, 10% CO_2 incubator. cr421 and cr437 RSK4 KO cells (See Mammalian cell culture) were seeded directly into 96-well plates at a density of 2-3 x 10^3/well. Cells were treated with increasing concentrations of 0-100 nM (2-fold dilutions) paclitaxel (Taxol) or 0-100 µM (2-fold dilutions) cisplatin (See Drug treatments; Cisplatin, Paclitaxel). Media were removed (gentle tap on tissue) 48-72 h post-drug treatment and cells were fixed and stained with 0.5% (w/v) crystal violet in 25% (v/v) methanol for 30 min - 1 h at RT. Plates were thoroughly washed and air-dried o/n. Crystal violet was reconstituted in 10% (v/v) acetic acid under gentle agitation for 1 h at RT. Absorbance was read at 595 nm using the Sunrise™ microplate reader (Tecan, Männedorf, Switzerland). Technical replicates (3-6) were averaged and normalised to the DMSO control values (i.e. the '0'). Values were plotted following the log(inhibitor) vs. response curve in Prism (GraphPad Software, CA, USA) and IC50 (inhibitory concentration) was derived.

2.30 Caspase-Glo 3/7 activity assay

The Caspase-Glo® 3/7 assay (Promega, Southampton, UK) was performed as per the manufacturer's protocol. Briefly, the Caspase-Glo® 3/7 Buffer and lyophilized Caspase-Glo® 3/7 Substrate were equilibrated to RT before transferring the contents of Caspase-Glo® 3/7 Buffer into the Caspase-Glo® 3/7 Substrate vial (i.e. the Caspase-Glo® 3/7 Reagent). Equal volume of Caspase-Glo® 3/7 Reagent to samples (i.e. 100 µl) was added per 96-well of a solid white flat bottom 96-well luminescence plate (Corning Inc., NY, USA). Plates were incubated at RT in the dark for 30 mins and luminescence was recorded using the PHERAstar microplate reader (BMG Labtech, Aylesbury, UK).

2.31 Immunostaining & confocal microscopy

A549 or HEK293A cells were grown on 12 mm round glass coverslips, and when reached the desired confluency, fixed with 4% PFA in PBS for 10 min at RT. For HEK293A cells, coverslips were pre-coated with 50 µg/mL poly-D-Lysine (Sigma Life Sciences, MO, USA) to enhance adhesion. Cells were PBS-washed three times

and permeabilised with 0.1% Triton-X100 (Sigma Life Sciences, MO, USA) in PBS for 5 min at RT. Cells were PBS-washed three times and blocked in 5% BSA in PBS for 1 h at RT. Following staining with the appropriate primary antibodies **(Table S 13)** in 1% BSA in PBS for 1 h at RT, coverslips were PBS-washed three times and incubated with the appropriate secondary antibodies **(Table S 14)** in 1% BSA in PBS for 1 h at RT. Coverslips were PBS-washed three times, counterstained with Hoechst (Invitrogen™, Thermo Fisher Scientific, MA, USA) and mounted on microscope slides with Fluoro-Gel (Laborimpex, Brussels, Belgium). For actin cytoskeleton staining, cells grown on coverslips were fixed, permeablised and blocked as described above, before staining with 1X (165 nM) Alexa Fluor™ 488® Phalloidin (F-actin) (Invitrogen™, Thermo Fisher Scientific, MA, USA) in PBS for 1 h at RT. For EGF stimulation, cells grown on coverslips were serum-starved o/n with 0.5% FCS and stimulated with 100 ng/mL EGF for 15 min (See EGF stimulation), before fixing with 4% PFA. For mitochondrial staining, cells grown on coverslips were incubated with 250 nM MitoTracker® Red CMXRos (Invitrogen™, Thermo Fisher Scientific, MA, USA) prepared in culture medium without FCS, for 15-20 min at 37 °C, before fixing with 4% PFA. Images were captured using the Zeiss LSM-780 inverted laser scanning confocal microscope (FILM, Imperial College London, UK) equipped with a 63X/1.40 numerical aperture (NA) Plan Apochromat Oil immersion objective lens (Carl Zeiss MicroImaging, Jena, Germany).

2.32 Animal experiments

All animal experiments were performed under a UK Home office approved project license and following institutional welfare guidelines.

2.32.1 Xenograft mouse model experiments

To assess tumour growth *in vivo* downstream of RSK4 KO in the absence of chemotherapeutic treatment, 5 x 10^6 A549-NT, cr421 (RSK4#1) or cr437 (RSK4#2) A549 cells were injected subcutaneously into the flanks of female BALB/c-nu/nu nude mice (Yulan Wang[25]). When tumours reached 50 mm^3, daily tumour measurements

[25] Key Laboratory of Magnetic Resonance in Biological Systems, National Centre for Magnetic Resonance in Wuhan, State Key Laboratory of Magnetic Resonance and Atomic and Molecular Physics, Wuhan Institute of Physics and Mathematics, Chinese Academy of Sciences, Wuhan, China.

for 46 days were performed by caliper and volumes calculated based on the ellipsoid volume formula: V= (length (mm)) x (width (mm)) x (height (mm)) x π/6.

To assess tumour growth *in vivo* downstream of RSK4 KO following a cycle of cisplatin treatment, 5 x 10^6 A549-NT or cr437 (RSK4#2) A549 cells were injected subcutaneously into the flanks of female BALB/c-nu/nu nude mice (Yulan Wang[1]). When tumours reached 50 mm^3, mice were treated ± 5 mg/kg cisplatin (dissolved in DMSO) in PBS (See Drug treatments; Cisplatin) intraperitoneally (IP) twice-weekly (vehicle control: DMSO+PBS IP injection), for 46 days. End-point (day 46) tumour measurements were performed by caliper and volumes calculated based on the ellipsoid volume formula: V= (length (mm)) x (width (mm)) x (height (mm)) x π/6.

To assess metastasis *in vivo* downstream of RSK4 KO, 1 x 10^6 A549-NT or cr437 (RSK4#2) A549 cells were tail vein-injected into SCID (severe combined immunodeficient) mice (n=8/condition) and tumours left to develop for 8 weeks (Yulan Wang[1]). The animals were then sacrificed and their lungs extracted, formalin-fixed and paraffin-embedded (FFPE). 10 microtome slices per lung over a depth of 600 µm (each separated by 60 µm) were H&E (haematoxylin and eosin) stained and analysed microscopically for the presence of tumour nodules (i.e. lung area colonised (%) and number of tumour nodules) (Francesco Mauri, Imperial College London, London, UK).

To assess *in vivo* efficacy of trovafloxacin following a cycle of cisplatin treatment, 5 x 10^6 luciferase-expressing A549 cells (A549-Luc) were injected subcutaneously into the flanks of female BALB/c-nu/nu nude mice (Rajat Roy, Silvia Ottaviani, Joel Abrahams, Imperial College London, London, UK). When tumours reached 50 mm^3, mice were treated ± 5 mg/kg cisplatin (dissolved in DMSO) in PBS (See Drug treatments; Cisplatin) intraperitoneally (IP) weekly and ± 175 mg/kg trovafloxacin (Shaw et al., 2007; Thadepalli et al., 1997) (dissolved in Milli-Q water) (See Drug treatments; Trovafloxacin) by daily oral gavage (vehicle controls: DMSO+PBS IP injection, Milli-Q water oral gavage), for 14 days. Following injection of luciferin, representative images from each condition were acquired using a luminometric small-animal imager at day 0 and 14, and

percentage change in tumour volume at day 14 was plotted. Animals were sacrificed, tumours extracted and snap frozen or FFPE for further analysis.

2.32.2 $Kras^{LSL\text{-}G12D/+}/p53^{flox/flox}$ (KP) driven genetically-engineered mouse model

To assess *in vivo* efficacy of trovafloxacin following a cycle of cisplatin treatment in an autochthonous conditional tumour model, we utilised the $Kras^{LSL\text{-}G12D/+;p53^{flox/flox}}$ (KP) NSCLC mouse model (Tyler Jacks, Koch Institute for Integrative Cancer Research, MIT, MA, USA). To generate sporadic lung tumours, the lungs of this mice were infected via intratracheal intubation with 1 x 10^6 pfu (plaque-forming unit) adenovirus expressing Cre recombinase (Gene Transfer Vector Core, MA, USA), as previously described, (DuPage, Dooley & Jacks, 2009) to induce concomitant activation of oncogenic KRAS and deletion of tumour suppressor p53 (Jackson et al., 2005) (David Hancock, Christopher Moore, Miriam Molina Arcas, Julian Downward, The Francis Crick Institute, London, UK). Mice were allowed to develop lung tumours as detected by micro-computerised tomography (CT) scanning (scan 1) (SkyScan 1176, Accela, Prague, Czech Republic). They were then treated ± 5 mg/kg Cisplatin (dissolved in DMSO) in PBS (See Drug treatments; Cisplatin) intraperitoneally (IP) weekly and ± 175 mg/kg trovafloxacin (Shaw et al., 2007; Thadepalli et al., 1997) (dissolved in Milli-Q water) (See Drug treatments; Trovafloxacin) by daily oral gavage (5 days/week) (vehicle controls: DMSO+PBS IP injection, Milli-Q water oral gavage), for 3 weeks. At the end of the treatment period mice were re-scanned (scan 2). Micro-CT analysis was performed in SkyScan 1176. Micro-CT data were reconstructed using NRecon software (SkyScan), imaged using DataViewer and tumour volumes were calculated using the CT-analyser program (CTAn, SkyScan). Changes in the volume (mm^3) of individual tumours from scan 1 to scan 2 were calculated and expressed as percentage volume change of either individual tumours or total tumour burden. Animals were sacrificed, lungs extracted and either snap frozen or NBF (neutral buffered formalin)/EtOH fixed and paraffin embedded for further analysis.

2.33 Immunohistochemistry (IHC) & Tissue MicroArrays (TMAs)

Commercial tissue microarrays (TMAs) (LC1006, LC10010, LC1201) containing 64 LUAD (lung adenocarcinoma), 51 LUSC (lung squamous cell carcinoma), 12 LCC (large cell carcinoma), 56 SCLC (small cell lung cancer) and 25 normal lung samples were purchased from US Biomax, Inc. (Rockville, MD, USA).

A post-mortem home-made TMA containing syngeneic primary tumour/metastasis samples from 98 lung cancer patients was prepared. This protocol received full approval by an accredited Research Ethics Committee (Reference: 06/Q0406/154). Briefly, 12,580 post-mortem examinations performed at Hammersmith Hospital (London, UK) between January 1970 and December 2005 were reviewed from the Royal Postgraduate Medical School archives, and searched for metastatic lung cancer samples. This resulted in 499 cases, of which patients who underwent anticancer treatment, as determined by post-mortem reports and medical notes, were excluded (n=286). FFPE tissue blocks pertaining to 213 patients were retrieved in total. Tissues were further screened based on: (1) confirmed histopathologic metastatic lung cancer diagnosis, (2) autolytic degeneration of the target tissues, (3) complete post-mortem dissection of all organs and (4) post-mortem interval <24 h from death. Histotype classification and metastatic distribution was confirmed following examination of newly cut H&E sections by a consultant pulmonary pathologist (Francesco Mauri, Imperial College London, London, UK). The suitability of both primary and metastatic tissues for IHC was confirmed by preliminary immunostaining for two pan-cytokeratin (CK) markers: MNF116 (Dako, Cambridge, UK), incubated at 1:200 dilution for 1 h and CK CAM5.2 (BD Biosciences, NJ, USA), incubated at 1:20 dilution for 1 h following 0.1% trypsin in PBS incubation for 10 min. Specimens with unsatisfactory MNF116/CK CAM5.2 staining were discarded. Considering the above quality criteria, a total of 98 cases were suitable for this experiment. A TMA was then constructed by re-embedding 1 mm cores from the most representative and best preserved areas of the tumours in microarray blocks.

Unlike the rest of this work, where the RSK4 Abcam antibody (ab76117) was used, IHC was performed using the RSK4 Sigma Prestige antibody (HPA002852) **(Table S 8)**. This is because the RSK4 Abcam (ab76117) antibody

did not adequately work by IHC, while it also detects a nuclear signal (by Immunofluorescence) that is not specific to RSK4 (as assessed by knocking-down RSK4; data not shown). Signal specificity for the RSK4 Sigma Prestige antibody (HPA002852) was determined using RSK4-silenced paraffin embedded A549 cells. RSK4 expression levels were semi-quantified using an IHC score, calculated by multiplying staining intensity with the percentage of positive cells (Herberger et al., 2007).

2.34 Statistical analysis

All statistical analyses were performed in Prism (GraphPad Software, CA, USA). Normally distributed continuous variables were assessed by an unpaired Student's *t*-test or two-way ANOVA, and $P \leq 0.05$ was interpreted to denote statistical significance. All results are presented as the mean ± SEM.

3. RSK4 targeting: A new therapeutic strategy against drug resistance and metastasis in non-small cell lung cancer

3.1 Introduction

Lung cancer is the most commonly diagnosed cancer and the leading cause of cancer death globally, accounting for 11.6% of all new cancer cases and 18.4% of the total cancer-related deaths in 2018 (Bray et al., 2018). In the UK, lung cancer is the third most common cancer in males and the second most common cancer in females, while it is ranked first in terms of mortality rates in both sexes (Bray et al., 2018). Non-small cell lung cancer (NSCLC) accounts for 80%-85% of lung cancer cases of which lung adenocarcinoma (LUAD; 40%) prevails. The five-year survival rate for lung cancer is less than five percent for distant tumours and this is due to late stage diagnosis and the onset of metastatic drug-resistant disease. Hence, a better understanding of the mechanisms underlying these biological processes is urgently required to improve clinical outcome.

The p90 (90 kDa) Ribosomal Protein S6 Kinases (RPS6KAs; RSKs) are highly conserved serine/threonine protein kinases that signal downstream of the RAS/MAPK pathway **(Figure 6)** and are implicated in diverse cellular processes including protein synthesis, transcriptional regulation, cell survival, migration and invasion (Lara, Seckl & Pardo, 2013). RSK constitutes a family of four human isoforms (RSK1-4), which are 73%-80% identical at the protein level, and are uniquely characterised by the presence of two functional and non-identical kinase catalytic domains **(Figure 7)**. While RSK1 and RSK2, the most studied isoforms in cancer, are considered to be tumour promoters, RSK3 and RSK4 are thought to act in a tumour suppressive manner (Houles & Roux, 2018). However, this notion is being challenged with reports indicating that RSK1 suppresses lung cancer cell migration and invasion (Lara et al., 2011), and RSK3/4 mediate resistance to PI3K inhibitors in breast cancer (Serra et al., 2013). Thus, questioning the effectiveness of pan-RSK inhibitors for cancer treatment and paving the way for the development of RSK isoform-specific inhibitors.

RSK4, unlike RSK1-3, is predominantly cytosolic, constitutively active and does not require PDK1 for its activation. Therefore, RSK4 is emerging as a distinct RSK isoform, while its role in cancer has been conflicting (Houles & Roux, 2018; Dummler et al., 2005). RSK4 mRNA and/or protein expression is significantly downregulated in breast, colon, renal, endometrial and ovarian cancers compared to their normal cell and/or

tissue counterparts, where it is thought to exert a tumour suppressive role (Houles & Roux, 2018). For instance, RSK4 overexpression reduced MDA-MB-231 xenograft tumour growth and suppressed MDA-MB-231 cell metastatic dissemination *in vivo* (Thakur et al., 2008). In colon cancer, RSK4 overexpression inhibited HCT-116 cell growth *in vitro* and suppressed HCT-116 cell invasion (Ye et al., 2018). Conversely, RSK4 is overexpressed in renal and melanoma cancers compared to normal tissues, where it is thought to promote tumour growth. For example, RSK4 downregulation sensitised melanoma and renal cancer cell lines to sunitinib treatment and prevented their migration and invasion *in vitro* (Fan et al., 2013; Bender & Ullrich, 2012).

It is possible that RSK4 acts as a tumour suppressor or tumour promoter in a tissue-specific manner. Therefore, an in depth understanding of RSK4 molecular mechanisms of action in different cancers is required. To our knowledge, the role of RSK4 in lung cancer remains elusive. The human A549 cell line is a KRAS (G12S)-driven lung adenocarcinoma, the most prevalent type of lung cancer. A549 cells are easy to maintain, transfect and have a short doubling time compared to other lung adenocarcinoma cells. Therefore, this cell line represents an excellent model to study lung cancer. In the current study, RSK4 silencing sensitises A549 cells to chemotherapeutic compounds cisplatin and paclitaxel (taxol) and prevents their migration and invasiveness *in vitro* and *in vivo*. Conversely, RSK4 overexpression renders cells more resistant to chemotherapy and enhances their migratory capabilities. These phenotypic processes are associated with the modulation of anti-apoptotic proteins c-IAP1 and c-IAP2 and epithelial-mesenchymal transition (EMT). A small-molecule inhibitor screen (Kathryn Chapman, personal communication) identified several (but not all) floxacins as potent allosteric inhibitors of RSK4 activation. The most potent, trovafloxacin, reproduced all biological and molecular effects of RSK4 silencing *in vitro* and *in vivo* and it is predicted to bind a novel allosteric site as revealed by our RSK4 N-terminal kinase domain crystal structure (Filippo Prischi, collaboration) and mathematical Markov Transient Analysis (MTA) (Mauricio Barahona, collaboration). Further, RSK4 is overexpressed in the majority of NSCLC biopsies, which correlates with poor overall survival in lung adenocarcinoma patients. Collectively, our data implicate RSK4 as a promising novel therapeutic target in lung cancer.

3.2 Results

3.2.1 RSK4 emerges as a potent regulator of chemo-sensitivity in lung and bladder cancer cells

A kinome RNA interference screen previously performed in T24 bladder cancer cells treated with or without paclitaxel (taxol) or cisplatin identified RSK4 as a potent regulator of both taxol and cisplatin response in these cells (Uwais Mufti, personal communication). The role of RSK4 in chemo-sensitivity was reproduced in two additional bladder cancer cell lines, TCCSUP and J82 (Uwais Mufti, personal communication) and in an RNA interference screen in A549 lung adenocarcinoma cells (Swanton et al., 2007). Here, RSK4 siRNA silencing sensitised both T24 and A549 cell lines to taxol and cisplatin, while RSK4 downregulation in the absence of chemotherapy did not alter cell viability **(Figure 11a)**. This effect was reproduced in additional lung cancer cell lines, HOP62 and H1299 (Chrysostomou et al., Unpublished), while RSK4 overexpression rendered lung cancer cells more resistant to chemotherapy **(Figure S 1a, b)**. The drug sensitisation in RSK4-depleted cells was associated with potentiation of apoptosis in both T24 and A549 cells treated with cisplatin, as assessed by a caspase 3/7 activation assay **(Figure 11b)**. In the absence of chemotherapeutic drugs, RSK4 silencing decreased cellular inhibitor of apoptosis protein-1 (c-IAP1) and c-IAP2 protein and mRNA levels **(Figure 11c-e)**, which were previously shown to promote drug resistance in lung cancer by inhibiting apoptosis (Pardo et al., 2003). This was associated with upregulation of total and cleaved caspase-7 and cleaved poly (ADP-ribose) polymerase-1 (PARP-1) protein levels **(Figure 11f, g)**, while RSK4 overexpression decreased the cleavage of caspase-3, -7 and PARP-1 **(Figure S 1c)**. However, caspase-9 cleavage was not detected in RSK4-slienced cells **(Figure 11f, g)**, suggesting that the proteolytic cleavage and activation of caspase-3 and -7 might occur independently of caspase-9 activation. RSK1 siRNA silencing was previously shown to promote resistance to taxol in A549 cells (Swanton et al., 2007). Here, we show that RSK1 downregulation, in contrast to RSK4, renders A549 cells more resistant to both taxol and cisplatin treatment **(Figure S 2a, b)**. While RSK1 knockdown decreased c-IAP1 at the protein and mRNA level, it significantly upregulated c-IAP2 levels, suggesting that c-IAP2 might play a more prominent role in the regulation of chemo-sensitivity in our setting **(Figure S 2c, d)**. Collectively, RSK4 downregulation sensitises lung cancer cells to clinically relevant chemotherapeutic compounds, via a mechanism that might, at least in part, involve c-IAP family members. Interestingly, RSK1

silencing opposes this phenotype, suggesting that the use of a pan-RSK inhibitor might be ineffective in lung adenocarcinoma.

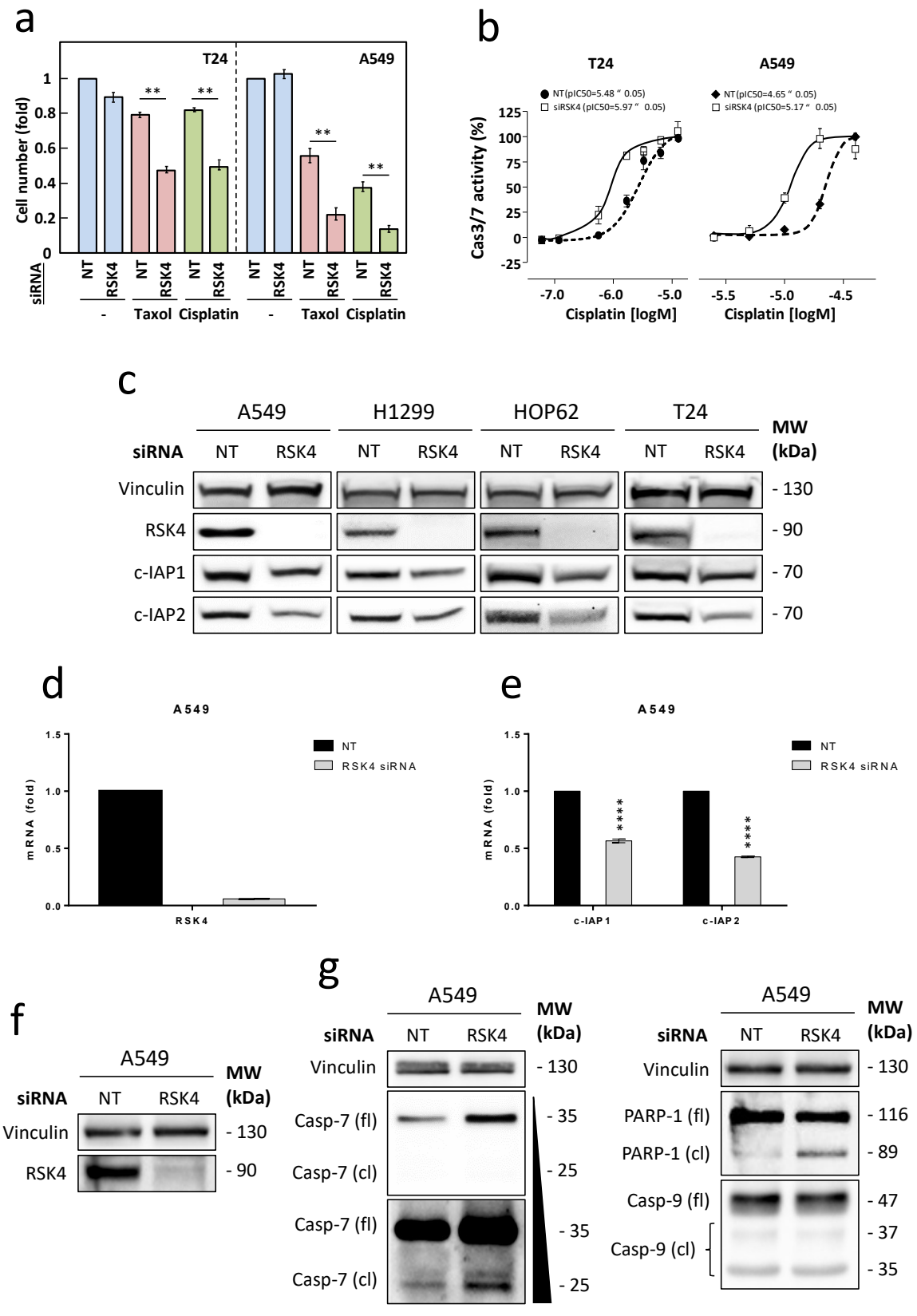

Figure 11| RSK4 emerges as a potent regulator of chemo-sensitivity in lung and bladder cancer cells. (a) RSK4 siRNA knockdown sensitises lung and bladder cancer cells to chemotherapy. Cell viability was determined by crystal violet staining of T24 (bladder cancer; left) or A549 (lung cancer; right) cells transfected (24-48 h) with a final concentration of 20 nM NT (non-targeting) or RSK4 siRNAs, before treated with 2-fold serially diluted paclitaxel (taxol) (0-100 nM) or cisplatin (0-100 µM) for 48-72 h. Data plotted as a fold change of IC_{50} relative to the untreated NT condition and represent mean ± SEM of three independent biological replicates performed in quadruplicates. **(b)** RSK4 silencing potentiates caspase-3/7 activation of cisplatin treated T24 (left) and A549 (right) cells. T24 or A549 cells were transfected (24-48 h) with a final concentration of 20 nM NT (non-targeting) or RSK4 siRNAs, before treated with 2-fold serially diluted cisplatin (0-100 µM) and caspase-3/7 activity assessed through the cleavage of DEVD-aminoluciferin substrate. Data plotted as a percentage change relative to the untreated NT condition and represent mean ± SEM of three independent biological replicates performed in quadruplicates. **(c)** RSK4 downregulation decreases c-IAP1 and c-IAP2 protein levels in lung and bladder cancer cell lines. Immunoblotting of RSK4, c-IAP1 and c-IAP2 in whole cell A549, H1299 (lung), HOP62 (lung) and T24 (bladder) extracts transfected (48-72 h) with a final concentration of 20 nM NT (non-targeting) or RSK4 siRNAs. Vinculin was used as a loading control. Data are representative of three independent biological replicates. **(d, e)** RSK4 downregulation decreases mRNA expression of c-IAP1 and c-IAP2 in A549 cells. qRT-PCR analysis of **(d)** RSK4, **(e)** c-IAP1 (BIRC2) and c-IAP2 (BIRC3) mRNAs in A549 cells transfected (48-72 h) with a final concentration of 20 nM NT (non-targeting) or RSK4 siRNAs. Ct values were normalised to HPRT housekeeping gene and shown as a fold change relative to NT control condition. Data represent mean ± SEM of three independent biological replicates performed in triplicates. **(f, g)** RSK4 silencing increases total and cleaved caspase-7 and cleaved PARP-1 protein levels in A549 cells. Immunoblotting of RSK4, Caspase-7, PARP-1 and Caspase-9 in whole cell A549 extracts transfected (48-72 h) with a final concentration of 20 nM NT (non-targeting) or RSK4 siRNAs. Vinculin was used as a loading control. Data are representative of two independent biological replicates. Statistical significance was assessed by an unpaired Student's t-test in GraphPad Prism. **; $P \leq 0.01$, ****; $P \leq 0.0001$. fl; full length, cl; cleaved. The work presented in **b** was performed by Kathryn Chapman (personal communication). The knockdown of RSK4 (including loading control) in experiment **f** is shown again in **Figure 29b** (same lysate).

3.2.2 CRISPR/Cas9-mediated knockout of RSK4 impairs xenograft tumour growth and enhances cisplatin response in vivo

To compensate the transient RSK4 knockdown results, we utilised our CRISPR/Cas9-mediated RSK4 knockout (KO) clones: cr421 (partial RSK4 KO) and cr437 (complete RSK4 KO) (Rajat Roy, personal communication). Here, we show that both RSK4 KO clones were sensitised to cisplatin treatment *in vitro* in a manner that depends on RSK4 expression, while cell viability was unaffected in the absence of drug **(Figure 12a)**. Similarly, RSK4 KO decreased the protein and mRNA levels of c-IAP1 and c-IAP2 **(Figure 12b, c)**. To assess the effect of RSK4 silencing on tumour growth *in vivo*, RSK4 KO clones cr421, cr437 or A549 control cells were injected subcutaneously into the flanks of nude mice and, when tumours reached 50 mm^3, tumour volumes were measured daily for 46 days (Yulan Wang, collaboration). Tumour growth was significantly delayed for both RSK4 KO clones as compared to non-targeted A549 tumours **(Figure 12d)**. To evaluate the response of RSK4 KO to cisplatin treatment *in vivo*, cr437 or A549 control cells were injected subcutaneously into the flanks of nude mice and, when tumours reached 50 mm^3, mice were treated with/without cisplatin intraperitoneally (IP) twice-weekly and tumour volumes were measured at day 46 (Yulan Wang, collaboration). Here, we show that cisplatin treatment significantly decreased tumour growth compared to non-targeted/non-drug treated tumours **(Figure 12e)**. Collectively, RSK4 downregulation in combination with chemotherapy impairs lung adenocarcinoma tumour growth *in vitro* and *in vivo* in a xenograft mouse model.

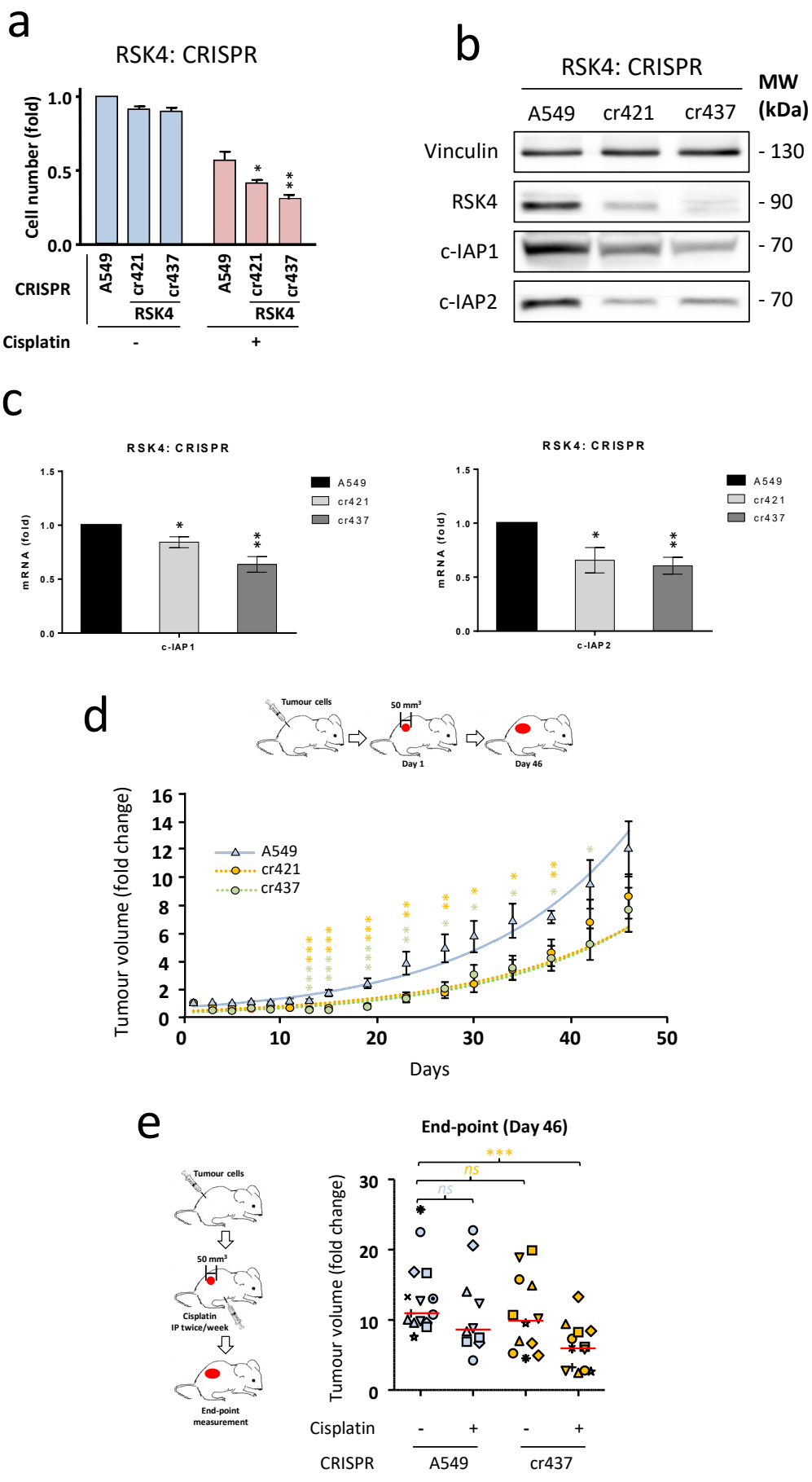
a
RSK4: CRISPR
Cell number (fold)
1.0
0.5
0.0
A549
cr421
cr437
A549
cr421
cr437
CRISPR
RSK4
RSK4
Cisplatin
-
+
b
RSK4: CRISPR
MW (kDa)
A549
cr421
cr437
Vinculin
- 130
RSK4
- 90
c-IAP1
- 70
c-IAP2
- 70
c
RSK4: CRISPR
mRNA (fold)
A549
cr421
cr437
c-IAP1
RSK4: CRISPR
mRNA (fold)
A549
cr421
cr437
c-IAP2
d
Tumour cells
50 mm³
Day 1
Day 46
Tumour volume (fold change)
A549
cr421
cr437
Days
e
End-point (Day 46)
Tumour cells
50 mm³
Cisplatin IP twice/week
End-point measurement
***
ns
ns
Tumour volume (fold change)
Cisplatin
CRISPR
A549
cr437

Figure 12| CRISPR/Cas9-mediated knockout of RSK4 impairs xenograft tumour growth and enhances cisplatin response *in vivo*. (a) RSK4 CRISPR/Cas9-mediated knockout (KO) clones (A549 cells): cr421 (partial RSK4 KO) and cr437 (complete RSK4 KO) are sensitised to chemotherapy. Cell viability was determined by crystal violet staining of A549 (non-targeted; control), cr421 and cr437 cells treated with 2-fold serially diluted cisplatin (0-100 μM) for 48-72 h. Data plotted as a fold change of IC_{50} relative to the untreated A549 control condition and represent mean ± SEM of three independent biological replicates performed in quadruplicates. **(b)** RSK4 knockout decreases c-IAP1 and c-IAP2 protein levels. Immunoblotting of RSK4, c-IAP1 and c-IAP2 in whole cell A549 (control), cr421 and cr437 extracts. Vinculin was used as a loading control. Data are representative of three independent biological replicates. **(c)** RSK4 knockout decreases mRNA expression of c-IAP1 and c-IAP2. qRT-PCR analysis of c-IAP1 (BIRC2; left) and c-IAP2 (BIRC3; right) mRNAs in A549 (control), cr421 and cr437 cells. Ct values were normalised to HPRT housekeeping gene and shown as a fold change relative to A549 control condition. Data represent mean ± SEM of three independent biological replicates performed in triplicates. **(d)** CRISPR/Cas9-mediated knockout of RSK4 impairs xenograft tumour growth. 5 x 10^6 A549 control, cr421 or cr437 cells were injected subcutaneously into the flanks of female BALB/c-nu/nu nude mice and, when tumours reached 50 mm^3 (day 1), tumour volumes were measured by caliper daily for 46 days. cr421 and cr437 tumour volumes are plotted as a fold change relative to A549 control tumour volume and represent mean ± SEM. **(e)** CRISPR/Cas9-mediated knockout of RSK4 enhances cisplatin response *in vivo*. 5 x 10^6 A549 control or cr437 cells were injected subcutaneously into the flanks of female BALB/c-nu/nu nude mice and, when tumours reached 50 mm^3 (day 1), mice were treated with or without cisplatin intraperitoneally (IP) twice-weekly and tumour volumes were measured by caliper at day 46 (end-point measurement). Tumour volumes are plotted as a fold change relative to the untreated A549 control tumour volumes and represent mean ± SEM. Statistical significance was assessed by an **(c)** unpaired Student's t-test or **(d, e)** two-way ANOVA in GraphPad Prism. ns; non-significant ($P > 0.05$), *; $P \leq 0.05$, **; $P \leq 0.01$, ***; $P \leq 0.001$. The work presented in **d-e** was performed by Yulan Wang (collaboration).

3.2.3 RSK4 downregulation inhibits A549 cell migration and invasion in vitro and metastatic dissemination in vivo

Contrary to RSK1, RSK4 siRNA silencing was previously shown to inhibit the migration and invasion of A549 cells *in vitro* (Lara et al., 2011). In corroboration with these results, RSK4 downregulation hindered the migration of A549 cells, while RSK4 overexpression enhanced their migratory potential **(Figure 13a, b)**. These results were reproduced in several lung and bladder cancer cell lines **(Figure S 3a-d)**. Brightfield microscopy of RSK4-silenced A549 cells revealed extensive cell clustering, a phenotype that is reminiscent of mesenchymal-epithelial transition (MET) **(Figure 13c)**. Indeed, RSK4 knockdown upregulated the epithelial marker E-cadherin, while it downregulated the mesenchymal markers N-cadherin and vimentin **(Figure 13d)**. Conversely, overexpression of RSK4 led to the reverse **(Figure 13d)**. However, only N-cadherin appeared to be regulated at the mRNA level by RSK4 **(Figure S 4 & Figure S 6)**. Contrary to RSK4, RSK1 downregulation enhanced the migration of A549 cells, an effect associated with a mesenchymal-like appearance of RSK1-silenced cells and induction of epithelial-mesenchymal transition (EMT) markers with the exception of N-cadherin **(Figure S 5 & Figure S 6)**. EMT represents one of the earliest events of the invasion-metastasis cascade in epithelial tumours (Lambert, Pattabiraman & Weinberg, 2017). To assess metastasis *in vivo* downstream of RSK4 depletion, cr437 or A549 control cells were tail vein-injected into nude mice and allowed to form lung micro-metastases (Yulan Wang, collaboration).

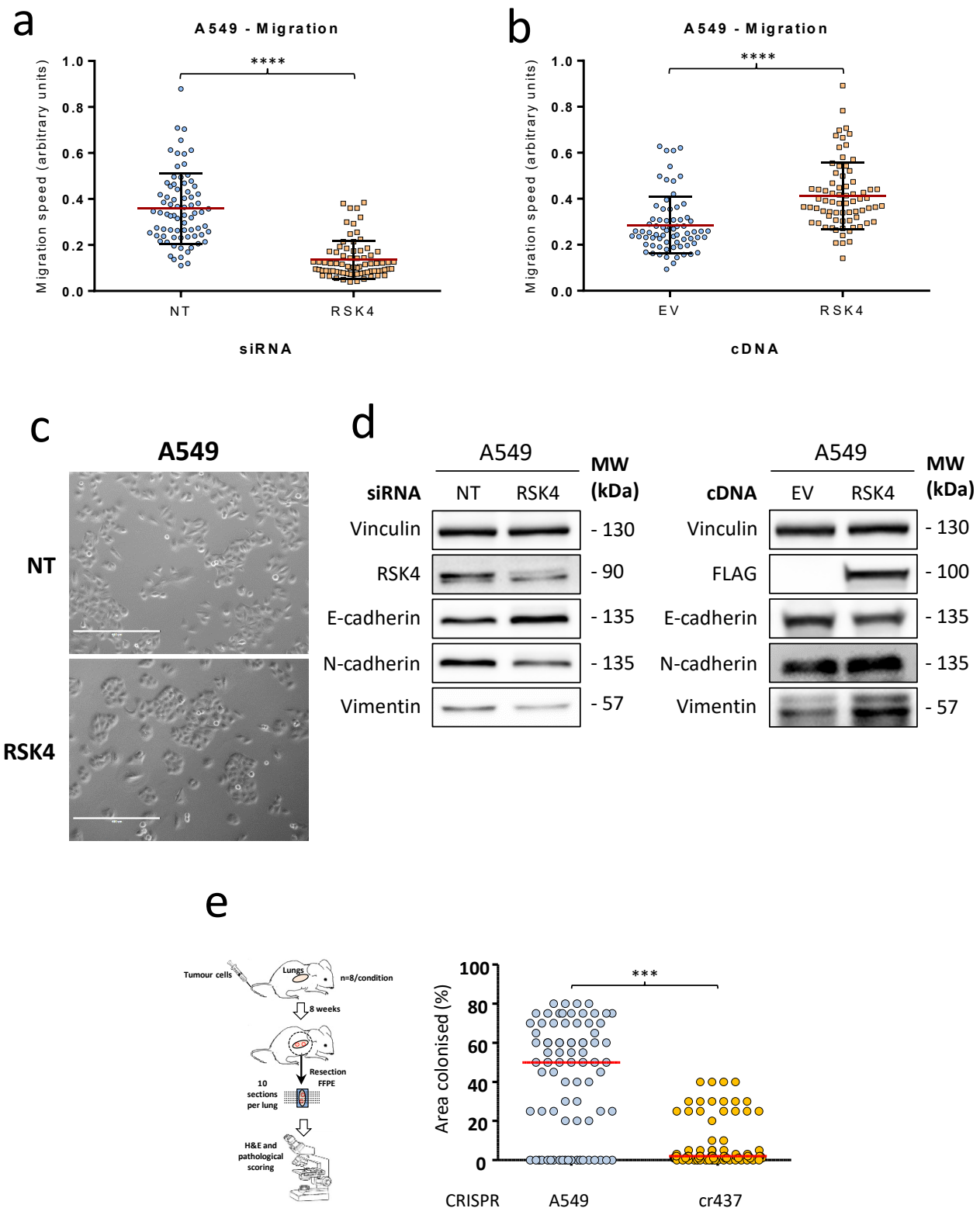

Figure 13| RSK4 downregulation inhibits A549 cell migration *in vitro* and metastatic dissemination *in vivo*. **(a, b)** RSK4 regulates A549 cell migration. Migration speed of A549 cells transfected (24-48 h) with **(a)** a final concentration of 20 nM NT (non-targeting) or RSK4 siRNAs or **(b)** a final concentration of 2.5 µg EV (empty vector) or RSK4 cDNAs. Time-lapse brightfield imaging was performed for 18 h (1 image/10 min) (Zeiss Axiovert 100 Inverted Widefield Microscope, MRC, Imperial College London) and migrating cells were tracked manually in FIJI Image-J. Migration speed was analysed using "Cell Migration analysis.R" script written in RStudio 0.99.89 by Dr Olivier

Pardo (Division of Cancer, Imperial College London, London, UK; o.pardo@imperial.ac.uk). Data are presented as a scatter plot showing migration speed (arbitrary units) of individual cells and the mean ± SD of three independent biological replicates performed in quintuplicates. **(c, d)** RSK4 controls the EMT programme. **(c)** Brightfield images of NT (non-targeting) or RSK4 siRNA-transfected A549 cells. (scale bars: 400 µm). **(d)** Immunoblotting of RSK4 (or FLAG), E-cadherin, N-cadherin and Vimentin in whole cell A549 extracts transfected (48-72 h) with a final concentration of 20 nM NT (non-targeting) or RSK4 siRNAs (left), or transfected (24-48 h) with a final concentration of 2.5 µg EV (empty vector) or RSK4 cDNAs (right). Vinculin was used as a loading control. Data are representative of three independent biological replicates. **(e)** CRISPR/Cas9-mediated knockout of RSK4 inhibits metastatic dissemination *in vivo*. 1 x 10^6 A549 control (NT) or cr437 cells were tail vein-injected into female BALB/c-nu/nu nude mice (n=8/condition) and allowed to form lung micro-metastases (8 weeks). Animals were sacrificed and their lungs extracted, formalin-fixed and paraffin-embedded (FFPE). 10 microtome slices per lung over a depth of 600 µm (each separated by 60 µm) were H&E stained and analysed microscopically for the presence of tumour nodules. Lung area colonised by, and the number of (See **Figure S 3e**), tumour nodules were quantified. Data are presented as a scatter plot showing percentage of area colonised per microtome slice and the mean ± SD. Statistical significance was assessed by an unpaired Student's t-test in GraphPad Prism. ***; $P \leq 0.001$, ****; $P \leq 0.0001$. The work presented in **e** was performed by Yulan Wang (collaboration) and Francesco Mauri (collaboration).

Lungs were extracted, formalin-fixed and paraffin-embedded (FFPE) and analysed microscopically for the presence of tumour nodules (Francesco Mauri, collaboration). Evidently, RSK4 KO cells were significantly less able to colonise the lungs of injected mice compared to control cells **(Figure 13e & Figure S 3e)**. In short, RSK4 downregulation prevents the metastatic dissemination of lung cancer cells *in vivo* and emerges as a regulator of the EMT programme. RSK1 acts in an opposing manner, providing additional evidence for the requirement of RSK isoform-specific inhibitors.

3.2.4 RSK4 is overexpressed in lung cancer and correlates with poor outcome in adenocarcinoma patients

To assess whether targeting RSK4 would be clinically relevant, we first compared RSK4 protein expression between primary lung cancer and normal lung tissue microarrays (TMAs) (Francesco Mauri, collaboration). While RSK4 was undetectable in non-cancerous specimens, it was expressed in nearly 60% of lung cancer samples **(Figure 14a, b)**. Immunoblotting of RSK4 in several NSCLC cell lines showed expression of RSK4 in all lung adenocarcinoma (LUAD) cells (i.e. A549, EKVX, HOP-62, H23 and H322M), while it was poorly expressed in large cell carcinoma (LCC) cells HOP-92 and H460 and the lung squamous cell carcinoma (LUSC) cell line H226 **(Figure S 7a)**. Importantly, RSK4 was undetectable in normal lung cells ATII (alveolar type II pneumocytes) and NL20 (bronchial epithelium) **(Figure S 7a)**. RSK1 on the other hand was expressed in all NSCLC cells as well as normal lung cell lines **(Figure S 7a)**. Taken together so far, RSK4, unlike RSK1, is overexpressed in lung cancer cells and tissues compared to their normal counterparts, suggesting that RSK4 might be important in lung cancer.

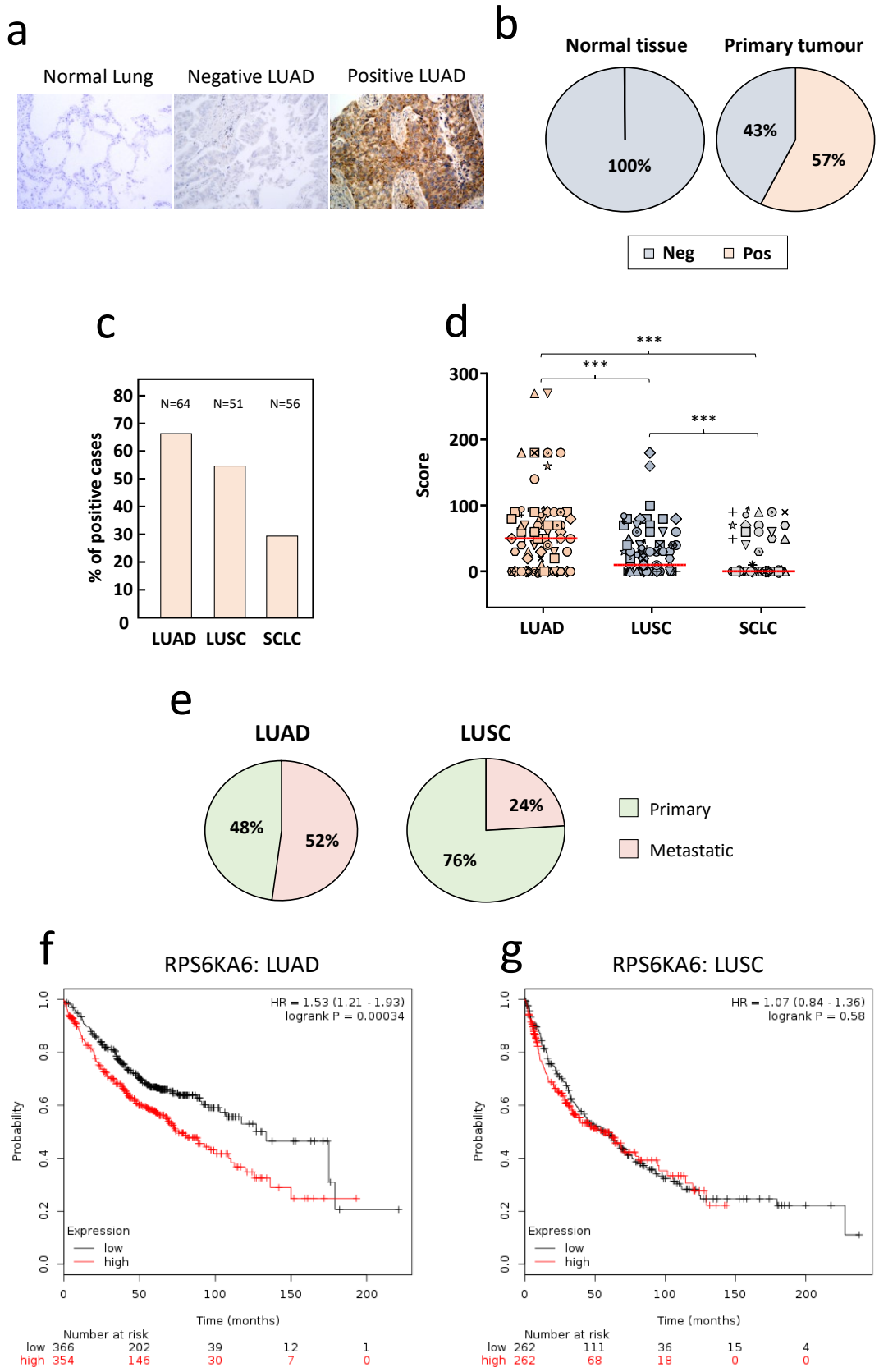

Figure 14| RSK4 is overexpressed in lung cancer and correlates with poor outcome in adenocarcinoma patients. **(a-e)** Normal lung (N=25) and lung cancer (N=183) FFPE samples were stained with H&E and RSK4 antibody prior to DAB development. **(a)** Examples of RSK4 staining in normal lung, RSK4-negative and RSK4-positive lung adenocarcinoma (LUAD) samples. **(b)** Percentage of normal tissue or primary tumour samples with negative (neg) or positive (pos) RSK4 staining. **(c)** Percentage of lung cancer subtypes with positive

RSK4 staining. LUAD; lung adenocarcinoma, LUSC; lung squamous cell carcinoma, SCLC; small cell lung cancer. **(d)** Semi-quantitative score for RSK4 staining in each lung cancer subtype. **(e)** RSK4 staining score was compared between matched primary and metastatic LUAD (N=26) and LUSC (N=20) lesions from post-mortem cases and the percentage of cases where metastatic lesions expressed more or less RSK4 than the primary are represented as a pie chart. **(f, g)** Kaplan-Meier analysis of RPS6KA6 (RSK4) mRNA expression (gene chip) in **(f)** LUAD (P=3.4×10^{-4}) and **(g)** LUSC (non-significant) patients (Nagy et al., 2018). Statistical significance was assessed by an unpaired Student's t-test in GraphPad Prism. ***; $P \leq 0.001$. The work presented in **a-e** was performed by Francesco Mauri (collaboration).

To investigate whether RSK4 expression is particularly important in specific subtypes of lung cancer, we stratified our clinical samples into LUAD, LUSC and small cell lung cancer (SCLC). RSK4 was more frequently and intensely expressed in LUAD specimens compared to LUSC and SCLC samples, suggesting that this kinase might be more important in LUADs **(Figure 14c, d)**. Further, in a post-mortem TMA containing syngeneic primary tumour/metastasis lung cancer patient samples, RSK4 was expressed at higher levels in the majority of LUAD metastatic lesions (52%) compared to primary LUAD tumours (48%), while only 24% of LUSC metastases had similar RSK4 expression levels **(Figure 14e)**. Therefore, RSK4 might be required for the metastatic dissemination of LUADs. To assess whether RSK4 expression impacts lung cancer survival, we utilised the Kaplan-Meier plotter database. High RSK4 mRNA (gene chip) expression correlated with poorer prognosis in lung cancer patients (P=4.5×10^{-3}) **(Figure S 8a)**. Following stratification into lung cancer subtypes, high RSK4 expression correlated with worst prognosis in LUAD patients (P=3.4×10^{-4}), while it did not affect LUSC survival **(Figure 14f, g)**. Interestingly, RSK1 mRNA expression did not affect the survival of either LUAD or LUSC patients **(Figure S 8c, d)**. Collectively, RSK4 is overexpressed in LUADs and this is associated with decreased overall patient survival, suggesting that inhibition of RSK4 might be beneficial in this setting.

3.2.5 A fluoroquinolone antibiotic reproduces the effects of RSK4 silencing in vitro

A small-molecule inhibitor screen identified several floxacins as non-ATP competitive reversible inhibitors of RSK4 activation, as determined by a high throughput homogeneous time resolved fluorescence (HTRF)-based assay (Kathryn Chapman, personal communication). Trovafloxacin was a potent inhibitor of RSK4 activation (and not RSK1) (Kathryn Chapman, personal communication), and sensitised A549 cells to cisplatin (IC_{50}= 7.5 µM) as compared to cisplatin only treated A549 cells **(Figure 15a)**. This was associated with potentiation of caspase-3/7 activity in cells treated with both trovafloxacin and cisplatin **(Figure 15b)**.

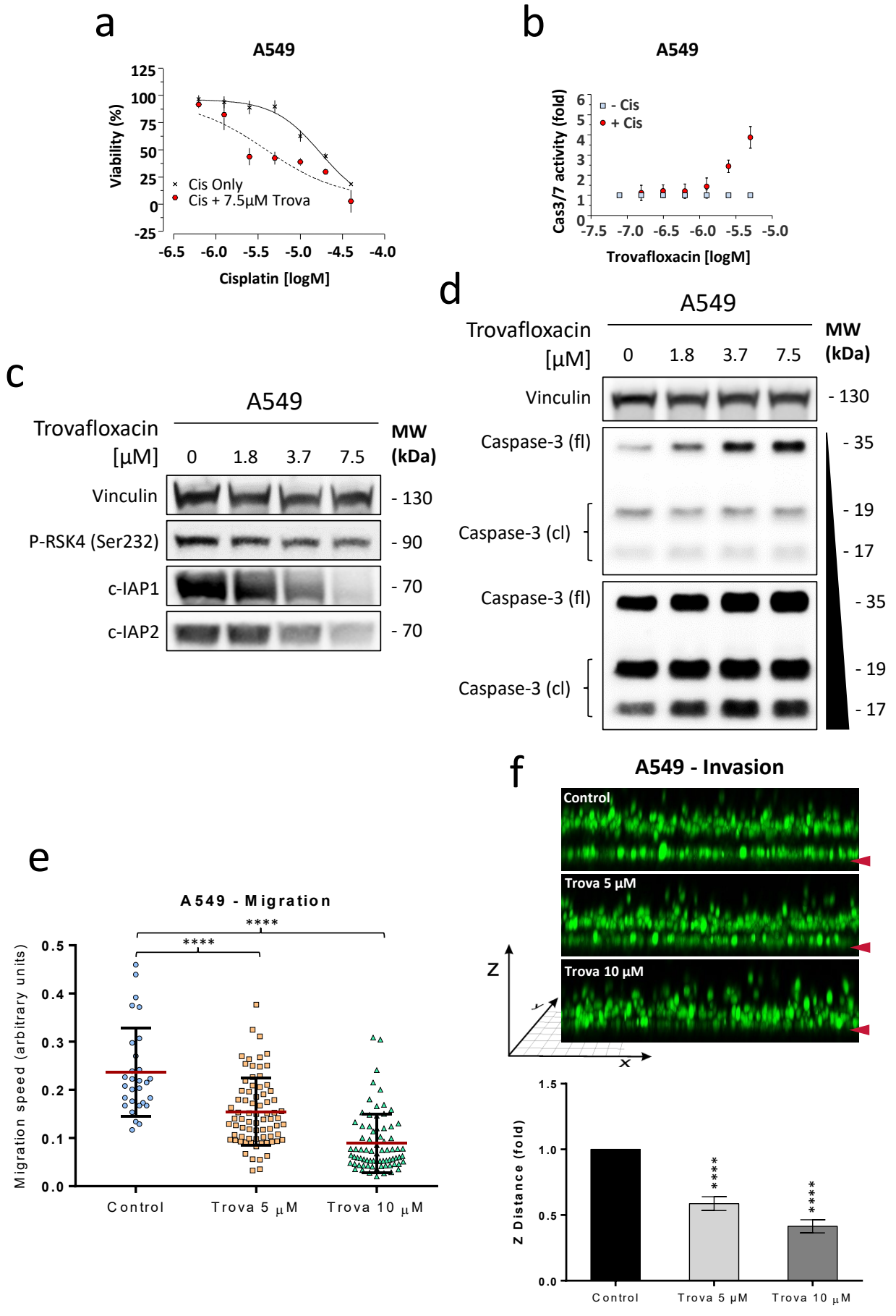
a
A549
Viability (%)
Cis Only
Cis + 7.5µM Trova
Cisplatin [logM]
b
A549
- Cis
+ Cis
Cas3/7 activity (fold)
Trovafloxacin [logM]
c
A549
Trovafloxacin [µM]
MW (kDa)
Vinculin
P-RSK4 (Ser232)
c-IAP1
c-IAP2
d
A549
Trovafloxacin [µM]
MW (kDa)
Vinculin
Caspase-3 (fl)
Caspase-3 (cl)
e
A549 - Migration
Migration speed (arbitrary units)
Control
Trova 5 µM
Trova 10 µM
f
A549 - Invasion
Control
Trova 5 µM
Trova 10 µM
Z Distance (fold)

Figure 15| Trovafloxacin, an inhibitor of RSK4 activation, reproduces the biological and molecular effects of RSK4 silencing *in vitro*. **(a)** Trovafloxacin treatment sensitises A549 cells to chemotherapy. Cell viability was determined by crystal violet staining. A549 cells were incubated with or without 7.5 µM trovafloxacin prior to treatment with 2-fold serially diluted cisplatin (0-100 µM) for 48-72 h. Data plotted as percentage change relative to the cisplatin only treated cells and represent mean ± SEM of three independent biological replicates performed in quadruplicates. **(b)** Trovafloxacin treatment potentiates caspase-3/7 activation of cisplatin treated A549 cells. A549 cells were incubated with increasing concentrations of trovafloxacin prior to treatment with or without 12.5 µM cisplatin treatment for 48-72 h. Caspase-3/7 activity was assessed through the cleavage of DEVD-aminoluciferin substrate. Data plotted as a fold change relative to the untreated condition (-Cis) and represent mean ± SEM of three independent biological replicates performed in quadruplicates. **(c)** Immunoblotting of Phospho-RSK4 (Ser232), c-IAP1 and c-IAP2 in whole cell A549 extracts incubated with increasing concentrations of trovafloxacin (0-7.5 µM) for 24 h. Vinculin was used as a loading control. Data are representative of three independent biological replicates. **(d)** Immunoblotting of Caspase-3 in whole cell A549 extracts incubated with increasing concentrations of trovafloxacin (0-7.5 µM) for 24 h. Vinculin was used as a loading control. Data are representative of two independent biological replicates. **(e)** Trovafloxacin treatment inhibits A549 cell migration. Migration speed of A549 cells treated with 10 µM DMSO (control), 5 µM trovafloxacin or 10 µM trovafloxacin. Time-lapse brightfield imaging was performed for 18 h (1 image/10 min) (Zeiss Axiovert 100 Inverted Widefield Microscope, MRC, Imperial College London) and migrating cells were tracked manually in FIJI Image-J. Migration speed was analysed using "Cell Migration analysis.R" script written in RStudio 0.99.89 by Dr Olivier Pardo (Division of Cancer, Imperial College London, London, UK; o.pardo@imperial.ac.uk). Data are presented as a scatter plot showing migration speed (arbitrary units) of individual cells and the mean ± SD of three independent biological replicates performed in quintuplicates. **(f)** Trovafloxacin treatment inhibits A549 cell invasion. 3D collagen invasion of A549 cells treated with 10 µM DMSO (control), 5 µM trovafloxacin or 10 µM trovafloxacin. DMSO- or trovafloxacin-treated cells were coated with type-I rat-tail collagen and treated with 1 µg/mL EGF to encourage invasion of cells upwards through the polymerised collagen matrix. 131 stacks of 500 µm were taken at 7 sites per well using the Zeiss AxioObserver Inverted Widefield Microscope (FILM, Imperial College London, UK). Images were deconvoluted using Huygens deconvolution software (FILM, Imperial College London, UK) and analysed using FIJI Image-J's 3D object counter plugin and macro script written by Stephen Rothery (FILM, Imperial College London, UK). The Z distances were normalised to the median, averaged per condition, and normalised to control. **(f, top)** Representative images of each condition. **(f, bottom)** Quantification shown as fold change relative to the control. Statistical significance was assessed by an unpaired Student's t-test in GraphPad Prism. ****; $P \leq 0.0001$. Red arrowheads indicate the bottom of the well. fl; full length, cl; cleaved. The work presented in **a-b** was performed by Kathryn Chapman (personal communication).

Similar chemo-sensitisation and caspase3/7 activation results were obtained with taxol (Chrysostomou et al., Unpublished). Crucially, the floxacins that were unable to inhibit RSK4 activation (e.g. ciprofloxacin) failed to sensitise cells to chemotherapy (Kathryn Chapman, personal communication). Increasing concentrations of trovafloxacin (0-7.5 µM) decreased RSK4 activity as determined by immunoblotting against anti-phospho-RSK4 Ser232 **(Figure 15c)**, a site that is indispensable for RSK4 activation and downstream substrate phosphorylation (Dummler et al., 2005) . This was associated with downregulation of both c-IAP1 and c-IAP2 proteins and upregulation of total and cleaved caspase-3 levels **(Figure 15c, d)**. Further, trovafloxacin treatment reduced the migration of A549 cells in a time-lapse random migration assay, and hindered their invasion through a collagen matrix **(Figure 15e, f)**. Taken together, trovafloxacin reproduces the biological and molecular effects of RSK4 silencing *in vitro*.

3.2.6 Trovafloxacin inhibits tumour growth and sensitises tumours to chemotherapy in vivo

To assess the effect of trovafloxacin on tumour growth *in vivo*, luciferase-expressing A549 cells (A549-Luc) were injected subcutaneously into the flanks of nude mice and when tumours became palpable, mice were

treated weekly with or without intraperitoneal injections of cisplatin and daily oral gavage of trovafloxacin for 14 days (Rajat Roy, personal communication). Following injection of luciferin, bioluminescent whole-animal imaging was performed on the last day of treatment. Here, we show that administration of trovafloxacin in combination with cisplatin significantly reduced tumour volume compared to vehicle-only treated animals **(Figure 16a, b)**.

Considering that ectopic (subcutaneous) xenograft models do not fully recapitulate lung tumour microenvironment, we utilised the *Kras*$^{LSL\text{-}G12D/+}$;*p53*$^{flox/flox}$ (KP) NSCLC genetically engineered mouse (GEM) model, where sporadic lung tumours are triggered through adenoviral Cre-recombinase delivery (David Hancock, Christopher Moore, Miriam Molina Arcas, Julian Downward; collaboration) (DuPage, Dooley & Jacks, 2009). Here, the total tumour burden was reduced in trovafloxacin/cisplatin-treated animals compared to the vehicle-only treated conditions **(Figure 17a-c)**. This was associated with decreased c-IAP2 levels and increased caspase-3 cleavage in cells isolated from KP tumours **(Figure 17d)**. Interestingly, ciprofloxacin, which does not inhibit RSK4 activation, failed to reproduce these molecular changes **(Figure 17e)**. In short, RSK4 is emerging as a promising target in lung adenocarcinomas and RSK4-targeting floxacins may improve the clinical outcome of these patients.

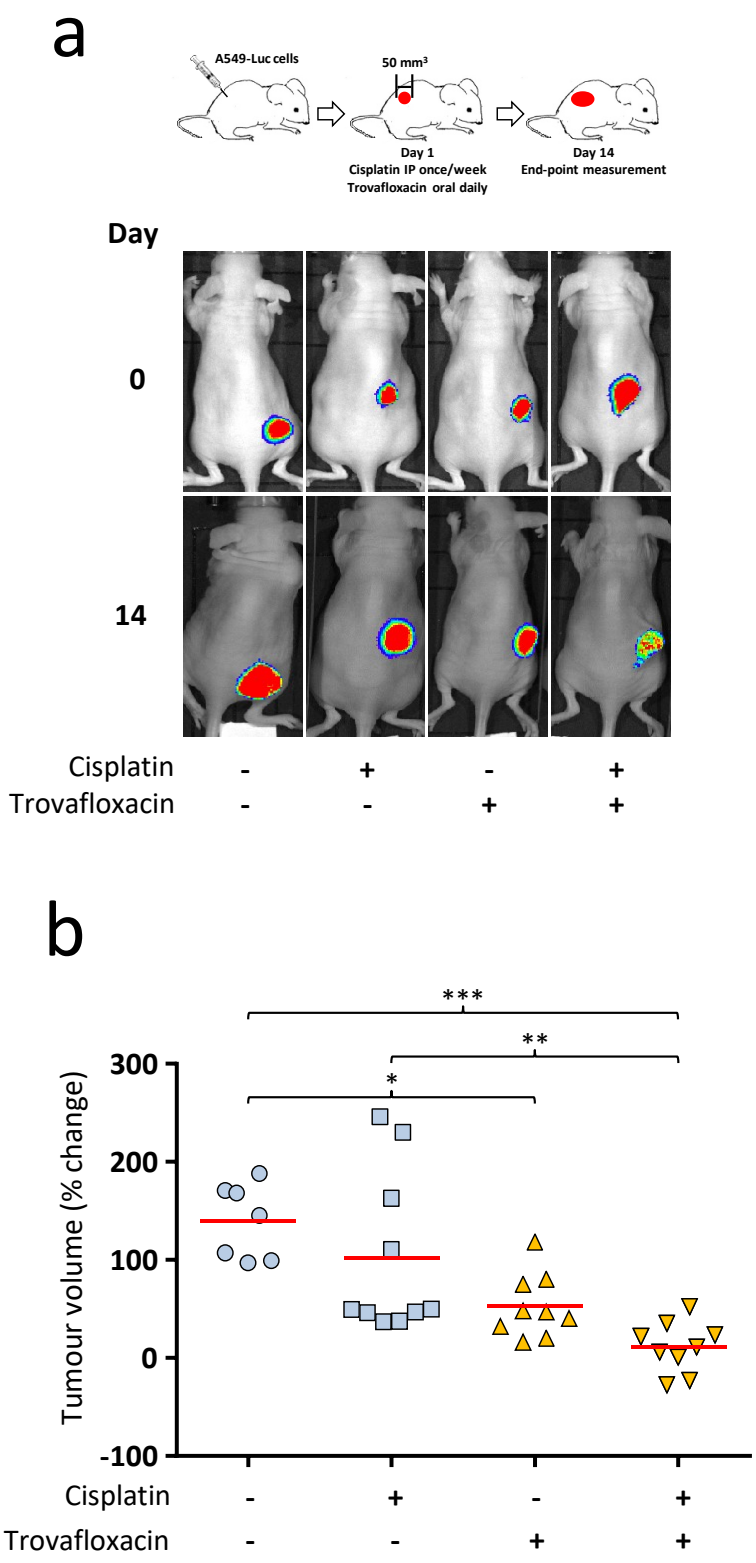

Figure 16| Trovafloxacin enhances cisplatin efficacy in A549 xenografts. **(a, b)** 5 x 10^6 luciferase-expressing A549 cells (A549-Luc) were injected subcutaneously into the flanks of female BALB/c-nu/nu nude mice and when tumours reached 50 mm^3 mice were treated with or without cisplatin intraperitoneally weekly and trovafloxacin by daily oral gavage for 14 days. Following injection of luciferin, bioluminescent whole-animal imaging was performed on the first and last day of treatment. **(a)** Representative images from each condition acquired with a luminometric small-animal imager, showing luciferase signal at day 0 and 14. **(b)** Percentage change in tumour volume at day 14. Red bar represents the median. Statistical significance was assessed by an unpaired Student's t-test in GraphPad Prism. *; $P \leq 0.05$, **; $P \leq 0.01$, ***; $P \leq 0.001$. The work presented in **a-b** was performed by Rajat Roy, Silvia Ottaviani and Joel Abrahams (collaboration).

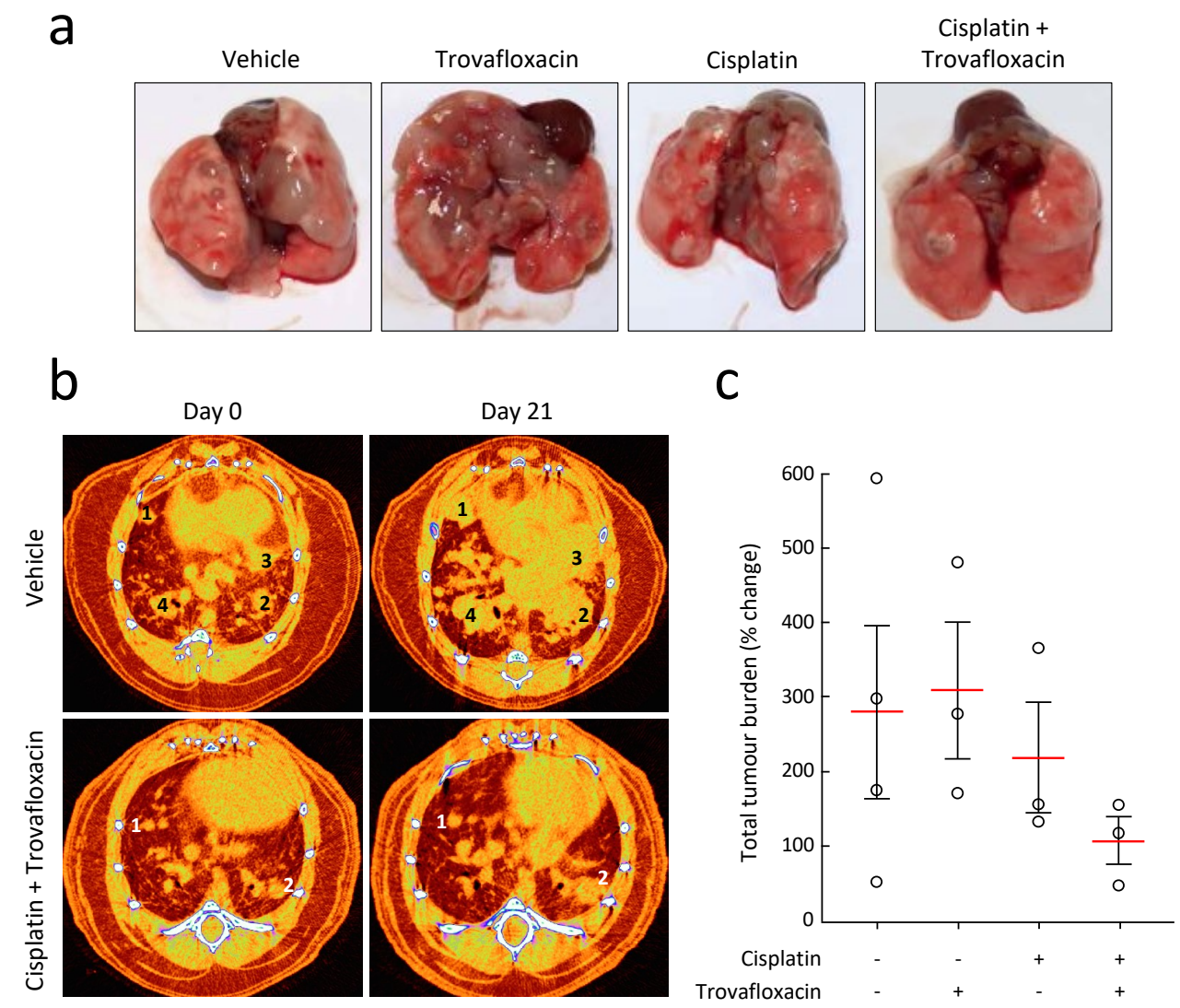

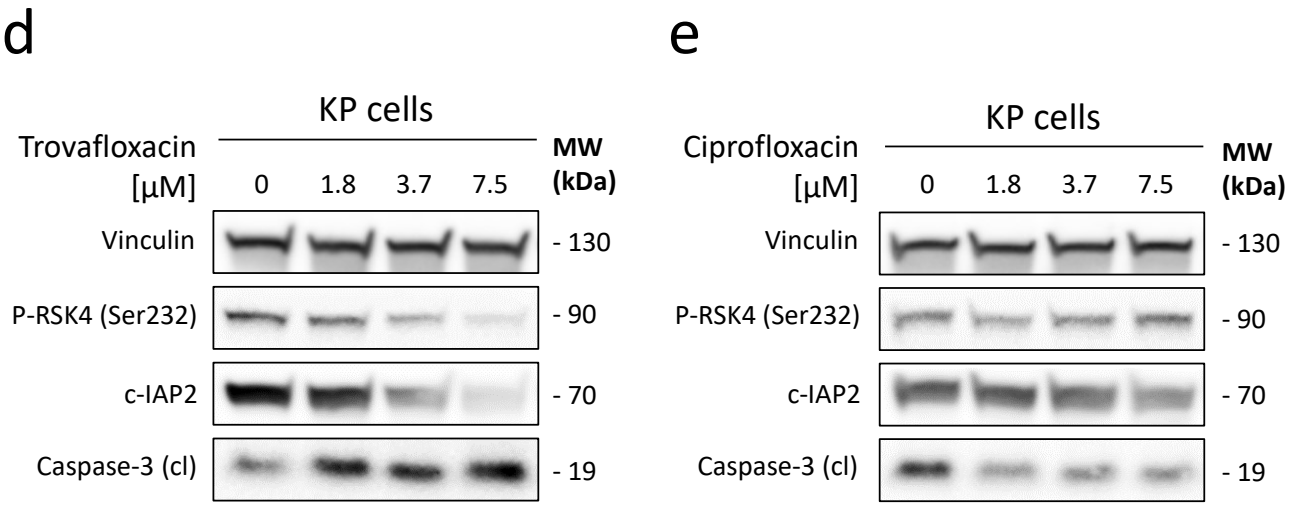

Figure 17| Trovafloxacin sensitises lung adenocarcinoma tumours to cisplatin in the Kras$^{LSL\text{-}G12D/+}$;p53$^{flox/flox}$ (KP)-driven genetically engineered mouse model. **(a-c)** KP mice were infected with 1 x 10^6 pfu (plaque-forming unit) adenovirus expressing *Cre* recombinase via intratracheal intubation to induce concomitant activation of oncogenic *Kras* and deletion of tumour suppressor *Tp53*. Mice were allowed to develop lung tumours as detected by micro-computerised tomography (CT) scanning (scan 1; day 0). They were then treated

± cisplatin intraperitoneally (IP) weekly and ± Trovafloxacin by daily oral gavage (5 days/week) for 3 weeks. Mice were re-scanned at the end of the treatment period (scan 2; day 21). Micro-CT analysis was performed in SkyScan 1176. Micro-CT data were reconstructed using NRecon software (SkyScan), imaged using DataViewer and tumour volumes were calculated using the CT-analyser program (CTAn, SkyScan). **(a)** Representative images of resected lungs from each condition. **(b)** Representative Micro-CT scans from vehicle-only and combination (cisplatin + trovafloxacin) treated animals taken prior to (scan 1; day 0) and at the end of the treatment (scan 2; day 21). Individual tumours followed during the treatment are indicated by numbers. **(c)** Changes in the volume (mm^3) of individual tumours from scan 1 to scan 2 were calculated and expressed as percentage volume change of total tumour burden. Each data point represents an individual animal. Red line indicates the median. **(d, e)** Trovafloxacin, but not ciprofloxacin, decreases RSK4 activity, downregulates c-IAP2 and induces caspase-3 cleavage in cells isolated from KP tumours. Immunoblotting of Phospho-RSK4 (Ser232), c-IAP2 and cleaved (cl) Caspase-3 in whole KP cell extracts incubated with increasing concentrations of **(d)** trovafloxacin (0-7.5 µM) or **(e)** ciprofloxacin (0-7.5 µM) for 24 h. Vinculin was used as a loading control. Data are representative of three independent biological replicates. The work presented in **a-c** was performed by David Hancock, Christopher Moore, Miriam Molina Arcas and Julian Downward (collaboration).

3.3 Discussion

In this report, we provide evidence that supports a tumour promoting role for RSK4 in lung cancer. Overexpressing this kinase increases the resistance of lung cancer cells to chemotherapeutic compounds and enhances their migratory capabilities *in vitro* **(Figure 13 & Figure S 1)**. Conversely, RSK4 silencing by siRNA or CRISPR/Cas9-mediated knockout, sensitises these cells to chemotherapy and inhibits their invasiveness *in vitro* and *in vivo* **(Figure 11, Figure 12 & Figure 13)**. Further, RSK4 is overexpressed in lung cancer cell lines and tissues, and this appears to be particularly important in metastasised lung adenocarcinomas **(Figure 14, Figure S 7 & Figure S 8)**. Our data are consistent with the role of RSK4 in renal and melanoma cancers, where silencing of this kinase sensitised renal and melanoma cell lines to sunitinib treatment, and prevented their migration *in vitro* (Bender & Ullrich, 2012). RSK4 was also overexpressed in renal cell carcinoma (RCC) and this correlated with poor prognosis in RCC patients (Fan et al., 2013). However, data presented in this study conflicts with the proposed tumour suppressive role of RSK4 in breast cancer (Thakur et al., 2008; Thakur et al., 2007; Thakur et al., 2005). Indeed, immunoblotting analysis of RSK4 in a panel of NCI-60 cell lines showed undetectable expression of this kinase in breast cancer cell lines (MCF7, MDA-MB-231, Hs 578T and BT-549) compared to A549 lung cancer cells **(Figure S 7b)**. In addition, Kaplan Meir-plotter indicated that high expression of RSK4 (mRNA; gene chip and RNA-seq data) correlates with better prognosis in breast cancer patients (P=1.8×10^{-6}) **(Figure S 8b)**. Hence, RSK4 might indeed function differently in a tissue- or disease-specific manner. It is also possible that these discrepancies might be due to differentially expressed alternatively spliced variants of RSK4. At least two protein-coding RSK4 transcript variants are reported in Ensembl: RSK4 variant I (NM_014496.5) and RSK4 variant II (NM_001330512.1), the latter of which we have cloned and is under investigation.

Inhibitor of apoptosis proteins (IAPs) constitute a family of anti-apoptotic molecules that are highly expressed in cancers and promote chemotherapy drug resistance by antagonising apoptosis promoting signals (Rathore et al., 2017). Here, we propose that the chemo-sensitisation effect of RSK4 inhibition is mediated, at least in part, due to downregulation of c-IAP-1 and c-IAP2 and concurrent upregulation of total and cleaved caspase-

3 and -7 **(Figure 11c, g & Figure 15c, d)**. IAPs are characterised by the presence of baculoviral IAP repeat (BIR) domains, which bind caspases and a C-terminal RING domain, which equips them with an E3 ubiquitin ligase activity (Gyrd-Hansen & Meier, 2010). c-IAP1 and c-IAP2 were shown to bind and prevent caspase-3 cleavage (Kavanagh et al., 2014; Burke, Smith & Smith, 2010) as well as ubiquitinate both caspase-3 and -7, the latter of which promotes their degradation via the proteasome (Choi et al., 2009; Huang et al., 2000). The fact that c-IAPs target caspase-3 and -7 directly might explain why caspase-9, which initiates apoptosis by proteolytically cleaving caspase-3 and -7, is not altered following RSK4 silencing. Therefore, RSK4 might not participate in the classical mitochondrial apoptosis pathway, rather it could impact apoptosis by targeting c-IAPs directly. Further, the fact that c-IAP1 and c-IAP2 prevent both caspase cleavage and target caspases for proteasomal degradation, might account for the upregulation of total and cleaved caspase levels downstream of RSK4 gene silencing or pharmacological inhibition **(Figure 11g & Figure 15 d)**. Lastly, RSK4 downregulation results in PARP-1 cleavage **(Figure 11g)**, which could be mediated following activation of caspase-3 and -7, both of which were reported to cleave and inactivate PARP-1 with similar efficiency (Walsh et al., 2008). PARP participates in the repair of DNA single-strand breaks (SSBs) and its inhibition can lead to double-strand breaks (DSBs) and γH2AX phosphorylation in the chromatin, which is required for the assembly of DNA repair molecules (Redon et al., 2010). Indeed, RSK4 silencing increased the number of γH2AX nuclear foci as detected with the anti-phospho Ser139 antibody (Chrysostomou et al., Unpublished).

EMT represents one of the earliest events during the invasion-metastasis cascade while the loss of E-cadherin alone is sufficient to promote cancer metastasis (Devlin & Verschuren, 2018; Fan et al., 2012; Sawada et al., 2008). Hence, targeting molecules that promote this process represents an attractive therapeutic strategy. Here, we show that RSK4 silencing induces an epithelial-like (MET) phenotype, which could be attributed to upregulation of E-cadherin and concurrent downregulation of the mesenchymal markers N-cadherin and vimentin **(Figure 13 & Figure S 3)**. Although it is unclear at this stage how RSK4 regulates the EMT programme, RSK1 silencing, which we show induces a mesenchymal-like phenotype (i.e. EMT), decreases total and Ser780

phosphorylation levels of retinoblastoma (Rb) protein **(Figure S 5)**. Crucially, depletion of Rb was shown to induce EMT-like changes by downregulating E-cadherin in breast cancer cells (Arima et al., 2008).

While there are several potent pan-RSK inhibitors available, including the N-terminal kinase domain (NTKD) inhibitors SL-0101 and BI-D1870, these are ATP-competitive inhibitors with several off-target effects (Bain et al., 2007). Further, in light of data suggesting a tumour suppressive role for RSK1, the application of a pan-RSK inhibitor might be ineffective in lung adenocarcinomas. In agreement with this, treatment of A549 cells with the pan-RSK inhibitor SL-0101 enhanced their migration and invasion *in vitro*, thereby phenocopying the effects of RSK1 silencing (Chrysostomou et al., Unpublished). Our small-molecule inhibitor screen identified several (but not all) floxacins (e.g. moxifloxacin, trovafloxacin and levofloxacin) as potent allosteric inhibitors of RSK4 activation (Kathryn Chapman, personal communication). Trovafloxacin, a fluoroquinolone antibiotic, was among the most potent RSK4 inhibitors and reproduced all biological and molecular effects of RSK4 silencing *in vitro* and *in vivo* **(Figure 15, Figure 16 & Figure 17)**. An attempt to co-crystallise trovafloxacin bound to RSK4 NTKD was not successful as resulting crystals either did not contain the drug or failed to diffract. However, as revealed through our RSK4 NTKD crystal structure, mathematical modelling and molecular docking simulations, trovafloxacin is predicted to bind a second AMP-PNP site within the NTKD that is not conserved among classical AGC kinases, implying a level of specificity for this drug (Chrysostomou et al., Unpublished). To complement our *in-silico* methods we carried out a hydrogen deuterium exchange mass spectrometry analysis, which provided additional evidence for RSK4/trovafloxacin binding (Mark Skehel, collaboration). Crucially, the floxacins that were unable to inhibit RSK4 activation (e.g. ciprofloxacin) failed to sensitise cells to chemotherapy or impair their invasiveness, indicating that these effects occur independently of their role as antibiotics (Kathryn Chapman, personal communication). Nonetheless, trovafloxacin has been associated with hepatotoxicity and thus has been withdrawn from the market. Hepatotoxicity has been suggested to be caused by oxidation of a cyclopropylamine moiety within trovafloxacin (Sun et al., 2007), therefore necessitating the development of trovafloxacin analogues that retain their capacity to bind RSK4, but are devoid of this moiety or other putative toxicity causing moieties.

To conclude, here we have identified RSK4 as a potent mediator of tumour metastasis and chemotherapy drug resistance in lung adenocarcinoma. The results presented in this study implicate RSK4 as a novel therapeutic target for the treatment of lung cancer patients. Our small-molecule inhibitor screen identified certain floxacins that were able to inhibit RSK4 and phenocopy the effects of RSK4 gene silencing. Based on our RSK4 NTKD crystal structure and *in-silico* modelling, trovafloxacin is predicted to bind a potential allosteric site on RSK4. Through subsequent medicinal chemistry we will seek to develop floxacin-based analogues that are able to bind RSK4 with greater affinity and are devoid of toxicity-inducing moieties. Ultimately, RSK4-targeting floxacins could be re-purposed and used in combination with chemotherapy to improve survival of lung cancer patients.

4. RSK1 vs RSK4: Tandem affinity purification, global proteomics & phosphoproteomics – LC-MS/MS

4.1 Introduction

RSK family members have been reported to exert overlapping functions and this is due to their high degree of sequence homology (Houles & Roux, 2018). RSKs are highly conserved serine/threonine protein kinases, implicated in the phosphorylation of numerous substrates downstream of the RAS/MAPK pathway **(Figure 6)**. Indeed, RSKs phosphorylate several substrates redundantly, including rpS6, which is involved in protein synthesis (Meyuhas, 2008). While RSK1 and RSK2 represent the most studied RSK members and are typically thought to act in a tumour promoting manner, RSK3 and RSK4 are the least studied isoforms and are generally thought to suppress tumour growth. Nevertheless, this notion is being challenged and distinct biological functions are being attributed to distinct RSK isoforms; notably, the opposing regulation of lung adenocarcinoma cell migration/invasion (Lara et al., 2011) and response to chemotherapeutic agents **(Chapter 3, p.118)** between RSK1 and RSK4.

The role of RSK4 has also been controversial in cancer. While RSK4 was shown to suppress breast cancer growth *in vitro* and *in vivo* (Thakur et al., 2008), it was shown to exert tumour promoting properties in renal, melanoma (Fan et al., 2013; Bender & Ullrich, 2012) and lung cancers (Lara et al., 2011) **(Chapter 3, p.118)**. These discrepancies might relate to tissue-specific roles of RSK4 or the presence of RSK4 alternatively spliced variants with divergent biological functions. Indeed, two protein-coding transcript variants of RSK4 have been reported: RSK4 variant I (NM_014496.5) and RSK4 variant II (NM_001330512.1), the latter of which is so far unstudied **(Figure S 9)**. Importantly, to date, no RSK4 specific phosphorylation substrates or interactors have been reported. Therefore, to further understand the underlying mechanisms by which RSK1 and RSK4 transcript variants modulate cellular processes, it is crucial to elucidate their respective interacting/binding partners and substrates.

Tandem affinity purification (TAP) combined with qualitative mass spectrometry represents an efficient system for the isolation and identification of protein-protein interactions. To identify common as well as exclusive binding partners, we have performed TAP downstream of RSK1, RSK4 variant I and RSK4 variant II

transient overexpression in HEK293A cells, followed by qualitative mass spectrometric analysis (MS/MS). MS/MS data were searched against the human protein database UniProtKB/Swiss-Prot and Cytoscape (pathway) analysis was performed to integrate and visualise data in the context of signalling pathways[26] **(Figure 18)**. In this study, we report that RSK1 and RSK4 (variants I & II[27]) interact with proteins involved in the regulation of p53 (*TP53*) activity as well as proteins regulating DNA damage repair pathways including non-homologous end joining (NHEJ), homologous recombination (HR) and nucleotide excision repair (NER) pathways. Interestingly, these kinases were also found to interact with proteins involved in immune response, metabolism and neurodegeneration.

The application of quantitative mass spectrometry-based proteomics coupled with phosphopeptide enrichment strategies (e.g. immobilised metal affinity chromatography [IMAC] and TiO_2) represents a highly sensitive and powerful tool for large scale identification and quantification of phosphorylation changes in biological samples. To identify which of our TAP binding partners may be substrates for our kinases and assess the larger scale effect of our RSK isoforms on the phosphoproteome, we performed quantitative mass spectrometric global phosphoproteomics analysis of A549 cells transiently silenced for RSK1 or RSK4. Here, we show that RSK1 and RSK4 modulate substrates involved in DNA damage repair pathways including homologous recombination and non-homologous end joining.

[26] For simplicity, TAP and phosphoproteomics/proteomics hits are referred to with their gene names in pathway analysis and supplementary tables.
[27] In this section, unless otherwise specified, RSK4 will refer to both RSK4 variant I and RSK4 variant II.

4.2 Results

4.2.1 Tandem Affinity Purification (TAP) – LC-MS/MS

HEK293[28] cells transfected with FLAG-HA-HA[29]-tagged EV (empty vector control), RSK1, RSK4 variant I and RSK4 variant II fusion constructs were EGF (epidermal growth factor) stimulated to activate RSKs and promote their association with prospective interacting partners. Following TAP, resulting immunocomplexes were analysed by liquid chromatography tandem mass spectrometry (LC-MS/MS) (Mark Skehel, MRC Laboratory of Molecular Biology, Cambridge, UK). LC-MS/MS data were then searched against the human protein database UniProtKB/Swiss-Prot using the Mascot search engine and validated using the Scaffold proteome software, resulting in a total of 764 identified proteins. Hits detected in the EV control condition were excluded and resulting proteins (N=633) were subjected to pathway analysis (Olivier Pardo, Imperial College London, London, UK) **(Figure 18, Table S 15-Table S 21)**.

Following RAS/MAPK pathway stimulation, ERK1/2 directly interact with and phosphorylate RSKs (Anjum & Blenis, 2008). Analysis of our TAP data revealed that both RSK1 and RSK4 immunoprecipitate with ERK1 (*MAPK3*), indicating pathway activation **(Table S 18)**. Full RSK kinase activation also depends on PDK1 (*PDPK1*) binding and phosphorylation. Unlike RSK1-3, RSK4 activation was shown to be PDK1 independent (Dummler et al., 2005); nevertheless, we were able to detect both RSK1 and RSK4 interacting with PDK1 in our cells **(Table S 15 & Table S 21)**. Interestingly, RSK1 co-purifies with all RSK family members (RSK2 [*RPS6KA3*], RSK3 [*RPS6KA2*] and RSK4 [*RPS6KA6*]), as well as the structurally related homolog MSK1 (*RPS6KA5*), while both RSK4 variants reciprocally immunoprecipitate with RSK1, suggesting that some RSK functions might be dependent on heterodimerisation with other RSK family members **(Table S 15-Table S 17)**. Although RSK4 variant I and II differ only in the first exon **(Figure S 9)**, the variant II of RSK4 had more common interactors with RSK1 (N=76) than with RSK4 variant I (N=54), or overlapping interactors between RSK1 and RSK4 variant I (N=40) **(Figure 18)**. For example, RSK1 and RSK4 variant II (and not variant I) interact with components of both the small 40S

[28] cDNA transfection is more efficient in HEK293A cells compared to A549 cells.
[29] N-terminal FLAG-HA-HA tags.

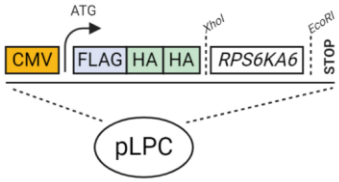
ATG
XhoI
EcoRI
CMV
FLAG
HA
HA
RPS6KA6
STOP
pLPC

0 Cloning
1 HEK293 cells
2 Anti-FLAG
3 Anti-HA
4 SDS-PAGE
5 LC-MS/MS
1st elution
2nd elution
- Transient cDNA transfection
- Starvation & EGF stimulation
- Whole-cell lysate preparation
- Bind to Anti-FLAG beads
- Wash
- 3XFLAG peptide elution
- Bind to Anti-HA beads
- Wash
- 2X Laemmli buffer elution
- Denaturation & separation by SDS-PAGE
- Gel lanes excised
- Reduction, alkylation, trypsin digestion & extraction
- Analysis by LC-MS/MS

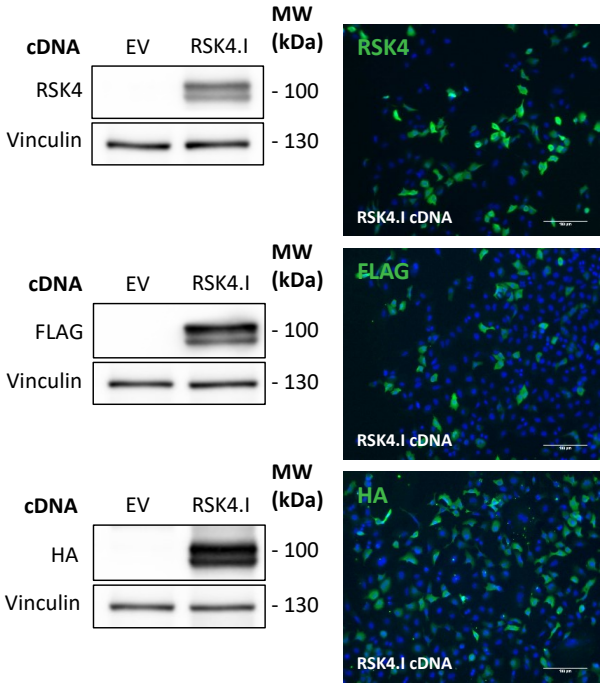
cDNA
EV
RSK4.I
MW (kDa)
RSK4
- 100
Vinculin
- 130
cDNA
EV
RSK4.I
MW (kDa)
FLAG
- 100
Vinculin
- 130
cDNA
EV
RSK4.I
MW (kDa)
HA
- 100
Vinculin
- 130

RSK4
RSK4.I cDNA
FLAG
RSK4.I cDNA
HA
RSK4.I cDNA

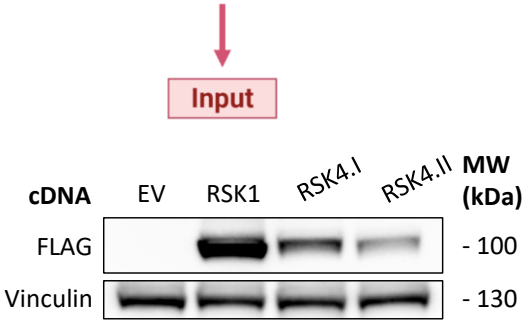
Input
cDNA
EV
RSK1
RSK4.I
RSK4.II
MW (kDa)
FLAG
- 100
Vinculin
- 130

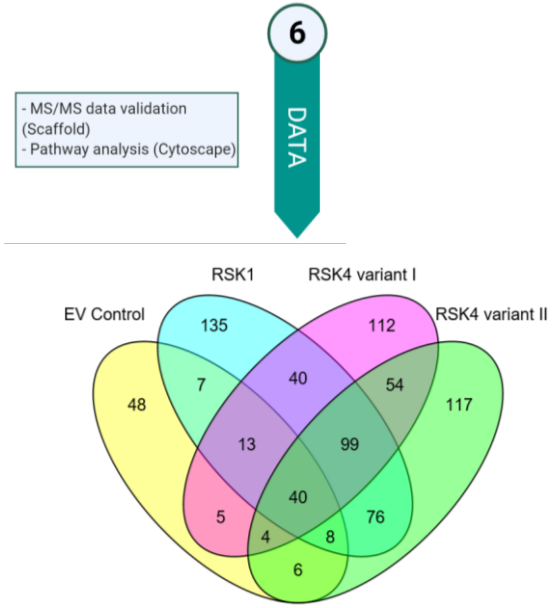
6 DATA
- MS/MS data validation (Scaffold)
- Pathway analysis (Cytoscape)
RSK1
RSK4 variant I
EV Control
RSK4 variant II
135
112
48
7
40
54
117
13
99
40
5
76
4
8
6

Figure 18| Tandem affinity purification workflow. (0) RSK1, RSK4 variant I (RSK4.I) and RSK4 variant II (RSK4.II) were PCR-cloned into N-terminal FLAG-HA-HA pLPC vectors and efficient expression and detection was assessed by western blotting and immunofluorescence. **(1)** Vectors were transiently transfected in HEK293A cells and following serum starvation and EGF stimulation, whole cell lysates were prepared for immunoprecipitation. **(2, 3)** Lysates were sequentially affinity purified with anti-FLAG and anti-HA conjugated beads, and eluted with 3XFLAG peptide and 2X Laemmli buffer, respectively. **(4)** Eluates were denatured and separated by SDS-PAGE, gel lanes were excised and **(5)** in-gel reduced, alkylated and trypsin digested. Extracted digests were analysed by LC-MS/MS and **(6)** data were searched against the human protein database UniProtKB/Swiss-Prot using the Mascot search engine and validated using the Scaffold proteome software, resulting in a total of 764 identified proteins. Hits detected in the EV Control condition were excluded and resulting proteins (N=633) were subjected to pathway analysis. LC-MS/MS was performed by Mark Skehel (collaboration) and pathway analysis by Olivier Pardo (personal communication).

(e.g. RPS2, RPS7) and large 60S (e.g. RPL10A, RPL26L1) ribosomal subunits, and several members of the heat shock protein (HSP) family, such as HSP40 (*DNAJ*) and HSP27 (*HSPB1*) **(Table S 15, Table S 17 & Table S 19)**. Lastly, RSK1 and RSK4 associate with several heterogeneous nuclear ribonucleoproteins (hnRNPs) (e.g. HNRNPH1, HNRNPU, HNRNPF), suggesting their possible involvement in alternative splicing and/or nucleocytoplasmic mRNA transport **(Table S 18)** (Geuens, Bouhy & Timmerman, 2016).

Data from our TAP screen were then used to build directed functional networks in Cytoscape using the Reactome FI (functional interaction) plugin (Wu, Feng & Stein, 2010). Modules were then isolated based on network connectivity and, following gene ontology (GO) enrichment analysis, four major sub-networks emerged: 1) DNA damage repair and cell death, 2) immune response, 3) metabolism and 4) neurodegeneration related pathways **(Figure 19)**. The DNA damage repair and cell death network is organised into six smaller interconnected nodes that include proteins involved in NHEJ, HR, NER, cell death and mitochondria, and proteins regulating PLK1 (polo-like kinase 1) and p53 activity **(Figure 19)**. Within this network, RSK1 and both RSK4 transcript variants interact with positive or negative modulators of p53. For instance, common interactors include the catalytic subunit of DNA-dependent protein kinase (DNA-PKcs; *PRKDC* or *XRCC7*); the transcriptional co-regulator RNA helicase p68 (*DDX5*); and the demethylase KDM1A **(Figure 19)**. RSK1 also exclusively interacts with several proteins that converge on p53 either directly or indirectly, such as all three catalytic subunits of protein kinase CK2 (previously known as casein kinase II): CSNK2A1, CSNK2A2 and CSNK2B; transcription initiation factor TFIID subunit TAF4; double-strand break repair protein MRE11A; cell-cycle and apoptosis regulator protein 2 (CCAR2) and methyltransferase PRMT1 **(Figure 19)**. Interestingly, both RSK4 transcript variants, unlike RSK1, interact with p53, suggesting that RSK4 may play a more prominent role

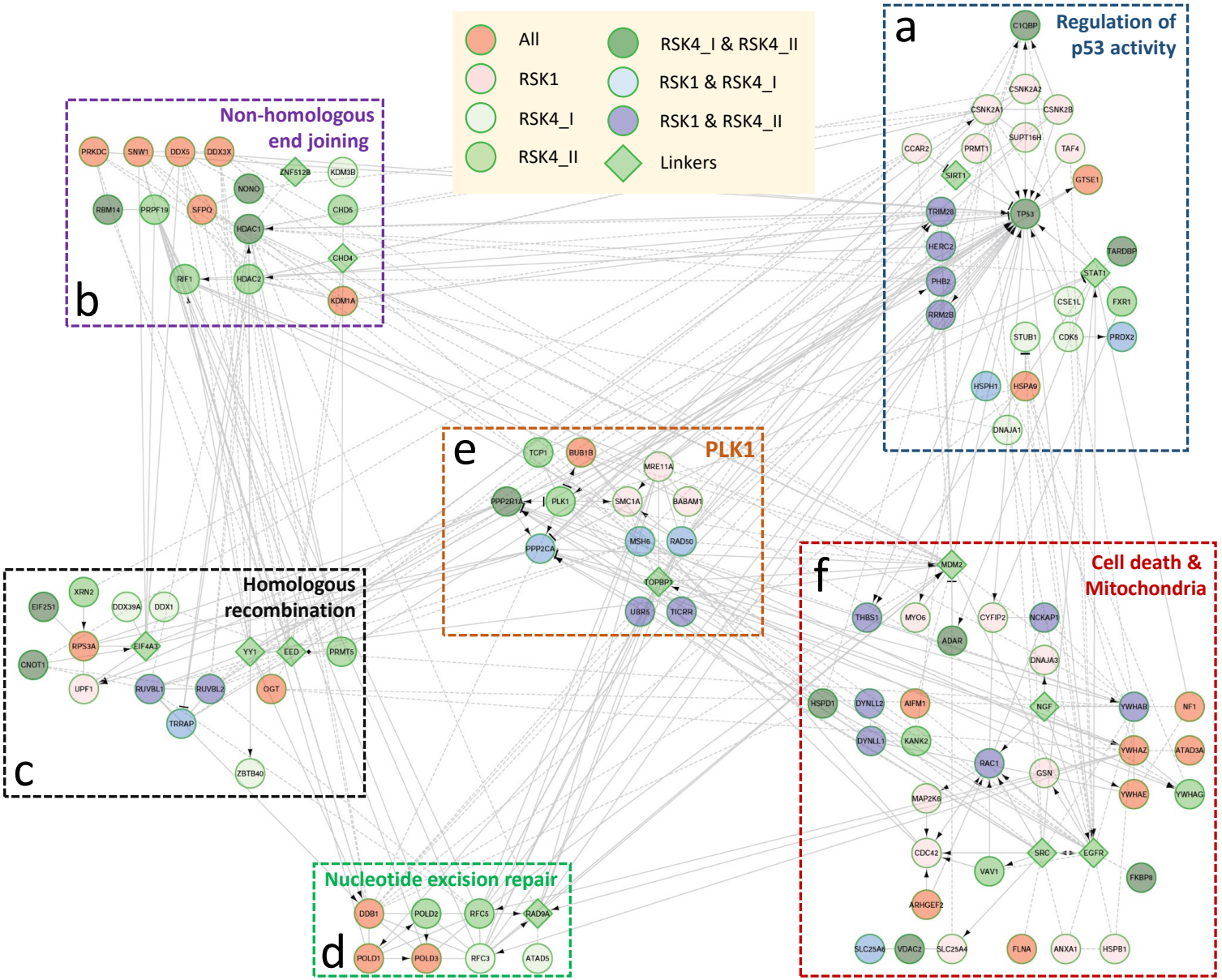
All
RSK1
RSK4_I
RSK4_II
RSK4_I & RSK4_II
RSK1 & RSK4_I
RSK1 & RSK4_II
Linkers
a
Regulation of p53 activity
b
Non-homologous end joining
c
Homologous recombination
d
Nucleotide excision repair
e
PLK1
f
Cell death & Mitochondria

Figure 19| RSK1 and RSK4 interact with proteins involved in DNA damage response and p53 activity. RSK1, RSK4 variant I and RSK4 variant II were affinity purified from HEK293A cells and complexes were analysed by LC-MS/MS. LC-MS/MS data were searched against the human protein database UniProtKB/Swiss-Prot and integrated into signalling networks following Cytoscape analysis: **(a)** Regulation of p53 activity, **(b)** Non-homologous end joining, **(c)** Homologous recombination, **(d)** Nucleotide excision repair, **(e)** PLK1, **(f)** Cell death & Mitochondria. Arrows indicate positive regulation whereas blunt arrows indicate negative regulation. LC-MS/MS was performed by Mark Skehel (collaboration) and pathway analysis by Olivier Pardo (personal communication).

in p53 regulation than RSK1 **(Figure 19)**. In short, these data propose that both RSK1 and RSK4 might be involved in the regulation of p53 activity and/or function. Considering that p53 is a key promoter of DNA damage repair pathways, it is not surprising that RSK1 and RSK4 interact with proteins involved in DNA-damage response (DDR). For instance, RSK4 immunoprecipitates with HDAC1 and ATP-dependent RNA helicase DDX1, which are involved in DNA double-strand break (DSB) repair by NHEJ and HR, respectively **(Figure 19)**. Similarly, RSK1 co-purifies with MRE11A and RAD50, key components of DSB repair by both HR and NHEJ pathways **(Figure 19)**. Further, RSK1 and RSK4 interact with proteins involved in DNA single-strand break (SSB) repair, including DNA damage-binding protein 1 (DDB1) and DNA polymerases delta 1 (POLD1) and 2 (POLD2), all of which are required during NER **(Figure 19)** (Jackson & Bartek, 2009).

RSK1 and RSK4 were also found to be associated with proteins involved in immune response, including targets of type I and type II interferons (IFN), T-cell development and inflammatory cytokine production **(Figure S 10)**. RSK4 co-purifies with several ATP-dependent RNA helicases including DDX41, which is involved in the induction of type I IFN response (Platanias, 2005), while RSK1 interacts with CDC42 and RAC1 RHO GTPases, both of which are essential for T-cell development **(Figure S 10)** (Smits et al., 2010; Dumont et al., 2009). Further, RSK1 and RSK4 interact with several members of the mitochondrial transporter family SLC25 (e.g. SLC25A1[30], SLC25A3[31], and SLC25A5[32]), which participate in numerous metabolic pathways **(Figure S 11)** (Palmieri, 2013). Finally, both RSK1 and RSK4 associated with neurodegeneration related proteins such as neurofibromin (NF1) (Parkinson's disease), CYFIP1 (schizophrenia and autism) and LSD1/KDM1A (Alzheimer's disease) **(Figure S 12)**.

[30] Tricarboxylate (citrate) transport protein.
[31] Phosphate carrier protein.
[32] ADP/ATP translocase.

4.2.2 A549 cell global proteomics and phosphoproteomics profiling – LC-MS/MS

To complement our TAP screen, we profiled the phosphoproteome and total proteome of A549 cells following treatment with NT (non-targeting control), RSK1 or RSK4 siRNAs (Howard Desmond, Paul Huang, The Institute of Cancer Research, London, UK). IMAC-enriched (phosphoproteome) and total proteome samples were analysed by LC-MS/MS. LC-MS/MS data were then processed by MaxQuant and searched against the human protein database UniProtKB/Swiss-Prot using the Andromeda search engine, followed by pathway analysis (Olivier Pardo, Imperial College London, London, UK). Differentially altered phosphoproteomics and total proteomics hits were visualised in a volcano plot, showing normalised (to control) fold change of serine-threonine-tyrosine (STY) phosphorylation or total protein (x-axis), plotted against *P*-values (y-axis) as determined by multiple t-test analysis **(Figure 20, Figure 24 & Table S 22-Table S 25)**.

RSK1 downregulation significantly decreased the phosphorylation of rpS6[33] (*RPS6*), a component of the 40S ribosomal subunit and a well-characterised S6K and RSK phosphorylation substrate **(Table S 23)** (Meyuhas, 2008). Further, the phosphorylation of 40S ribosomal protein RPS3A (Tyr256 or Ser263) and 60S ribosomal protein RPL23A (Ser43) was decreased in the RSK1-silenced condition, while the former also co-purified with RSK1 (and RSK4) in our TAP data **(Figure 27 & Table S 23)**. The total protein levels of 60S ribosomal proteins RPL14 and RPL22L1 were also decreased following RSK1 silencing **(Table S 25)**. Hence, in conjunction with the TAP results, this may suggest that RSK1 plays a more prominent role than RSK4 in modulating the activity and/or function ribosomes.

Following functional network building and GO enrichment analysis of the phosphoproteomics data, both RSK1 and RSK4 hits were enriched in pathways involved in DDR, including NHEJ and HR **(Figure 21 & Figure 22)**, corroborating TAP data. For example, RSK1 downregulation was associated with decreased phosphorylation of DNA-PKcs (Ser3205), a vital component of NHEJ pathway **(Figure 21)** (Davis, Chen & Chen, 2014). Interestingly, DNA-PKcs was shown to interact with both RSK1 and RSK4 in our TAP **(Figure 27)**. Further, RSK4

[33] Sequence window within the five conserved serine residues of rpS6 (Ser235, Ser236, Ser240, Ser244 and Ser247).

a

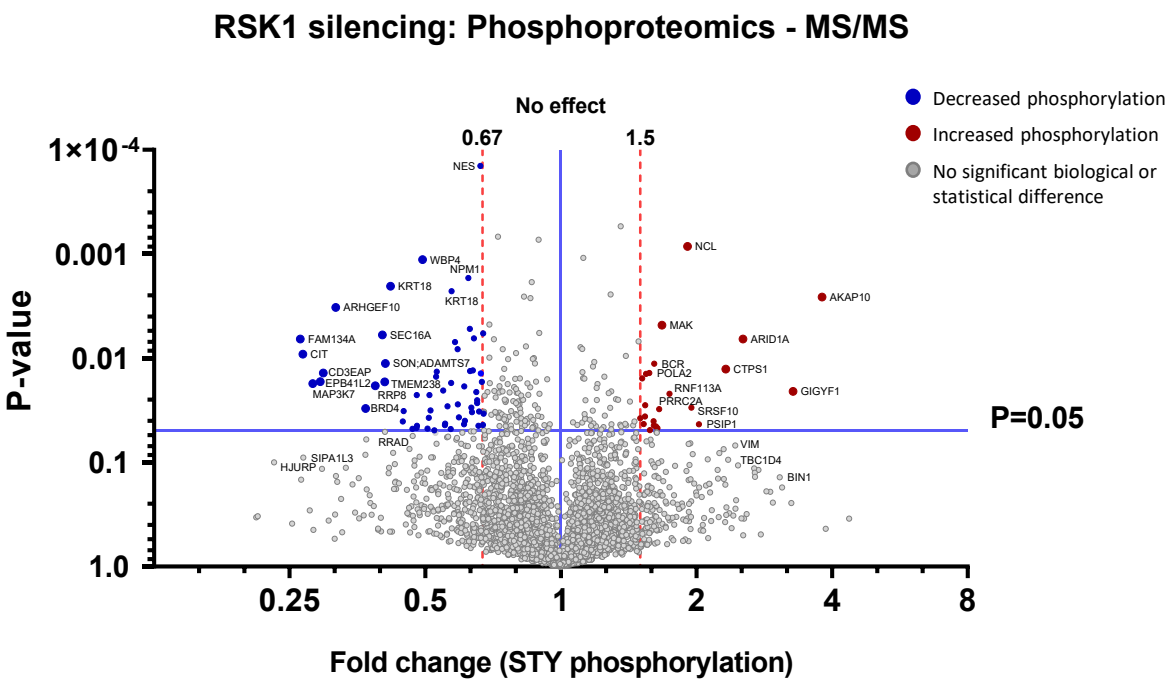

b

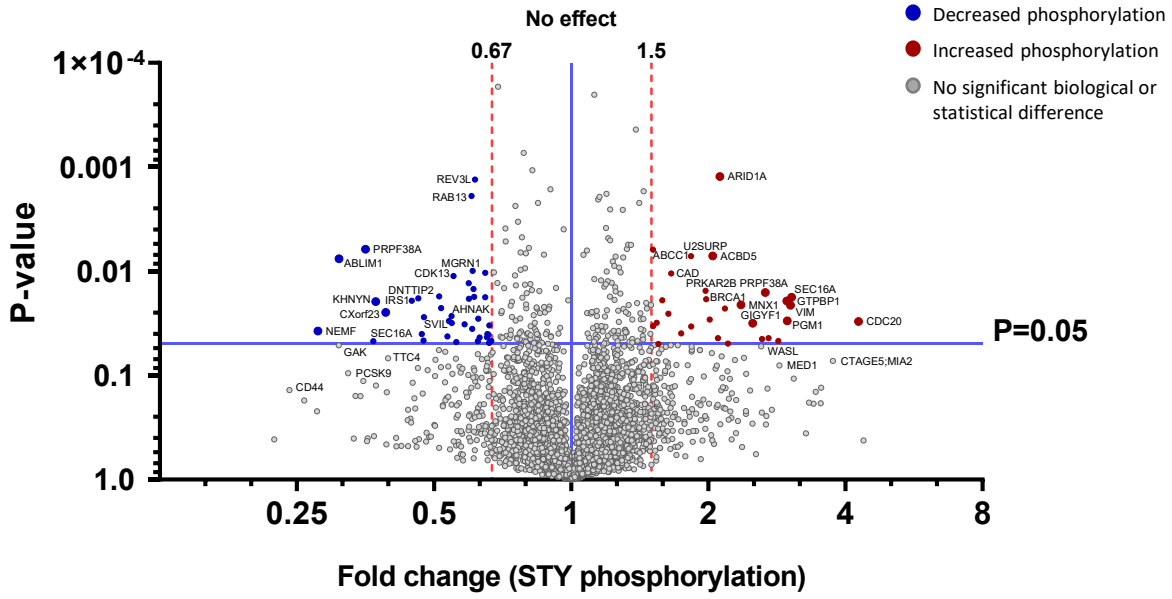

Figure 20| Volcano plot analysis of phosphoproteomics hits. Volcano plots show normalised (to control) fold change of serine-threonine-tyrosine (STY) phosphorylation changes (x-axis) downstream of **(a)** RSK1 and **(b)** RSK4 silencing, plotted against P-values (y-axis) as determined by multiple t-test analysis in Prism (GraphPad Software). $P \leq 0.05$ was interpreted to denote statistical significance. Data points in the upper left (ratio < 0.67) and upper right (ratio > 1.5) sections represent the most significant hits. LC-MS/MS was performed by Howard Desmond and Paul Huang (collaboration).

downregulation increased the phosphorylation of promyelocytic leukemia (PML; Ser36/38/40) protein, which is involved in repairing DSBs by HR **(Figure 22)** (Chang et al., 2018). In addition to DDR, RSK4 hits were also involved in mRNA splicing, spliceosome formation and mRNA transport **(Figure S 13)**.

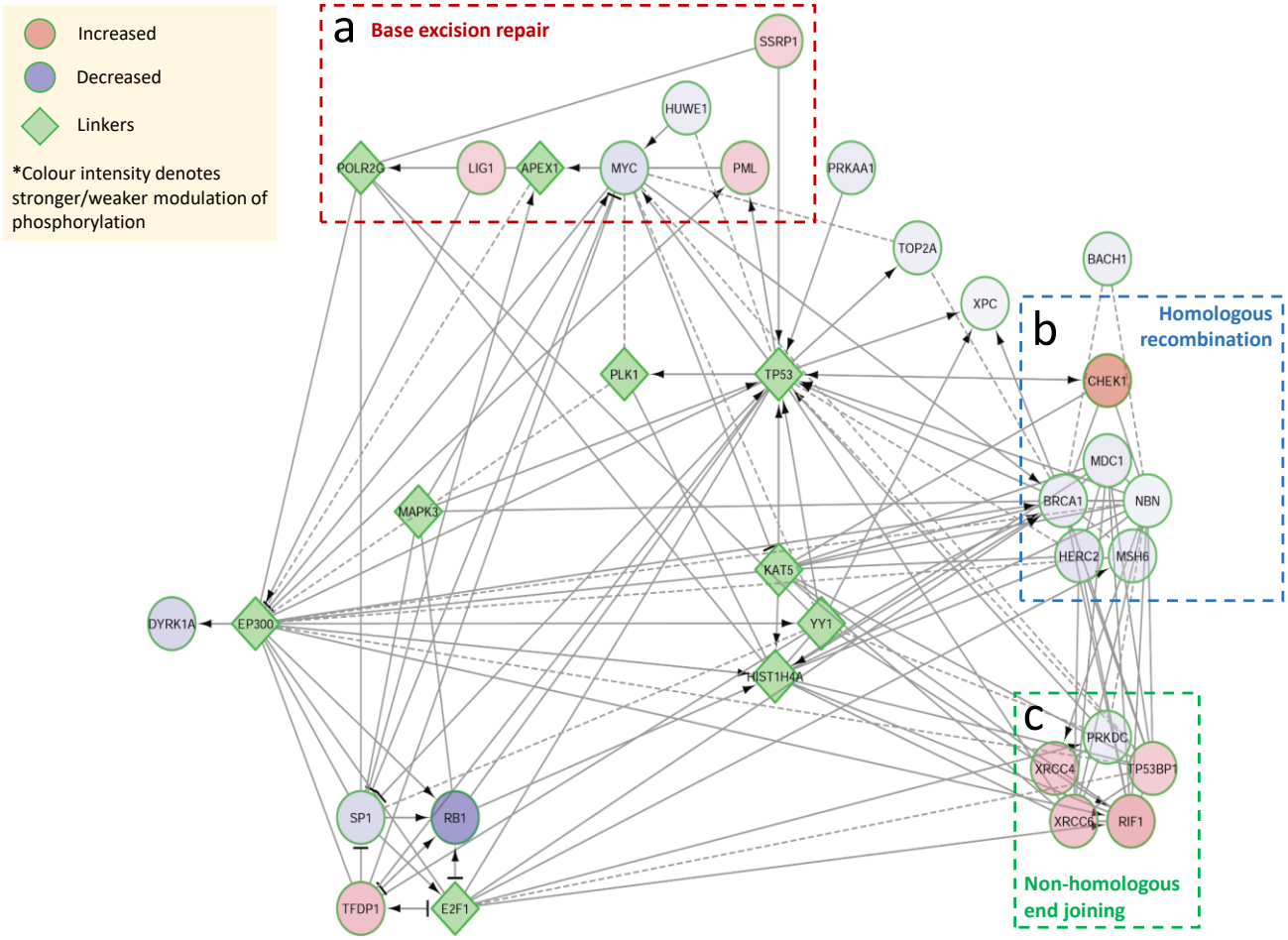

Figure 21| RSK1 modulates the phosphorylation of proteins involved in DNA damage response. RSK1 was transiently downregulated in A549 cells, lysates were trypsin digested and labelled with tandem mass tag (TMT) isobaric labelling reagents. Pooled and labelled samples (80%) were subjected to IMAC phosphopeptide enrichment and analysed by LC-MS/MS. LC-MS/MS data were searched against the human protein database UniProtKB/Swiss-Prot and integrated into signalling networks following Cytoscape analysis: **(a)** Base excision repair, **(b)** Homologous recombination, **(c)** Non-homologous end joining. Arrows indicate positive regulation whereas blunt arrows indicate negative regulation. LC-MS/MS was performed by Howard Desmond and Paul Huang (collaboration) and pathway analysis by Olivier Pardo (personal communication).

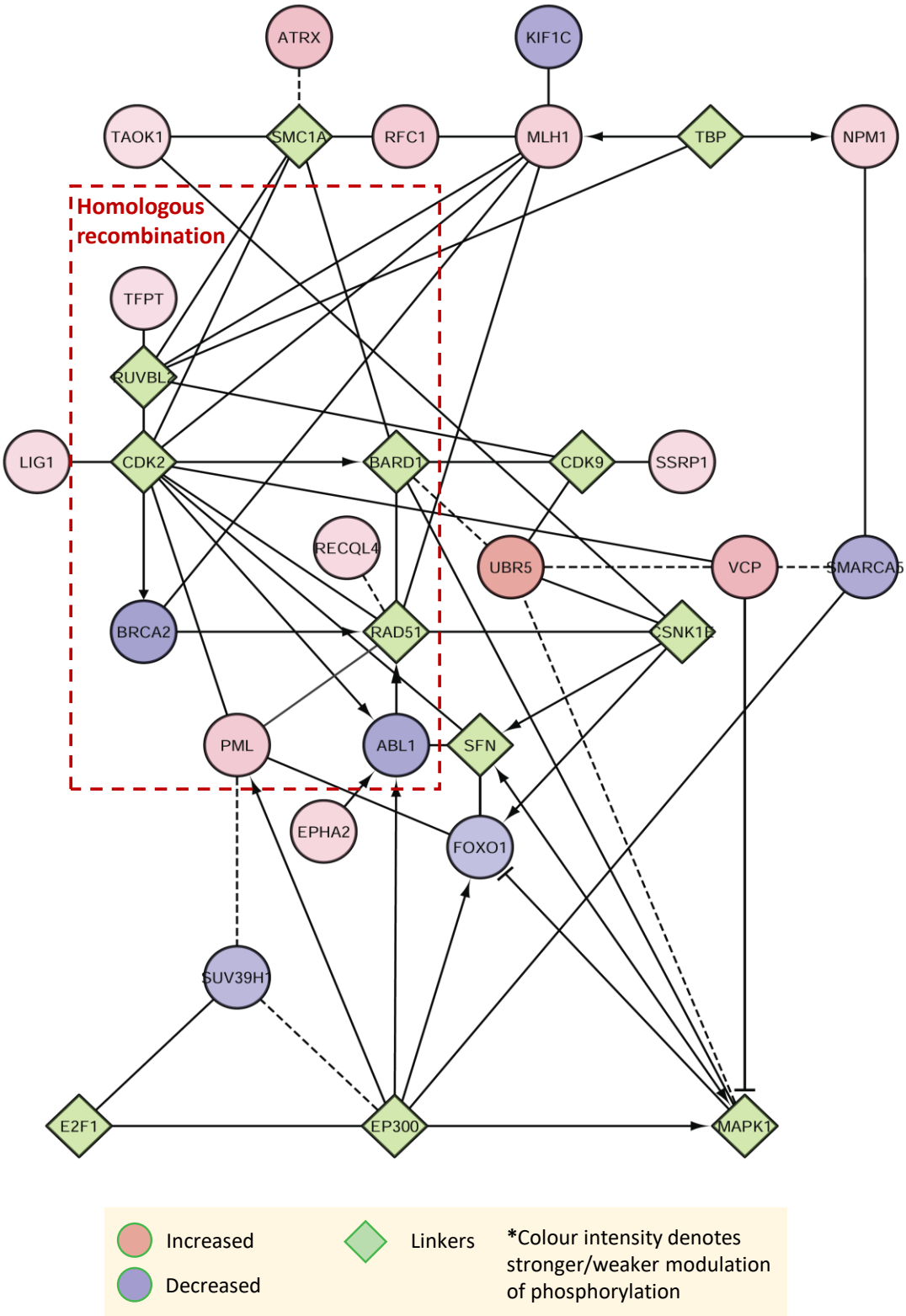

Figure 22| RSK4 modulates the phosphorylation of proteins involved in homologous recombination. RSK4 was transiently downregulated in A549 cells, lysates were trypsin digested and labelled with tandem mass tag (TMT) isobaric labelling reagents. Pooled and labelled samples (80%) were subjected to IMAC phosphopeptide enrichment and analysed by LC-MS/MS. LC-MS/MS data were searched against the human protein database UniProtKB/Swiss-Prot and integrated into signalling networks following Cytoscape analysis. Arrows indicate positive regulation whereas blunt arrows indicate negative regulation. LC-MS/MS was performed by Howard Desmond and Paul Huang (collaboration) and pathway analysis by Olivier Pardo (personal communication).

To identify mutually or differentially regulated phosphoproteomics hits between RSK1 and RSK4, we visualised our data in a Venn diagram **(Figure 23)**. Here, we show that RSK1 and RSK4 differentially regulate the phosphorylation of vimentin (VIM), ribosomal RNA-processing protein 8 (RRP8), serine/arginine-rich splicing factor 10 (SRSF10), pre-mRNA-splicing factor 38A (PRPF38A) and protein transport protein SEC16A; while the phosphorylation of AAT-rich interactive domain-containing protein 1A (ARID1A) and GRB10-interacting GYF protein 1 (GIGYF1) is mutually increased, and the phosphorylation of nestin (NES), E3 ubiquitin-protein ligase MGRN1 and bystin (BYSL) is mutually decreased, in response to RSK1 or RSK4 silencing **(Figure 23)**. Considering that the majority of these phosphorylation sites have not been experimentally characterised yet, phospho-specific antibodies raised against these sites and subsequent mutational studies are required to validate these changes and demonstrate their functional significance, respectively.

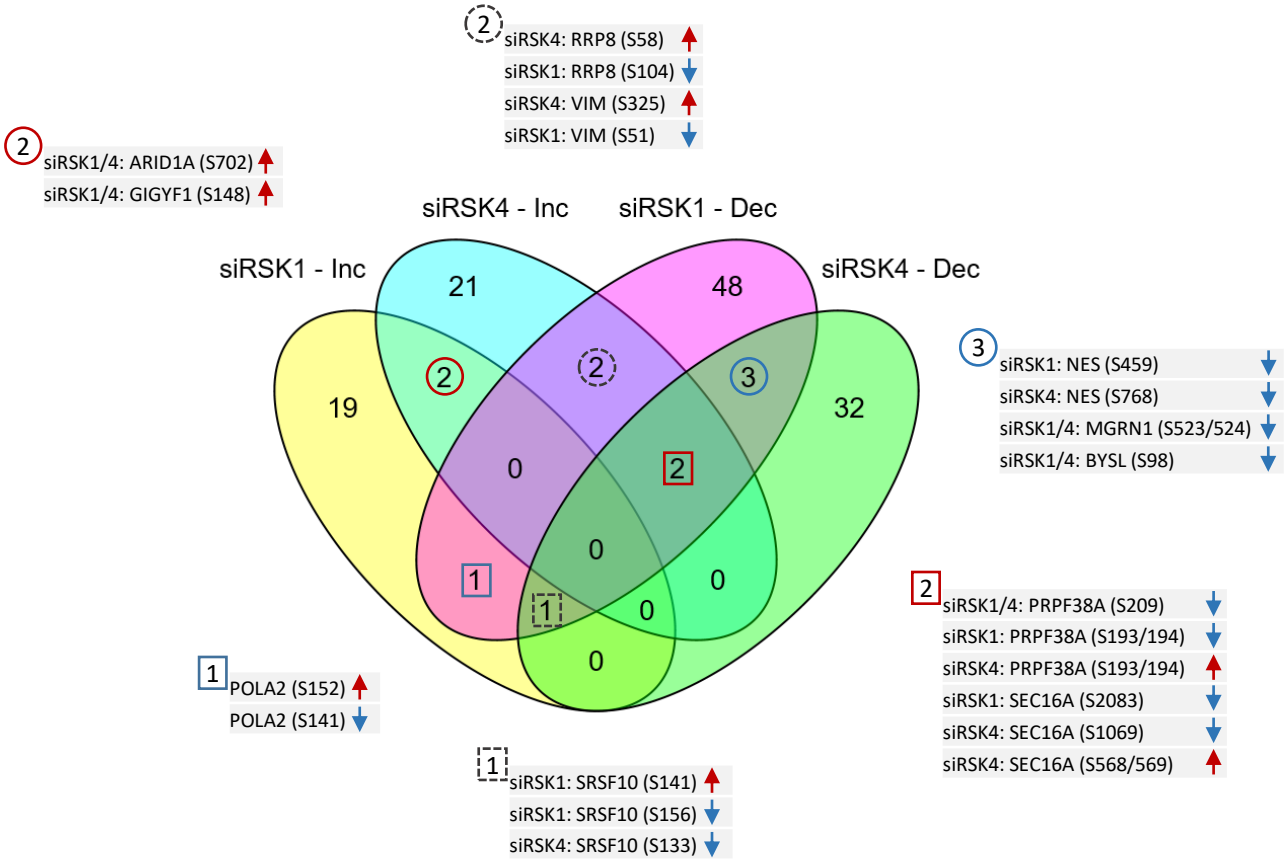

Figure 23| Identification of mutually and differentially regulated phosphoproteomics hits between RSK1 and RSK4. Venn diagram of RSK1 increased phosphorylation (siRSK1 - Inc), RSK4 increased phosphorylation (siRSK4 - Inc), RSK1 decreased phosphorylation (siRSK1 - Dec) and RSK4 decreased phosphorylation (siRSK4 - Dec) hits: AT-rich interactive domain-containing protein 1A (ARID1A: Ser702); GRB10-interacting GYF protein 1 (GIGYF1: Ser148); Ribosomal RNA-processing protein 8 (RRP8: Ser58, Ser104); Vimentin (VIM: Ser325, Ser51); Nestin (NES: Ser459, Ser768); E3 ubiquitin-protein ligase (MGRN1: Ser523/524); Bystin (BYSL: Ser98); Pre-mRNA-splicing factor 38A (PRPF38A: Ser209, Ser193/194); Protein transport protein SEC16A (Ser2083, Ser1069, Ser568/569); Serine/arginine-rich splicing factor 10 (SRSF10: Ser141, Ser156, Ser133); DNA polymerase alpha subunit B (POLA2: Ser152, Ser141).

Due to insufficient RSK1 total proteomics hits we were unable to derive RSK1-regulated functional pathways. Interestingly though, RSK1 knockdown decreased the expression of both fatty acid desaturase-1 (FADS1) and -2 (FADS2), potentially implicating RSK1 in fatty acid metabolism **(Figure 24a & Table S 25)**. Pathway analysis of RSK4 total proteomics hits revealed proteins involved in autophagy (p62; SQSTM1), cell attachment and migration (ANTXR1), mRNA transcription (YAP1) and iron homeostasis (FTH1) **(Figure 25)**. Further, RSK4 silencing decreased the expression of calpain-2 (CAPN2) and calpain-4 (CAPN4; CAPNS1), which are cysteine proteases with important implications in cancer **(Figure 24b & Table S 25)** (Storr et al., 2011). To identify mutually or differentially regulated proteins between RSK1 and RSK4, we visualised our data in a Venn diagram **(Figure 26)**. While no differentially regulated proteins were identified, RSK1 and RSK4, among others, mutually regulate the expression of proteins involved in ubiquitination (UBE2G2), G1/S phase transition (CDK6) and nuclear protein import (TNPO2) **(Figure 26)**. Lastly, to examine whether phosphoproteomics changes correlate with changes at the proteomic level, we integrated our phosphoproteomics and proteomics data in a Venn diagram **(Figure S 14)**. Although no correlation was observed between RSK1 phospho and total proteomics hits, RSK4 silencing decreased the phosphorylation of insulin receptor substrate 1 (IRS1; Ser636/639), which resulted in upregulation of its total protein levels **(Figure S 14)**. In corroboration, Ser636/639 phosphorylation negatively regulates the stability of IRS1 and was previously shown to be mediated by mTORC1 (Tzatsos, 2009).

While, RSK1 and RSK2 were shown to regulate the expression of several transcription factors (TFs), including CREB and c-Fos (Houles & Roux, 2018), to date, no RSK4-regulated TF has been identified. Here, in an attempt to identify TFs that might explain the total proteomic changes downstream of RSK4 downregulation, we utilised the iRegulon plugin from Cytoscape, which identifies putative TFs for a given set of targets (Olivier Pardo, Imperial College London, London, UK). Some of the major transcription factors that emerged as possibly regulating many of the identified total proteomics targets include NFE2, MAFK and histone acetyltransferase EP300 **(Figure S 15)**. Further validation would now be required to assess whether they are modulated by RSK4.

a

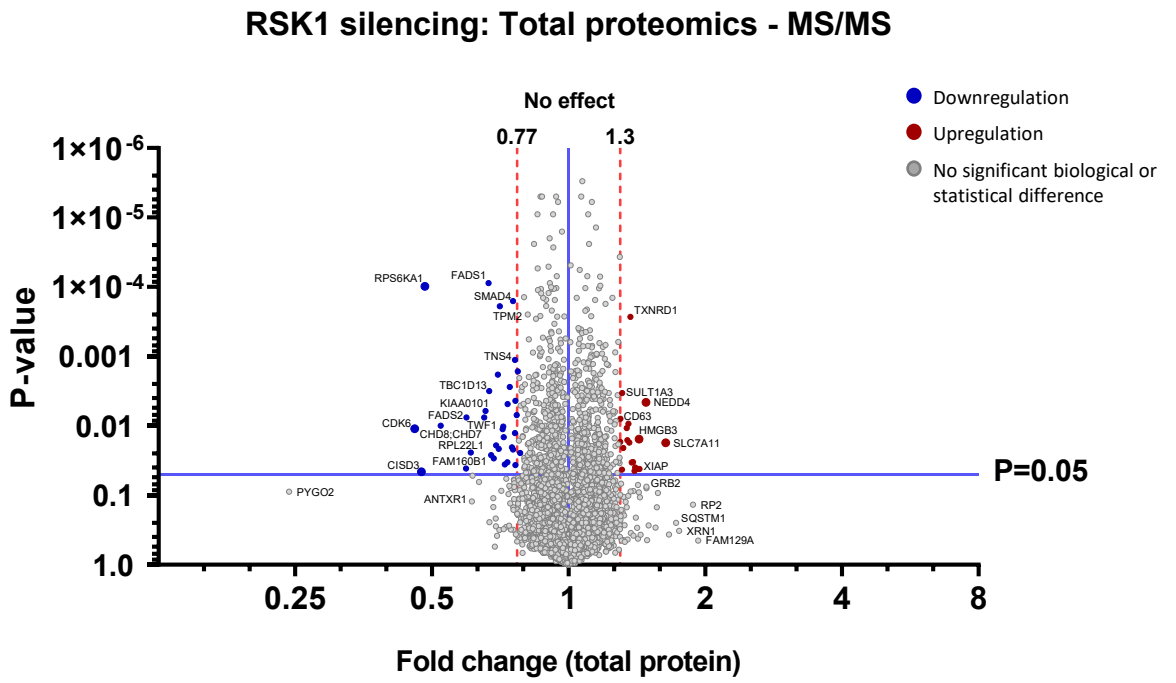

b

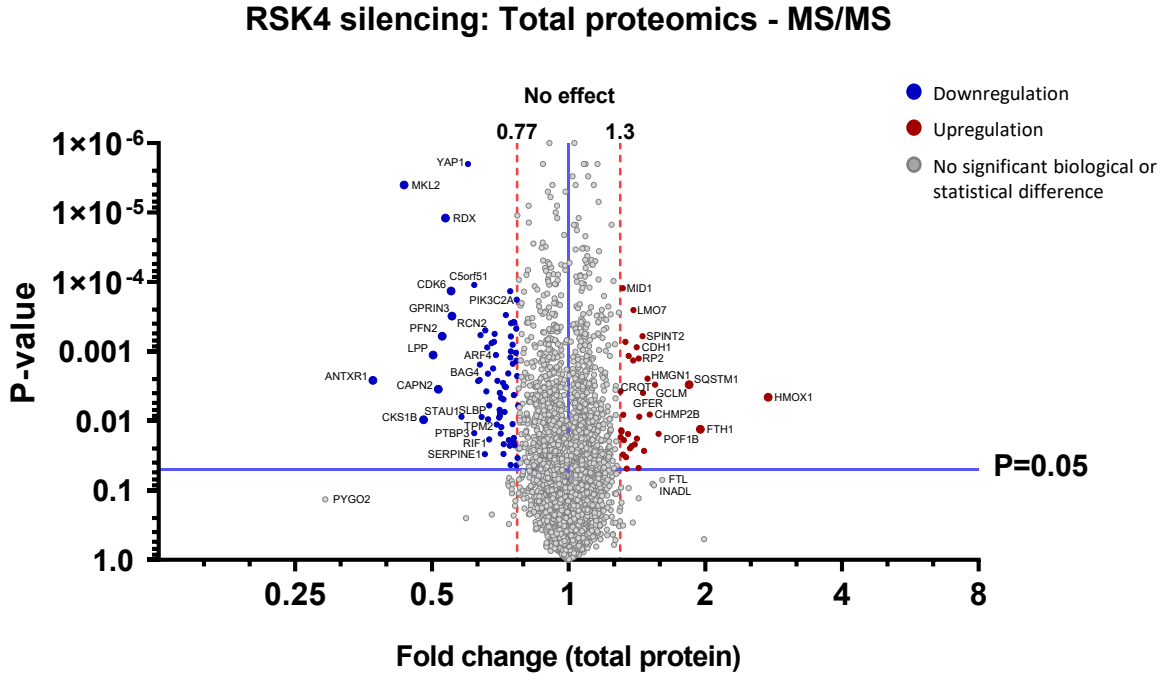

Figure 24| Volcano plot analysis of total proteomics hits. Volcano plots show normalised (to control) fold change of total protein changes (x-axis) downstream of **(a)** RSK1 and **(b)** RSK4 silencing, plotted against P-values (y-axis) as determined by multiple t-test analysis in Prism (GraphPad Software). $P \leq 0.05$ was interpreted to denote statistical significance. Data points in the upper left (ratio < 0.77) and upper right (ratio > 1.3) sections represent the most significant hits. LC-MS/MS was performed by Howard Desmond and Paul Huang (collaboration).

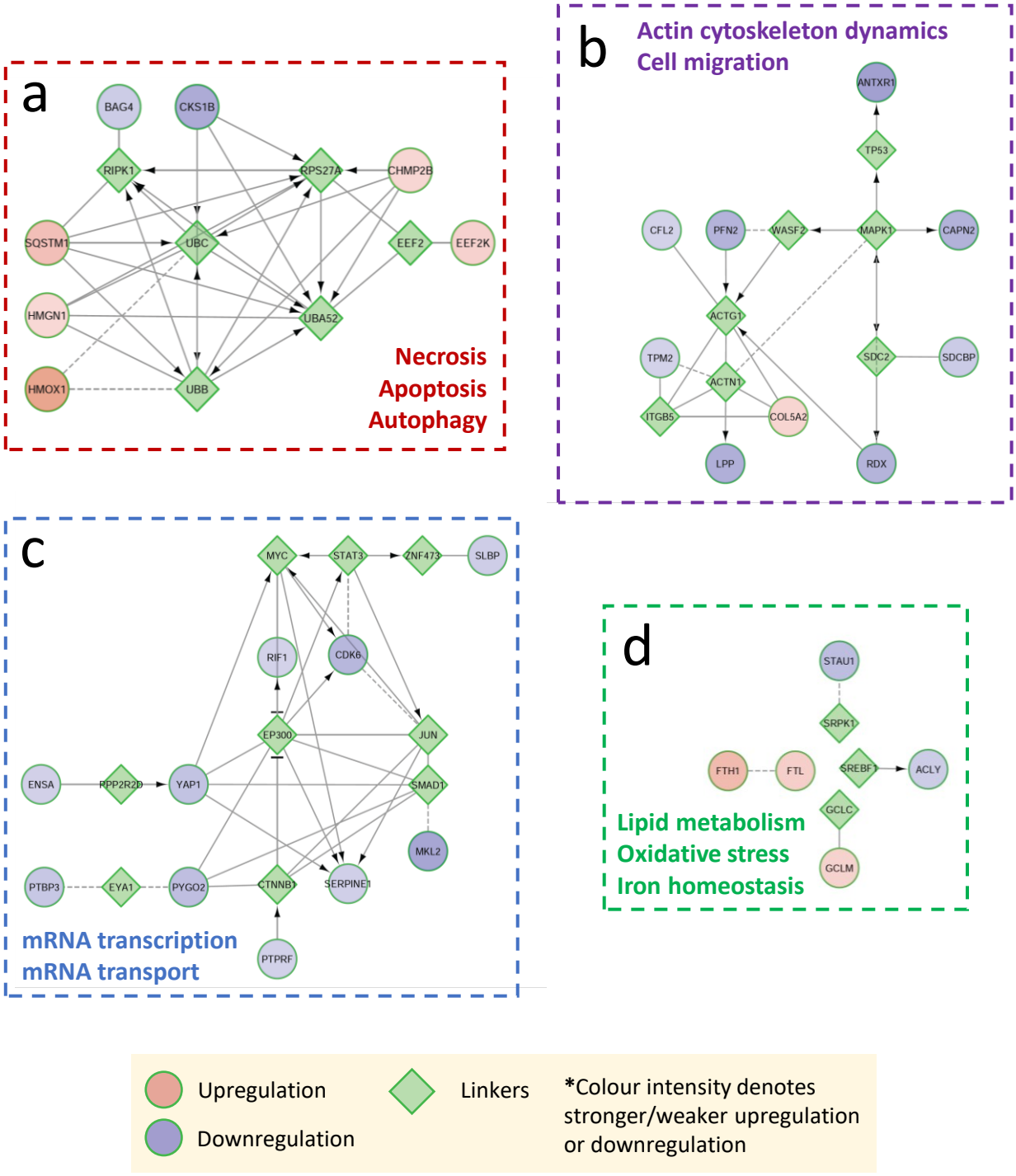

Figure 25| RSK4 modulates the expression of proteins involved in key cellular pathways. RSK4 was transiently downregulated in A549 cells, lysates were trypsin digested and labelled with tandem mass tag (TMT) isobaric labelling reagents. Pooled and labelled samples (20%) were fractionated by strong cation-exchange (SCX) chromatography and analysed by LC-MS/MS. LC-MS/MS data were searched against the human protein database UniProtKB/Swiss-Prot and integrated into signalling networks following Cytoscape analysis: **(a)** Necrosis, Apoptosis, Autophagy, **(b)** Actin cytoskeleton dynamics & Cell migration, **(c)** mRNA transcription & transport, **(d)** Lipid metabolism, Oxidative stress, Iron homeostasis. Arrows indicate positive regulation whereas blunt arrows indicate negative regulation. LC-MS/MS was performed by Howard Desmond and Paul Huang (collaboration) and pathway analysis by Olivier Pardo (personal communication).

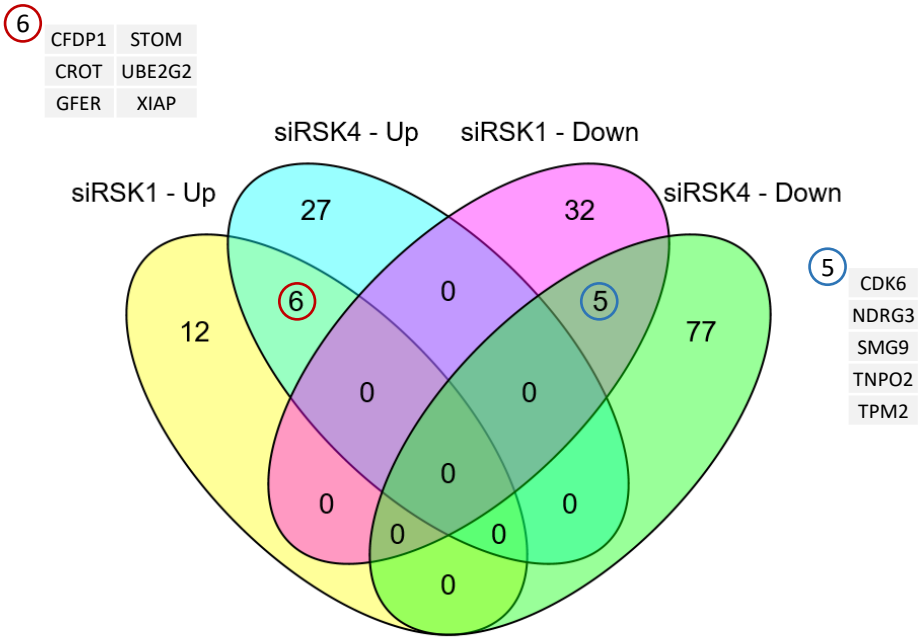

Figure 26| Identification of mutually and differentially regulated total proteomics hits between RSK1 and RSK4. Venn diagram of RSK1 upregulated (siRSK1 - Up), RSK4 upregulated (siRSK4 - Up), RSK1 downregulated (siRSK1 - Down) and RSK4 downregulated (siRSK4 - Down) hits: Craniofacial development protein 1 (CFDP1); Peroxisomal carnitine O-octanoyltransferase (CROT); FAD-linked sulfhydryl oxidase ALR (GFER); Erythrocyte band 7 integral membrane protein (STOM); Ubiquitin-conjugating enzyme E2 G2 (UBE2G2); E3 ubiquitin-protein ligase (XIAP); Cyclin-dependent kinase 6 (CDK6); NDRG3; SMG9; Transportin-2 (TNPO2); Tropomyosin beta chain (TPM2).

Direct kinase-substrate interaction is a prerequisite for substrate phosphorylation. Therefore, to examine whether the phosphorylation of our TAP hits is modulated in response to RSK1 or RSK4 knockdown, we integrated our TAP and phosphoproteomics data in a Venn diagram **(Figure 27 & Figure S 16)**. Here, we show that SEC16A interacts with and its phosphorylation is modulated by both RSK1 and RSK4, albeit at different sites **(Figure 27)**. RSK1 exclusively interacts with and modulates the phosphorylation of heat shock protein 27 (HSP27 or HSPB1; Ser82), while RSK4 exclusively interacts with and modulates the phosphorylation of LIM and SH3 protein 1 (LASP1; Ser146) and catenin delta-1 (CTNND1 or p120-catenin; Ser47) **(Figure S 16)**. Whether RSK1 or RSK4 directly phosphorylate these proteins or participate in a multi-protein complex involved in their regulation remains to be explored.

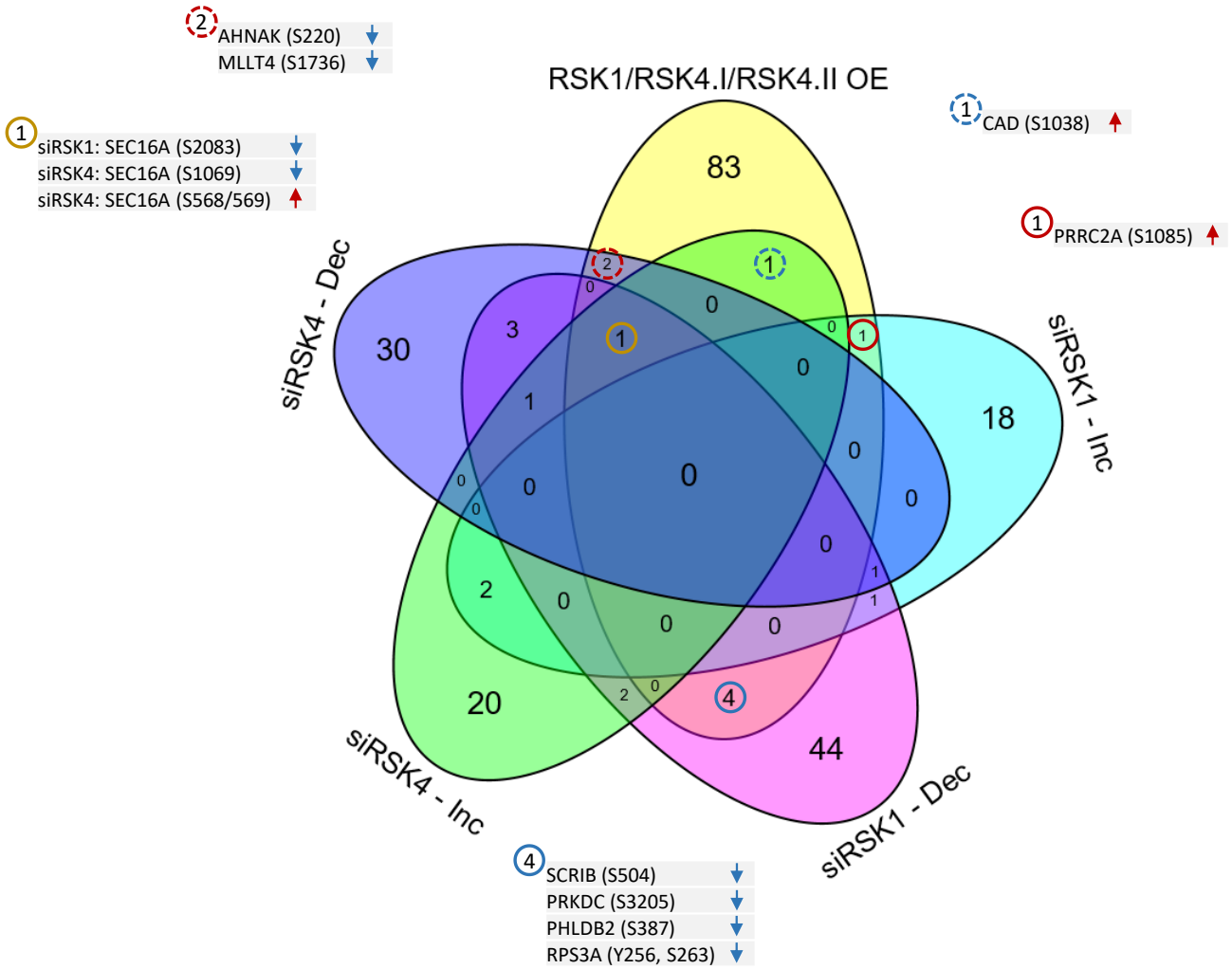

Figure 27| Identification of shared hits between tandem affinity purification and phosphoproteomics screens. Venn diagram of RSK1/RSK4.I/RSK4.II interacting partners (OE [overexpression] & affinity purification) integrated with RSK1 increased phosphorylation (siRSK1 - Inc), decreased phosphorylation (siRSK1 - Dec), and RSK4 increased phosphorylation (siRSK4 - Inc), decreased phosphorylation (siRSK4 - Dec) hits: Neuroblast differentiation-associated protein (AHNAK: Ser220); Afadin (MLLT4: Ser1736); Carbamoyl-phosphate synthetase 2, aspartate transcarbamylase, and dihydroorotase (CAD: Ser1038); Proline Rich Coiled-Coil 2A (PRRC2A: Ser1085); Protein scribble homolog (SCRIB: Ser504); DNA-dependent protein kinase catalytic subunit (PRKDC: Ser3205); Pleckstrin homology-like domain family B member 2 (PHLDB2: Ser387); 40S ribosomal protein S3a (RPS3A: Tyr256, Ser263); Protein transport protein SEC16A (Ser2083, Ser1069, Ser568/569).

4.3 Discussion

RSKs are emerging as key downstream effectors of the RAS/MAPK pathway and therefore have been implicated in tumourigenesis. Protein phosphorylation regulates most intracellular signalling pathways; hence, RSKs, as downstream kinases of a pathway that is hyper-activated in cancer, represent attractive therapeutic targets. While several pan-RSK kinase inhibitors have been developed and tested *in vitro* and *in vivo* (e.g. BI-D1870, SL0101 and FMK) (Casalvieri et al., 2017), the appearance of distinct biological functions between RSK family members is paving the way for the development of RSK isoform-specific inhibitors. Mass spectrometry-based proteomics combined with affinity tag-based protein purification or phosphopeptide enrichment strategies represent a powerful system to study complex signalling pathways and dissect out exclusive proteins or pathways between functionally related members of a kinase family.

Here, in an attempt to isolate RSK1 and RSK4 interacting partners, we affinity purified these kinases from whole cell HEK293A extracts and analysed co-purified interactors by LC-MS/MS. To identify prospective phosphorylation substrates we complemented this approach with a phosphoproteomics-based LC-MS/MS in response to RSK1 or RSK4 silencing in A549 cells. Following pathway analysis, RSK1 and RSK4 could potentially emerge as key regulators of the DDR and p53 activity **(Figure 19)**. Both kinases interact with the DNA-PKcs, a DNA damage sensor and core NHEJ pathway component, while RSK1 also positively regulates its phosphorylation (Ser3205) **(Figure 27)**. The protein kinase activity of DNA-PKcs was reported to be controlled by autophosphorylation, the closely related DDR kinases ATM and ATR and the mitosis regulator PLK1 (Davis, Chen & Chen, 2014). DNA-PKcs was implicated in the regulation of mitosis following PLK1-mediated Ser3205 phosphorylation, which promotes its localisation to the midbody during cytokinesis (Douglas et al., 2014). Interestingly, RSK1 was previously identified as a mediator of mitotic arrest in association with PLK1 (Li et al., 2012), therefore it remains to be investigated whether RSK1 is also involved in DNA-PKcs/PLK1-mediated mitotic processing. Further, in response to ionising radiation, p53 is stabilised via an ATM-independent mechanism that involves phosphorylation and activation of AKT (Ser473) by DNA-PKcs, which in turn

inactivates GSK-3β and MDM2 (Boehme, Kulikov & Blattner, 2008). It remains to be explored whether RSK1 (or RSK4) regulate p53 stability by converging on DNA-PKcs following DNA damage.

In concordance with our TAP data, RSK1 and RSK4 associate with several hnRNPs, including HNRNPH1, HNRNPU and HNRNPF, while RSK4 variant II exclusively interacts with HNRNPK **(Table S 17 & Table S 18)**. hnRNPs are RNA-biding proteins known to regulate transcription, mRNA transport and stabilisation and cap-independent translation (Geuens, Bouhy & Timmerman, 2016). In response to DNA damage HNRNPK is upregulated in a manner that depends on ATM and ATR kinase activity and inhibition of MDM2-mediated ubiquitin degradation. HNRNPK then acts as a transcriptional cofactor for p53 to promote DNA damage-induced cell-cycle arrest (Moumen et al., 2005). Hence, RSK4 (variant II) could be implicated in the induction of p53-responsive genes in a complex with HNRNPK.

In addition to hnRNPs well-established roles in mRNA transcription and protein translation, hnRNPs are also involved in alternative splicing of pre-mRNAs by intron retention or exon skipping (Geuens, Bouhy & Timmerman, 2016). Here, we show that RSK4 positively regulates Ser133 phosphorylation of SRSF10 **(Figure 23)**. Interestingly, SRSF10 is a splicing factor that controls BCL-X[34] (pre-mRNA) splicing in a complex that involves stimulatory HNRNPF and HNRNPH and repressor HNRNPK. Following DNA damage, SRSF10 is dephosphorylated at serines 131 and 133, which causes the dissociation of SRSF10 and HNRNPK from HNRNPF/H-bound BCL-X, thereby promoting the splicing of pro-apoptotic BCL-X**S** (Shkreta et al., 2016). Crucially, SRSF10 displays both the -3 and -5 preferred arginines (**R**-S-**R**-S-R-pSer133) for phosphorylation by RSKs, making it a good candidate for phosphorylation by RSK4. Thus, it would be interesting to test whether RSK4 is involved in the alternative splicing of anti- or pro-apoptotic proteins following DNA damage.

RSK1 and RSK4 variant II were shown to interact with several HSP proteins, including HSP40 members and HSPB1, while RSK1 also positively regulates Ser82 phosphorylation of HSPB1 **(Table S 15, Table S 17 & Figure S 16)**. HSPs participate in protein aggregation and folding while they also protect cells against DNA damage

[34] BCL-X alternative splicing gives rise to anti-apoptotic BCL-X**L** and pro-apoptotic BCL-X**S** variants.

(Sottile & Nadin, 2018). HSPB1 phosphorylation occurs at serines 15, 78 and 82, which are mediated by several kinases including AKT (PKB), PKC, PKD, MK2 and MK3. Interestingly, phosphorylation of HSPB1 was reported to exert tumour suppressive properties by inhibiting activation of the RAF/MEK/ERK pathway and suppressing hepatocellular carcinoma cell growth (Matsushima-Nishiwaki et al., 2008). HSPB1 displays the preferred -3 arginine residue (L-S-**R**-Q-L-pSer82) for phosphorylation by RSKs (Romeo, Zhang & Roux, 2012), rendering this protein a potential RSK1 substrate. Considering the putative tumour suppressive properties of RSK1 in lung adenocarcinoma (Lara et al., 2011) **(Chapter 3, p.118)**, it is appealing to validate this phosphorylation and assess whether it functions similarly in our setting.

RSK4 silencing decreases the migration of lung adenocarcinoma cells (Lara et al., 2011), and this is, at least in part, mediated by induction of mesenchymal-epithelial transition (MET) **(Figure 13)**. Based on our total proteomics screen, RSK4 positively regulates the expression of the trans-membrane protein anthrax toxin receptor 1 (ANTXR1)/tumour endothelium marker 8 (TEM8) **(Figure 24b)**. ANTXR1 was shown to promote endothelial cell adhesion and migration, an important angiogenesis characteristic; mediate cell spreading by linking protective antigen (PA) or collagen I ligands to actin cytoskeleton; and its silencing inhibited the migration and invasion of lung cancer cells *in vitro* (Gong et al., 2018; Werner, Kowalczyk & Faundez, 2006; Hotchkiss et al., 2005). Therefore, it is possible that RSK4 might be mediating cell migration, at least in part, through ANTXR1. Here, we further show that RSK4 interacts with and positively regulates LASP1 Ser146 phosphorylation **(Figure S 16)**. LASP1 is scaffold protein that predominantly localises at focal contacts where it interacts with motility-related proteins, such as F-actin and zyxin. Phosphorylation of LASP1 by PKA decreases its binding affinity for focal contact proteins and induces its nuclear translocation, while dephosphorylation relocalises LASP1 to the cytoplasm (Mihlan et al., 2013). Nuclear LASP1 correlates with highly aggressive breast cancer and is linked to poor long-term breast cancer patient survival (Frietsch et al., 2010; Grunewald et al., 2007). Interestingly, LASP1 also displays the -3 arginine residue upstream of Ser146 (P-E-**R**-R-D-pSer146), which is preferred for phosphorylation by RSKs (Romeo, Zhang & Roux, 2012). Therefore,

it is possible that RSK4 phosphorylates LASP1 directly, although this, and its functional importance in lung cancer, remain to be validated.

The conflicting roles of RSK4 in tumourigenesis could be explained by differentially expressed spliced variants of this kinase. Here, we cloned a novel, previously unstudied RSK4 variant, and identified several of its unique interacting partners. Although this variant only differs from the "canonical" isoform in its first exon (i.e. 81 bp coding for the first 27 aa of the protein) **(Figure S 9)**, unlike variant I, it displays a predicted N-terminal site for myristoylation, a post-translational lipid modification, which targets proteins to the plasma membrane. Therefore, it would be interesting to test whether the two variants differentially localise in the cell and whether this may help explain (or be explained by) their different interactors.

In the current study we employed two complementary proteomics strategies in an attempt to identify prospective interactors and substrates of two RSK kinases. These approaches are indispensable tools for elucidating the underlying mechanisms involved in the distinct phenotypes mediated downstream of highly homologous kinases. Considering the opposing roles of RSK1 and RSK4 in modulating lung adenocarcinoma cell migration/invasion and chemotherapeutic response (Lara et al., 2011) **(Chapter 3, p.118)**, it will be crucial to validate and assert functional roles for these hits. Evidently, both kinases associate with several p53 regulators, while RSK4 interacts directly with this potent tumour suppressor. The functional importance of this interaction remains to be explored.

5. RSK1 and RSK4 impinge on the MDM2-p53 pathway

5.1 Introduction

RSKs are emerging as important downstream effectors of the RAS/MAPK pathway in cancer (Houles & Roux, 2018). According to the analysis of our tandem affinity purification (TAP) and global phosphoproteomics screens, RSK1 and RSK4 putative binding partners and substrates are enriched in pathways controlling the DNA-damage response (DDR), in particular non-homologous end joining (NHEJ) and homologous recombination (HR) **(Figure 19, Figure 21 & Figure 22)**. Not surprisingly, many of those interacting partners converge on p53 and/or are regulated by p53 themselves. Interestingly, unlike RSK1, RSK4 was shown to interact directly with this potent tumour suppressor **(Figure 19)**. Considering that RSK1 and RSK4 were also suggested to interact in our TAP, here, we sought to assess the role of RSK1 and RSK4 on the p53 pathway in lung adenocarcinoma.

TP53, the gene that encodes cellular tumour antigen p53, is the most frequently mutated gene in human cancer (Kandoth et al., 2013). In response to acute DNA damage, oncogene activation or hyperproliferative signals, p53 is activated and regulates the transcription of genes involved in cell cycle arrest and senescence, DNA damage repair and apoptosis; all of which are critical cellular processes associated with tumour suppression (Fischer, 2017; Bieging, Mello & Attardi, 2014). The DDR pathway is initiated in response to DNA replication stress, DNA single- or double-strand breaks (SSBs or DSBs), which trigger the activation of ataxia-telangiectasia mutated (ATM), ataxia telangiectasia and RAD3-related (ATR) and the catalytic subunit of DNA-dependent protein kinase (DNA-PKcs; PRKDC); the most upstream DDR serine/threonine protein kinases. ATM, ATR and DNA-PKcs phosphorylate and activate p53 directly (e.g. at Ser15) or indirectly via phosphorylation of the serine/threonine protein kinases CHK1 (ATR: Ser317, Ser345) and CHK2 (ATM: Thr68), both of which activate p53 through Ser20 phosphorylation (Blackford & Jackson, 2017; Marechal & Zou, 2013). DNA damage-induced Ser15 and Ser20 phosphorylation stabilises p53 by disrupting its interaction with E3 ubiquitin ligase MDM2 and/or occluding C-terminal lysine residues from MDM2-mediated ubiquitination (Hafner et al., 2019).

RPS6KA6 (RSK4) was among five novel modulators of p53-depednent proliferation arrest identified in a large-scale RNAi screen (Berns et al., 2004)[35]. RSK4 downregulation did not alter p53 expression, rather it decreased both the mRNA and protein levels of G1-checkpoint CDK inhibitor $p21^{Cip1/WAF1}$; an effect suggested to be, at least in part, responsible for bypassing p53-induced cell cycle arrest (Berns et al., 2004). Contrary to the aforementioned study, RSK4 knockdown was shown to promote cell cycle arrest in GRC-1 renal carcinoma cells (Fan et al., 2013). The precise underlying mechanism of this phenotype remains unclear since RSK4 downregulation did not alter p21 expression, although it was associated with p53 protein upregulation in this setting (Fan et al., 2013). RSK1 on the other hand, was previously shown to interact with and activated by p53 in Saos osteosarcoma cells, which was required for p53-dependent induction of NF-κB pathway (Bohuslav et al., 2004).

Malmlof and colleagues, using pharmacological inhibitors of MEK/ERK and PI3K/AKT pathways, demonstrated that Ser166 phosphorylation of MDM2 is mediated downstream of the MEK/ERK pathway in HepG2 (hepatocyte) cells and PI3K/AKT pathway in A549 cells (Malmlof et al., 2007). Another report, using MEK/ERK and pan-RSK kinase inhibitors, suggested that VEGFA-induced Ser166 phosphorylation of MDM2 is mediated downstream of the MER/ERK pathway and specifically by the RSK family in endothelial cells (Aiken & Birot, 2016). Although both studies indicate Ser166 phosphorylation of MDM2 occurs downstream of the MEK/ERK/RSK pathway, it remains unclear which RSK family members are involved in this mechanism or whether these kinases phosphorylate MDM2 directly. Here, we show that RSK1 or RSK4 downregulation decreases Ser166 phosphorylation of MDM2, while RSK2 or RSK3 knockdown increases Ser166 phosphorylation levels. We show that RSK1 and RSK4 phosphorylate MDM2 at Ser166 directly, thereby regulating p53 and its target genes $p21^{Cip1/WAF1}$ and PUMA.

[35] RNAi library results were validated in a modified primary human BJ fibroblast cell system.

5.2 Results

5.2.1 RSK1 and RSK4 co-immunoprecipitate and co-localise with mitochondria

To validate RSK1/RSK4 interaction we performed co-immunoprecipitation (Co-IP) assays in HEK293A cells, which exhibit higher cDNA transfection efficiency than A549 cells. However, this interaction was not conclusive when immunoprecipitating endogenous RSK1 or RSK4 (data not shown) due to RSK1/RSK4 antibody cross-reactivity **(Figure S 17a-c)**. To overcome this, we created empty vector (EV) control, RSK1 or RSK4 stable expressing cell lines by transfecting our dual-tagged (FLAG-HA) EV, RSK1 or RSK4 vectors in HEK293A cells, and selecting for plasmid-positive clones with puromycin treatment **(Figure S 17d, e)**. FLAG-tagged RSK1 stable expression was more efficient than RSK4, therefore we transiently transfected this cell line with Myc-tagged RSK4, pulled-down RSK1 with anti-FLAG (M2)-conjugated magnetic beads and probed for RSK4 using an anti-Myc antibody **(Figure 28a)**. Here, we show that RSK4 co-immunoprecipitates with RSK1 in HEK293A cells, while RSK4 was undetectable in the EV control condition **(Figure 28a)**. The previously reported subcellular localisation of RSK1 (cytoplasmic/perinuclear/nuclear) and RSK4 (cytoplasmic/perinuclear) (Dummler et al., 2005), which we recapitulated in our setting, suggests that the RSK1/RSK4 interaction may occur within perinuclear regions **(Figure 28b)**. Interestingly, cytosolic RSK1 and RSK4 co-localise with mitochondria as determined by double staining for RSK1 or RSK4 and MitoTracker (mitochondrial stain) **(Figure 28c, d)**. In short, these data suggest that RSK1 and RSK4 might form heterodimers at mitochondria.

5.2.2 RSK1 and RSK4 immunoprecipitate with p53 and regulate its protein levels

Considering that RSK4 co-immunoprecipitates with RSK1, and RSK4 was shown to interact with p53 in our TAP, we sought to validate the interaction between RSK4 and p53 and assess the possibility of a RSK1/p53 association. We transiently transfected GFP-tagged p53 in our FLAG-tagged EV, RSK1 or RSK4 stables, pulled-down complexes with anti-FLAG (M2)-conjugated magnetic beads and probed for p53 using an anti-GFP antibody **(Figure 29a)**. Here, we show that p53 co-immunoprecipitates with both RSK1 and RSK4 in HEK293A cells, indicating that these kinases could be involved in regulating p53 activity **(Figure 29a)**. Therefore, we next sought to test how manipulation of RSK1 or RSK4 levels affects p53. RSK1 or RSK4 transient knockdown, in p53

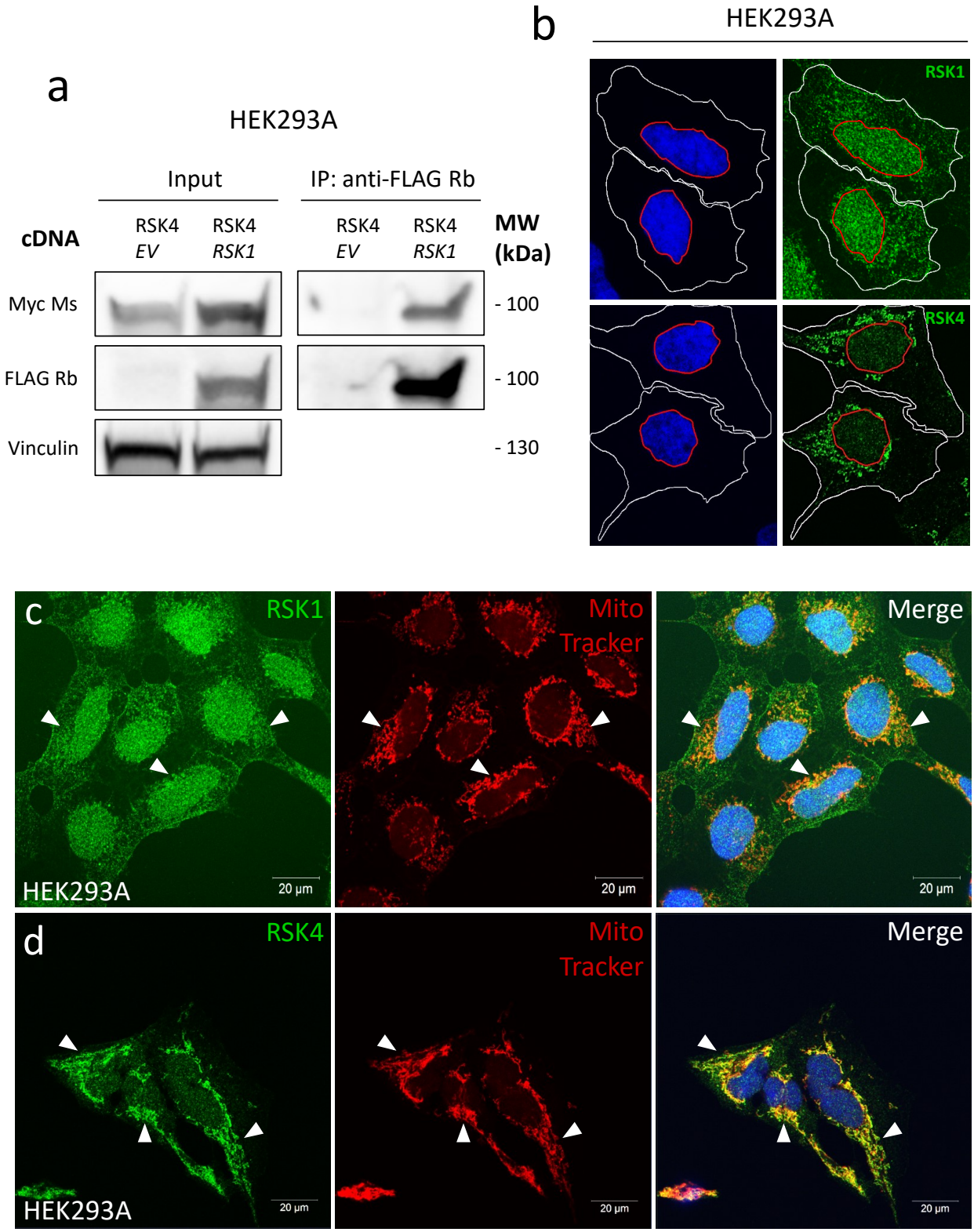

Figure 28| RSK1 and RSK4 co-immunoprecipitate and co-localise with mitochondria. **(a)** HEK293A FLAG-tagged EV (empty vector) and RSK1 stables (See **Figure S 17**) were transiently transfected with Myc-tagged RSK4, complexes pulled-down with anti-FLAG Rb (rabbit)-conjugated magnetic beads, followed by immunoblotting with anti-Myc Ms (mouse), anti-FLAG Rb (rabbit) and anti-Vinculin (loading control). Data are representative of two independent biological replicates. **(b-d)** Confocal microscopy of HEK293A cells grown on 12 mm coverslips and stained for **(b)** RSK1 (top), **(b)** RSK4 (bottom), or dual-stained for **(c)** RSK1 and mitochondria (MitoTracker), or **(d)** RSK4 and mitochondria (MitoTracker), and counterstained with Hoechst. Confocal images were captured on an inverted Zeiss LSM-780 (FILM, Imperial College London, UK). White arrows indicate areas of colocalisation (scale bars: 20 µm). Data are representative of two independent biological replicates. (See **Figure S 23** for RSK1/RSK4 siRNA and mitochondria).

WT A549 lung adenocarcinoma cells, upregulated p53 protein levels **(Figure 29b)**. Conversely, overexpressing these kinases reduced p53 protein, indicating that RSK1/4 might be regulating p53 transcriptionally or post-translationally **(Figure 29c)**. Interestingly, RSK1 or RSK4 downregulation (or overexpression) did not affect p53 mRNA **(Figure S 17c-f & Figure S 18a, b)**. Considering that p53 levels are largely regulated post-translationally by MDM2, we next investigated the effect of RSK1/4 manipulation on MDM2. RSK1 or RSK4 silencing decreased, while RSK1 or RSK4 cDNA expression increased, MDM2 Ser166 phosphorylation **(Figure 29b, c)**, which is a well-characterised site associated with increased MDM2 E3 ubiquitin ligase activity and subsequent p53 proteasomal degradation (Meek & Knippschild, 2003). Concurrent RSK1/4 downregulation enhanced the effects of single RSK1 or RSK4 siRNA, suggesting these kinases regulate MDM2 and p53 in a synergistic manner **(Figure 29d)**. Lastly, MDM2 modulation appears to be mediated post-translationally since MDM2 mRNA and total protein levels were unaffected downstream of RSK1 or RSK4 manipulation **(Figure S 18c-e)**. Collectively, these data implicate RSK1 and RSK4 in the regulation of p53 stability by impinging on MDM2 activity.

5.2.3 Pharmacological inhibition of p90RSKs reproduces RSK1 and RSK4 siRNA effects

There are four, highly homologous, RSK family members (RSK1-4), of which only RSK4 is constitutively active (Dummler et al., 2005). To determine the net effect of pan-RSK inhibition, we firstly stimulated A549 cells with EGF[36] to activate all RSKs, and subsequently treated cells with the well-characterised pan-RSK ATP-competitive inhibitor BI-D1870. Pathway activation was determined by the induction of phosphorylated ERK1/2. BI-D1870 treatment reduced RSK activity as determined with a phospho-RSK1/2/4 (Ser363) antibody and the reduction of rpS6 Ser235/236 phosphorylation, a well-documented RSK (and S6K) substrate (Meyuhas, 2008) **(Figure 30a)**. The reduction of RSK activity correlated with decreased Ser166 phosphorylation levels of MDM2 and p53 upregulation in both starved and EGF stimulated conditions **(Figure 30a)**. EGF stimulation in the absence of BI-D1870 strongly induced MDM2 Ser166 phosphorylation, which decreased following pan-RSK inhibition, suggesting that RAS/MAPK pathway activation positively regulates MDM2 activity through RSKs **(Figure 30a)**. Further, BI-D1870 being an ATP-competitive inhibitor, these effects are dependent on RSKs' kinase activity.

[36] EGF stimulation induces (among others) RAS/MAPK and PI3K/AKT pathway activation (Scaltriti & Baselga, 2006).

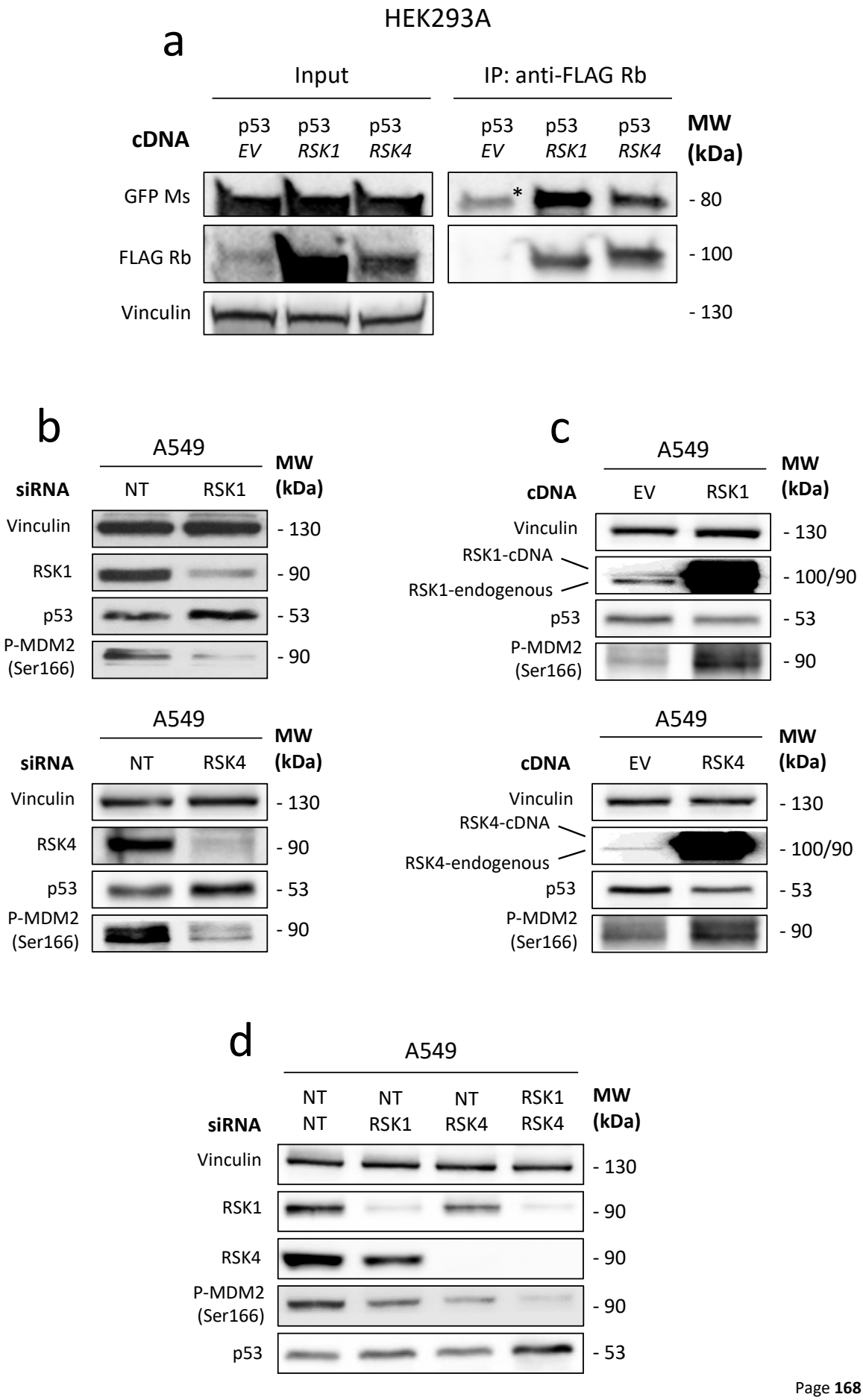
a
HEK293A
Input
IP: anti-FLAG Rb
cDNA
p53 EV
p53 RSK1
p53 RSK4
MW (kDa)
GFP Ms
FLAG Rb
Vinculin
*
- 80
- 100
- 130
b
A549
siRNA
NT
RSK1
RSK4
MW (kDa)
Vinculin
RSK1
RSK4
p53
P-MDM2 (Ser166)
- 130
- 90
- 53
c
A549
cDNA
EV
RSK1
RSK4
RSK1-cDNA
RSK1-endogenous
RSK4-cDNA
RSK4-endogenous
- 100/90
d
NT NT
NT RSK1
NT RSK4
RSK1 RSK4

Figure 29| RSK1 and RSK4 immunoprecipitate with p53 and regulate its protein levels. **(a)** HEK293A FLAG-tagged EV (empty vector), RSK1 and RSK4 stables (See **Figure S 17**) were transiently transfected with GFP-tagged p53, complexes pulled-down with anti-FLAG Rb (rabbit)-conjugated magnetic beads, followed by immunoblotting with anti-GFP Ms (mouse), anti-FLAG Rb (rabbit) and anti-Vinculin (loading control). Asterisk indicates background p53 levels immunoprecipitated with EV control. Data are representative of two independent biological replicates. **(b)** Immunoblotting of RSK1, RSK4, p53 and Phospho-MDM2 (Ser166) in whole cell A549 extracts transfected (48-72 h) with a final concentration of 20 nM NT (non-targeting), RSK1 (top) or RSK4 (bottom) siRNAs. Data are representative of three independent biological replicates. **(c)** Immunoblotting of RSK1, RSK4, p53 and Phospho-MDM2 (Ser166) in whole cell A549 extracts transfected (24-48 h) with a final concentration of 2.5 µg EV (empty vector), RSK1 (top) or RSK4 (bottom) cDNAs. Data are representative of three independent biological replicates. **(d)** Immunoblotting of RSK1, RSK4, p53 and Phospho-MDM2 (Ser166) in whole cell A549 extracts transfected (48-72 h) with a final concentration of 40 nM NT+NT, NT+RSK1, NT+RSK4 or RSK1+RSK4 siRNAs. Vinculin was used as a loading control. Data are representative of three independent biological replicates. The work presented in **d** was performed by Alex Power (personal communication). The knockdown of RSK4 (including loading control) in experiment **b** is shown again in **Figure 11f** (same lysate). The overexpression of RSK1 and RSK4 (including loading controls) in **c** are shown again in **Figure S 17a, b** at lower exposure (same lysate).

To assess whether RSK2 or RSK3 promote MDM2 Ser166 phosphorylation we transiently knocked-down all RSK family members individually **(Figure S 18f)**. Interestingly, contrary to RSK1 and RSK4, these RSK isoforms seem to negatively regulate MDM2 activity as their downregulation increased Ser116 phosphorylation of MDM2. Also, combined downregulation of all RSK isoforms cancelled out changes on Ser166 phosphorylation levels, indicating that RSK2/3 might counteract the effects of RSK1/4 **(Figure 30c)**. There is a possibility that the increase in Ser166 phosphorylation observed may be the consequence of a corresponding increase in RSK1/4 activity downstream of RSK2/3 silencing, and this possibility would require further investigation.

In addition to A549 cells, RSK1 and RSK4 impact on MDM2 phosphorylation was conserved across different cancer cell lines. Here, we show that knocking-down RSK1 or RSK4 decreased Ser166 phosphorylation of MDM2 in wild type (MCF7 breast cancer) and mutant (H23[37] lung and T24[38] bladder cancer) p53 cell lines, indicating this effect occurs independently of p53 status **(Figure 31a & Figure S 19a-d)**. In the p53 WT MCF7 cell line, RSK4 depletion upregulated p53, which also correlated with PUMA upregulation at the protein level **(Figure S 19b)**. Taken together, RSKs are emerging as potent modulators of MDM2 activity downstream of the RAS/MAPK pathway, with RSK1 and RSK4 appearing to promote MDM2 phosphorylation.

[37] Missense p53 mutation: p.M246I.
[38] Homozygous-TP53: c.378C>G; p.Y126Ter.

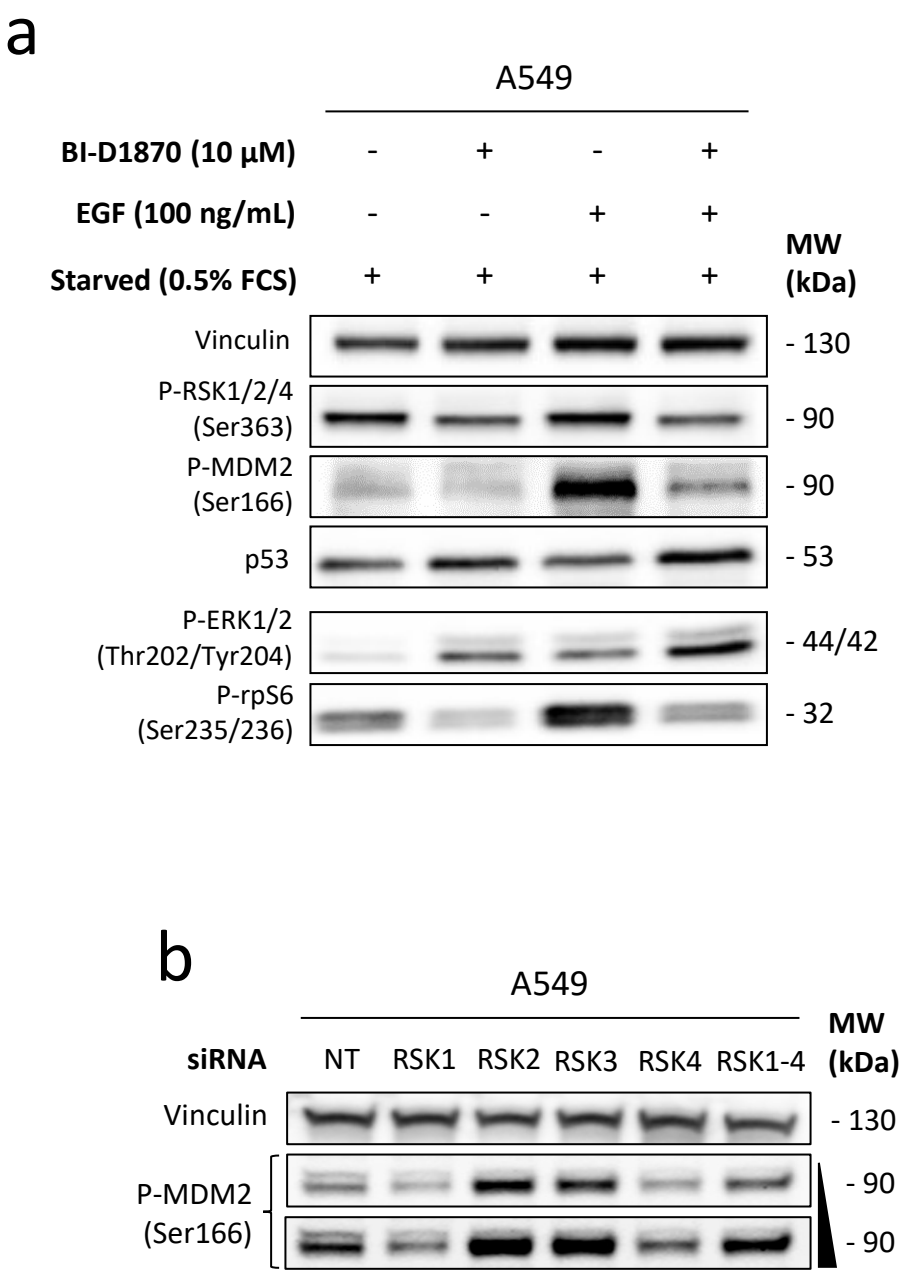

Figure 30| Pharmacological inhibition of p90RSKs reproduces RSK1 and RSK4 siRNA silencing effects. **(a)** Immunoblotting for the indicated proteins in whole cell A549 extracts serum-starved overnight with 0.5% FCS, stimulated with ± 100 ng/mL EGF (epidermal growth factor) for 15 min, and treated with ± 10 µM BI-D1870 (pan-RSK ATP-competitive inhibitor) for 30 min. Vinculin was used as a loading control. Data are representative of three independent biological replicates. **(b)** Immunoblotting of Phospho-MDM2 (Ser166) in whole cell A549 extracts transfected (48-72 h) with a final concentration of 20 nM NT (non-targeting), RSK1, RSK2, RSK3, RSK4 or RSK1-4 siRNAs. Vinculin was used as a loading control. Data are representative of three independent biological replicates. The work presented in **a** was performed by Alex Power (personal communication).

5.2.4 RSK1 and RSK4 phosphorylate MDM2 at Ser166

The prototypical consensus phosphorylation motif in RSK substrates includes a -3 and -5 position arginine residues relative to the phosphoacceptor site. RSKs display a stronger requirement for the -3 arginine residue, and tend to phosphorylate serine rather than threonine residues (Romeo, Zhang & Roux, 2012) **(Figure 31b)**. MDM2 displays both required arginine residues and has a serine residue as the phosphoacceptor site, thereby rendering MDM2 a potential RSK1 and RSK4 substrate **(Figure 31b)**. To test this possibility, we incubated increasing amounts of full length recombinant MDM2 protein with or without recombinant active RSK1 or RSK4 kinases in the presence of ATP **(Figure 31c, d)**. Phosphorylated MDM2 was detected by immunoblotting for MDM2 phospho-Ser166. Recombinant RSK1 and RSK4 were able to phosphorylate MDM2 at this site, suggesting that MDM2 is a *bona fide* substrate for these kinases **(Figure 31c, d)**. Considering that kinase-substrate interaction is a prerequisite for protein phosphorylation, we attempted to co-immunoprecipitate Myc-tagged MDM2 with our FLAG-tagged RSK1 or RSK4 fusion proteins, but this approach failed (data not shown). This may be due to the N-terminal tag of MDM2 interfering with this interaction and this possibility would need to be tested by using a C-terminal-tagged version of MDM2. In short, our data suggest that MDM2 may be a direct downstream phospho-target for RSK1 and RSK4.

5.2.5 RSK1 and RSK4 downregulation stabilises p53 and enhances expression of p53-responsive genes

Under non-stressed conditions, MDM2 maintains low p53 levels by targeting this tumour suppressor for ubiquitin-dependent proteasomal degradation, while genotoxic stress inhibits MDM2/p53 interaction, thereby stabilising p53 (Moll & Petrenko, 2003). To assess whether RSK1 and RSK4 modulate the stability of p53, we treated NT control, RSK1- or RSK4-silenced A549 cells with the protein synthesis inhibitor cycloheximide over a period of 90 min and assessed p53 protein amount by immunoblotting **(Figure 32a & Figure S 22)**. The half-life of p53 was considerably extended following RSK1 or RSK4 silencing as indicated by densitometry, thus confirming stabilisation of p53 **(Figure 32a & Figure S 22)**. p53 is a well-documented transcriptional effector of genes involved in cell cycle arrest, DNA repair and apoptosis (Fischer, 2017), including $p21^{Cip1/WAF1}$ and PUMA. Here, RSK1 or RSK4 depletion, upregulated the levels of both proteins and

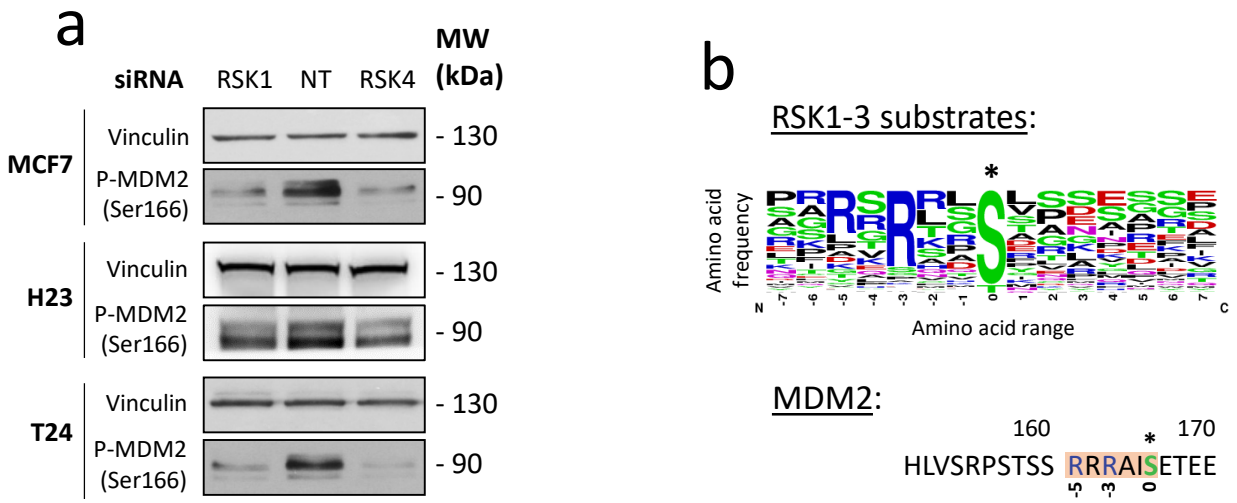

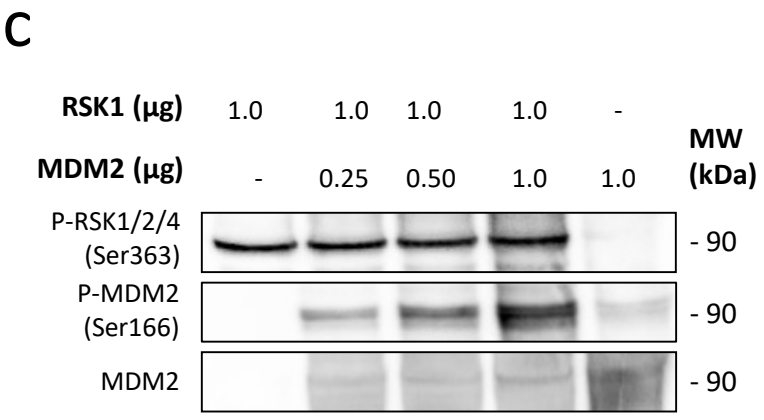

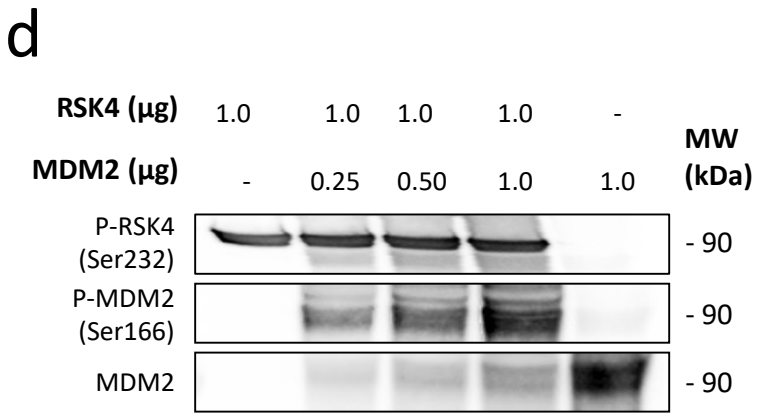

Figure 31| RSK1 and RSK4 phosphorylate MDM2 at Ser166. **(a)** Immunoblotting of Phospho-MDM2 (Ser166) in whole cell MCF7 (top), H23 (middle) and T24 (bottom) extracts transfected (48-72 h) with a final concentration of 20 nM NT (non-targeting), RSK1 or RSK4 siRNAs. Vinculin was used as a loading control. Data are representative of three independent biological replicates. **(b)** The amino acid sequences (-7 to +7 relative to the phosphoacceptor site; x-axis) of RSK substrates (Lara, Seckl & Pardo, 2013), were aligned and a sequence logo was created using WebLogo (Crooks et al., 2004). The height of amino acids within the stack indicates relative amino acid frequency (y-axis). MDM2 shares the -3 and -5 position arginine residues and the serine phosphoacceptor residue (denoted with an asterisk). **(c, d)** *In vitro* kinase assay of full length human recombinant MDM2 (0.25-1.0 µg) incubated with **(c)** ± recombinant RSK1 (1.0 µg) or **(d)** ± recombinant RSK4 (1.0 µg) in the presence of ATP. Phosphorylation or total protein were detected by immunoblotting with anti-Phospho-RSK1/2/4 (Ser363), anti-Phospho-RSK4 (Ser232), anti-Phospho-MDM2 (Ser166) and anti-MDM2. Data are representative of two independent biological replicates.

this mostly correlated with changes in the corresponding mRNAs **(Figure 32b-d)**. Conversely, overexpressing these kinases, decreased $p21^{Cip1/WAF1}$ and PUMA protein levels **(Figure S 20a-c)**. Taken together, our data indicate that RSK1 and RSK4 regulate p53 stability and subsequent expression of p53 target genes. However, it remains to be tested whether RSK1/4 promote p53 ubiquitination in an MDM2 Ser166-dependent manner.

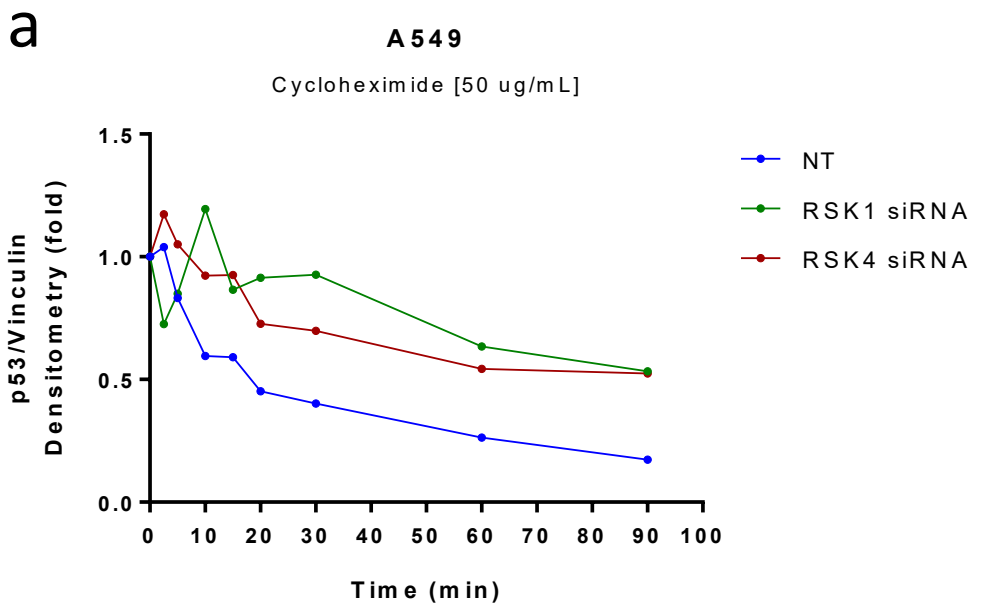

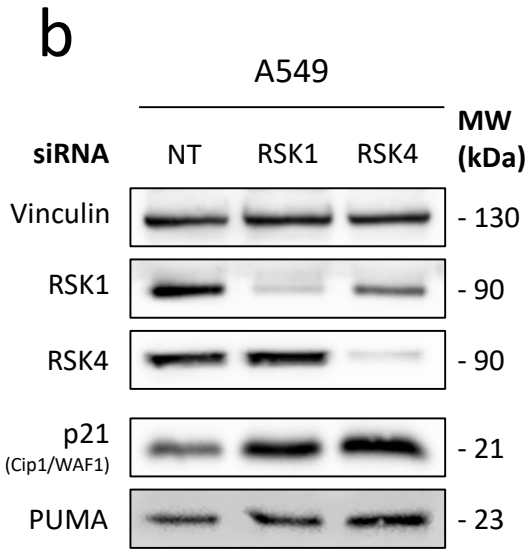

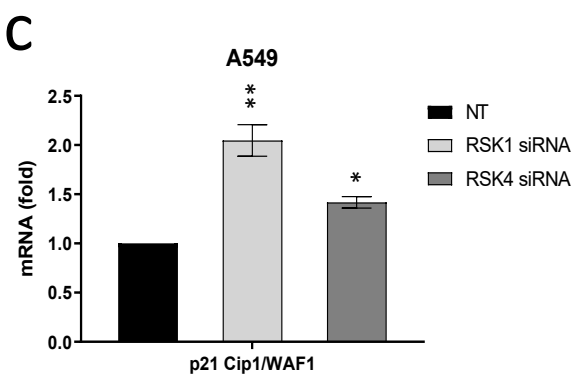

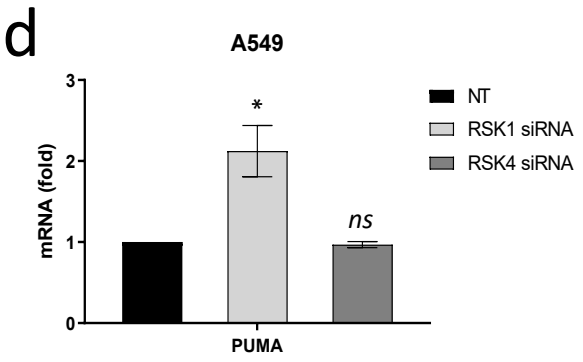

Figure 32| RSK1 and RSK4 downregulation stabilises p53 and enhances expression of p53-responsive genes. (a) Quantification of p53 protein levels following cycloheximide treatment (50 µg/mL) of NT (non-targeting), RSK1 or RSK4 siRNA-transfected cells (See **Figure S 22** for Immunoblotting analysis). The amount of p53 was quantified by densitometry in ImageJ software, normalised to Vinculin (loading control) and shown as a fold change relative to NT control condition. Data are representative of two independent biological replicates. **(b)** Immunoblotting of RSK1, RSK4, $p21^{Cip1/WAF1}$ and PUMA in whole cell A549 extracts transfected (48-72 h) with a final concentration of 20 nM NT (non-targeting), RSK1 or RSK4 siRNAs. Vinculin was used as a loading control. Data are representative of three independent biological replicates. **(c, d)** qRT-PCR analysis of **(c)** $p21^{Cip1/WAF1}$ (CDKN1A) and **(d)** PUMA (BBC3) mRNAs in A549 cells transfected (48-72 h) with a final concentration of 20 nM NT (non-targeting), RSK1 or RSK4 siRNAs. *Ct* values were normalised to HPRT housekeeping gene and shown as a fold change relative to NT control condition. Data represent mean ± SEM of three independent biological replicates performed in triplicates. Statistical significance was assessed by an unpaired Student's *t*-test in GraphPad Prism. *ns*; non-significant ($P > 0.05$), *; $P \leq 0.05$, **; $P \leq 0.01$. The work presented in **a** was performed by Alex Power (personal communication).

5.2.6 p53 regulates RSK4 protein and mRNA levels

p53 primarily functions as a transcription factor of genes associated with tumour suppression (Fischer, 2017). Crucially, p53 also promotes the expression of its principal antagonist MDM2, thereby creating an autoregulatory feedback loop that maintains low p53 levels under non-stressed conditions (Moll & Petrenko, 2003). Hence, to test the existence of such a feedback mechanism between p53 and RSK1/4, we transiently knocked-down p53 in our cells. Here, p53 siRNA silencing substantially reduced RSK4 protein levels, which correlated with a 50% reduction in its mRNA levels **(Figure 33a, b)**. Interestingly, this effect appears to be specific to RSK4, since RSK1 protein levels did not change following p53 downregulation **(Figure 33a, b)**. To our surprise, analysis of RSK1 and RSK4 expression in wild-type (WT) p53 versus mutant (MUT) p53 TCGA lung adenocarcinoma (LUAD) samples, indicated that RSK1 (and not RSK4) expression was significantly lower in MUT p53 samples compared to WT p53 samples **(Figure 34a-d)**. Collectively, while RSK1 and RSK4 regulate p53 stability, p53 may in turn regulate the expression of RSK isoforms. In particular, our data suggest that RSK4 may be a transcriptional target of p53. The possibility that p53 might also form a protein-protein complex with RSK1 and/or RSK4, to mediate an as of yet unknown function, requires further investigation.

5.2.7 Chronic depletion of RSK4 promotes MDM2-independent pathway rewiring of 53

To assess the effects of RSK4 chronic depletion on MDM2 and p53, we utilised our CRISPR-mediated RSK4 knockout cell lines (Rajat Roy, personal communication). Two RSK4 CRISPR clones, one with partial (cr421) and one with complete (cr437) RSK4 knockout, manifest decreased Ser166 phosphorylation of MDM2 **(Figure 35a & Figure S 21)**. Unlike the transient knockdown of RSK4 **(Figure 29b bottom)**, p53 levels in both knockout clones were reduced as compared to the parental cells, despite persistent reduction of Ser166

phosphorylation **(Figure 35a, b)**. This discrepancy between p53 protein levels and MDM2 phosphorylation was associated with a decrease in p53 mRNA levels **(Figure 35c)**, suggesting that RSK4 CRISPR cells adapted to acute increase in p53 stability by reducing p53 expression in an MDM2-independent manner.

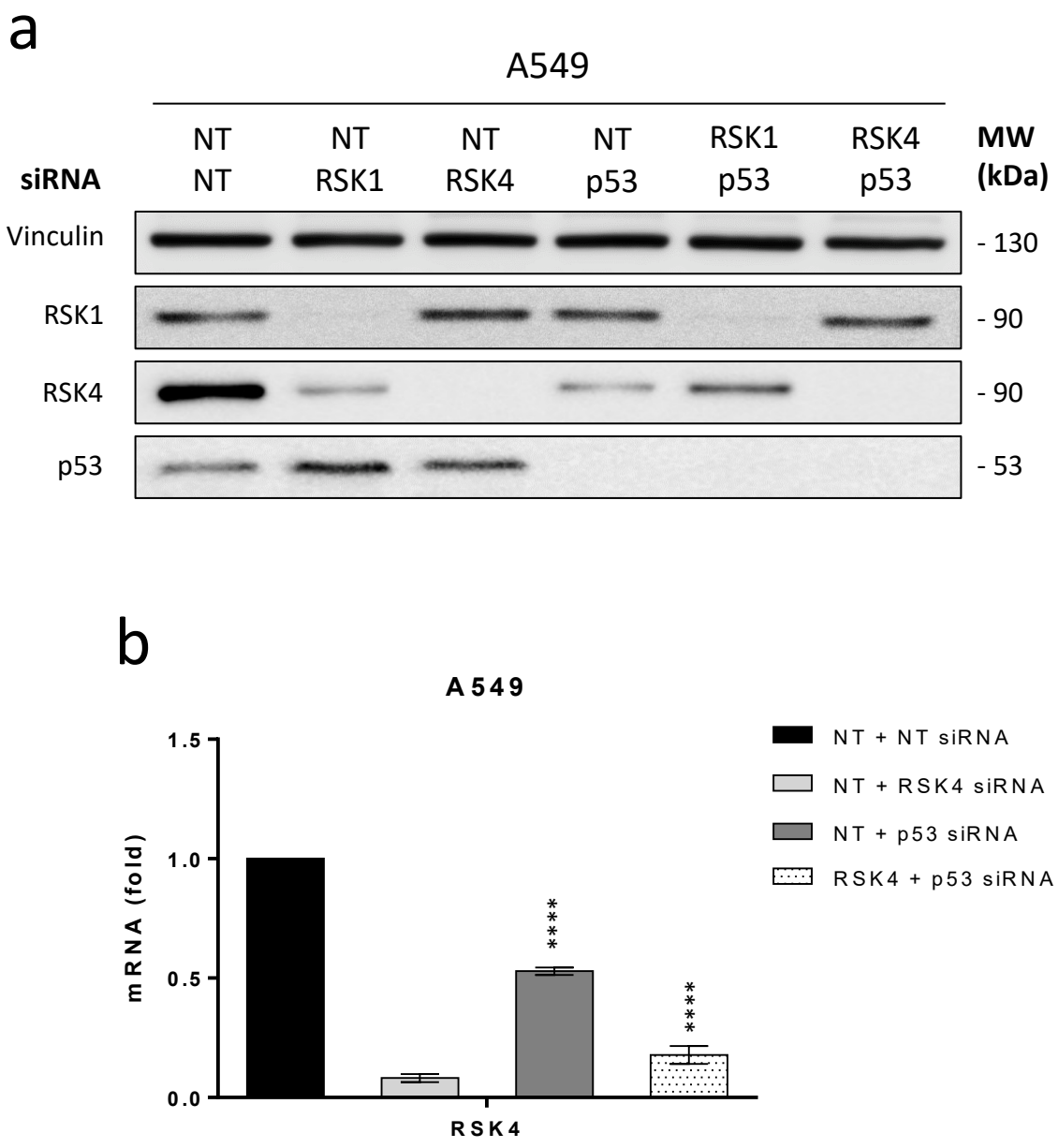

Figure 33| p53 regulates RSK4 protein and mRNA levels. **(a)** Immunoblotting of RSK1, RSK4 and p53 in whole cell A549 extracts transfected (48-72 h) with a final concentration of 40 nM NT+NT (non-targeting), NT+RSK1, NT+RSK4, NT+p53, RSK1+p53 and RSK4+p53 siRNAs. Vinculin was used as a loading control. Data are representative of three independent biological replicates. **(b)** qRT-PCR analysis of RSK4 (RPS6KA6) mRNA in A549 cells transfected (48-72 h) with a final concentration of 40 nM NT+NT, NT+RSK4, NT+p53 and RSK4+p53 siRNAs. *Ct* values were normalised to HPRT housekeeping gene and shown as a fold change relative to NT+NT control condition. Data represent mean ± SEM of three independent biological replicates performed in triplicates. Statistical significance was assessed by an unpaired Student's *t*-test in GraphPad Prism. ****; $P \leq 0.0001$.

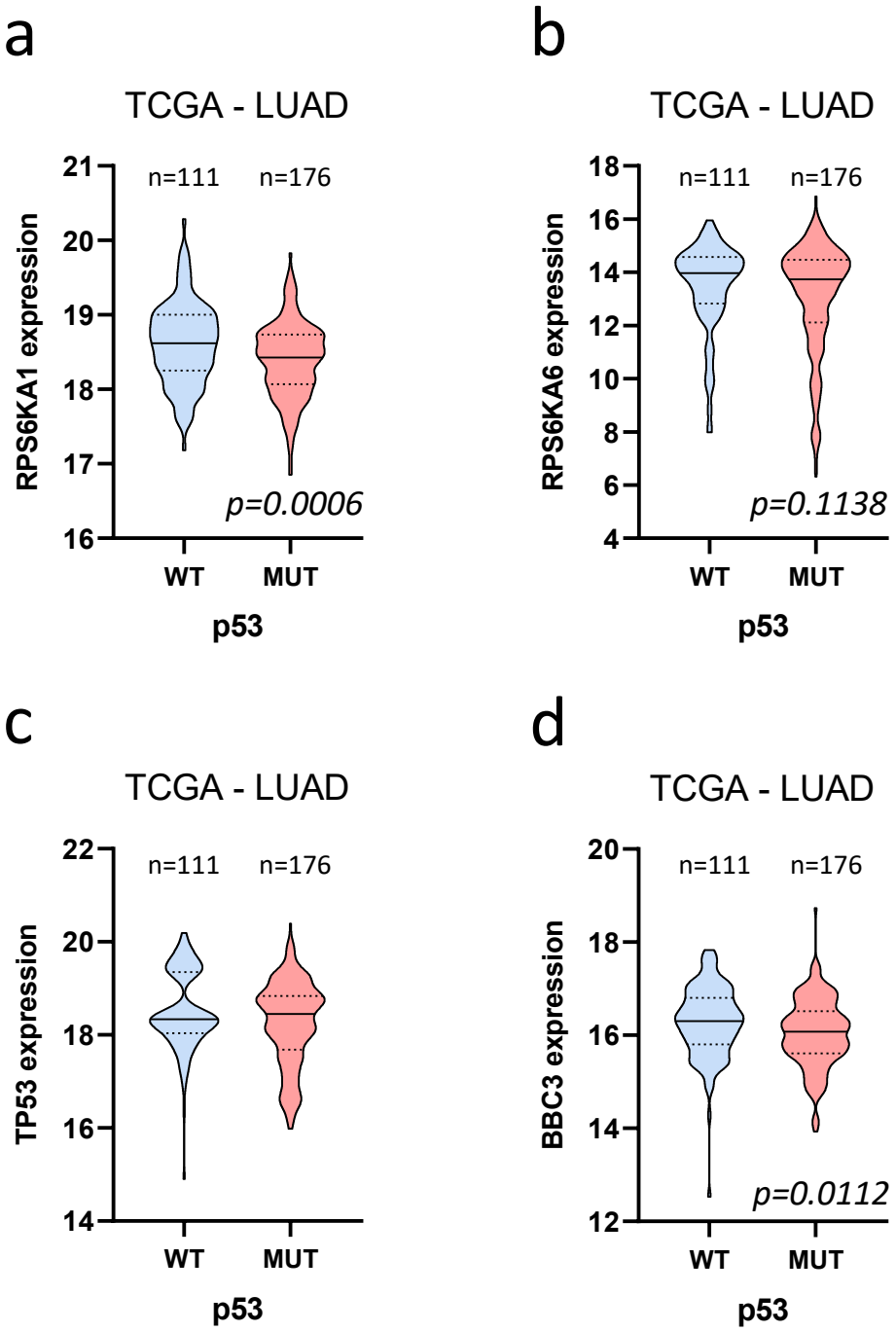

Figure 34| RSK1 and RSK4 expression in wild-type vs mutant p53 TCGA lung adenocarcinoma samples. **(a-d)** Analysis of **(a)** RPS6KA1 (RSK1), **(b)** RPS6KA6 (RSK4), **(c)** TP53 and **(d)** BBC3 (PUMA) gene expression in wild-type (WT) p53 (n=111) versus mutant (MUT) p53 (n=176) TCGA lung adenocarcinoma (LUAD) samples. Statistical significance was assessed by an unpaired Student's *t*-test in GraphPad Prism.

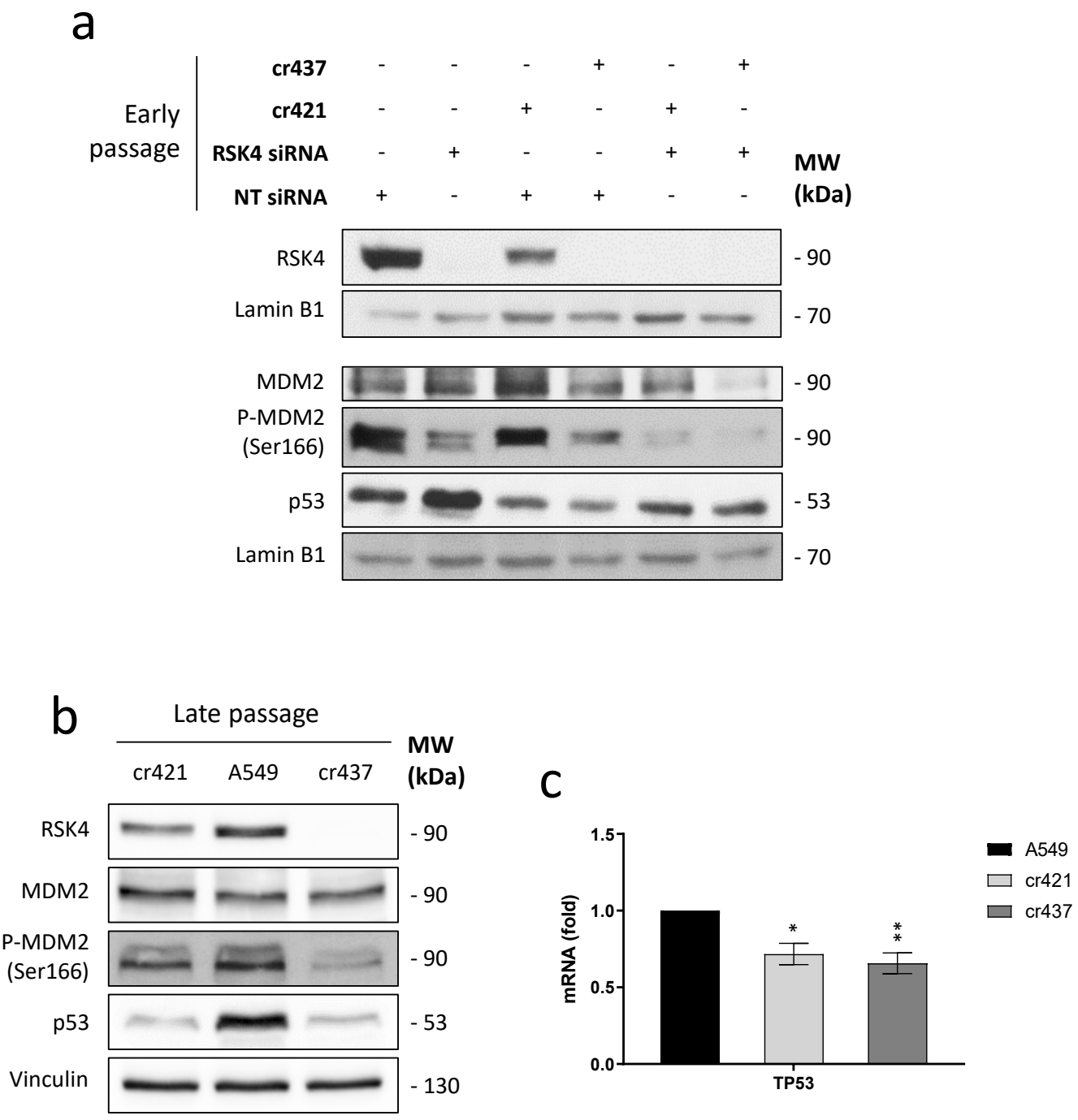

Figure 35| Chronic depletion of RSK4 promotes MDM2-independent pathway rewiring of p53. **(a)** Immunoblotting of RSK4, MDM2, Phospho-MDM2 (Ser166) and p53 in (early passage) whole cell A549 (control) extracts transfected (48-72 h) with a final concentration of 20 nM NT (non-targeting) or RSK4 siRNAs; whole cell cr421 extracts (partial RSK4 KO) transfected (48-72 h) with a final concentration of 20 nM NT or RSK4 siRNAs; and whole cell cr437 extracts (complete RSK4 KO) transfected (48-72 h) with a final concentration of 20 nM NT or RSK4 siRNAs. Lamin B1 was used as a loading control. Data are representative of three independent biological replicates. **(b)** Immunoblotting of RSK4, MDM2, Phospho-MDM2 (Ser166) and p53 in (late passage) whole cell A549 (control), cr421 and cr437 extracts. Vinculin was used as a loading control. Data are representative of three independent biological replicates. **(c)** qRT-PCR analysis of TP53 mRNA in A549 (control), cr421 and cr437 cells. *Ct* values were normalised to HPRT housekeeping gene and shown as a fold change relative to A549 control condition. Data represent mean ± SEM of three independent biological replicates performed in triplicates. Statistical significance was assessed by an unpaired Student's *t*-test in GraphPad Prism. *; $P \leq 0.05$, **; $P \leq 0.01$. (See **Figure S 21** for qRT-PCR analysis).

5.3 Discussion

In this study, we report a mechanism by which RSK1 and RSK4 antagonise p53. RSK1 or RSK4 expression reduced the levels of p53 protein, which we propose is mediated, at least in part, by modulation of MDM2 ubiquitin ligase activity **(Figure 29c)**. MDM2 gene amplification is a frequent phenomenon in human cancers and its oncogenic properties are mostly driven through the negative regulation of tumour suppressor p53, therefore MDM2 activity is tightly regulated in cells (Wade, Li & Wahl, 2013; Forslund et al., 2008) .

RAS-driven PI3K/AKT and RAF/MEK/ERK (MAPK) pathways display extensive signalling crosstalk and were both shown to regulate MDM2 activity or expression in a mutual or opposing manner depending on the cellular context and growth factor specificity. While AKT interacts with and directly phosphorylates Ser166 and Ser186 of MDM2, which enhances MDM2-mediated ubiquitination and degradation of p53 (Ogawara et al., 2002), no such role was proposed for the RAF/MEK/ERK. For instance, activated RAS and RAF promote MDM2 transcription via a p53-independent mechanism, resulting in p53 degradation (Ries et al., 2000), while others demonstrated with pharmacological inhibitors that MDM2 Ser166 phosphorylation is mediated downstream of the MEK/ERK pathway (Aiken & Birot, 2016; Malmlof et al., 2007). In agreement with the aforementioned studies, we demonstrate that Ser166 phosphorylation is induced downstream of EGF stimulation **(Figure 30a)**, and provide evidence that this phosphorylation is mediated by RSK1 and RSK4 **(Figure 30 & Figure 31)**. This appears to be specific to these RSK isoforms, since RSK2 and RSK3 antagonise MDM2 activity, suggesting this mechanism is not conserved across all RSK family members **(Figure 30c)**. This is somewhat unexpected considering that no difference in the phosphorylation consensus sequence required for phosphorylation by the four RSK isoforms is known. Hence, it is possible that this discrepancy is due to distinct sub-cellular localisation of the four RSK kinases, which may provide differential access to substrates. Surprisingly, at this stage we were unable to demonstrate direct protein-protein interaction between RSK1/4 and MDM2 **(Figure S 19e)**. Considering that MDM2 Ser166 phosphorylation is induced within 10 min of EGF stimulation, this might be due to a very transient interaction between these proteins. Another possibility could be that, at least RSK1, regulates this phosphorylation indirectly by impinging on AKT activity **(Figure S 20d)**. Here, we show that RSK1

regulates the activating phosphorylation of AKT (Ser473) **(Figure S 20d)**, which could be mediated through its inhibitory phosphorylation of DEPTOR, a well-known negative regulator of AKT (Zhao, Xiong & Sun, 2011).

How p53 integrates upstream signals and chooses between cell survival (i.e. cell cycle arrest and DNA repair) and cell death (i.e. apoptosis) is a highly complex process that is still not fully resolved. This might be dependent on the cell type and extend of DNA damage. Here, depletion of RSK1 or RSK4 stabilises p53 and enhances expression of the *bona-fide* p53 transcriptional targets $p21^{Cip1/WAF1}$ (*CDKN1A*) and PUMA (*BBC3*), which promote G1 cell cycle arrest and intrinsic apoptosis, respectively **(Figure 32 & Figure S 22)**. Following DNA damage, p53 promotes the transcription of $p21^{Cip1/WAF1}$, which inhibits CDK2 and CDK4/6 activities. In turn cyclin-E-CDK2 and cyclin-D-CDK4/6 complexes fail to phosphorylate Rb, which then sequesters E2F and prevents transcription of E2F target genes that promote S phase entry (Abukhdeir & Park, 2008). Hence, a possibility that remains to be explored is whether DNA damage inhibits RSK1 or RSK4 activity to induce p53-mediated cell cycle arrest. Interestingly, RSK1 was previously shown to regulate $p21^{Cip1/WAF1}$ directly by phosphorylation at Ser116 and Ser146 (Neise et al., 2013), the latter of which is also phosphorylated by AKT and was shown to activate, rather than inhibit, the cyclin-D1-CDK4 complex (Li, Dowbenko & Lasky, 2002). This implicates RSK1 directly in promoting cell cycle progression. PUMA on the other hand, is a BCL-2 family BH-3 only pro-apoptotic protein that accounts for the majority of p53-dependent cell death in response to DNA damage. This is mediated by promoting the assembly of BAK-BAX channel across the outer mitochondrial membranes, resulting in the cytoplasmic efflux of cytochrome c and subsequent caspase activation (Yu & Zhang, 2008). Our preliminary data indicates that the knockdown of RSK4, but not RSK1, promotes caspase-7 cleavage, suggesting that RSK4 antagonises p53-dependent apoptosis downstream of PUMA (data not shown). However, whether caspase cleavage is indeed dependent on PUMA activity in our setting requires further investigation. Conversely, RSK2 was previously shown to interact with and phosphorylate p53 (Ser15) and ATM (Ser1981), which is required for maintaining genomic stability by promoting cell cycle arrest and DNA repair (Lim et al., 2013; Cho et al., 2005). Hence, RSKs impinge on p53 activity and/or expression through distinct mechanisms, culminating in different biological outcomes.

Following RAS/MAPK pathway stimulation, ERK1/2 phosphorylate a broad spectrum of cytosolic and nuclear substrates, including the highly conserved serine/threonine kinases RSK1-4 (Anjum & Blenis, 2008). A prerequisite for cytosolic substrate phosphorylation by ERK1/2 involves the formation of ERK dimers, while nuclear substrates are phosphorylated by ERK monomers (Casar, Pinto & Crespo, 2008). In concordance, it is possible that RSK1-RSK4 heterodimer formation **(Figure 28a)** is required for the phosphorylation of conserved substrates in the cytoplasm, including MDM2. It was previously reported that RSK4, unlike RSK1-3, is a cytosolic protein regardless of growth factor stimulation (Dummler et al., 2005). Consistent with these studies, we found RSK4 localised in perinuclear/cytoplasmic regions, while RSK1 is mostly perinuclear/nuclear **(Figure 28b)**. Importantly, both RSK1 and RSK4 co-localise with mitochondria, although it is unclear yet in which mitochondrial sub-compartment and what the functional significance of this might be **(Figure 28c, d)**. Interestingly though, RSK1-3 were previously shown to phosphorylate BAD (Ser112, Ser155), which localises at mitochondrial membranes and promotes apoptosis in a complex with BCL-XL (Tan et al., 2000; Tan et al., 1999). In keeping with our TAP screen, RSK1 and RSK4 interact with several members of the SLC25 mitochondrial transporter family, including SLC25A1 and SLC25A5, which are embedded within the inner mitochondrial membrane and regulate numerous metabolic pathways (Palmieri, 2013). Therefore, raising the possibility that these kinases are involved in the mitochondrial/cytoplasmic transport of keys metabolites. Interestingly, our preliminary data indicate that RSK4 downregulation alters the mitochondrial network **(Figure S 23)**, which plays key roles in metabolic pathways, neurodegeneration and apoptosis (Westermann, 2010).

Here, we propose a mechanism by which RSK1 and RSK4 antagonise p53 in an MDM2-dependent manner. However, the presence of additional mechanisms between RSK1/4 and p53 regulation should not be excluded. RSK1 and RSK4 interact directly with p53, thus these kinases could regulate p53 activity by phosphorylation **(Figure 29a)**. Further, p53 positively regulates RSK4 mRNA and protein levels, possibly engaging in a feedback loop to counteract RSK4 antagonistic activity **(Figure 33)**. Nevertheless, analysis of RSK4 expression in WT p53 versus MUT p53 TCGA LUAD samples, did not indicate a statistically significant difference **(Figure 34)**. Analysis of publicly available ChIP-seq datasets also failed to provide evidence for p53 binding within up to 10 kb of

RPS6KA6 (RSK4) transcription start site (data not shown). Therefore, it is possible that p53 regulates RSK4 indirectly via an intermediate protein, likely a transcriptional regulator. Finally, chronic depletion of RSK4 using CRISPR-Cas9 technology resulted in suppression of p53 protein independently of MDM2 activity **(Figure 35)**. This manifests the importance of p53 as a tumour suppressor and the plasticity of protein circuitry in cancer cells to suppress p53 and favour cancer cell survival.

6. Discussion and Future Directions

Lung cancer remains the principal cancer killer worldwide and this is due to late diagnosis and the onset of drug resistant metastatic disease. Intra-tumour heterogeneity, mediated by extensive remodelling of the tumour microenvironment as well as genetic and epigenetic diversity, promotes tumour evolution by fuelling drug resistance and metastasis (Shibue & Weinberg, 2017; Caswell & Swanton, 2017). Metastasis is responsible for 90% of cancer-associated deaths and yet this multistep process remains poorly understood (Chaffer & Weinberg, 2011). Epithelial-mesenchymal transition (EMT) represents one of the earliest events of the invasion-metastasis cascade, while the plasticity of cancer cells to transition between epithelial and mesenchymal states has been considered the hallmark of metastatic dissemination in epithelial cancers, despite emerging reports of alternative dissemination modes (Jolly et al., 2017). Crucially, cancer cells that have undergone EMT acquire resistance to molecular targeted therapy, chemotherapy and immunotherapy. As resistant residual carcinoma cells often manifest EMT activation, elucidating the mechanisms underlying these processes and targeting their key pathway components might improve clinical responses (Shibue & Weinberg, 2017).

The RAS/MAPK pathway is one of the most persistently activated pathways in cancer. RAS mutations are found in 25% of all human cancers, of which KRAS mutations prevail (Haigis, 2017). Activating KRAS mutations account for the majority of molecular alterations in lung adenocarcinomas (LUADs), the most commonly diagnosed lung cancer subtype. Aberrant KRAS activation is indispensable for tumour initiation and progression and is linked to poor outcome in surgically resected LUADs (Nadal et al., 2014). Critically, RAS mutations have not been adequately targeted to date and tumours with these mutations are resistant to tyrosine kinase inhibitors (TKIs) targeting EGFR mutations, the second most frequent oncogenic drivers in LUAD (Mao et al., 2010). Further, persistent KRAS activation is involved in resistance to anti-EGFR therapies by encouraging EGF-dependent downstream signalling (Chong & Janne, 2013). KRAS downstream signalling is partly mediated through the RAF/MEK/ERK pathway, which controls key cellular processes including cell proliferation, differentiation, survival and growth, and has been widely associated with RAS-driven oncogenesis (Ryan et al., 2015). Although several potent BRAF, MEK1/2 and ERK1/2 inhibitors have been

developed and showed promising clinical responses, resistance almost invariably emerges, which results in persistent ERK signalling in the presence of the inhibitor. This is mainly due to activating mutations or amplification of upstream/downstream pathway components and dependency on parallel pathways. Crucially, the RAF/MEK/ERK pathway is characterised by the presence of several negative feedback loops, which are responsible for its fine-tuning. This is problematic for efficient therapeutic targeting, as RAF, MEK or ERK inhibitors relieve the inhibitory effects of ERK-dependent negative feedback loops, resulting in further activation of the pathway and the acquisition of resistance (Caunt et al., 2015; Ryan et al., 2015; Lito, Rosen & Solit, 2013).

The ability of cancer cells to adapt to such therapeutic interventions manifests the complexity of this pathway, the presence of several autoregulatory feedback loops and the plasticity of the protein circuitry to rewire, all of which can reactivate the pathway or shift the dependency on parallel pathways. Hence, identifying and targeting downstream components of this pathway that are important oncogenic drivers has been an attractive therapeutic strategy. Unlike the restricted downstream targets of RAF and MEK, the kinases ERK1 and ERK2 were shown to phosphorylate over 200 nuclear and cytoplasmic substrates, many critical for cancer progression (Ryan et al., 2015). The p90 (90 kDa) ribosomal S6 kinase (RSK) family of serine/threonine kinases are major effectors of ERK1/2 kinases and have been shown to drive cancer growth, motility, invasion and metastasis (Sulzmaier & Ramos, 2013; Romeo et al., 2013).

RSKs are emerging as major effectors of the RAS/MAPK pathway in cancer, and direct RSK targeting represents a valuable alternative approach to the inhibition of upstream pathway components (Houles & Roux, 2018; Romeo & Roux, 2011). RSKs are likely to phosphorylate a more limited substrate repertoire as compared to ERK1/2, thus targeting RSKs would presumably generate less severe side effects while retaining potential anti-cancer properties. Three major classes of pan-RSK inhibitors exist to date: the reversible N-terminal kinase domain (NTKD) inhibitors SL-0101 and BI-D1870, and the irreversible C-terminal kinase domain (CTKD) inhibitor FMK (Casalvieri et al., 2017). Although they have been instrumental in better understanding RSK signalling, these are ATP-competitive inhibitors and therefore have been associated with several off-target

effects (Bain et al., 2007). Accumulating evidence also supports the presence of a RSK-dependent negative feedback loop that is similar to the ERK1/2-mediated inhibition of RAS/MAPK pathway. RSK2 was shown to phosphorylate SOS, a well-known guanine nucleotide exchange factor (GEF), and RAS activator (Douville & Downward, 1997). While it is unclear whether this phosphorylation results in RAS/MAPK inhibition, skeletal muscle lysates from RSK2 knockout mice and BI-D1870-treated HEK293 cells demonstrated increased phosphorylation of ERK1/2 (Sapkota et al., 2007; Dufresne et al., 2001), suggesting that pan-RSK inhibition may result in sustained pathway activation and promote rather than inhibit cancer progression. Interesingly, in the current study we show that taking out RSK4 decreases the phosphorylation of ERK1/2, suggesting that selective inhibition of RSK4 may not result in RAS/MAPK reactivation **(Figure S 26b)**. Lastly, the differential expression of RSK isoforms in tissues and the emergence of isoform-specific roles in cancer, renders the use of pan-RSK inhibitors ineffective, and demonstrates the need for the development of isoform-selective RSK inhibitors (Houles & Roux, 2018; Casalvieri et al., 2017).

In this study, we identified RSK4, a member of the RSK (RSK1-4) family of kinases, as a key mediator of drug resistance and metastasis in lung cancer. We propose that RSK4 regulates these processes, at least in part, by impinging on key anti-apoptotic proteins (c-IAP1 and c-IAP2) and the EMT programme. Although, to formally demonstrate whether c-IAPs are indeed involved in drug resistance in our setting, drug sensitivity will be assessed in the presence of RSK4 siRNA or in RSK4 KO cell lines followed by re-expression of c-IAP1 or c-IAP2. Further, the manipulation of EMT or MET markers in the same setting will provide unequivocal evidence for their participation in migration and/or invasion. Crucially, this work provides evidence for the requirement of RSK-specific inhibitors as opposed to pan-RSK inhibitors. RSK1 exerts opposing effects to RSK4 on drug response and cell migration/invasion and may act as a potent tumour suppressor in lung cancer. Our small-molecule inhibitor screen identified trovafloxacin as a potent allosteric inhibitor of RSK4 activation as determined by a HTRF assay. Considering that no RSK4 exclusive phosphorylation substrate has been reported to date, it has been challenging to manifest inhibition of RSK4 activity by assessing substrate phosphorylation in cells. For instance, rpS6 is redundantly phosphorylated by all S6K and RSK family members. Therefore, the

alternative would be to perform an *in vitro* kinase assay with recombinant RSK4 and rpS6 proteins treated with/without trovafloxacin. Nevertheless, trovafloxacin reproduces all molecular and biological effects of RSK4 silencing *in vitro* and *in vivo*. Further, preliminary data show that trovafloxacin does not inhibit RSK1 activation in cells (data not shown), although the formal demonstration of that would require the development of a RSK1 HTRF-based activation assay, which is complicated by the fact that RSK1, unlike RSK4, requires both ERK1/2 and PDK1 for its activation. Lastly, although RSK4 CRISPR/Cas9-mediated KO or pharmacological inhibition impairs tumour growth *in vivo* **(Figure 12d, e & Figure 16)**, it remains unclear whether this effect is mediated through the molecular changes observed *in vitro*. To demonstrate this, immunohistochemical analysis of apoptosis (e.g. cleaved caspase-3, cleaved PARP, c-IAPs), proliferation (e.g. Ki-67) and EMT/MET (e.g. N-cadherin and E-cadherin) markers will be carried out in FFPE tissue sections of our tumour xenografts. Taken together, RSK4 is emerging as a novel therapeutic target in lung cancer and RSK4-targeting floxacins could be re-purposed and used in combination with chemotherapy to improve survival of lung cancer patients.

Trovafloxacin is a fluoroquinolone-based broad spectrum antibiotic that exerts its antibacterial action by inhibiting type II topoisomerases DNA gyrase and topoisomerase IV, both essential bacterial enzymes for managing DNA tangles and supercoils (Brighty & Gootz, 1997; Gootz et al., 1996). Floxacin antibiotics that were inactive against RSK4 (e.g. ciprofloxacin), could not reproduce the effects of RSK4 silencing, suggesting the effects of trovafloxacin are not dependent on the antibacterial activity of these compounds (Kathryn Chapman, personal communication). Nevertheless, the possibility that some of the effects of trovafloxacin could be mediated independently of RSK4 should not be excluded. Trovafloxacin was previously profiled against a panel of over 200 kinases and was shown to inhibit the discoidin domain-containing receptor 2 (DDR2) by 69±2% at an *in vitro* concentration of 10 µM (Kathryn Chapman, personal communication). DDR2 is a tyrosine kinase collagen receptor involved in ECM remodelling, cell migration, proliferation and differentiation (Leitinger, 2014). In fact, DDR2 is a target of several FDA-approved kinase inhibitors, including imatinib and dasatinib (Day et al., 2008). Interestingly, DDR2 activating mutations were sensitive to dasatinib treatment in lung cancer (Xu et al., 2015; Hammerman et al., 2011). Trovafloxacin was also shown to inhibit

plasma membrane pannexin 1 channels (PANX1), which release nucleotide “find-me” signals during apoptosis to promote phagocytic clearance (Poon et al., 2014). Hence, trovafloxacin treatment may result in dysregulated apoptotic cell fragmentation. Furthermore, this fluoroquinolone was reported to inhibit fatty acid binding protein 4 (FABP4), which plays crucial roles in metabolic disorders including atherosclerosis and insulin resistance (Wang et al., 2014). To distinguish between trovafloxacin’s off-target effects and effects mediated through inhibition of RSK4 activity, a mutated version of RSK4 that is resistant to trovafloxacin binding (based on mathematical modelling and molecular docking simulations; data not shown), will be expressed in trovafloxacin-treated cells and phenotypic rescue will be assessed.

In mice, treatment with the combination of trovafloxacin and lipopolysaccharide (LPS), which induces tumour necrosis factor alpha (TNFα) production (van der Bruggen et al., 1999), caused liver injury as determined by monitoring plasma alanine aminotransferase (ALT) activity. However, treatment with trovafloxacin alone did not alter ALT activity up to 1000 mg/kg (Shaw et al., 2007). Therefore, the LPS-induced inflammatory response via TNFα production promotes the hepatotoxicity of trovafloxacin in mice. Interestingly, the mechanisms underlying the cytotoxicity of trovafloxacin in response to TNFα were subsequently shown to be mediated by activation of ERK1/2 signalling *in vitro* (Beggs et al., 2015). In patients, the administration of trovafloxacin as an antibacterial agent was associated with several cases of hepatotoxicity so that this drug has been withdrawn from the market (Stahlmann, 2002). Trovafloxacin-induced hepatotoxicity was proposed to be mediated through the oxidation of a cyclopropylamine moiety to reactive intermediates (i.e. alpha, beta-unsaturated aldehyde) that could form adducts with hepatic proteins (Sun et al., 2007). Collectively, the aforementioned studies demonstrate the requirement for the design and synthesis of novel trovafloxacin-based analogues that retain their capacity to bind RSK4 but are devoid of these reactive side chains.

This work proposes a tumour promoting role for RSK4, which contradicts the tumour suppressive properties reported for this kinase in breast and colon cancers (Ye et al., 2018; Thakur et al., 2008). It is possible that RSK4 exerts its divergent roles in a context- or disease-specific manner and therefore further studies are required to elucidate the underlying molecular mechanisms accounting for these discrepancies. In addition, we show

that expression of RSK4 does not affect the survival of lung squamous cell carcinoma (LUSC) patients, while it correlates with patient outcome in lung adenocarcinoma (LUAD). Hence, pharmacological inhibition of RSK4 might be more beneficial in selective cancer types and/or subtypes. There is also a possibility that RSK4 conflicting roles might be due to differentially expressed alternatively spliced variants. At least two protein-coding RSK4 transcript variants are reported in Ensembl: RSK4 variant I (NM_014496.5), which is considered the "canonical" variant, and RSK4 variant II (NM_001330512.1), which has not been previously studied. Alternative splicing increases proteomic diversity and changes in alternative splicing have been associated with human diseases, while it is often deregulated in cancer (Tazi, Bakkour & Stamm, 2009). For instance, alternative splicing can produce several variants of the transmembrane glycoprotein CD44, which were shown to differentially affect cancer progression (Prochazka, Tesarik & Turanek, 2014). For this reason, we have recently cloned the variant II of RSK4 and are currently exploring its functional significance in lung cancer as well as breast cancer cell lines. Interestingly, reconstructing RSK4 spliced variants based on publicly available genome assemblies and protein sequences, revealed that RSK4 variant II contains all the necessary information (i.e. exons), which following alternative splicing (i.e. exon skipping), could give rise to RSK4 variant I **(Figure S 9)**. Hence, RSK4 variant II might be the "canonical" variant of RSK4, an observation that requires further validation. For this purpose, it will be crucial to develop tools for the specific downregulation and mRNA or protein quantification of RSK4 spliced variants across a diverse panel of cancer cell lines and/or tissues. Once their tissue specificity is better understood, further work will aim at highlighting the biological effects of these variants. With this in mind, it is worth noticing that our tandem-affinity purification (TAP) screen identified >100 exclusive interacting partners for RSK4 variant I vs variant II in HEK293A cells. Further validation of these targets could be the first step towards understanding the functional differences between these two RSK4 proteins.

RSK4 is emerging as a functionally distinct RSK family member in that is does not require PDK1 for its activation and manifests high baseline activity in the absence of growth factor stimulation that was interpreted as a constitutive activation state (Dummler et al., 2005). However, our preliminary data indicates increased Ser232

phosphorylation of RSK4 following stimulation with EGF **(Figure S 26a)**. Crucially, this residue corresponds to the PDK1 phosphorylation site in RSK1-3 (Dummler et al., 2005). While it is unclear at this stage whether this phosphorylation is mediated by ERK1/2 or requires the input from additional kinases, this observation challenges the notion that RSK4 is constitutively active. The transient knockdown of ERK1/2 and/or PDK1 in the presence or absence of growth factor stimulation will formally demonstrate whether RSK4 receives inputs from both kinases. It has also been postulated that RSK4, because of the lack of PDK1 requirement, exhibits enhanced autophosphorylation (Dummler et al., 2005). Assessing Ser232 phosphorylation levels of NTKD or CTKD catalytically inactive mutants, immunoprecipitated from ERK1/2- and/or PDK1-deficient cells, will provide unequivocal evidence for the level of contribution from autophosphorylation, ERK1/2 and PDK1. In fact, RSK4 was co-purified with PDK1 in our TAP, suggesting it might indeed be involved in RSK4 activation. The possibility that RSK4 might receive inputs from additional kinases should not be excluded. For instance, in dendritic cells RSKs were shown to be activated not only by ERK1/2, but also by p38 through the MK2 and MK3 kinases (Zaru et al., 2007). A targeted drug screen using a commercially-available compound library targeting various signalling pathways would enable us to assess the possible contribution from additional kinases.

Unlike RSK1-3, RSK4 was reported not to translocate to the nucleus following pathway activation (Dummler et al., 2005). Similarly, we demonstrate that RSK4 is mostly cytosolic and localises in the perinuclear region, especially at the mitochondrial level. While EGF stimulation fails to induce its nuclear translocation, it causes RSK4 to spread in the cytoplasm **(Figure S 27)**, an effect that may be associated with changes at the mitochondrial structure. Interestingly, PDGF stimulation, which also activates the RAS/MAPK pathway, was shown to promote mitochondrial fragmentation in vascular smooth muscle cells (Salabei & Hill, 2013). Cycles of mitochondrial fission/fusion regulate mitochondrial distribution and proliferation, allow the mixing of mitochondrial DNA and metabolites and ensure cellular adaptations to fluctuating energy requirements (Westermann, 2010). There is mounting evidence depicting the critical role these dynamic processes play in neurodegeneration and apoptosis (Knott et al., 2008; Arnoult, 2007). Hence, it would be particularly

interesting to dissect out the mechanisms by which RSK4 might impact mitochondrial dynamics and ultimately identify the functional significance, and possible disease relevance, of this regulation.

RSK family members display high degree of sequence homology and this was once thought to suggest overlapping functions. While a certain degree of redundancy is expected, accumulating evidence supports the existence of RSK isoform-specific roles in cancer (Houles & Roux, 2018; Lara, Seckl & Pardo, 2013). To identify common or exclusive binding partners of RSK1 and RSK4, we carried out a TAP of these kinases followed by mass-spectrometric analysis. We complemented this approach with a global phosphoproteomics and proteomics analysis in a RSK1 or RSK4 transiently depleted background. RSK1 and RSK4 putative binding partners and substrates were enriched in pathways controlling the DNA-damage response (DDR), in particular non-homologous end joining (NHEJ) and homologous recombination (HR). The tumour suppressor p53 lays at the centre of these pathways and we therefore investigated the regulation of this protein by RSK1/4 further. Here, we propose a mechanism by which both kinases regulate p53 stability through direct phosphorylation of MDM2 at Ser166, a well-characterised site associated with increased ubiquitin ligase activity of MDM2 and subsequent proteasomal degradation of p53 (Meek & Knippschild, 2003). This was further associated with induction of two *bona fide* p53 transcriptional targets, $p21^{Cip1/WAF1}$ and PUMA, although the downstream effects of this regulation remain to be explored. In addition to the well documented roles of p53 in DNA repair, cell cycle arrest and apoptosis, p53 was implicated in the regulation of several metabolic processes (Kastenhuber & Lowe, 2017). For instance, p53 was shown to reduce mitochondrial pyruvate uptake and upregulate glycolysis in a PUMA-dependent manner. Interestingly, a novel p53 target, TIGAR (TP53-induced glycolysis and apoptosis regulator) was also reported to regulate glycolysis and protect cells against oxidative stress-induced apoptosis (Kim et al., 2019; Bensaad et al., 2006). In addition, although p53 remains one of the best characterised MDM2 targets, MDM2 interacts with several other proteins including HNRNPK, Slug and IGF-1R, which it targets for proteasomal degradation (Riley & Lozano, 2012). For instance, HNRNPK was stabilised in response to DNA damage via a mechanism that involves inhibition of MDM2-mediated ubiquitin degradation (Moumen et al., 2005). Considering that RSK4 (variant II) co-purifies with HNRNPK in our TAP it

would be interesting to test whether RSK4 participates in this mechanism. In summary, while RSK1 and RSK4 regulate p53 and MDM2 in a mutual manner, the diversity of pathways downstream of these master regulators may still explain different functional consequences of signalling from these two kinases.

Surprisingly, throughout this study we have observed that RSK1 silencing decreases RSK4 protein levels **(e.g. Figure 29d)**, suggesting that the RSK4 antibody might be cross-reacting with RSK1 antigen. However, RSK1 siRNA deconvolution shows that all, except one, oligonucleotides decrease RSK4 mRNA levels by 30%-50%, raising the possibility that RSK1 might be involved in the transcriptional regulation of RSK4 **(Figure S 24a)**. Interestingly, no transcription factor was reported to control RSK4 gene expression to date. RSK1 is known to phosphorylate several transcription factors including CREB, c-Fos and ERα (Houles & Roux, 2018), and the involvement of these in RSK4 transcription could be further investigated. Alternatively, the use of a siRNA library targeting all known transcription factors followed by RSK1 silencing and quantification of RSK4 mRNA levels, will assist in identifying candidate transcriptions factors involved. Further, RSK2 or RSK3 silencing similarly decreased RSK4 protein levels **(Figure S 24b)**. Whether this is a siRNA off-target effect or indeed constitutes a true regulation of RSK4 expression remains to be determined.

A major caveat of siRNAs is their off-target silencing through partial sequence complementarity with the 3'-UTRs of unintended transcripts (Jackson & Linsley, 2010). This hinders our understanding of gene function and may lead to false positive or negative phenotypes, thus complicating data interpretation. This hurdle can be mitigated by siRNA pooling, chemical modification (e.g. 2'-O-methyl modification) of siRNAs to weaken/disrupt their interaction with partially bound transcripts, by avoiding siRNAs ≥30bp in length, which may induce an interferon response, and by reducing the concentration of siRNAs to the minimum amount that generates the desired response (Cullen, 2006). In the current work, data from siRNA experiments were confirmed with RSK4 KO cell lines and the pharmacological inhibitor of RSK4. The specificity of siRNA experiments can be further established by rescuing the phenotype following expression of a mutated form of RSK4 that is resistant to siRNA binding/silencing, or by transfecting multiple independent siRNAs that are designed to target different regions of RSK4 while exerting the same effect (Cullen, 2006). Similarly, CRISPR/Cas9-mediated genome

editing is also prone to off-target activity by inducing mutations at unintended genomic sites (Zhang et al., 2015). Off-target sites can be detected by several methods, including deep sequencing, GUIDE-seq and ChIP-seq, all of which have varying degrees of precision and sensitivity. Several strategies have also been reported to reduce off-target effects, including reduction of Cas9-sgRNA concentration, expression of a Cas9 D10A nickase version, which generates single-strand breaks, and the truncation of sgRNA 3' or 5' end (Zhang et al., 2015). To assess whether the effects of CRISPR/Cas9-mediated KO of RSK4 are indeed the result of RSK4 deletion, RSK4 will be re-expressed in these cells and downstream assays will be performed. To determine which of these effects are dependent upon the kinase activity of RSK4, we will utilise our RSK4 kinase active and dead mutants **(Figure S 25)**.

RSK4, is an X-linked gene and therefore one of its alleles undergoes random X-chromosome inactivation in 'XX' cells. Hence, this feature should be considered before interpreting RSK4 background levels in female cancers or comparing them with male cancers (i.e. 'XY' cells), since differential X-chromosome activation status due to duplications, reactivations or X-chromosome inactivation escape, might alter the expression levels of this kinase and potentially its function (Berletch et al., 2011; Thakur et al., 2007; Spatz, Borg & Feunteun, 2004). Whether RSK4 acts in a tumour suppressive or tumour promoting manner remains elusive. Genetic or epigenetic mechanisms (Niskakoski et al., 2014; Li et al., 2014; Dewdney et al., 2011), distinct upstream/downstream signalling and differential expression patterns, compensatory or counteracting signals from other RSK family members, or the presence of alternatively spliced variants could contribute towards the discrepancies in the reported roles of this kinase in cancer. Nevertheless, our work established RSK4 as a potent tumour promoter in lung cancer and its therapeutic targeting could improve the clinical outcome for lung adenocarcinoma patients.

7. References

Abukhdeir, A. M. & Park, B. H. (2008) P21 and p27: roles in carcinogenesis and drug resistance. *Expert Reviews in Molecular Medicine.* 10 e19. Available from: doi: https://dx.doi.org/10.1017/S1462399408000744.

Aiken, J. & Birot, O. (2016) The Vascular Endothelial Growth Factor-A phosphorylates Murine Double Minute-2 on its Serine 166 via the Extracellular Signal-Regulated Kinase 1/2 and p90 Ribosomal S6 Kinase in primary human endothelial cells. *Biochemical & Biophysical Research Communications.* 478 (4), 1548-1554. Available from: doi: https://dx.doi.org/10.1016/j.bbrc.2016.08.150.

Alexandrov, L. B., Nik-Zainal, S., Wedge, D. C., Aparicio, S. A. J. R., Behjati, S., Biankin, A. V., Bignell, G. R., Bolli, N., Borg, A., Borresen-Dale, A., Boyault, S., Burkhardt, B., Butler, A. P., Caldas, C., Davies, H. R., Desmedt, C., Eils, R., Eyfjord, J. E., Foekens, J. A., Greaves, M., Hosoda, F., Hutter, B., Ilicic, T., Imbeaud, S., Imielinski, M., Jager, N., Jones, D. T. W., Jones, D., Knappskog, S., Kool, M., Lakhani, S. R., Lopez-Otin, C., Martin, S., Munshi, N. C., Nakamura, H., Northcott, P. A., Pajic, M., Papaemmanuil, E., Paradiso, A., Pearson, J. V., Puente, X. S., Raine, K., Ramakrishna, M., Richardson, A. L., Richter, J., Rosenstiel, P., Schlesner, M., Schumacher, T. N., Span, P. N., Teague, J. W., Totoki, Y., Tutt, A. N. J., Valdes-Mas, R., van Buuren, M. M., van 't Veer, L., Vincent-Salomon, A., Waddell, N., Yates, L. R., Australian Pancreatic Cancer Genome Initiative, ICGC Breast Cancer Consortium, ICGC MMML-Seq Consortium, ICGC PedBrain, Zucman-Rossi, J., Futreal, P. A., McDermott, U., Lichter, P., Meyerson, M., Grimmond, S. M., Siebert, R., Campo, E., Shibata, T., Pfister, S. M., Campbell, P. J. & Stratton, M. R. (2013) Signatures of mutational processes in human cancer. *Nature.* 500 (7463), 415-421. Available from: doi: https://dx.doi.org/10.1038/nature12477.

Andreeff, M., Kelly, K. R., Yee, K., Assouline, S., Strair, R., Popplewell, L., Bowen, D., Martinelli, G., Drummond, M. W., Vyas, P., Kirschbaum, M., Iyer, S. P., Ruvolo, V., Gonzalez, G. M. N., Huang, X., Chen, G., Graves, B., Blotner, S., Bridge, P., Jukofsky, L., Middleton, S., Reckner, M., Rueger, R., Zhi, J., Nichols, G. & Kojima, K. (2016) Results of the Phase I Trial of RG7112, a Small-Molecule MDM2 Antagonist in Leukemia. *Clinical Cancer Research.* 22 (4), 868-876. Available from: doi: https://dx.doi.org/10.1158/1078-0432.CCR-15-0481.

Anjum, R. & Blenis, J. (2008) The RSK family of kinases: emerging roles in cellular signalling. *Nature Reviews Molecular Cell Biology.* 9 (10), 747-758. Available from: doi: http://dx.doi.org/10.1038/nrm2509.

Anwar, A., Norris, D. A. & Fujita, M. (2011) Ubiquitin proteasomal pathway mediated degradation of p53 in melanoma. *Archives of Biochemistry & Biophysics.* 508 (2), 198-203. Available from: doi: https://dx.doi.org/10.1016/j.abb.2010.12.012.

Arechavaleta-Velasco, F., Zeferino-Toquero, M., Estrada-Moscoso, I., Imani-Razavi, F. S., Olivares, A., Perez-Juarez, C. E. & Diaz-Cueto, L. (2016) Ribosomal S6 kinase 4 (RSK4) expression in ovarian tumors and its regulation by antineoplastic drugs in ovarian cancer cell lines. *Medical Oncology.* 33 (2), 11. Available from: doi: https://dx.doi.org/10.1007/s12032-015-0724-6.

Arima, Y., Inoue, Y., Shibata, T., Hayashi, H., Nagano, O., Saya, H. & Taya, Y. (2008) Rb depletion results in deregulation of E-cadherin and induction of cellular phenotypic changes that are characteristic of the epithelial-to-mesenchymal transition. *Cancer Research.* 68 (13), 5104-5112. Available from: doi: https://dx.doi.org/10.1158/0008-5472.CAN-07-5680.

Arnoult, D. (2007) Mitochondrial fragmentation in apoptosis. *Trends in Cell Biology.* 17 (1), 6-12. Available from: doi: https://dx.doi.org/10.1016/j.tcb.2006.11.001.

Aronheim, A., Engelberg, D., Li, N., al-Alawi, N., Schlessinger, J. & Karin, M. (1994) Membrane targeting of the nucleotide exchange factor Sos is sufficient for activating the Ras signaling pathway. *Cell.* 78 (6), 949-961. Available from: doi: https://dx.doi.org/10.1016/0092-8674(94)90271-2.

Au, N. H. C., Gown, A. M., Cheang, M., Huntsman, D., Yorida, E., Elliott, W. M., Flint, J., English, J., Gilks, C. B. & Grimes, H. L. (2004) P63 expression in lung carcinoma: a tissue microarray study of 408 cases. *Applied Immunohistochemistry & Molecular Morphology.* 12 (3), 240-247. Available from: doi: https://www.ncbi.nlm.nih.gov/pubmed/15551738.

Bach, I., Robinson, D., Thomas, N., Ropers, H. H. & Cremers, F. P. (1992) Physical fine mapping of genes underlying X-linked deafness and non fra (X)-X-linked mental retardation at Xq21. *Human Genetics.* 89 (6), 620-624. Available from: doi: https://www.ncbi.nlm.nih.gov/pubmed/1511979.

Bain, J., Plater, L., Elliott, M., Shpiro, N., Hastie, C. J., McLauchlan, H., Klevernic, I., Arthur, J. S. C., Alessi, D. R. & Cohen, P. (2007) The selectivity of protein kinase inhibitors: a further update. *Biochemical Journal.* 408 (3), 297-315. Available from: doi: https://dx.doi.org/10.1042/BJ20070797.

Batlle, E., Sancho, E., Franci, C., Dominguez, D., Monfar, M., Baulida, J. & Garcia De Herreros, A. (2000) The transcription factor snail is a repressor of E-cadherin gene expression in epithelial tumour cells. *Nature Cell Biology.* 2 (2), 84-89. Available from: doi: https://dx.doi.org/10.1038/35000034.

Bean, J., Brennan, C., Shih, J., Riely, G., Viale, A., Wang, L., Chitale, D., Motoi, N., Szoke, J., Broderick, S., Balak, M., Chang, W., Yu, C., Gazdar, A., Pass, H., Rusch, V., Gerald, W., Huang, S., Yang, P., Miller, V., Ladanyi, M., Yang, C. & Pao, W. (2007) MET amplification occurs with or without T790M mutations in EGFR mutant lung tumors with acquired resistance to gefitinib or erlotinib. *Proceedings of the National Academy of Sciences of the United States of America.* 104 (52), 20932-20937. Available from: doi: https://dx.doi.org/10.1073/pnas.0710370104.

Beggs, K. M., Maiuri, A. R., Fullerton, A. M., Poulsen, K. L., Breier, A. B., Ganey, P. E. & Roth, R. A. (2015) Trovafloxacin-induced replication stress sensitizes HepG2 cells to tumor necrosis factor-alpha-induced cytotoxicity mediated by extracellular signal-regulated kinase and ataxia telangiectasia and Rad3-related. *Toxicology.* 331 35-46. Available from: doi: https://dx.doi.org/10.1016/j.tox.2015.03.002.

Bender, C. & Ullrich, A. (2012) PRKX, TTBK2 and RSK4 expression causes Sunitinib resistance in kidney carcinoma- and melanoma-cell lines. *International Journal of Cancer.* 131 (2), E45-55. Available from: doi: http://dx.doi.org/10.1002/ijc.26486.

Bensaad, K., Tsuruta, A., Selak, M. A., Vidal, M. N. C., Nakano, K., Bartrons, R., Gottlieb, E. & Vousden, K. H. (2006) TIGAR, a p53-inducible regulator of glycolysis and apoptosis. *Cell.* 126 (1), 107-120. Available from: doi: https://dx.doi.org/10.1016/j.cell.2006.05.036.

Berletch, J. B., Yang, F., Xu, J., Carrel, L. & Disteche, C. M. (2011) Genes that escape from X inactivation. *Human Genetics.* 130 (2), 237-245. Available from: doi: http://dx.doi.org/10.1007/s00439-011-1011-z.

Berndt, N., Hamilton, A. D. & Sebti, S. M. (2011) Targeting protein prenylation for cancer therapy. *Nature Reviews.Cancer.* 11 (11), 775-791. Available from: doi: https://dx.doi.org/10.1038/nrc3151.

Berns, K., Hijmans, E. M., Mullenders, J., Brummelkamp, T. R., Velds, A., Heimerikx, M., Kerkhoven, R. M., Madiredjo, M., Nijkamp, W., Weigelt, B., Agami, R., Ge, W., Cavet, G., Linsley, P. S., Beijersbergen, R. L. & Bernards, R. (2004) A large-scale RNAi screen in human cells identifies new components of the p53 pathway. *Nature.* 428 (6981), 431-437. Available from: doi: http://dx.doi.org/10.1038/nature02371.

Bieging, K. T., Mello, S. S. & Attardi, L. D. (2014) Unravelling mechanisms of p53-mediated tumour suppression. *Nature Reviews.Cancer.* 14 (5), 359-370. Available from: doi: https://dx.doi.org/10.1038/nrc3711.

Blackford, A. N. & Jackson, S. P. (2017) ATM, ATR, and DNA-PK: The Trinity at the Heart of the DNA Damage Response. *Molecular Cell.* 66 (6), 801-817. Available from: doi: https://dx.doi.org/10.1016/j.molcel.2017.05.015.

Blanpain, C., Lowry, W. E., Geoghegan, A., Polak, L. & Fuchs, E. (2004) Self-renewal, multipotency, and the existence of two cell populations within an epithelial stem cell niche. *Cell.* 118 (5), 635-648. Available from: doi: https://dx.doi.org/10.1016/j.cell.2004.08.012.

Blasco, R. B., Francoz, S., Santamaria, D., Canamero, M., Dubus, P., Charron, J., Baccarini, M. & Barbacid, M. (2011) c-Raf, but not B-Raf, is essential for development of K-Ras oncogene-driven non-small cell lung carcinoma. *Cancer Cell.* 19 (5), 652-663. Available from: doi: https://dx.doi.org/10.1016/j.ccr.2011.04.002.

Blumenschein, G. R. J., Smit, E. F., Planchard, D., Kim, D., Cadranel, J., De Pas, T., Dunphy, F., Udud, K., Ahn, M., Hanna, N. H., Kim, J., Mazieres, J., Kim, S., Baas, P., Rappold, E., Redhu, S., Puski, A., Wu, F. S. & Janne, P. A. (2015) A randomized phase II study of the MEK1/MEK2 inhibitor trametinib (GSK1120212) compared with docetaxel in KRAS-mutant advanced non-small-cell lung cancer (NSCLC) . *Annals of Oncology.* 26 (5), 894-901. Available from: doi: https://dx.doi.org/10.1093/annonc/mdv072.

Bode, A. M. & Dong, Z. (2004) Post-translational modification of p53 in tumorigenesis. *Nature Reviews.Cancer.* 4 (10), 793-805. Available from: doi: https://dx.doi.org/10.1038/nrc1455.

Boehme, K. A., Kulikov, R. & Blattner, C. (2008) p53 stabilization in response to DNA damage requires Akt/PKB and DNA-PK. *Proceedings of the National Academy of Sciences of the United States of America.* 105 (22), 7785-7790. Available from: doi: https://dx.doi.org/10.1073/pnas.0703423105.

Bohuslav, J., Chen, L., Kwon, H., Mu, Y. & Greene, W. C. (2004) p53 induces NF-kappaB activation by an IkappaB kinase-independent mechanism involving phosphorylation of p65 by ribosomal S6 kinase 1. *Journal of Biological Chemistry.* 279 (25), 26115-26125. Available from: doi: https://dx.doi.org/10.1074/jbc.M313509200.

Bolos, V., Peinado, H., Perez-Moreno, M. A., Fraga, M. F., Esteller, M. & Cano, A. (2003) The transcription factor Slug represses E-cadherin expression and induces epithelial to mesenchymal transitions: a comparison with Snail and E47 repressors. *Journal of Cell Science.* 116 (Pt 3), 499-511. Available from: doi: https://dx.doi.org/10.1242/jcs.00224.

Bonni, A., Brunet, A., West, A. E., Datta, S. R., Takasu, M. A. & Greenberg, M. E. (1999) Cell survival promoted by the Ras-MAPK signaling pathway by transcription-dependent and -independent mechanisms. *Science.* 286 (5443), 1358-1362. Available from: doi: https://www2.scopus.com/record/display.uri?eid=2-s2.0-0032698075&origin=inward.

Bos, J. L., Rehmann, H. & Wittinghofer, A. (2007) GEFs and GAPs: critical elements in the control of small G proteins. *Cell.* 129 (5), 865-877. Available from: doi: https://dx.doi.org/10.1016/j.cell.2007.05.018.

Brady, C. A., Jiang, D., Mello, S. S., Johnson, T. M., Jarvis, L. A., Kozak, M. M., Kenzelmann Broz, D., Basak, S., Park, E. J., McLaughlin, M. E., Karnezis, A. N. & Attardi, L. D. (2011) Distinct p53 transcriptional programs dictate acute DNA-damage responses and tumor suppression. *Cell.* 145 (4), 571-583. Available from: doi: https://dx.doi.org/10.1016/j.cell.2011.03.035.

Bray, F., Ferlay, J., Soerjomataram, I., Siegel, R. L., Torre, L. A. & Jemal, A. (2018) Global cancer statistics 2018: GLOBOCAN estimates of incidence and mortality worldwide for 36 cancers in 185 countries. *CA: A Cancer Journal for Clinicians.* 68 (6), 394-424. Available from: doi: https://dx.doi.org/10.3322/caac.21492.

Brighty, K. E. & Gootz, T. D. (1997) The chemistry and biological profile of trovafloxacin. *Journal of Antimicrobial Chemotherapy.* 39 (Suppl B), 1-14. Available from: doi: https://dx.doi.org/10.1093/jac/39.suppl_2.1.

Brown, D. M. & Ruoslahti, E. (2004) Metadherin, a cell surface protein in breast tumors that mediates lung metastasis. *Cancer Cell.* 5 (4), 365-374. Available from: doi: https://dx.doi.org/10.1016/S1535-6108(04)00079-0.

Brown, R. L., Reinke, L. M., Damerow, M. S., Perez, D., Chodosh, L. A., Yang, J. & Cheng, C. (2011) CD44 splice isoform switching in human and mouse epithelium is essential for epithelial-mesenchymal transition and breast cancer progression. *Journal of Clinical Investigation.* 121 (3), 1064-1074. Available from: doi: https://dx.doi.org/10.1172/JCI44540.

Bruning, J. C., Gillette, J. A., Zhao, Y., Bjorbaeck, C., Kotzka, J., Knebel, B., Avci, H., Hanstein, B., Lingohr, P., Moller, D. E., Krone, W., Kahn, C. R. & Muller-Wieland, D. (2000) Ribosomal subunit kinase-2 is required for growth factor-stimulated transcription of the c-Fos gene. *Proceedings of the National Academy of Sciences of the United States of America.* 97 (6), 2462-2467. Available from: doi: https://dx.doi.org/10.1073/pnas.97.6.2462.

Bruno, M. D., Bohinski, R. J., Huelsman, K. M., Whitsett, J. A. & Korfhagen, T. R. (1995) Lung cell-specific expression of the murine surfactant protein A (SP-A) gene is mediated by interactions between the SP-A promoter and thyroid transcription factor-1. *Journal of Biological Chemistry.* 270 (12), 6531-6536. Available from: doi: https://dx.doi.org/10.1074/jbc.270.12.6531.

Burgess, A. W., Cho, H., Eigenbrot, C., Ferguson, K. M., Garrett, T. P. J., Leahy, D. J., Lemmon, M. A., Sliwkowski, M. X., Ward, C. W. & Yokoyama, S. (2003) An open-and-shut case? Recent insights into the activation of EGF/ErbB receptors. *Molecular Cell.* 12 (3), 541-552. Available from: doi: https://dx.doi.org/10.1016/S1097-2765(03)00350-2.

Burke, S. P., Smith, L. & Smith, J. B. (2010) cIAP1 cooperatively inhibits procaspase-3 activation by the caspase-9 apoptosome. *Journal of Biological Chemistry.* 285 (39), 30061-30068. Available from: doi: https://dx.doi.org/10.1074/jbc.M110.125955.

Byles, V., Zhu, L., Lovaas, J. D., Chmilewski, L. K., Wang, J., Faller, D. V. & Dai, Y. (2012) SIRT1 induces EMT by cooperating with EMT transcription factors and enhances prostate cancer cell migration and metastasis. *Oncogene.* 31 (43), 4619-4629. Available from: doi: https://dx.doi.org/10.1038/onc.2011.612.

Cai, J., Ma, H., Huang, F., Zhu, D., Zhao, L., Yang, Y., Bi, J. & Zhang, T. (2014) Low expression of RSK4 predicts poor prognosis in patients with colorectal cancer. *International Journal of Clinical & Experimental Pathology.* 7 (8), 4959-4970. Available from: doi: https://www.ncbi.nlm.nih.gov/pmc/articles/PMC4152057/.

Carpenter, G., King, L. J. & Cohen, S. (1978) Epidermal growth factor stimulates phosphorylation in membrane preparations in vitro. *Nature.* 276 (5686), 409-410. Available from: doi: https://www.ncbi.nlm.nih.gov/pubmed/309559.

Carriere, A., Cargnello, M., Julien, L., Gao, H., Bonneil, E., Thibault, P. & Roux, P. P. (2008) Oncogenic MAPK signaling stimulates mTORC1 activity by promoting RSK-mediated raptor phosphorylation. *Current Biology.* 18 (17), 1269-1277. Available from: doi: https://dx.doi.org/10.1016/j.cub.2008.07.078.

Casalvieri, K. A., Matheson, C. J., Backos, D. S. & Reigan, P. (2017) Selective Targeting of RSK Isoforms in Cancer. *Trends in Cancer.* 3 (4), 302-312. Available from: doi: https://dx.doi.org/10.1016/j.trecan.2017.03.004.

Casar, B., Pinto, A. & Crespo, P. (2008) Essential role of ERK dimers in the activation of cytoplasmic but not nuclear substrates by ERK-scaffold complexes. *Molecular Cell.* 31 (5), 708-721. Available from: doi: https://dx.doi.org/10.1016/j.molcel.2008.07.024.

Caswell, D. R. & Swanton, C. (2017) The role of tumour heterogeneity and clonal cooperativity in metastasis, immune evasion and clinical outcome. *BMC Medicine.* 15 (1), 133. Available from: doi: https://dx.doi.org/10.1186/s12916-017-0900-y.

Caunt, C. J., Sale, M. J., Smith, P. D. & Cook, S. J. (2015) MEK1 and MEK2 inhibitors and cancer therapy: the long and winding road. *Nature Reviews.Cancer.* 15 (10), 577-592. Available from: doi: https://dx.doi.org/10.1038/nrc4000.

Chaffer, C. L. & Weinberg, R. A. (2011) A perspective on cancer cell metastasis. *Science.* 331 (6024), 1559-1564. Available from: doi: https://dx.doi.org/10.1126/science.1203543.

Chambers, A. F., Groom, A. C. & MacDonald, I. C. (2002) Dissemination and growth of cancer cells in metastatic sites. *Nature Reviews.Cancer.* 2 (8), 563-572. Available from: doi: https://dx.doi.org/10.1038/nrc865.

Chan, B. A. & Hughes, B. G. M. (2015) Targeted therapy for non-small cell lung cancer: current standards and the promise of the future. *Translational Lung Cancer Research.* 4 (1), 36-54. Available from: doi: https://dx.doi.org/10.3978/j.issn.2218-6751.2014.05.01.

Chang, F., Steelman, L. S., Lee, J. T., Shelton, J. G., Navolanic, P. M., Blalock, W. L., Franklin, R. A. & McCubrey, J. A. (2003) Signal transduction mediated by the Ras/Raf/MEK/ERK pathway from cytokine receptors to transcription factors: potential targeting for therapeutic intervention. *Leukemia.* 17 (7), 1263-1293. Available from: doi: https://dx.doi.org/10.1038/sj.leu.2402945.

Chang, H. R., Munkhjargal, A., Kim, M., Park, S. Y., Jung, E., Ryu, J., Yang, Y., Lim, J. & Kim, Y. (2018) The functional roles of PML nuclear bodies in genome maintenance. *Mutation Research.* 809 99-107. Available from: doi: https://dx.doi.org/10.1016/j.mrfmmm.2017.05.002.

Chen, H. H. W. & Kuo, M. T. (2010) Role of glutathione in the regulation of Cisplatin resistance in cancer chemotherapy. *Metal-Based Drugs.* 2010 Available from: doi: https://dx.doi.org/10.1155/2010/430939.

Chen, R. H., Abate, C. & Blenis, J. (1993) Phosphorylation of the c-Fos transrepression domain by mitogen-activated protein kinase and 90-kDa ribosomal S6 kinase. *Proceedings of the National Academy of Sciences of the United States of America.* 90 (23), 10952-10956. Available from: doi: https://dx.doi.org/10.1073/pnas.90.23.10952.

Chen, R. H., Sarnecki, C. & Blenis, J. (1992) Nuclear localization and regulation of erk- and rsk-encoded protein kinases. *Molecular & Cellular Biology.* 12 (3), 915-927. Available from: doi: https://www.ncbi.nlm.nih.gov/pmc/articles/PMC369523/.

Cho, H., Lai, C., Shao, L. & Yu, J. (2011) Identification of tumorigenic cells in Kras(G12D)-induced lung adenocarcinoma. *Cancer Research.* 71 (23), 7250-7258. Available from: doi: https://dx.doi.org/10.1158/0008-5472.CAN-11-0903.

Cho, Y., He, Z., Zhang, Y., Choi, H. S., Zhu, F., Choi, B. Y., Kang, B. S., Ma, W., Bode, A. M. & Dong, Z. (2005) The p53 protein is a novel substrate of ribosomal S6 kinase 2 and a critical intermediary for ribosomal S6 kinase 2 and histone H3 interaction. *Cancer Research.* 65 (9), 3596-3603. Available from: doi: https://dx.doi.org/10.1158/0008-5472.CAN-04-3935.

Choi, Y. E., Butterworth, M., Malladi, S., Duckett, C. S., Cohen, G. M. & Bratton, S. B. (2009) The E3 ubiquitin ligase cIAP1 binds and ubiquitinates caspase-3 and -7 via unique mechanisms at distinct steps in their processing. *Journal of Biological Chemistry.* 284 (19), 12772-12782. Available from: doi: https://dx.doi.org/10.1074/jbc.M807550200.

Chong, C. R. & Janne, P. A. (2013) The quest to overcome resistance to EGFR-targeted therapies in cancer. *Nature Medicine.* 19 (11), 1389-1400. Available from: doi: https://dx.doi.org/10.1038/nm.3388.

Clegg, L. X., Reichman, M. E., Miller, B. A., Hankey, B. F., Singh, G. K., Lin, Y. D., Goodman, M. T., Lynch, C. F., Schwartz, S. M., Chen, V. W., Bernstein, L., Gomez, S. L., Graff, J. J., Lin, C. C., Johnson, N. J. & Edwards, B. K. (2009) Impact of socioeconomic status on cancer incidence and stage at diagnosis: selected findings from the surveillance, epidemiology, and end results: National Longitudinal Mortality Study. *Cancer Causes & Control.* 20 (4), 417-435. Available from: doi: https://dx.doi.org/10.1007/s10552-008-9256-0.

Cohen, M. S., Zhang, C., Shokat, K. M. & Taunton, J. (2005) Structural bioinformatics-based design of selective, irreversible kinase inhibitors. *Science.* 308 (5726), 1318-1321. Available from: doi: https://dx.doi.org/10.1126/science1108367.

Colicelli, J. (2004) Human RAS superfamily proteins and related GTPases. *Science's Stke [Electronic Resource]: Signal Transduction Knowledge Environment.* 2004 (250), RE13. Available from: doi: https://dx.doi.org/10.1126/stke.2502004re13.

Collisson, E. A., Trejo, C. L., Silva, J. M., Gu, S., Korkola, J. E., Heiser, L. M., Charles, R., Rabinovich, B. A., Hann, B., Dankort, D., Spellman, P. T., Phillips, W. A., Gray, J. W. & McMahon, M. (2012) A central role for RAF->MEK->ERK signaling in the genesis of pancreatic ductal adenocarcinoma. *Cancer Discovery.* 2 (8), 685-693. Available from: doi: https://dx.doi.org/10.1158/2159-8290.CD-11-0347.

Cox, A. D., Fesik, S. W., Kimmelman, A. C., Luo, J. & Der, C. J. (2014) Drugging the undruggable RAS: Mission possible? *Nature Reviews.Drug Discovery.* 13 (11), 828-851. Available from: doi: https://dx.doi.org/10.1038/nrd4389.

Cox, J., Neuhauser, N., Michalski, A., Scheltema, R. A., Olsen, J. V. & Mann, M. (2011) Andromeda: a peptide search engine integrated into the MaxQuant environment. *Journal of Proteome Research.* 10 (4), 1794-1805. Available from: doi: https://dx.doi.org/10.1021/pr101065j.

Cremers, F. P., van de Pol, D. J., Diergaarde, P. J., Wieringa, B., Nussbaum, R. L., Schwartz, M. & Ropers, H. H. (1989) Physical fine mapping of the choroideremia locus using Xq21 deletions associated with complex syndromes. *Genomics.* 4 (1), 41-46. Available from: doi: http://dx.doi.org/10.1016/0888-7543(89)90312-1.

Crooks, G. E., Hon, G., Chandonia, J. & Brenner, S. E. (2004) WebLogo: a sequence logo generator. *Genome Research.* 14 (6), 1188-1190. Available from: doi: https://dx.doi.org/10.1101/gr.849004.

Cullen, B. R. (2006) Enhancing and confirming the specificity of RNAi experiments. *Nature Methods.* 3 (9), 677-681. Available from: doi: https://dx.doi.org/10.1038/nmeth913.

Dagogo-Jack, I. & Shaw, A. T. (2018) Tumour heterogeneity and resistance to cancer therapies. *Nature Reviews Clinical Oncology.* 15 (2), 81-94. Available from: doi: https://dx.doi.org/10.1038/nrclinonc.2017.166.

Davis, A. J., Chen, B. P. C. & Chen, D. J. (2014) DNA-PK: a dynamic enzyme in a versatile DSB repair pathway. *DNA Repair.* 17 21-29. Available from: doi: https://dx.doi.org/10.1016/j.dnarep.2014.02.020.

Day, E., Waters, B., Spiegel, K., Alnadaf, T., Manley, P. W., Buchdunger, E., Walker, C. & Jarai, G. (2008) Inhibition of collagen-induced discoidin domain receptor 1 and 2 activation by imatinib, nilotinib and dasatinib. *European Journal of Pharmacology.* 599 (1-3), 44-53. Available from: doi: https://dx.doi.org/10.1016/j.ejphar.2008.10.014.

De Cesare, D., Jacquot, S., Hanauer, A. & Sassone-Corsi, P. (1998) Rsk-2 activity is necessary for epidermal growth factor-induced phosphorylation of CREB protein and transcription of c-fos gene. *Proceedings of the National Academy of Sciences of the United States of America.* 95 (21), 12202-12207. Available from: doi: https://dx.doi.org/10.1073/pnas.95.21.12202.

De Craene, B. & Berx, G. (2013) Regulatory networks defining EMT during cancer initiation and progression. *Nature Reviews.Cancer.* 13 (2), 97-110. Available from: doi: https://dx.doi.org/10.1038/nrc3447.

De Palma, M., Biziato, D. & Petrova, T. V. (2017) Microenvironmental regulation of tumour angiogenesis. *Nature Reviews.Cancer.* 17 (8), 457-474. Available from: doi: https://dx.doi.org/10.1038/nrc.2017.51.

Dela Cruz, C. S., Tanoue, L. T. & Matthay, R. A. (2011) Lung cancer: epidemiology, etiology, and prevention. *Clinics in Chest Medicine.* 32 (4), 605-644. Available from: doi: https://dx.doi.org/10.1016/j.ccm.2011.09.001.

Devlin, J. R. & Verschuren, E. W. (2018) More than a Tumor Suppressor: E-Cadherin Loss Drives Lung Cancer Metastasis. *American Journal of Respiratory Cell & Molecular Biology.* 59 (2), 141-142. Available from: doi: https://dx.doi.org/10.1165/rcmb.2018-0063ED.

Dewdney, S. B., Rimel, B. J., Thaker, P. H., Thompson, D. M. J., Schmidt, A., Huettner, P., Mutch, D. G., Gao, F. & Goodfellow, P. J. (2011) Aberrant methylation of the X-linked ribosomal S6 kinase RPS6KA6 (RSK4) in endometrial cancers. *Clinical Cancer Research.* 17 (8), 2120-2129. Available from: doi: http://dx.doi.org/10.1158/1078-0432.CCR-10-2668.

Dirat, B., Bochet, L., Dabek, M., Daviaud, D., Dauvillier, S., Majed, B., Wang, Y. Y., Meulle, A., Salles, B., Le Gonidec, S., Garrido, I., Escourrou, G., Valet, P. & Muller, C. (2011) Cancer-associated adipocytes exhibit an activated phenotype and contribute to breast cancer invasion. *Cancer Research.* 71 (7), 2455-2465. Available from: doi: https://dx.doi.org/10.1158/0008-5472.CAN-10-3323.

Doehn, U., Hauge, C., Frank, S. R., Jensen, C. J., Duda, K., Nielsen, J. V., Cohen, M. S., Johansen, J. V., Winther, B. R., Lund, L. R., Winther, O., Taunton, J., Hansen, S. H. & Frodin, M. (2009) RSK is a principal effector of the RAS-ERK pathway for eliciting a coordinate promotile/invasive gene program and phenotype in epithelial cells. *Molecular Cell.* 35 (4), 511-522. Available from: doi: https://dx.doi.org/10.1016/j.molcel.2009.08.002.

Donaldson, J. G. & Jackson, C. L. (2011) ARF family G proteins and their regulators: roles in membrane transport, development and disease. *Nature Reviews Molecular Cell Biology.* 12 (6), 362-375. Available from: doi: https://dx.doi.org/10.1038/nrm3117.

Dongre, A. & Weinberg, R. A. (2019) New insights into the mechanisms of epithelial-mesenchymal transition and implications for cancer. *Nature Reviews Molecular Cell Biology.* 20 (2), 69-84. Available from: doi: https://dx.doi.org/10.1038/s41580-018-0080-4.

Douglas, P., Ye, R., Trinkle-Mulcahy, L., Neal, J. A., De Wever, V., Morrice, N. A., Meek, K. & Lees-Miller, S. P. (2014) Polo-like kinase 1 (PLK1) and protein phosphatase 6 (PP6) regulate DNA-dependent protein kinase catalytic subunit (DNA-PKcs) phosphorylation in mitosis. *Bioscience Reports.* 34 (3), Available from: doi: https://dx.doi.org/10.1042/BSR20140051.

Douville, E. & Downward, J. (1997) EGF induced SOS phosphorylation in PC12 cells involves P90 RSK-2. *Oncogene.* 15 (4), 373-383. Available from: doi: https://dx.doi.org/10.1038/sj.onc.1201214.

Downward, J. (2003) Targeting RAS signalling pathways in cancer therapy. *Nature Reviews.Cancer.* 3 (1), 11-22. Available from: doi: https://dx.doi.org/10.1038/nrc969.

Dufresne, S. D., Bjorbaek, C., El-Haschimi, K., Zhao, Y., Aschenbach, W. G., Moller, D. E. & Goodyear, L. J. (2001) Altered extracellular signal-regulated kinase signaling and glycogen metabolism in skeletal muscle from p90 ribosomal S6 kinase 2 knockout mice. *Molecular & Cellular Biology.* 21 (1), 81-87. Available from: doi: https://dx.doi.org/10.1128/MCB.21.1.81-87.2001.

Dummler, B. A., Hauge, C., Silber, J., Yntema, H. G., Kruse, L. S., Kofoed, B., Hemmings, B. A., Alessi, D. R. & Frodin, M. (2005) Functional characterization of human RSK4, a new 90-kDa ribosomal S6 kinase, reveals constitutive activation in most cell types. *Journal of Biological Chemistry.* 280 (14), 13304-13314. Available from: doi: http://dx.doi.org/10.1074/jbc.M408194200.

Dumont, C., Corsoni-Tadrzak, A., Ruf, S., de Boer, J., Williams, A., Turner, M., Kioussis, D. & Tybulewicz, V. L. J. (2009) Rac GTPases play critical roles in early T-cell development. *Blood.* 113 (17), 3990-3998. Available from: doi: https://dx.doi.org/10.1182/blood-2008-09-181180.

DuPage, M., Dooley, A. L. & Jacks, T. (2009) Conditional mouse lung cancer models using adenoviral or lentiviral delivery of Cre recombinase. *Nature Protocols.* 4 (7), 1064-1072. Available from: doi: https://dx.doi.org/10.1038/nprot.2009.95.

Ebisuya, M., Kondoh, K. & Nishida, E. (2005) The duration, magnitude and compartmentalization of ERK MAP kinase activity: mechanisms for providing signaling specificity. *Journal of Cell Science.* 118 (Pt 14), 2997-3002. Available from: doi: http://dx.doi.org/10.1242/jcs.02505.

el-Deiry, W. S., Kern, S. E., Pietenpol, J. A., Kinzler, K. W. & Vogelstein, B. (1992) Definition of a consensus binding site for p53. *Nature Genetics.* 1 (1), 45-49. Available from: doi: https://dx.doi.org/10.1038/ng0492-45.

Engelman, J. A., Zejnullahu, K., Mitsudomi, T., Song, Y., Hyland, C., Park, J. O., Lindeman, N., Gale, C., Zhao, X., Christensen, J., Kosaka, T., Holmes, A. J., Rogers, A. M., Cappuzzo, F., Mok, T., Lee, C., Johnson, B. E., Cantley, L. C. & Janne, P. A. (2007) MET amplification leads to gefitinib resistance in lung cancer by activating ERBB3 signaling. *Science.* 316 (5827), 1039-1043. Available from: doi: https://dx.doi.org/10.1126/science.1141478.

Erdjument-Bromage, H., Huang, F. & Neubert, T. A. (2018) Sample Preparation for Relative Quantitation of Proteins Using Tandem Mass Tags (TMT) and Mass Spectrometry (MS). *Methods in Molecular Biology.* 1741 135-149. Available from: doi: https://dx.doi.org/10.1007/978-1-4939-7659-1_11.

Erikson, E. & Maller, J. L. (1985) A protein kinase from Xenopus eggs specific for ribosomal protein S6. *Proceedings of the National Academy of Sciences of the United States of America.* 82 (3), 742-746. Available from: doi: http://dx.doi.org/10.1073/pnas.82.3.742.

Etienne-Manneville, S. & Hall, A. (2002) Rho GTPases in cell biology. *Nature.* 420 (6916), 629-635. Available from: doi: https://dx.doi.org/10.1038/nature01148.

Fan, L., Li, P., Yin, Z., Fu, G., Liao, D. J., Liu, Y., Zhu, J., Zhang, Y., Wang, L., Yan, Q., Guo, Y., Shao, C., Huang, G. & Wang, Z. (2013) Ribosomal s6 protein kinase 4: a prognostic factor for renal cell carcinoma. *British Journal of Cancer.* 109 (5), 1137-1146. Available from: doi: http://dx.doi.org/10.1038/bjc.2013.463.

Fan, L., Wang, H., Xia, X., Rao, Y., Ma, X., Ma, D., Wu, P. & Chen, G. (2012) Loss of E-cadherin promotes prostate cancer metastasis via upregulation of metastasis-associated gene 1 expression. *Oncology Letters.* 4 (6), 1225-1233. Available from: doi: https://dx.doi.org/10.3892/ol.2012.934.

Fasano, M., Della Corte, C. M., Papaccio, F., Ciardiello, F. & Morgillo, F. (2015) Pulmonary Large-Cell Neuroendocrine Carcinoma: From Epidemiology to Therapy. *Journal of Thoracic Oncology: Official Publication of the International Association for the Study of Lung Cancer.* 10 (8), 1133-1141. Available from: doi: https://dx.doi.org/10.1097/JTO.0000000000000589.

Felsher, D. W. & Bishop, J. M. (1999) Reversible tumorigenesis by MYC in hematopoietic lineages. *Molecular Cell.* 4 (2), 199-207. Available from: doi: https://dx.doi.org/10.1016/S1097-2765(00)80367-6.

Felsher, D. W. (2010) MYC Inactivation Elicits Oncogene Addiction through Both Tumor Cell-Intrinsic and Host-Dependent Mechanisms. *Genes & Cancer.* 1 (6), 597-604. Available from: doi: https://dx.doi.org/10.1177/1947601910377798.

Fischer, K. R., Durrans, A., Lee, S., Sheng, J., Li, F., Wong, S. T. C., Choi, H., El Rayes, T., Ryu, S., Troeger, J., Schwabe, R. F., Vahdat, L. T., Altorki, N. K., Mittal, V. & Gao, D. (2015) Epithelial-to-mesenchymal transition is not required for lung metastasis but contributes to chemoresistance. *Nature.* 527 (7579), 472-476. Available from: doi: https://dx.doi.org/10.1038/nature15748.

Fischer, M. (2017) Census and evaluation of p53 target genes. *Oncogene.* 36 (28), 3943-3956. Available from: doi: https://dx.doi.org/10.1038/onc.2016.502.

Flaherty, K. T., Infante, J. R., Daud, A., Gonzalez, R., Kefford, R. F., Sosman, J., Hamid, O., Schuchter, L., Cebon, J., Ibrahim, N., Kudchadkar, R., Burris, H. A. 3., Falchook, G., Algazi, A., Lewis, K., Long, G. V., Puzanov, I., Lebowitz, P., Singh, A., Little, S., Sun, P., Allred, A., Ouellet, D., Kim, K. B., Patel, K. & Weber, J. (2012) Combined BRAF and MEK inhibition in melanoma with BRAF V600 mutations. *New England Journal of Medicine.* 367 (18), 1694-1703. Available from: doi: https://dx.doi.org/10.1056/NEJMoa1210093.

Forslund, A., Zeng, Z., Qin, L., Rosenberg, S., Ndubuisi, M., Pincas, H., Gerald, W., Notterman, D. A., Barany, F. & Paty, P. B. (2008) MDM2 gene amplification is correlated to tumor progression but not to the presence of SNP309 or TP53 mutational status in primary colorectal cancers. *Molecular Cancer Research: MCR.* 6 (2), 205-211. Available from: doi: https://dx.doi.org/10.1158/1541-7786.MCR-07-0239.

Franklin, M. C., Carey, K. D., Vajdos, F. F., Leahy, D. J., de Vos, A. M. & Sliwkowski, M. X. (2004) Insights into ErbB signaling from the structure of the ErbB2-pertuzumab complex. *Cancer Cell.* 5 (4), 317-328. Available from: doi: https://dx.doi.org/10.1016/S1535-6108(04)00083-2.

Friedl, P., Borgmann, S. & Brocker, E. B. (2001) Amoeboid leukocyte crawling through extracellular matrix: lessons from the Dictyostelium paradigm of cell movement. *Journal of Leukocyte Biology.* 70 (4), 491-509. Available from: doi: https://www.ncbi.nlm.nih.gov/pubmed/11590185.

Friedl, P., Locker, J., Sahai, E. & Segall, J. E. (2012) Classifying collective cancer cell invasion. *Nature Cell Biology.* 14 (8), 777-783. Available from: doi: https://dx.doi.org/10.1038/ncb2548.

Friedl, P. & Wolf, K. (2003) Tumour-cell invasion and migration: diversity and escape mechanisms. *Nature Reviews.Cancer.* 3 (5), 362-374. Available from: doi: https://dx.doi.org/10.1038/nrc1075.

Frietsch, J. J., Grunewald, T. G. P., Jasper, S., Kammerer, U., Herterich, S., Kapp, M., Honig, A. & Butt, E. (2010) Nuclear localisation of LASP-1 correlates with poor long-term survival in female breast cancer. *British Journal of Cancer.* 102 (11), 1645-1653. Available from: doi: https://dx.doi.org/10.1038/sj.bjc.6605685.

Fruman, D. A., Chiu, H., Hopkins, B. D., Bagrodia, S., Cantley, L. C. & Abraham, R. T. (2017) The PI3K Pathway in Human Disease. *Cell.* 170 (4), 605-635. Available from: doi: https://dx.doi.org/10.1016/j.cell.2017.07.029.

Fujita, N., Sato, S. & Tsuruo, T. (2003) Phosphorylation of p27Kip1 at threonine 198 by p90 ribosomal protein S6 kinases promotes its binding to 14-3-3 and cytoplasmic localization. *Journal of Biological Chemistry.* 278 (49), 49254-49260. Available from: doi: https://dx.doi.org/10.1074/jbc.M306614200.

Fulda, S. & Vucic, D. (2012) Targeting IAP proteins for therapeutic intervention in cancer. *Nature Reviews.Drug Discovery.* 11 (2), 109-124. Available from: doi: https://dx.doi.org/10.1038/nrd3627.

Gaggioli, C., Hooper, S., Hidalgo-Carcedo, C., Grosse, R., Marshall, J. F., Harrington, K. & Sahai, E. (2007) Fibroblast-led collective invasion of carcinoma cells with differing roles for RhoGTPases in leading and following cells. *Nature Cell Biology.* 9 (12), 1392-1400. Available from: doi: https://dx.doi.org/10.1038/ncb1658.

Galluzzi, L., Vitale, I., Aaronson, S. A., Abrams, J. M., Adam, D., Agostinis, P., Alnemri, E. S., Altucci, L., Amelio, I., Andrews, D. W., Annicchiarico-Petruzzelli, M., Antonov, A. V., Arama, E., Baehrecke, E. H., Barlev, N. A., Bazan, N. G., Bernassola, F., Bertrand, M. J. M., Bianchi, K., Blagosklonny, M. V., Blomgren, K., Borner, C., Boya, P., Brenner, C., Campanella, M., Candi, E., Carmona-Gutierrez, D., Cecconi, F., Chan, F. K., Chandel, N. S., Cheng, E. H., Chipuk, J. E., Cidlowski, J. A., Ciechanover, A., Cohen, G. M., Conrad, M., Cubillos-Ruiz, J. R., Czabotar, P. E., D'Angiolella, V., Dawson, T. M., Dawson, V. L., De Laurenzi, V., De Maria, R., Debatin, K., DeBerardinis, R. J., Deshmukh, M., Di Daniele, N., Di Virgilio, F., Dixit, V. M., Dixon, S. J., Duckett, C. S., Dynlacht, B. D., El-Deiry, W. S., Elrod, J. W., Fimia, G. M., Fulda, S., Garcia-Saez, A. J., Garg, A. D., Garrido, C., Gavathiotis, E., Golstein, P., Gottlieb, E., Green, D. R., Greene, L. A., Gronemeyer, H., Gross, A., Hajnoczky, G., Hardwick, J. M., Harris, I. S., Hengartner, M. O., Hetz, C., Ichijo, H., Jaattela, M., Joseph, B., Jost, P. J., Juin, P. P., Kaiser, W. J., Karin, M., Kaufmann, T., Kepp, O., Kimchi, A., Kitsis, R. N., Klionsky, D. J., Knight, R. A., Kumar, S., Lee, S. W., Lemasters, J. J., Levine, B., Linkermann, A., Lipton, S. A., Lockshin, R. A., Lopez-Otin, C., Lowe, S. W., Luedde, T., Lugli, E., MacFarlane, M., Madeo, F., Malewicz, M., Malorni, W., Manic, G., Marine, J., Martin, S. J., Martinou, J., Medema, J. P., Mehlen, P., Meier, P., Melino, S., Miao, E. A., Molkentin, J. D., Moll, U. M., Munoz-Pinedo, C., Nagata, S., Nunez, G., Oberst, A., Oren, M., Overholtzer, M., Pagano, M., Panaretakis, T., Pasparakis, M., Penninger, J. M., Pereira, D. M., Pervaiz, S., Peter, M. E., Piacentini, M., Pinton, P., Prehn, J. H. M., Puthalakath, H., Rabinovich, G. A., Rehm, M., Rizzuto, R., Rodrigues, C. M. P., Rubinsztein, D. C., Rudel, T., Ryan, K. M., Sayan, E., Scorrano, L., Shao, F., Shi, Y., Silke, J., Simon, H., Sistigu, A., Stockwell, B. R., Strasser, A., Szabadkai, G., Tait, S. W. G., Tang, D., Tavernarakis, N., Thorburn, A., Tsujimoto, Y., Turk, B., Vanden Berghe, T., Vandenabeele, P., Vander Heiden, M. G., Villunger, A., Virgin, H. W., Vousden, K. H., Vucic, D., Wagner, E. F., Walczak, H., Wallach, D., Wang, Y., Wells, J. A., Wood, W., Yuan, J., Zakeri, Z., Zhivotovsky, B., Zitvogel, L., Melino, G. & Kroemer, G.

(2018) Molecular mechanisms of cell death: recommendations of the Nomenclature Committee on Cell Death 2018. *Cell Death & Differentiation.* 25 (3), 486-541. Available from: doi: https://dx.doi.org/10.1038/s41418-017-0012-4.

Geuens, T., Bouhy, D. & Timmerman, V. (2016) The hnRNP family: insights into their role in health and disease. *Human Genetics.* 135 (8), 851-867. Available from: doi: https://dx.doi.org/10.1007/s00439-016-1683-5.

Gomez, N. & Cohen, P. (1991) Dissection of the protein kinase cascade by which nerve growth factor activates MAP kinases. *Nature.* 353 (6340), 170-173. Available from: doi: https://dx.doi.org/10.1038/353170a0.

Gong, Q., Liu, C., Wang, C., Zhuang, L., Zhang, L. & Wang, X. (2018) Effect of silencing TEM8 gene on proliferation, apoptosis, migration and invasion of XWLC-05 lung cancer cells. *Molecular Medicine Reports.* 17 (1), 911-917. Available from: doi: https://dx.doi.org/10.3892/mmr.2017.7959.

Goody, R. S., Frech, M. & Wittinghofer, A. (1991) Affinity of guanine nucleotide binding proteins for their ligands: facts and artefacts. *Trends in Biochemical Sciences.* 16 (9), 327-328. Available from: doi: https://www.ncbi.nlm.nih.gov/pubmed/1949151.

Gootz, T. D., Zaniewski, R., Haskell, S., Schmieder, B., Tankovic, J., Girard, D., Courvalin, P. & Polzer, R. J. (1996) Activity of the new fluoroquinolone trovafloxacin (CP-99,219) against DNA gyrase and topoisomerase IV mutants of Streptococcus pneumoniae selected in vitro. *Antimicrobial Agents & Chemotherapy.* 40 (12), 2691-2697. Available from: doi: https://dx.doi.org/10.1128/AAC.40.12.2691.

Gressner, A. M. & Wool, I. G. (1974) The phosphorylation of liver ribosomal proteins in vivo. Evidence that only a single small subunit protein (S6) is phosphorylated. *Journal of Biological Chemistry.* 249 (21), 6917-6925. Available from: doi: http://www.jbc.org/content/249/21/6917.long.

Grunewald, T. G. P., Kammerer, U., Kapp, M., Eck, M., Dietl, J., Butt, E. & Honig, A. (2007) Nuclear localization and cytosolic overexpression of LASP-1 correlates with tumor size and nodal-positivity of human breast carcinoma. *BMC Cancer.* 7 198. Available from: doi: https://dx.doi.org/10.1186/1471-2407-7-198.

Guazzi, S., Price, M., De Felice, M., Damante, G., Mattei, M. G. & Di Lauro, R. (1990) Thyroid nuclear factor 1 (TTF-1) contains a homeodomain and displays a novel DNA binding specificity. *EMBO Journal.* 9 (11), 3631-3639. Available from: doi: https://www.ncbi.nlm.nih.gov/pubmed/1976511.

Guo, W., Keckesova, Z., Donaher, J. L., Shibue, T., Tischler, V., Reinhardt, F., Itzkovitz, S., Noske, A., Zurrer-Hardi, U., Bell, G., Tam, W. L., Mani, S. A., van Oudenaarden, A. & Weinberg, R. A. (2012) Slug and Sox9 cooperatively determine the mammary stem cell state. *Cell.* 148 (5), 1015-1028. Available from: doi: https://dx.doi.org/10.1016/j.cell.2012.02.008.

Gutkind, J. S. (1998) The pathways connecting G protein-coupled receptors to the nucleus through divergent mitogen-activated protein kinase cascades. *Journal of Biological Chemistry.* 273 (4), 1839-1842. Available from: doi: http://dx.doi.org/10.1074/jbc.273.4.1839.

Gyrd-Hansen, M. & Meier, P. (2010) IAPs: from caspase inhibitors to modulators of NF-kappaB, inflammation and cancer. *Nature Reviews.Cancer.* 10 (8), 561-574. Available from: doi: https://dx.doi.org/10.1038/nrc2889.

Hafner, A., Bulyk, M. L., Jambhekar, A. & Lahav, G. (2019) The multiple mechanisms that regulate p53 activity and cell fate. *Nature Reviews Molecular Cell Biology.* 20 (4), 199-210. Available from: doi: https://dx.doi.org/10.1038/s41580-019-0110-x.

Haigis, K. M. (2017) KRAS Alleles: The Devil Is in the Detail. *Trends in Cancer.* 3 (10), 686-697. Available from: doi: https://dx.doi.org/10.1016/j.trecan.2017.08.006.

Hammerman, P. S., Sos, M. L., Ramos, A. H., Xu, C., Dutt, A., Zhou, W., Brace, L. E., Woods, B. A., Lin, W., Zhang, J., Deng, X., Lim, S. M., Heynck, S., Peifer, M., Simard, J. R., Lawrence, M. S., Onofrio, R. C., Salvesen, H. B., Seidel, D., Zander, T., Heuckmann, J. M., Soltermann, A., Moch, H., Koker, M., Leenders, F., Gabler, F., Querings, S., Ansen, S., Brambilla, E., Brambilla, C., Lorimier, P., Brustugun, O. T., Helland, A., Petersen, I., Clement, J. H., Groen, H., Timens, W., Sietsma, H., Stoelben, E., Wolf, J., Beer, D. G., Tsao, M. S., Hanna, M., Hatton, C., Eck, M. J., Janne, P. A., Johnson, B. E., Winckler, W., Greulich, H., Bass, A. J., Cho, J., Rauh, D., Gray, N. S., Wong, K., Haura, E. B., Thomas, R. K. & Meyerson, M. (2011) Mutations in the DDR2 kinase gene identify a novel therapeutic target in squamous cell lung cancer. *Cancer Discovery.* 1 (1), 78-89. Available from: doi: https://dx.doi.org/10.1158/2159-8274.CD-11-0005.

Hanahan, D. & Weinberg, R. A. (2011) Hallmarks of cancer: the next generation. *Cell.* 144 (5), 646-674. Available from: doi: http://dx.doi.org/10.1016/j.cell.2011.02.013.

Hancock, J. F., Cadwallader, K. & Marshall, C. J. (1991) Methylation and proteolysis are essential for efficient membrane binding of prenylated p21K-ras(B). *EMBO Journal.* 10 (3), 641-646. Available from: doi: https://www.ncbi.nlm.nih.gov/pmc/articles/PMC452695/.

Hancock, J. F. (2003) Ras proteins: different signals from different locations. *Nature Reviews Molecular Cell Biology.* 4 (5), 373-384. Available from: doi: https://dx.doi.org/10.1038/nrm1105.

Harding, J. & Burtness, B. (2005) Cetuximab: an epidermal growth factor receptor chemeric human-murine monoclonal antibody. *Drugs of Today.* 41 (2), 107-127. Available from: doi: https://www.ncbi.nlm.nih.gov/pubmed/15821783.

Hartsock, A. & Nelson, W. J. (2008) Adherens and tight junctions: structure, function and connections to the actin cytoskeleton. *Biochimica Et Biophysica Acta.* 1778 (3), 660-669. Available from: doi: https://dx.doi.org/10.1016/j.bbamem.2007.07.012.

Herberger, B., Puhalla, H., Lehnert, M., Wrba, F., Novak, S., Brandstetter, A., Gruenberger, B., Gruenberger, T., Pirker, R. & Filipits, M. (2007) Activated mammalian target of rapamycin is an adverse prognostic factor in patients with biliary tract adenocarcinoma. *Clinical Cancer Research.* 13 (16), 4795-4799. Available from: doi: https://dx.doi.org/10.1158/1078-0432.CCR-07-0738.

Hirsch, F. R., Varella-Garcia, M., Bunn, P. A. J., Di Maria, M. V., Veve, R., Bremmes, R. M., Baron, A. E., Zeng, C. & Franklin, W. A. (2003) Epidermal growth factor receptor in non-small-cell lung carcinomas: correlation between gene copy number and protein expression and impact on prognosis. *Journal of Clinical Oncology.* 21 (20), 3798-3807. Available from: doi: http://dx.doi.org/10.1200/JCO.2003.11.069.

Holohan, C., Van Schaeybroeck, S., Longley, D. B. & Johnston, P. G. (2013) Cancer drug resistance: an evolving paradigm. *Nature Reviews.Cancer.* 13 (10), 714-726. Available from: doi: https://dx.doi.org/10.1038/nrc3599.

Hoshino, R., Chatani, Y., Yamori, T., Tsuruo, T., Oka, H., Yoshida, O., Shimada, Y., Ari-i, S., Wada, H., Fujimoto, J. & Kohno, M. (1999) Constitutive activation of the 41-/43-kDa mitogen-activated protein kinase signaling pathway in human tumors. *Oncogene.* 18 (3), 813-822. Available from: doi: http://dx.doi.org/10.1038/sj.onc.1202367.

Hotchkiss, K. A., Basile, C. M., Spring, S. C., Bonuccelli, G., Lisanti, M. P. & Terman, B. I. (2005) TEM8 expression stimulates endothelial cell adhesion and migration by regulating cell-matrix interactions on collagen. *Experimental Cell Research.* 305 (1), 133-144. Available from: doi: https://dx.doi.org/10.1016/j.yexcr.2004.12.025.

Houles, T. & Roux, P. P. (2018) Defining the role of the RSK isoforms in cancer. *Seminars in Cancer Biology.* 48 53-61. Available from: doi: https://dx.doi.org/10.1016/j.semcancer.2017.04.016.

Huang, H. k., Joazeiro, C. A., Bonfoco, E., Kamada, S., Leverson, J. D. & Hunter, T. (2000) The inhibitor of apoptosis, cIAP2, functions as a ubiquitin-protein ligase and promotes in vitro monoubiquitination of caspases 3 and 7. *Journal of Biological Chemistry.* 275 (35), 26661-26664. Available from: doi: https://dx.doi.org/10.1074/jbc.C000199200.

Huang, R. Y., Guilford, P. & Thiery, J. P. (2012) Early events in cell adhesion and polarity during epithelial-mesenchymal transition. *Journal of Cell Science.* 125 (Pt 19), 4417-4422. Available from: doi: https://dx.doi.org/10.1242/jcs.099697.

Huang, S., Armstrong, E. A., Benavente, S., Chinnaiyan, P. & Harari, P. M. (2004) Dual-agent molecular targeting of the epidermal growth factor receptor (EGFR): combining anti-EGFR antibody with tyrosine kinase inhibitor. *Cancer Research.* 64 (15), 5355-5362. Available from: doi: http://dx.doi.org/10.1158/0008-5472.CAN-04-0562.

Hunter, J. C., Manandhar, A., Carrasco, M. A., Gurbani, D., Gondi, S. & Westover, K. D. (2015) Biochemical and Structural Analysis of Common Cancer-Associated KRAS Mutations. *Molecular Cancer Research: MCR.* 13 (9), 1325-1335. Available from: doi: https://dx.doi.org/10.1158/1541-7786.MCR-15-0203.

Imai, K. & Takaoka, A. (2006) Comparing antibody and small-molecule therapies for cancer. *Nature Reviews.Cancer.* 6 (9), 714-727. Available from: doi: https://dx.doi.org/10.1038/nrc1913.

Jackman, D. M., Yeap, B. Y., Sequist, L. V., Lindeman, N., Holmes, A. J., Joshi, V. A., Bell, D. W., Huberman, M. S., Halmos, B., Rabin, M. S., Haber, D. A., Lynch, T. J., Meyerson, M., Johnson, B. E. & Janne, P. A. (2006) Exon 19 deletion mutations of epidermal growth factor receptor are associated with prolonged survival in non-small cell lung cancer patients treated with gefitinib or erlotinib. *Clinical Cancer Research.* 12 (13), 3908-3914. Available from: doi: http://dx.doi.org/10.1158/1078-0432.CCR-06-0462.

Jackson, A. L. & Linsley, P. S. (2010) Recognizing and avoiding siRNA off-target effects for target identification and therapeutic application. *Nature Reviews.Drug Discovery.* 9 (1), 57-67. Available from: doi: https://dx.doi.org/10.1038/nrd3010.

Jackson, E. L., Willis, N., Mercer, K., Bronson, R. T., Crowley, D., Montoya, R., Jacks, T. & Tuveson, D. A. (2001) Analysis of lung tumor initiation and progression using conditional expression of oncogenic K-ras. *Genes & Development.* 15 (24), 3243-3248. Available from: doi: http://dx.doi.org/10.1101/gad.943001.

Jackson, E. L., Olive, K. P., Tuveson, D. A., Bronson, R., Crowley, D., Brown, M. & Jacks, T. (2005) The differential effects of mutant p53 alleles on advanced murine lung cancer. *Cancer Research.* 65 (22), 10280-10288. Available from: doi: https://dx.doi.org/10.1158/0008-5472.CAN-05-2193.

Jackson, S. P. & Bartek, J. (2009) The DNA-damage response in human biology and disease. *Nature.* 461 (7267), 1071-1078. Available from: doi: https://dx.doi.org/10.1038/nature08467.

Jamal-Hanjani, M., Wilson, G. A., McGranahan, N., Birkbak, N. J., Watkins, T. B. K., Veeriah, S., Shafi, S., Johnson, D. H., Mitter, R., Rosenthal, R., Salm, M., Horswell, S., Escudero, M., Matthews, N., Rowan, A., Chambers, T., Moore, D. A., Turajlic, S., Xu, H., Lee, S., Forster, M. D., Ahmad, T., Hiley, C. T., Abbosh, C., Falzon, M., Borg, E., Marafioti, T., Lawrence, D., Hayward, M., Kolvekar, S., Panagiotopoulos, N., Janes, S. M., Thakrar, R., Ahmed, A., Blackhall, F., Summers, Y., Shah, R., Joseph, L., Quinn, A. M., Crosbie, P. A., Naidu, B., Middleton, G., Langman, G., Trotter, S., Nicolson, M., Remmen, H., Kerr, K., Chetty, M., Gomersall, L., Fennell, D. A., Nakas, A., Rathinam, S., Anand, G., Khan, S., Russell, P., Ezhil, V., Ismail, B., Irvin-Sellers, M., Prakash, V., Lester, J. F., Kornaszewska, M., Attanoos, R., Adams, H., Davies, H., Dentro, S., Taniere, P., O'Sullivan, B., Lowe, H. L., Hartley, J. A., Iles, N., Bell, H., Ngai, Y., Shaw, J. A., Herrero, J., Szallasi, Z., Schwarz, R. F., Stewart, A., Quezada, S. A., Le Quesne, J., Van Loo, P., Dive, C., Hackshaw, A., Swanton, C. & TRACERx Consortium. (2017) Tracking the Evolution of Non-Small-Cell Lung Cancer. *New England Journal of Medicine.* 376 (22), 2109-2121. Available from: doi: https://dx.doi.org/10.1056/NEJMoa1616288.

Jang, S. & Atkins, M. B. (2013) Which drug, and when, for patients with BRAF-mutant melanoma? *Lancet Oncology.* 14 (2), e60-9. Available from: doi: https://dx.doi.org/10.1016/S1470-2045(12)70539-9.

Janne, P. A., Yang, J. C., Kim, D., Planchard, D., Ohe, Y., Ramalingam, S. S., Ahn, M., Kim, S., Su, W., Horn, L., Haggstrom, D., Felip, E., Kim, J., Frewer, P., Cantarini, M., Brown, K. H., Dickinson, P. A., Ghiorghiu, S. & Ranson, M. (2015) AZD9291 in EGFR inhibitor-resistant non-small-cell lung cancer. *New England Journal of Medicine.* 372 (18), 1689-1699. Available from: doi: https://dx.doi.org/10.1056/NEJMoa1411817.

Jemal, A., Miller, K. D., Ma, J., Siegel, R. L., Fedewa, S. A., Islami, F., Devesa, S. S. & Thun, M. J. (2018) Higher Lung Cancer Incidence in Young Women Than Young Men in the United States. *New England Journal of Medicine.* 378 (21), 1999-2009. Available from: doi: https://dx.doi.org/10.1056/NEJMoa1715907.

Jha, S., Morris, E. J., Hruza, A., Mansueto, M. S., Schroeder, G. K., Arbanas, J., McMasters, D., Restaino, C. R., Dayananth, P., Black, S., Elsen, N. L., Mannarino, A., Cooper, A., Fawell, S., Zawel, L., Jayaraman, L. & Samatar, A. A. (2016) Dissecting Therapeutic Resistance to ERK Inhibition. *Molecular Cancer Therapeutics.* 15 (4), 548-559. Available from: doi: https://dx.doi.org/10.1158/1535-7163.MCT-15-0172.

Jiang, Y., Ye, X., Ji, Y., Zhou, X., Yang, H., Wei, W. & Li, Q. (2017) Aberrant expression of RSK4 in breast cancer and its role in the regulation of tumorigenicity. *International Journal of Molecular Medicine.* 40 (3), 883-890. Available from: doi: https://dx.doi.org/10.3892/ijmm.2017.3069.

Joel, P. B., Smith, J., Sturgill, T. W., Fisher, T. L., Blenis, J. & Lannigan, D. A. (1998) pp90rsk1 regulates estrogen receptor-mediated transcription through phosphorylation of Ser-167. *Molecular & Cellular Biology.* 18 (4), 1978-1984. Available from: doi: https://dx.doi.org/10.1128/MCB.18.4.1978.

Johnson, L., Greenbaum, D., Cichowski, K., Mercer, K., Murphy, E., Schmitt, E., Bronson, R. T., Umanoff, H., Edelmann, W., Kucherlapati, R. & Jacks, T. (1997) K-ras is an essential gene in the mouse with partial functional overlap with N-ras. *Genes & Development.* 11 (19), 2468-2481. Available from: doi: https://www.ncbi.nlm.nih.gov/pmc/articles/PMC316567/.

Jolly, M. K., Ware, K. E., Gilja, S., Somarelli, J. A. & Levine, H. (2017) EMT and MET: necessary or permissive for metastasis? *Molecular Oncology.* 11 (7), 755-769. Available from: doi: https://dx.doi.org/10.1002/1878-0261.12083.

Jones, S. W., Erikson, E., Blenis, J., Maller, J. L. & Erikson, R. L. (1988) A Xenopus ribosomal protein S6 kinase has two apparent kinase domains that are each similar to distinct protein kinases. *Proceedings of the National*

Academy of Sciences of the United States of America. 85 (10), 3377-3381. Available from: doi: http://dx.doi.org/10.1073/pnas.85.10.3377.

Kandoth, C., McLellan, M. D., Vandin, F., Ye, K., Niu, B., Lu, C., Xie, M., Zhang, Q., McMichael, J. F., Wyczalkowski, M. A., Leiserson, M. D. M., Miller, C. A., Welch, J. S., Walter, M. J., Wendl, M. C., Ley, T. J., Wilson, R. K., Raphael, B. J. & Ding, L. (2013) Mutational landscape and significance across 12 major cancer types. *Nature.* 502 (7471), 333-339. Available from: doi: https://dx.doi.org/10.1038/nature12634.

Karachaliou, N., Pilotto, S., Lazzari, C., Bria, E., de Marinis, F. & Rosell, R. (2016) Cellular and molecular biology of small cell lung cancer: an overview. *Translational Lung Cancer Research.* 5 (1), 2-15. Available from: doi: https://dx.doi.org/10.3978/j.issn.2218-6751.2016.01.02.

Kastenhuber, E. R. & Lowe, S. W. (2017) Putting p53 in Context. *Cell.* 170 (6), 1062-1078. Available from: doi: https://dx.doi.org/10.1016/j.cell.2017.08.028.

Kavanagh, E., Rodhe, J., Burguillos, M. A., Venero, J. L. & Joseph, B. (2014) Regulation of caspase-3 processing by cIAP2 controls the switch between pro-inflammatory activation and cell death in microglia. *Cell Death & Disease.* 5 e1565. Available from: doi: https://dx.doi.org/10.1038/cddis.2014.514.

Keller, A., Nesvizhskii, A. I., Kolker, E. & Aebersold, R. (2002) Empirical statistical model to estimate the accuracy of peptide identifications made by MS/MS and database search. *Analytical Chemistry.* 74 (20), 5383-5392. Available from: doi: https://dx.doi.org/10.1021/ac025747h.

Kelly, S. E., Bachurski, C. J., Burhans, M. S. & Glasser, S. W. (1996) Transcription of the lung-specific surfactant protein C gene is mediated by thyroid transcription factor 1. *Journal of Biological Chemistry.* 271 (12), 6881-6888. Available from: doi: https://dx.doi.org/10.1074/jbc.271.12.6881.

Khayyata, S., Yun, S., Pasha, T., Jian, B., McGrath, C., Yu, G., Gupta, P. & Baloch, Z. (2009) Value of P63 and CK5/6 in distinguishing squamous cell carcinoma from adenocarcinoma in lung fine-needle aspiration specimens. *Diagnostic Cytopathology.* 37 (3), 178-183. Available from: doi: https://dx.doi.org/10.1002/dc.20975.

Khuder, S. A. (2001) Effect of cigarette smoking on major histological types of lung cancer: a meta-analysis. *Lung Cancer.* 31 (2-3), 139-148. Available from: doi: http://dx.doi.org/10.1016/S0169-5002(00)00181-1.

Kim, C. F. B., Jackson, E. L., Woolfenden, A. E., Lawrence, S., Babar, I., Vogel, S., Crowley, D., Bronson, R. T. & Jacks, T. (2005) Identification of bronchioalveolar stem cells in normal lung and lung cancer. *Cell.* 121 (6), 823-835. Available from: doi: https://dx.doi.org/10.1016/j.cell.2005.03.032.

Kim, J., Yu, L., Chen, W., Xu, Y., Wu, M., Todorova, D., Tang, Q., Feng, B., Jiang, L., He, J., Chen, G., Fu, X. & Xu, Y. (2019) Wild-Type p53 Promotes Cancer Metabolic Switch by Inducing PUMA-Dependent Suppression of Oxidative Phosphorylation. *Cancer Cell.* 35 (2), 191-203.e8. Available from: doi: https://dx.doi.org/10.1016/j.ccell.2018.12.012.

Knott, A. B., Perkins, G., Schwarzenbacher, R. & Bossy-Wetzel, E. (2008) Mitochondrial fragmentation in neurodegeneration. *Nature Reviews Neuroscience.* 9 (7), 505-518. Available from: doi: https://dx.doi.org/10.1038/nrn2417.

Koenig, A., Mueller, C., Hasel, C., Adler, G. & Menke, A. (2006) Collagen type I induces disruption of E-cadherin-mediated cell-cell contacts and promotes proliferation of pancreatic carcinoma cells. *Cancer Research.* 66 (9), 4662-4671. Available from: doi: https://dx.doi.org/10.1158/0008-5472.CAN-05-2804.

Kohn, M., Hameister, H., Vogel, M. & Kehrer-Sawatzki, H. (2003) Expression pattern of the Rsk2, Rsk4 and Pdk1 genes during murine embryogenesis. *Gene Expression Patterns.* 3 (2), 173-177. Available from: doi: http://dx.doi.org/10.1016/S1567-133X(03)00004-8.

Krebs, A. M., Mitschke, J., Lasierra Losada, M., Schmalhofer, O., Boerries, M., Busch, H., Boettcher, M., Mougiakakos, D., Reichardt, W., Bronsert, P., Brunton, V. G., Pilarsky, C., Winkler, T. H., Brabletz, S., Stemmler, M. P. & Brabletz, T. (2017) The EMT-activator Zeb1 is a key factor for cell plasticity and promotes metastasis in pancreatic cancer. *Nature Cell Biology.* 19 (5), 518-529. Available from: doi: https://dx.doi.org/10.1038/ncb3513.

Kreso, A. & Dick, J. E. (2014) Evolution of the cancer stem cell model. *Cell Stem Cell.* 14 (3), 275-291. Available from: doi: https://dx.doi.org/10.1016/j.stem.2014.02.006.

Lambert, A. W., Pattabiraman, D. R. & Weinberg, R. A. (2017) Emerging Biological Principles of Metastasis. *Cell.* 168 (4), 670-691. Available from: doi: https://dx.doi.org/10.1016/j.cell.2016.11.037.

Lamouille, S., Xu, J. & Derynck, R. (2014) Molecular mechanisms of epithelial-mesenchymal transition. *Nature Reviews Molecular Cell Biology.* 15 (3), 178-196. Available from: doi: http://dx.doi.org/10.1038/nrm3758.

Langley, R. R. & Fidler, I. J. (2011) The seed and soil hypothesis revisited--the role of tumor-stroma interactions in metastasis to different organs. *International Journal of Cancer.* 128 (11), 2527-2535. Available from: doi: https://dx.doi.org/10.1002/ijc.26031.

Lara, R., Mauri, F. A., Taylor, H., Derua, R., Shia, A., Gray, C., Nicols, A., Shiner, R. J., Schofield, E., Bates, P. A., Waelkens, E., Dallman, M., Lamb, J., Zicha, D., Downward, J., Seckl, M. J. & Pardo, O. E. (2011) An siRNA screen identifies RSK1 as a key modulator of lung cancer metastasis. *Oncogene.* 30 (32), 3513-3521. Available from: doi: https://dx.doi.org/10.1038/onc.2011.61.

Lara, R., Seckl, M. J. & Pardo, O. E. (2013) The p90 RSK family members: common functions and isoform specificity. *Cancer Research.* 73 (17), 5301-5308. Available from: doi: http://dx.doi.org/10.1158/0008-5472.CAN-12-4448.

Lee, C. K., Wu, Y., Ding, P. N., Lord, S. J., Inoue, A., Zhou, C., Mitsudomi, T., Rosell, R., Pavlakis, N., Links, M., Gebski, V., Gralla, R. J. & Yang, J. C. (2015) Impact of Specific Epidermal Growth Factor Receptor (EGFR) Mutations and Clinical Characteristics on Outcomes After Treatment With EGFR Tyrosine Kinase Inhibitors Versus Chemotherapy in EGFR-Mutant Lung Cancer: A Meta-Analysis. *Journal of Clinical Oncology.* 33 (17), 1958-1965. Available from: doi: https://dx.doi.org/10.1200/JCO.2014.58.1736.

Leitinger, B. (2014) Discoidin domain receptor functions in physiological and pathological conditions. *International Review of Cell & Molecular Biology.* 310 39-87. Available from: doi: https://dx.doi.org/10.1016/B978-0-12-800180-6.00002-5.

Lemmon, M. A. & Schlessinger, J. (2010) Cell signaling by receptor tyrosine kinases. *Cell.* 141 (7), 1117-1134. Available from: doi: https://dx.doi.org/10.1016/j.cell.2010.06.011.

Li, H., Zhu, H., Xu, C. J. & Yuan, J. (1998) Cleavage of BID by caspase 8 mediates the mitochondrial damage in the Fas pathway of apoptosis. *Cell.* 94 (4), 491-501. Available from: doi: https://dx.doi.org/10.1016/S0092-8674(00)81590-1.

Li, Q., Gao, H., Yang, H., Wei, W. & Jiang, Y. (2019) Estradiol promotes the progression of ER+ breast cancer through methylation-mediated RSK4 inactivation. *OncoTargets and Therapy.* 12 5907-5916. Available from: doi: https://dx.doi.org/10.2147/OTT.S208988.

Li, Q., Jiang, Y., Wei, W., Ji, Y., Gao, H. & Liu, J. (2014) Frequent epigenetic inactivation of RSK4 by promoter methylation in cancerous and non-cancerous tissues of breast cancer. *Medical Oncology.* 31 (1), 793. Available from: doi: http://dx.doi.org/10.1007/s12032-013-0793-3.

Li, R., Chen, D., Zhou, R., Jia, S., Yang, J., Clegg, J. S. & Yang, W. (2012) Involvement of polo-like kinase 1 (Plk1) in mitotic arrest by inhibition of mitogen-activated protein kinase-extracellular signal-regulated kinase-ribosomal S6 kinase 1 (MEK-ERK-RSK1) cascade. *Journal of Biological Chemistry.* 287 (19), 15923-15934. Available from: doi: https://dx.doi.org/10.1074/jbc.M111.312413.

Li, Y., Dowbenko, D. & Lasky, L. A. (2002) AKT/PKB phosphorylation of p21Cip/WAF1 enhances protein stability of p21Cip/WAF1 and promotes cell survival. *Journal of Biological Chemistry.* 277 (13), 11352-11361. Available from: doi: https://dx.doi.org/10.1074/jbc.M109062200.

Lim, H. C., Xie, L., Zhang, W., Li, R., Chen, Z., Wu, G., Cui, S., Tan, E. K. & Zeng, L. (2013) Ribosomal S6 Kinase 2 (RSK2) maintains genomic stability by activating the Atm/p53-dependent DNA damage pathway. *PLoS ONE [Electronic Resource].* 8 (9), e74334. Available from: doi: https://dx.doi.org/10.1371/journal.pone.0074334.

Lito, P., Rosen, N. & Solit, D. B. (2013) Tumor adaptation and resistance to RAF inhibitors. *Nature Medicine.* 19 (11), 1401-1409. Available from: doi: https://dx.doi.org/10.1038/nm.3392.

Little, A. S., Smith, P. D. & Cook, S. J. (2013) Mechanisms of acquired resistance to ERK1/2 pathway inhibitors. *Oncogene.* 32 (10), 1207-1215. Available from: doi: https://dx.doi.org/10.1038/onc.2012.160.

Liu, J., Yang, H., Chen, Z. & Jiang, Y. (2011) [Abnormal expression of RSK-4 and its clinical significance in breast cancer]. *Chung-Hua Chung Liu Tsa Chih [Chinese Journal of Oncology].* 33 (6), 452-456. Available from: doi: https://www.ncbi.nlm.nih.gov/pubmed/21875487.

Liu, Y., Sun, L., Xiong, Z., Sun, X., Zhang, S., Ma, J. & Han, C. (2017) Meta-analysis of the impact of de novo and acquired EGFR T790M mutations on the prognosis of patients with non-small cell lung cancer receiving EGFR-TKIs. *OncoTargets and Therapy.* 10 2267-2279. Available from: doi: https://dx.doi.org/10.2147/OTT.S133082.

LLeonart, M. E., Vidal, F., Gallardo, D., Diaz-Fuertes, M., Rojo, F., Cuatrecasas, M., Lopez-Vicente, L., Kondoh, H., Blanco, C., Carnero, A. & Ramon y Cajal, S. (2006) New p53 related genes in human tumors: significant downregulation in colon and lung carcinomas. *Oncology Reports.* 16 (3), 603-608. Available from: doi: https://dx.doi.org/10.3892/or.16.3.603.

Lopez-Vicente, L., Armengol, G., Pons, B., Coch, L., Argelaguet, E., Lleonart, M., Hernandez-Losa, J., de Torres, I. & Ramon y Cajal, S. (2009) Regulation of replicative and stress-induced senescence by RSK4, which is down-regulated in human tumors. *Clinical Cancer Research.* 15 (14), 4546-4553. Available from: doi: http://dx.doi.org/10.1158/1078-0432.CCR-08-3159.

Lopez-Vicente, L., Pons, B., Coch, L., Teixido, C., Hernandez-Losa, J., Armengol, G. & Ramon Y Cajal, S. (2011) RSK4 inhibition results in bypass of stress-induced and oncogene-induced senescence. *Carcinogenesis.* 32 (4), 470-476. Available from: doi: http://dx.doi.org/10.1093/carcin/bgr003.

Luzzi, K. J., MacDonald, I. C., Schmidt, E. E., Kerkvliet, N., Morris, V. L., Chambers, A. F. & Groom, A. C. (1998) Multistep nature of metastatic inefficiency: dormancy of solitary cells after successful extravasation and limited survival of early micrometastases. *American Journal of Pathology.* 153 (3), 865-873. Available from: doi: https://dx.doi.org/10.1016/S0002-9440(10)65628-3.

Lynch, T. J., Bell, D. W., Sordella, R., Gurubhagavatula, S., Okimoto, R. A., Brannigan, B. W., Harris, P. L., Haserlat, S. M., Supko, J. G., Haluska, F. G., Louis, D. N., Christiani, D. C., Settleman, J. & Haber, D. A. (2004) Activating mutations in the epidermal growth factor receptor underlying responsiveness of non-small-cell lung cancer to gefitinib. *New England Journal of Medicine.* 350 (21), 2129-2139. Available from: doi: http://dx.doi.org/10.1056/NEJMoa040938.

MacKenzie, S. J., Baillie, G. S., McPhee, I., Bolger, G. B. & Houslay, M. D. (2000) ERK2 mitogen-activated protein kinase binding, phosphorylation, and regulation of the PDE4D cAMP-specific phosphodiesterases. The involvement of COOH-terminal docking sites and NH2-terminal UCR regions. *Journal of Biological Chemistry.* 275 (22), 16609-16617. Available from: doi: https://dx.doi.org/10.1074/jbc.275.22.16609.

Magnuson, B., Ekim, B. & Fingar, D. C. (2012) Regulation and function of ribosomal protein S6 kinase (S6K) within mTOR signalling networks. *Biochemical Journal.* 441 (1), 1-21. Available from: doi: https://dx.doi.org/10.1042/BJ20110892.

Mahmood, M. Q., Ward, C., Muller, H. K., Sohal, S. S. & Walters, E. H. (2017) Epithelial mesenchymal transition (EMT) and non-small cell lung cancer (NSCLC): a mutual association with airway disease. *Medical Oncology.* 34 (3), 45. Available from: doi: https://dx.doi.org/10.1007/s12032-017-0900-y.

Mainardi, S., Mijimolle, N., Francoz, S., Vicente-Duenas, C., Sanchez-Garcia, I. & Barbacid, M. (2014) Identification of cancer initiating cells in K-Ras driven lung adenocarcinoma. *Proceedings of the National Academy of Sciences of the United States of America.* 111 (1), 255-260. Available from: doi: https://dx.doi.org/10.1073/pnas.1320383110.

Malmlof, M., Roudier, E., Hogberg, J. & Stenius, U. (2007) MEK-ERK-mediated phosphorylation of Mdm2 at Ser-166 in hepatocytes. Mdm2 is activated in response to inhibited Akt signaling. *Journal of Biological Chemistry.* 282 (4), 2288-2296. Available from: doi: https://dx.doi.org/10.1074/jbc.M604953200.

Mantovani, A., Allavena, P., Sica, A. & Balkwill, F. (2008) Cancer-related inflammation. *Nature.* 454 (7203), 436-444. Available from: doi: https://dx.doi.org/10.1038/nature07205.

Mao, C., Qiu, L., Liao, R., Du, F., Ding, H., Yang, W., Li, J. & Chen, Q. (2010) KRAS mutations and resistance to EGFR-TKIs treatment in patients with non-small cell lung cancer: a meta-analysis of 22 studies. *Lung Cancer.* 69 (3), 272-278. Available from: doi: https://dx.doi.org/10.1016/j.lungcan.2009.11.020.

Marechal, A. & Zou, L. (2013) DNA damage sensing by the ATM and ATR kinases. *Cold Spring Harbor Perspectives in Biology.* 5 (9), Available from: doi: https://dx.doi.org/10.1101/cshperspect.a012716.

Martincorena, I., Raine, K. M., Gerstung, M., Dawson, K. J., Haase, K., Van Loo, P., Davies, H., Stratton, M. R. & Campbell, P. J. (2018) Universal Patterns of Selection in Cancer and Somatic Tissues. *Cell.* 173 (7), 1823. Available from: doi: https://dx.doi.org/10.1016/j.cell.2018.06.001.

Matsushima-Nishiwaki, R., Takai, S., Adachi, S., Minamitani, C., Yasuda, E., Noda, T., Kato, K., Toyoda, H., Kaneoka, Y., Yamaguchi, A., Kumada, T. & Kozawa, O. (2008) Phosphorylated heat shock protein 27 represses growth of hepatocellular carcinoma via inhibition of extracellular signal-regulated kinase. *Journal of Biological Chemistry.* 283 (27), 18852-18860. Available from: doi: https://dx.doi.org/10.1074/jbc.M801301200.

May, M., Colleaux, L., Murgia, A., Aylsworth, A., Nussbaum, R., Fontes, M. & Schwartz, C. (1995) Molecular analysis of four males with mental retardation and deletions of Xq21 places the putative MR region in Xq21.1 between DXS233 and CHM. *Human Molecular Genetics.* 4 (8), 1465-1466. Available from: doi: http://dx.doi.org/10.1093/hmg/4.8.1465.

Meek, D. W. & Knippschild, U. (2003) Posttranslational modification of MDM2. *Molecular Cancer Research: MCR.* 1 (14), 1017-1026. Available from: doi: https://www.ncbi.nlm.nih.gov/pubmed/14707285.

Mendez, M. G., Kojima, S. & Goldman, R. D. (2010) Vimentin induces changes in cell shape, motility, and adhesion during the epithelial to mesenchymal transition. *FASEB Journal.* 24 (6), 1838-1851. Available from: doi: https://dx.doi.org/10.1096/fj.09-151639.

Mengoli, M. C., Longo, F. R., Fraggetta, F., Cavazza, A., Dubini, A., Ali, G., Guddo, F., Gilioli, E., Bogina, G., Nannini, N., Barbisan, F., De Rosa, N., Falconieri, G., Rossi, G. & Graziano, P. (2018) The 2015 World Health Organization Classification of lung tumors: new entities since the 2004 Classification. *Pathologica.* 110 (1), 39-67. Available from: doi: http://dx.doi.org/10.1097/JTO.0000000000000630.

Meyuhas, O. (2008) Physiological roles of ribosomal protein S6: one of its kind. *International Review of Cell & Molecular Biology.* 268 1-37. Available from: doi: http://dx.doi.org/10.1016/S1937-6448(08)00801-0.

Midha, A., Dearden, S. & McCormack, R. (2015) EGFR mutation incidence in non-small-cell lung cancer of adenocarcinoma histology: a systematic review and global map by ethnicity (mutMapII). *American Journal of Cancer Research.* 5 (9), 2892-2911. Available from: doi: https://www.ncbi.nlm.nih.gov/pmc/articles/PMC4633915/.

Mihlan, S., Reis, C., Thalheimer, P., Herterich, S., Gaetzner, S., Kremerskothen, J., Pavenstadt, H. J., Lewandrowski, U., Sickmann, A. & Butt, E. (2013) Nuclear import of LASP-1 is regulated by phosphorylation and dynamic protein-protein interactions. *Oncogene.* 32 (16), 2107-2113. Available from: doi: https://dx.doi.org/10.1038/onc.2012.216.

Mise, N., Savai, R., Yu, H., Schwarz, J., Kaminski, N. & Eickelberg, O. (2012) Zyxin is a transforming growth factor-beta (TGF-beta)/Smad3 target gene that regulates lung cancer cell motility via integrin alpha5beta1. *Journal of Biological Chemistry.* 287 (37), 31393-31405. Available from: doi: https://dx.doi.org/10.1074/jbc.M112.357624.

Mok, T. S., Wu, Y., Ahn, M., Garassino, M. C., Kim, H. R., Ramalingam, S. S., Shepherd, F. A., He, Y., Akamatsu, H., Theelen, W. S. M. E., Lee, C. K., Sebastian, M., Templeton, A., Mann, H., Marotti, M., Ghiorghiu, S., Papadimitrakopoulou, V. A. & AURA3 Investigators. (2017) Osimertinib or Platinum-Pemetrexed in EGFR T790M-Positive Lung Cancer. *New England Journal of Medicine.* 376 (7), 629-640. Available from: doi: https://dx.doi.org/10.1056/NEJMoa1612674.

Moldvay, J., Jackel, M., Bogos, K., Soltesz, I., Agocs, L., Kovacs, G. & Schaff, Z. (2004) The role of TTF-1 in differentiating primary and metastatic lung adenocarcinomas. *Pathology Oncology Research.* 10 (2), 85-88. Available from: doi: https://www.ncbi.nlm.nih.gov/pubmed/15188024.

Molina, M. A., Codony-Servat, J., Albanell, J., Rojo, F., Arribas, J. & Baselga, J. (2001) Trastuzumab (herceptin), a humanized anti-Her2 receptor monoclonal antibody, inhibits basal and activated Her2 ectodomain cleavage in breast cancer cells. *Cancer Research.* 61 (12), 4744-4749. Available from: doi: https://www.ncbi.nlm.nih.gov/pubmed/11406546.

Moll, U. M. & Petrenko, O. (2003) The MDM2-p53 interaction. *Molecular Cancer Research: MCR.* 1 (14), 1001-1008. Available from: doi: https://mcr.aacrjournals.org/content/1/14/1001.

Mora, A., Komander, D., van Aalten, D. M. F. & Alessi, D. R. (2004) PDK1, the master regulator of AGC kinase signal transduction. *Seminars in Cell & Developmental Biology.* 15 (2), 161-170. Available from: doi: https://dx.doi.org/10.1016/j.semcdb.2003.12.022.

Morrison, S. J. & Weissman, I. L. (1994) The long-term repopulating subset of hematopoietic stem cells is deterministic and isolatable by phenotype. *Immunity.* 1 (8), 661-673. Available from: doi: https://dx.doi.org/10.1016/1074-7613(94)90037-X.

Moumen, A., Masterson, P., O'Connor, M. J. & Jackson, S. P. (2005) hnRNP K: an HDM2 target and transcriptional coactivator of p53 in response to DNA damage. *Cell.* 123 (6), 1065-1078. Available from: doi: https://dx.doi.org/10.1016/j.cell.2005.09.032.

Mukherjee, S. (2010) *The Emperor of All Maladies: A Biography of Cancer.* New York, Scribnerhttps://www.pulitzer.org/winners/siddhartha-mukherjee.

Muller, P. A. J. & Vousden, K. H. (2014) Mutant p53 in cancer: new functions and therapeutic opportunities. *Cancer Cell.* 25 (3), 304-317. Available from: doi: https://dx.doi.org/10.1016/j.ccr.2014.01.021.

Myers, A. P., Corson, L. B., Rossant, J. & Baker, J. C. (2004) Characterization of mouse Rsk4 as an inhibitor of fibroblast growth factor-RAS-extracellular signal-regulated kinase signaling. *Molecular & Cellular Biology.* 24 (10), 4255-4266. Available from: doi: http://dx.doi.org/10.1128/MCB.24.10.4255-4266.2004.

Nadal, E., Chen, G., Prensner, J. R., Shiratsuchi, H., Sam, C., Zhao, L., Kalemkerian, G. P., Brenner, D., Lin, J., Reddy, R. M., Chang, A. C., Capella, G., Cardenal, F., Beer, D. G. & Ramnath, N. (2014) KRAS-G12C mutation is associated with poor outcome in surgically resected lung adenocarcinoma. *Journal of Thoracic Oncology: Official Publication of the International Association for the Study of Lung Cancer.* 9 (10), 1513-1522. Available from: doi: https://dx.doi.org/10.1097/JTO.0000000000000305.

Nag, S., Qin, J., Srivenugopal, K. S., Wang, M. & Zhang, R. (2013) The MDM2-p53 pathway revisited. *Journal of Biomedical Research.* 27 (4), 254-271. Available from: doi: https://dx.doi.org/10.7555/JBR.27.20130030.

Nagy, A., Lanczky, A., Menyhart, O. & Gyorffy, B. (2018) Author Correction: Validation of miRNA prognostic power in hepatocellular carcinoma using expression data of independent datasets. *Scientific Reports.* 8 (1), 11515. Available from: doi: https://dx.doi.org/10.1038/s41598-018-29514-3.

Neise, D., Sohn, D., Stefanski, A., Goto, H., Inagaki, M., Wesselborg, S., Budach, W., Stuhler, K. & Janicke, R. U. (2013) The p90 ribosomal S6 kinase (RSK) inhibitor BI-D1870 prevents gamma irradiation-induced apoptosis and mediates senescence via RSK- and p53-independent accumulation of p21WAF1/CIP1. *Cell Death & Disease.* 4 e859. Available from: doi: https://dx.doi.org/10.1038/cddis.2013.386.

Nesvizhskii, A. I., Keller, A., Kolker, E. & Aebersold, R. (2003) A statistical model for identifying proteins by tandem mass spectrometry. *Analytical Chemistry.* 75 (17), 4646-4658. Available from: doi: https://dx.doi.org/10.1021/ac0341261.

Niskakoski, A., Kaur, S., Staff, S., Renkonen-Sinisalo, L., Lassus, H., Jarvinen, H. J., Mecklin, J., Butzow, R. & Peltomaki, P. (2014) Epigenetic analysis of sporadic and Lynch-associated ovarian cancers reveals histology-specific patterns of DNA methylation. *Epigenetics: Official Journal of the DNA Methylation Society.* 9 (12), 1577-1587. Available from: doi: http://dx.doi.org/10.4161/15592294.2014.983374.

Noonan, D. M., De Lerma Barbaro, A., Vannini, N., Mortara, L. & Albini, A. (2008) Inflammation, inflammatory cells and angiogenesis: decisions and indecisions. *Cancer & Metastasis Reviews.* 27 (1), 31-40. Available from: doi: https://dx.doi.org/10.1007/s10555-007-9108-5.

Ogawara, Y., Kishishita, S., Obata, T., Isazawa, Y., Suzuki, T., Tanaka, K., Masuyama, N. & Gotoh, Y. (2002) Akt enhances Mdm2-mediated ubiquitination and degradation of p53. *Journal of Biological Chemistry.* 277 (24), 21843-21850. Available from: doi: https://dx.doi.org/10.1074/jbc.M109745200.

Oliner, J. D., Pietenpol, J. A., Thiagalingam, S., Gyuris, J., Kinzler, K. W. & Vogelstein, B. (1993) Oncoprotein MDM2 conceals the activation domain of tumour suppressor p53. *Nature.* 362 (6423), 857-860. Available from: doi: https://dx.doi.org/10.1038/362857a0.

Ono, M. & Kuwano, M. (2006) Molecular mechanisms of epidermal growth factor receptor (EGFR) activation and response to gefitinib and other EGFR-targeting drugs. *Clinical Cancer Research.* 12 (24), 7242-7251. Available from: doi: https://dx.doi.org/10.1158/1078-0432.CCR-06-0646.

Paez, J. G., Janne, P. A., Lee, J. C., Tracy, S., Greulich, H., Gabriel, S., Herman, P., Kaye, F. J., Lindeman, N., Boggon, T. J., Naoki, K., Sasaki, H., Fujii, Y., Eck, M. J., Sellers, W. R., Johnson, B. E. & Meyerson, M. (2004) EGFR mutations in lung cancer: correlation with clinical response to gefitinib therapy. *Science.* 304 (5676), 1497-1500. Available from: doi: https://dx.doi.org/10.1126/science.1099314.

Palmieri, F. (2013) The mitochondrial transporter family SLC25: identification, properties and physiopathology. *Molecular Aspects of Medicine.* 34 (2-3), 465-484. Available from: doi: https://dx.doi.org/10.1016/j.mam.2012.05.005.

Panic, L., Tamarut, S., Sticker-Jantscheff, M., Barkic, M., Solter, D., Uzelac, M., Grabusic, K. & Volarevic, S. (2006) Ribosomal protein S6 gene haploinsufficiency is associated with activation of a p53-dependent checkpoint during gastrulation. *Molecular & Cellular Biology.* 26 (23), 8880-8891. Available from: doi: https://dx.doi.org/10.1128/MCB.00751-06.

Pardo, O. E., Lesay, A., Arcaro, A., Lopes, R., Ng, B. L., Warne, P. H., McNeish, I. A., Tetley, T. D., Lemoine, N. R., Mehmet, H., Seckl, M. J. & Downward, J. (2003) Fibroblast growth factor 2-mediated translational control of IAPs blocks mitochondrial release of Smac/DIABLO and apoptosis in small cell lung cancer cells. *Molecular & Cellular Biology.* 23 (21), 7600-7610. Available from: doi: https://dx.doi.org/10.1128/MCB.23.21.7600-7610.2003.

Parkin, D. M., Bray, F., Ferlay, J. & Pisani, P. (2005) Global cancer statistics, 2002. *CA: A Cancer Journal for Clinicians.* 55 (2), 74-108. Available from: doi: http://dx.doi.org/10.3322/canjclin.55.2.74.

Peinado, H., Olmeda, D. & Cano, A. (2007) Snail, Zeb and bHLH factors in tumour progression: an alliance against the epithelial phenotype? *Nature Reviews.Cancer.* 7 (6), 415-428. Available from: doi: https://dx.doi.org/10.1038/nrc2131.

Perkins, D. N., Pappin, D. J., Creasy, D. M. & Cottrell, J. S. (1999) Probability-based protein identification by searching sequence databases using mass spectrometry data. *Electrophoresis.* 20 (18), 3551-3567. Available from: doi: https://www.ncbi.nlm.nih.gov/pubmed/10612281.

Platanias, L. C. (2005) Mechanisms of type-I- and type-II-interferon-mediated signalling. *Nature Reviews.Immunology.* 5 (5), 375-386. Available from: doi: https://dx.doi.org/10.1038/nri1604.

Poon, I. K. H., Chiu, Y., Armstrong, A. J., Kinchen, J. M., Juncadella, I. J., Bayliss, D. A. & Ravichandran, K. S. (2014) Unexpected link between an antibiotic, pannexin channels and apoptosis. *Nature.* 507 (7492), 329-334. Available from: doi: https://dx.doi.org/10.1038/nature13147.

Pritchard, C. A., Samuels, M. L., Bosch, E. & McMahon, M. (1995) Conditionally oncogenic forms of the A-Raf and B-Raf protein kinases display different biological and biochemical properties in NIH 3T3 cells. *Molecular & Cellular Biology.* 15 (11), 6430-6442. Available from: doi: https://www.ncbi.nlm.nih.gov/pubmed/7565795.

Prochazka, L., Tesarik, R. & Turanek, J. (2014) Regulation of alternative splicing of CD44 in cancer. *Cellular Signalling.* 26 (10), 2234-2239. Available from: doi: https://dx.doi.org/10.1016/j.cellsig.2014.07.011.

Psaila, B. & Lyden, D. (2009) The metastatic niche: adapting the foreign soil. *Nature Reviews.Cancer.* 9 (4), 285-293. Available from: doi: https://dx.doi.org/10.1038/nrc2621.

Public Health England (PHE). (2017) Chapter 2: major causes of death and how they have changed. In: Public Health England (ed.).*Health Profile for England.* , London, PHE. https://www.gov.uk/government/publications/health-profile-for-england/chapter-2-major-causes-of-death-and-how-they-have-changed.

Qian, B., Li, J., Zhang, H., Kitamura, T., Zhang, J., Campion, L. R., Kaiser, E. A., Snyder, L. A. & Pollard, J. W. (2011) CCL2 recruits inflammatory monocytes to facilitate breast-tumour metastasis. *Nature.* 475 (7355), 222-225. Available from: doi: https://dx.doi.org/10.1038/nature10138.

Qian, H., Xu, T., Cai, X., Ji, T. & Guo, H. (2015) Prognostic value of TTF-1 expression in patients with non-small cell lung cancer: A meta-analysis. *Clinica Chimica Acta.* 451 (Pt B), 208-214. Available from: doi: https://dx.doi.org/10.1016/j.cca.2015.01.023.

Ramos, J. W. (2008) The regulation of extracellular signal-regulated kinase (ERK) in mammalian cells. *International Journal of Biochemistry & Cell Biology.* 40 (12), 2707-2719. Available from: doi: https://dx.doi.org/10.1016/j.biocel.2008.04.009.

Ran FA, Hsu PD, Wright J, Agarwala V, Scott DA & Zhang F. (2013) Genome engineering using the CRISPR-Cas9 system. *Nature Protocols.* 8 (11), 2281-2308. Available from: doi: https://dx.doi.org/10.1038/nprot.2013.143.

Rathore, R., McCallum, J. E., Varghese, E., Florea, A. & Busselberg, D. (2017) Overcoming chemotherapy drug resistance by targeting inhibitors of apoptosis proteins (IAPs). *Apoptosis.* 22 (7), 898-919. Available from: doi: https://dx.doi.org/10.1007/s10495-017-1375-1.

Rawlins, E. L., Okubo, T., Xue, Y., Brass, D. M., Auten, R. L., Hasegawa, H., Wang, F. & Hogan, B. L. M. (2009) The role of Scgb1a1+ Clara cells in the long-term maintenance and repair of lung airway, but not alveolar, epithelium. *Cell Stem Cell.* 4 (6), 525-534. Available from: doi: https://dx.doi.org/10.1016/j.stem.2009.04.002.

Ray-Coquard, I., Blay, J., Italiano, A., Le Cesne, A., Penel, N., Zhi, J., Heil, F., Rueger, R., Graves, B., Ding, M., Geho, D., Middleton, S. A., Vassilev, L. T., Nichols, G. L. & Bui, B. N. (2012) Effect of the MDM2 antagonist RG7112 on the P53 pathway in patients with MDM2-amplified, well-differentiated or dedifferentiated liposarcoma: an exploratory proof-of-mechanism study. *Lancet Oncology.* 13 (11), 1133-1140. Available from: doi: https://dx.doi.org/10.1016/S1470-2045(12)70474-6.

Redon, C. E., Nakamura, A. J., Zhang, Y., Ji, J. J., Bonner, W. M., Kinders, R. J., Parchment, R. E., Doroshow, J. H. & Pommier, Y. (2010) Histone gammaH2AX and poly(ADP-ribose) as clinical pharmacodynamic biomarkers. *Clinical Cancer Research.* 16 (18), 4532-4542. Available from: doi: https://dx.doi.org/10.1158/1078-0432.CCR-10-0523.

Rekhtman, N. (2010) Neuroendocrine tumors of the lung: an update. *Archives of Pathology & Laboratory Medicine.* 134 (11), 1628-1638. Available from: doi: https://dx.doi.org/10.1043/2009-0583-RAR.1.

Richards, S. A., Dreisbach, V. C., Murphy, L. O. & Blenis, J. (2001) Characterization of regulatory events associated with membrane targeting of p90 ribosomal S6 kinase 1. *Molecular & Cellular Biology.* 21 (21), 7470-7480. Available from: doi: http://dx.doi.org/10.1128/MCB.21.21.7470-7480.2001.

Ridley, A. J. (2011) Life at the leading edge. *Cell.* 145 (7), 1012-1022. Available from: doi: https://dx.doi.org/10.1016/j.cell.2011.06.010.

Riedl, S. J. & Shi, Y. (2004) Molecular mechanisms of caspase regulation during apoptosis. *Nature Reviews Molecular Cell Biology.* 5 (11), 897-907. Available from: doi: https://dx.doi.org/10.1038/nrm1496.

Ries, S., Biederer, C., Woods, D., Shifman, O., Shirasawa, S., Sasazuki, T., McMahon, M., Oren, M. & McCormick, F. (2000) Opposing effects of Ras on p53: transcriptional activation of mdm2 and induction of p19ARF. *Cell.* 103 (2), 321-330. Available from: doi: https://dx.doi.org/10.1016/S0092-8674(00)00123-9.

Rigaut, G., Shevchenko, A., Rutz, B., Wilm, M., Mann, M. & Seraphin, B. (1999) A generic protein purification method for protein complex characterization and proteome exploration. *Nature Biotechnology.* 17 (10), 1030-1032. Available from: doi: https://dx.doi.org/10.1038/13732.

Riley, M. F. & Lozano, G. (2012) The Many Faces of MDM2 Binding Partners. *Genes & Cancer.* 3 (3-4), 226-239. Available from: doi: https://dx.doi.org/10.1177/1947601912455322.

Rivera, V. M., Miranti, C. K., Misra, R. P., Ginty, D. D., Chen, R. H., Blenis, J. & Greenberg, M. E. (1993) A growth factor-induced kinase phosphorylates the serum response factor at a site that regulates its DNA-binding activity. *Molecular & Cellular Biology.* 13 (10), 6260-6273. Available from: doi: https://dx.doi.org/10.1128/MCB.13.10.6260.

Roberts, P. J. & Der, C. J. (2007) Targeting the Raf-MEK-ERK mitogen-activated protein kinase cascade for the treatment of cancer. *Oncogene.* 26 (22), 3291-3310. Available from: doi: http://dx.doi.org/10.1038/sj.onc.1210422.

Romeo, Y., Moreau, J., Zindy, P., Saba-El-Leil, M., Lavoie, G., Dandachi, F., Baptissart, M., Borden, K. L. B., Meloche, S. & Roux, P. P. (2013) RSK regulates activated BRAF signalling to mTORC1 and promotes melanoma growth. *Oncogene.* 32 (24), 2917-2926. Available from: doi: https://dx.doi.org/10.1038/onc.2012.312.

Romeo, Y. & Roux, P. P. (2011) Paving the way for targeting RSK in cancer. *Expert Opinion on Therapeutic Targets.* 15 (1), 5-9. Available from: doi: https://dx.doi.org/10.1517/14728222.2010.531014.

Romeo, Y., Zhang, X. & Roux, P. P. (2012) Regulation and function of the RSK family of protein kinases. *Biochemical Journal.* 441 (2), 553-569. Available from: doi: http://dx.doi.org/10.1042/BJ20110289.

Rosell, R., Moran, T., Queralt, C., Porta, R., Cardenal, F., Camps, C., Majem, M., Lopez-Vivanco, G., Isla, D., Provencio, M., Insa, A., Massuti, B., Gonzalez-Larriba, J. L., Paz-Ares, L., Bover, I., Garcia-Campelo, R., Moreno, M. A., Catot, S., Rolfo, C., Reguart, N., Palmero, R., Sanchez, J. M., Bastus, R., Mayo, C., Bertran-Alamillo, J., Molina, M. A., Sanchez, J. J., Taron, M. & Spanish Lung Cancer Group. (2009) Screening for epidermal growth factor receptor mutations in lung cancer. *New England Journal of Medicine.* 361 (10), 958-967. Available from: doi: https://dx.doi.org/10.1056/NEJMoa0904554.

Roux, P. P., Ballif, B. A., Anjum, R., Gygi, S. P. & Blenis, J. (2004) Tumor-promoting phorbol esters and activated Ras inactivate the tuberous sclerosis tumor suppressor complex via p90 ribosomal S6 kinase. *Proceedings of the National Academy of Sciences of the United States of America.* 101 (37), 13489-13494. Available from: doi: http://dx.doi.org/10.1073/pnas.0405659101.

Roux, P. P. & Blenis, J. (2004) ERK and p38 MAPK-activated protein kinases: a family of protein kinases with diverse biological functions. *Microbiology & Molecular Biology Reviews.* 68 (2), 320-344. Available from: doi: http://dx.doi.org/10.1128/MMBR.68.2.320-344.2004.

Roux, P. P., Richards, S. A. & Blenis, J. (2003) Phosphorylation of p90 ribosomal S6 kinase (RSK) regulates extracellular signal-regulated kinase docking and RSK activity. *Molecular & Cellular Biology.* 23 (14), 4796-4804. Available from: doi: https://dx.doi.org/10.1128/MCB.23.14.4796-4804.2003.

Rowbotham, S. P. & Kim, C. F. (2014) Diverse cells at the origin of lung adenocarcinoma. *Proceedings of the National Academy of Sciences of the United States of America.* 111 (13), 4745-4746. Available from: doi: https://dx.doi.org/10.1073/pnas.1401955111.

Rozakis-Adcock, M., Fernley, R., Wade, J., Pawson, T. & Bowtell, D. (1993) The SH2 and SH3 domains of mammalian Grb2 couple the EGF receptor to the Ras activator mSos1. *Nature.* 363 (6424), 83-85. Available from: doi: https://dx.doi.org/10.1038/363083a0.

Russell, P. A., Wainer, Z., Wright, G. M., Daniels, M., Conron, M. & Williams, R. A. (2011) Does lung adenocarcinoma subtype predict patient survival?: A clinicopathologic study based on the new International Association for the Study of Lung Cancer/American Thoracic Society/European Respiratory Society international multidisciplinary lung adenocarcinoma classification. *Journal of Thoracic Oncology: Official Publication of the International Association for the Study of Lung Cancer.* 6 (9), 1496-1504. Available from: doi: https://dx.doi.org/10.1097/JTO.0b013e318221f701.

Ryan, M. B. & Corcoran, R. B. (2018) Therapeutic strategies to target RAS-mutant cancers. *Nature Reviews Clinical Oncology.* 15 (11), 709-720. Available from: doi: https://dx.doi.org/10.1038/s41571-018-0105-0.

Ryan, M. B., Der, C. J., Wang-Gillam, A. & Cox, A. D. (2015) Targeting RAS-mutant cancers: is ERK the key?. *Trends in Cancer.* 1 (3), 183-198. Available from: doi: https://dx.doi.org/10.1016/j.trecan.2015.10.001.

Salabei, J. K. & Hill, B. G. (2013) Mitochondrial fission induced by platelet-derived growth factor regulates vascular smooth muscle cell bioenergetics and cell proliferation. *Redox Biology.* 1 542-551. Available from: doi: https://dx.doi.org/10.1016/j.redox.2013.10.011.

Sanchez-Tillo, E., Lazaro, A., Torrent, R., Cuatrecasas, M., Vaquero, E. C., Castells, A., Engel, P. & Postigo, A. (2010) ZEB1 represses E-cadherin and induces an EMT by recruiting the SWI/SNF chromatin-remodeling protein BRG1. *Oncogene.* 29 (24), 3490-3500. Available from: doi: https://dx.doi.org/10.1038/onc.2010.102.

Sapkota, G. P., Cummings, L., Newell, F. S., Armstrong, C., Bain, J., Frodin, M., Grauert, M., Hoffmann, M., Schnapp, G., Steegmaier, M., Cohen, P. & Alessi, D. R. (2007) BI-D1870 is a specific inhibitor of the p90 RSK (ribosomal S6 kinase) isoforms in vitro and in vivo. *Biochemical Journal.* 401 (1), 29-38. Available from: doi: https://dx.doi.org/10.1042/BJ20061088.

Satoh, T., Fantl, W. J., Escobedo, J. A., Williams, L. T. & Kaziro, Y. (1993) Platelet-derived growth factor receptor mediates activation of ras through different signaling pathways in different cell types. *Molecular & Cellular Biology.* 13 (6), 3706-3713. Available from: doi: https://www.ncbi.nlm.nih.gov/pubmed/8388543.

Sawada, K., Mitra, A. K., Radjabi, A. R., Bhaskar, V., Kistner, E. O., Tretiakova, M., Jagadeeswaran, S., Montag, A., Becker, A., Kenny, H. A., Peter, M. E., Ramakrishnan, V., Yamada, S. D. & Lengyel, E. (2008) Loss of E-cadherin promotes ovarian cancer metastasis via alpha 5-integrin, which is a therapeutic target. *Cancer Research.* 68 (7), 2329-2339. Available from: doi: https://dx.doi.org/10.1158/0008-5472.CAN-07-5167.

Scaltriti, M. & Baselga, J. (2006) The epidermal growth factor receptor pathway: a model for targeted therapy. *Clinical Cancer Research.* 12 (18), 5268-5272. Available from: doi: https://dx.doi.org/10.1158/1078-0432.CCR-05-1554.

Scheffzek, K., Ahmadian, M. R., Kabsch, W., Wiesmuller, L., Lautwein, A., Schmitz, F. & Wittinghofer, A. (1997) The Ras-RasGAP complex: structural basis for GTPase activation and its loss in oncogenic Ras mutants. *Science.* 277 (5324), 333-338. Available from: doi: https://dx.doi.org/10.1126/science.277.5324.333.

Schliekelman, M. J., Taguchi, A., Zhu, J., Dai, X., Rodriguez, J., Celiktas, M., Zhang, Q., Chin, A., Wong, C., Wang, H., McFerrin, L., Selamat, S. A., Yang, C., Kroh, E. M., Garg, K. S., Behrens, C., Gazdar, A. F., Laird-Offringa, I. A., Tewari, M., Wistuba, I. I., Thiery, J. P. & Hanash, S. M. (2015) Molecular portraits of epithelial, mesenchymal, and hybrid States in lung adenocarcinoma and their relevance to survival. *Cancer Research.* 75 (9), 1789-1800. Available from: doi: https://dx.doi.org/10.1158/0008-5472.CAN-14-2535.

Schouten, G. J., Vertegaal, A. C., Whiteside, S. T., Israel, A., Toebes, M., Dorsman, J. C., van der Eb, A. J. & Zantema, A. (1997) IkappaB alpha is a target for the mitogen-activated 90 kDa ribosomal S6 kinase. *EMBO Journal.* 16 (11), 3133-3144. Available from: doi: http://dx.doi.org/10.1093/emboj/16.11.3133.

Schumacher, D., Strilic, B., Sivaraj, K. K., Wettschureck, N. & Offermanns, S. (2013) Platelet-derived nucleotides promote tumor-cell transendothelial migration and metastasis via P2Y2 receptor. *Cancer Cell.* 24 (1), 130-137. Available from: doi: https://dx.doi.org/10.1016/j.ccr.2013.05.008.

Serra, V., Eichhorn, P. J. A., Garcia-Garcia, C., Ibrahim, Y. H., Prudkin, L., Sanchez, G., Rodriguez, O., Anton, P., Parra, J., Marlow, S., Scaltriti, M., Perez-Garcia, J., Prat, A., Arribas, J., Hahn, W. C., Kim, S. Y. & Baselga, J. (2013) RSK3/4 mediate resistance to PI3K pathway inhibitors in breast cancer. *Journal of Clinical Investigation.* 123 (6), 2551-2563. Available from: doi: http://dx.doi.org/10.1172/JCI66343.

Sharma, S. V., Gajowniczek, P., Way, I. P., Lee, D. Y., Jiang, J., Yuza, Y., Classon, M., Haber, D. A. & Settleman, J. (2006) A common signaling cascade may underlie "addiction" to the Src, BCR-ABL, and EGF receptor oncogenes. *Cancer Cell.* 10 (5), 425-435. Available from: doi: https://dx.doi.org/10.1016/j.ccr.2006.09.014.

Sharrocks, A. D., Yang, S. H. & Galanis, A. (2000) Docking domains and substrate-specificity determination for MAP kinases. *Trends in Biochemical Sciences.* 25 (9), 448-453. Available from: doi: https://dx.doi.org/10.1016/S0968-0004(00)01627-3.

Shaw, P. J., Hopfensperger, M. J., Ganey, P. E. & Roth, R. A. (2007) Lipopolysaccharide and trovafloxacin coexposure in mice causes idiosyncrasy-like liver injury dependent on tumor necrosis factor-alpha. *Toxicological Sciences.* 100 (1), 259-266. Available from: doi: https://dx.doi.org/10.1093/toxsci/kfm218.

Shibue, T. & Weinberg, R. A. (2017) EMT, CSCs, and drug resistance: the mechanistic link and clinical implications. *Nature Reviews Clinical Oncology.* 14 (10), 611-629. Available from: doi: https://dx.doi.org/10.1038/nrclinonc.2017.44.

Shigematsu, H., Lin, L., Takahashi, T., Nomura, M., Suzuki, M., Wistuba, I. I., Fong, K. M., Lee, H., Toyooka, S., Shimizu, N., Fujisawa, T., Feng, Z., Roth, J. A., Herz, J., Minna, J. D. & Gazdar, A. F. (2005) Clinical and biological features associated with epidermal growth factor receptor gene mutations in lung cancers. *Journal of the National Cancer Institute.* 97 (5), 339-346. Available from: doi: https://dx.doi.org/10.1093/jnci/dji055.

Shiozawa, Y., Pedersen, E. A., Havens, A. M., Jung, Y., Mishra, A., Joseph, J., Kim, J. K., Patel, L. R., Ying, C., Ziegler, A. M., Pienta, M. J., Song, J., Wang, J., Loberg, R. D., Krebsbach, P. H., Pienta, K. J. & Taichman, R. S. (2011) Human prostate cancer metastases target the hematopoietic stem cell niche to establish footholds in mouse bone marrow. *Journal of Clinical Investigation.* 121 (4), 1298-1312. Available from: doi: https://dx.doi.org/10.1172/JCI43414.

Shkreta, L., Toutant, J., Durand, M., Manley, J. L. & Chabot, B. (2016) SRSF10 Connects DNA Damage to the Alternative Splicing of Transcripts Encoding Apoptosis, Cell-Cycle Control, and DNA Repair Factors. *Cell Reports.* 17 (8), 1990-2003. Available from: doi: https://dx.doi.org/10.1016/j.celrep.2016.10.071.

Simanshu, D. K., Nissley, D. V. & McCormick, F. (2017) RAS Proteins and Their Regulators in Human Disease. *Cell.* 170 (1), 17-33. Available from: doi: https://dx.doi.org/10.1016/j.cell.2017.06.009.

Singh, A. & Settleman, J. (2010) EMT, cancer stem cells and drug resistance: an emerging axis of evil in the war on cancer. *Oncogene.* 29 (34), 4741-4751. Available from: doi: https://dx.doi.org/10.1038/onc.2010.215.

Smith, J. A., Poteet-Smith, C. E., Xu, Y., Errington, T. M., Hecht, S. M. & Lannigan, D. A. (2005) Identification of the first specific inhibitor of p90 ribosomal S6 kinase (RSK) reveals an unexpected role for RSK in cancer cell proliferation. *Cancer Research.* 65 (3), 1027-1034. Available from: doi: https://cancerres.aacrjournals.org/content/65/3/1027.long.

Smits, K., Iannucci, V., Stove, V., Van Hauwe, P., Naessens, E., Meuwissen, P. J., Arien, K. K., Bentahir, M., Plum, J. & Verhasselt, B. (2010) Rho GTPase Cdc42 is essential for human T-cell development. *Haematologica.* 95 (3), 367-375. Available from: doi: https://dx.doi.org/10.3324/haematol.2009.006890.

Soo, R. A., Kim, D. W., Yang, J. C. H., Stammberger, U., Xiong, H., Ihling, C. & Wu, Y. L. (2015) 3082 The highly selective c-Met inhibitor tepotinib in combination with gefitinib is active in Asian patients with c-Met-positive EGFR mutant NSCLC. *European Journal of Cancer.* 51 S625. Available from: doi: https://dx.doi.org/10.1016/S0959-8049(16)31723-3.

Soria, J., Wu, Y., Nakagawa, K., Kim, S., Yang, J., Ahn, M., Wang, J., Yang, J. C., Lu, Y., Atagi, S., Ponce, S., Lee, D. H., Liu, Y., Yoh, K., Zhou, J., Shi, X., Webster, A., Jiang, H. & Mok, T. S. K. (2015) Gefitinib plus chemotherapy versus placebo plus chemotherapy in EGFR-mutation-positive non-small-cell lung cancer after progression on first-line gefitinib (IMPRESS): a phase 3 randomised trial. *Lancet Oncology.* 16 (8), 990-998. Available from: doi: https://dx.doi.org/10.1016/S1470-2045(15)00121-7.

Sottile, M. L. & Nadin, S. B. (2018) Heat shock proteins and DNA repair mechanisms: an updated overview. *Cell Stress & Chaperones.* 23 (3), 303-315. Available from: doi: https://dx.doi.org/10.1007/s12192-017-0843-4.

Spatz, A., Borg, C. & Feunteun, J. (2004) X-chromosome genetics and human cancer. *Nature Reviews.Cancer.* 4 (8), 617-629. Available from: doi: http://dx.doi.org/10.1038/nrc1413.

Stahlmann, R. (2002) Clinical toxicological aspects of fluoroquinolones. *Toxicology Letters.* 127 (1-3), 269-277. Available from: doi: https://dx.doi.org/10.1016/S0378-4274(01)00509-4.

Stenhouse, G., Fyfe, N., King, G., Chapman, A. & Kerr, K. M. (2004) Thyroid transcription factor 1 in pulmonary adenocarcinoma. *Journal of Clinical Pathology.* 57 (4), 383-387. Available from: doi: http://dx.doi.org/10.1136/jcp.2003.007138.

Storr, S. J., Carragher, N. O., Frame, M. C., Parr, T. & Martin, S. G. (2011) The calpain system and cancer. *Nature Reviews.Cancer.* 11 (5), 364-374. Available from: doi: https://dx.doi.org/10.1038/nrc3050.

Sturgill, T. W., Ray, L. B., Erikson, E. & Maller, J. L. (1988) Insulin-stimulated MAP-2 kinase phosphorylates and activates ribosomal protein S6 kinase II. *Nature.* 334 (6184), 715-718. Available from: doi: http://dx.doi.org/10.1038/334715a0.

Suda, K., Murakami, I., Katayama, T., Tomizawa, K., Osada, H., Sekido, Y., Maehara, Y., Yatabe, Y. & Mitsudomi, T. (2010) Reciprocal and complementary role of MET amplification and EGFR T790M mutation in acquired resistance to kinase inhibitors in lung cancer. *Clinical Cancer Research.* 16 (22), 5489-5498. Available from: doi: https://dx.doi.org/10.1158/1078-0432.CCR-10-1371.

Sulzmaier, F. J. & Ramos, J. W. (2013) RSK isoforms in cancer cell invasion and metastasis. *Cancer Research.* 73 (20), 6099-6105. Available from: doi: https://dx.doi.org/10.1158/0008-5472.CAN-13-1087.

Sun, Q., Zhu, R., Foss, F. W. J. & Macdonald, T. L. (2007) Mechanisms of trovafloxacin hepatotoxicity: studies of a model cyclopropylamine-containing system. *Bioorganic & Medicinal Chemistry Letters.* 17 (24), 6682-6686. Available from: doi: https://dx.doi.org/10.1016/j.bmcl.2007.10.070.

Sun, Y., Cao, S., Yang, M., Wu, S., Wang, Z., Lin, X., Song, X. & Liao, D. J. (2013) Basic anatomy and tumor biology of the RPS6KA6 gene that encodes the p90 ribosomal S6 kinase-4. *Oncogene.* 32 (14), 1794-1810. Available from: doi: http://dx.doi.org/10.1038/onc.2012.200.

Surveillance Research Program (SRP). Howlader, N., Noone A. M., Krapcho, M., Miller, D., Brest, A., Yu, M., Ruhl, J., Tatalovich, Z., Mariotto, A., Lewis, D. R., Chen, H. S., Feuer, E. J., Cronin, K. A. (ed.) (2019) *SEER Cancer Statistics Review (CSR) 1975-2016.* Bethesda, MD, National Cancer Institute: SRP.https://seer.cancer.gov/csr/1975_2016/.

Sutherland, C., Leighton, I. A. & Cohen, P. (1993) Inactivation of glycogen synthase kinase-3 beta by phosphorylation: new kinase connections in insulin and growth-factor signalling. *Biochemical Journal.* 296 (Pt 1), 15-19. Available from: doi: https://www.ncbi.nlm.nih.gov/pubmed/8250835.

Sutherland, K. D. & Berns, A. (2010) Cell of origin of lung cancer. *Molecular Oncology.* 4 (5), 397-403. Available from: doi: https://dx.doi.org/10.1016/j.molonc.2010.05.002.

Sutherland, K. D., Proost, N., Brouns, I., Adriaensen, D., Song, J. & Berns, A. (2011) Cell of origin of small cell lung cancer: inactivation of Trp53 and Rb1 in distinct cell types of adult mouse lung. *Cancer Cell.* 19 (6), 754-764. Available from: doi: https://dx.doi.org/10.1016/j.ccr.2011.04.019.

Sutherland, K. D., Song, J., Kwon, M. C., Proost, N., Zevenhoven, J. & Berns, A. (2014) Multiple cells-of-origin of mutant K-Ras-induced mouse lung adenocarcinoma. *Proceedings of the National Academy of Sciences of the United States of America.* 111 (13), 4952-4957. Available from: doi: https://dx.doi.org/10.1073/pnas.1319963111.

Swanton, C., Marani, M., Pardo, O., Warne, P. H., Kelly, G., Sahai, E., Elustondo, F., Chang, J., Temple, J., Ahmed, A. A., Brenton, J. D., Downward, J. & Nicke, B. (2007) Regulators of mitotic arrest and ceramide metabolism are determinants of sensitivity to paclitaxel and other chemotherapeutic drugs. *Cancer Cell.* 11 (6), 498-512. Available from: doi: https://dx.doi.org/10.1016/j.ccr.2007.04.011.

Swarthout, J. T., Lobo, S., Farh, L., Croke, M. R., Greentree, W. K., Deschenes, R. J. & Linder, M. E. (2005) DHHC9 and GCP16 constitute a human protein fatty acyltransferase with specificity for H- and N-Ras. *Journal of Biological Chemistry.* 280 (35), 31141-31148. Available from: doi: http://dx.doi.org/10.1074/jbc.M504113200.

Szakacs, G., Paterson, J. K., Ludwig, J. A., Booth-Genthe, C. & Gottesman, M. M. (2006) Targeting multidrug resistance in cancer. *Nature Reviews.Drug Discovery.* 5 (3), 219-234. Available from: doi: https://dx.doi.org/10.1038/nrd1984.

Tabor, V., Bocci, M. & Larsson, L. (2013) Methods to study MYC-regulated cellular senescence. *Methods in Molecular Biology.* 1012 99-116. Available from: doi: http://dx.doi.org/10.1007/978-1-62703-429-6_8.

Tan, H., Yang, K., Li, Y., Shaw, T. I., Wang, Y., Blanco, D. B., Wang, X., Cho, J., Wang, H., Rankin, S., Guy, C., Peng, J. & Chi, H. (2017) Integrative Proteomics and Phosphoproteomics Profiling Reveals Dynamic Signaling Networks and Bioenergetics Pathways Underlying T Cell Activation. *Immunity.* 46 (3), 488-503. Available from: doi: https://dx.doi.org/10.1016/j.immuni.2017.02.010.

Tan, Y., Demeter, M. R., Ruan, H. & Comb, M. J. (2000) BAD Ser-155 phosphorylation regulates BAD/Bcl-XL interaction and cell survival. *Journal of Biological Chemistry.* 275 (33), 25865-25869. Available from: doi: https://dx.doi.org/10.1074/jbc.M004199200.

Tan, Y., Ruan, H., Demeter, M. R. & Comb, M. J. (1999) p90(RSK) blocks bad-mediated cell death via a protein kinase C-dependent pathway. *Journal of Biological Chemistry.* 274 (49), 34859-34867. Available from: doi: https://dx.doi.org/10.1074/jbc.274.49.34859.

Taneja, T. K. & Sharma, S. K. (2004) Markers of small cell lung cancer. *World Journal of Surgical Oncology.* 2 10. Available from: doi: https://dx.doi.org/10.1186/1477-7819-2-10.

Tang, D., Kang, R., Berghe, T. V., Vandenabeele, P. & Kroemer, G. (2019) The molecular machinery of regulated cell death. *Cell Research.* 29 (5), 347-364. Available from: doi: https://dx.doi.org/10.1038/s41422-019-0164-5.

Taylor, R. C., Cullen, S. P. & Martin, S. J. (2008) Apoptosis: controlled demolition at the cellular level. *Nature Reviews Molecular Cell Biology.* 9 (3), 231-241. Available from: doi: https://dx.doi.org/10.1038/nrm2312.

Tazi, J., Bakkour, N. & Stamm, S. (2009) Alternative splicing and disease. *Biochimica Et Biophysica Acta.* 1792 (1), 14-26. Available from: doi: https://dx.doi.org/10.1016/j.bbadis.2008.09.017.

Thadepalli, H., Reddy, U., Chuah, S. K., Thadepalli, F., Malilay, C., Polzer, R. J., Hanna, N., Esfandiari, A., Brown, P. & Gollapudi, S. (1997) In vivo efficacy of trovafloxacin (CP-99,217), a new quinolone, in experimental intra-abdominal abscesses caused by Bacteroides fragilis and Escherichia coli. *Antimicrobial Agents & Chemotherapy.* 41 (3), 583-586. Available from: doi: https://www.ncbi.nlm.nih.gov/pubmed/9055997.

Thakur, A., Rahman, K. W., Wu, J., Bollig, A., Biliran, H., Lin, X., Nassar, H., Grignon, D. J., Sarkar, F. H. & Liao, J. D. (2007) Aberrant expression of X-linked genes RbAp46, Rsk4, and Cldn2 in breast cancer. *Molecular Cancer Research: MCR.* 5 (2), 171-181. Available from: doi: http://dx.doi.org/10.1158/1541-7786.MCR-06-0071.

Thakur, A., Sun, Y., Bollig, A., Wu, J., Biliran, H., Banerjee, S., Sarkar, F. H. & Liao, D. J. (2008) Anti-invasive and antimetastatic activities of ribosomal protein S6 kinase 4 in breast cancer cells. *Clinical Cancer Research.* 14 (14), 4427-4436. Available from: doi: http://dx.doi.org/10.1158/1078-0432.CCR-08-0458.

Thakur, A., Xu, H., Wang, Y., Bollig, A., Biliran, H. & Liao, J. D. (2005) The role of X-linked genes in breast cancer. *Breast Cancer Research & Treatment.* 93 (2), 135-143. Available from: doi: http://dx.doi.org/10.1007/s10549-005-4516-0.

Theveneau, E. & Mayor, R. (2012) Cadherins in collective cell migration of mesenchymal cells. *Current Opinion in Cell Biology.* 24 (5), 677-684. Available from: doi: https://dx.doi.org/10.1016/j.ceb.2012.08.002.

Thiery, J. P., Acloque, H., Huang, R. Y. J. & Nieto, M. A. (2009) Epithelial-mesenchymal transitions in development and disease. *Cell.* 139 (5), 871-890. Available from: doi: https://dx.doi.org/10.1016/j.cell.2009.11.007.

Thomas, S., Quinn, B. A., Das, S. K., Dash, R., Emdad, L., Dasgupta, S., Wang, X., Dent, P., Reed, J. C., Pellecchia, M., Sarkar, D. & Fisher, P. B. (2013) Targeting the Bcl-2 family for cancer therapy. *Expert Opinion on Therapeutic Targets.* 17 (1), 61-75. Available from: doi: https://dx.doi.org/10.1517/14728222.2013.733001.

Thress, K. S., Paweletz, C. P., Felip, E., Cho, B. C., Stetson, D., Dougherty, B., Lai, Z., Markovets, A., Vivancos, A., Kuang, Y., Ercan, D., Matthews, S. E., Cantarini, M., Barrett, J. C., Janne, P. A. & Oxnard, G. R. (2015) Acquired EGFR C797S mutation mediates resistance to AZD9291 in non-small cell lung cancer harboring EGFR T790M. *Nature Medicine.* 21 (6), 560-562. Available from: doi: https://dx.doi.org/10.1038/nm.3854.

Toivola, D. M., Tao, G., Habtezion, A., Liao, J. & Omary, M. B. (2005) Cellular integrity plus: organelle-related and protein-targeting functions of intermediate filaments. *Trends in Cell Biology.* 15 (11), 608-617. Available from: doi: https://dx.doi.org/10.1016/j.tcb.2005.09.004.

Tomshine, J. C., Severson, S. R., Wigle, D. A., Sun, Z., Beleford, D. A. T., Shridhar, V. & Horazdovsky, B. F. (2009) Cell proliferation and epidermal growth factor signaling in non-small cell lung adenocarcinoma cell lines are dependent on Rin1. *Journal of Biological Chemistry.* 284 (39), 26331-26339. Available from: doi: https://dx.doi.org/10.1074/jbc.M109.033514.

Torre, L. A., Bray, F., Siegel, R. L., Ferlay, J., Lortet-Tieulent, J. & Jemal, A. (2015) Global cancer statistics, 2012. *CA: A Cancer Journal for Clinicians.* 65 (2), 87-108. Available from: doi: https://dx.doi.org/10.3322/caac.21262.

Toussaint, O., Medrano, E. E. & von Zglinicki, T. (2000) Cellular and molecular mechanisms of stress-induced premature senescence (SIPS) of human diploid fibroblasts and melanocytes. *Experimental Gerontology.* 35 (8), 927-945. Available from: doi: http://dx.doi.org/10.1016/S0531-5565(00)00180-7.

Travis, W. D., Brambilla, E., Noguchi, M., Nicholson, A. G., Geisinger, K. R., Yatabe, Y., Beer, D. G., Powell, C. A., Riely, G. J., Van Schil, P. E., Garg, K., Austin, J. H. M., Asamura, H., Rusch, V. W., Hirsch, F. R., Scagliotti, G., Mitsudomi, T., Huber, R. M., Ishikawa, Y., Jett, J., Sanchez-Cespedes, M., Sculier, J., Takahashi, T., Tsuboi, M., Vansteenkiste, J., Wistuba, I., Yang, P., Aberle, D., Brambilla, C., Flieder, D., Franklin, W., Gazdar, A., Gould, M., Hasleton, P., Henderson, D., Johnson, B., Johnson, D., Kerr, K., Kuriyama, K., Lee, J. S., Miller, V. A., Petersen, I., Roggli, V., Rosell, R., Saijo, N., Thunnissen, E., Tsao, M. & Yankelewitz, D. (2011) International association for the study of lung cancer/american thoracic society/european respiratory society international multidisciplinary classification of lung adenocarcinoma. *Journal of Thoracic Oncology: Official Publication of the International Association for the Study of Lung Cancer.* 6 (2), 244-285. Available from: doi: https://dx.doi.org/10.1097/JTO.0b013e318206a221.

Trivier, E., De Cesare, D., Jacquot, S., Pannetier, S., Zackai, E., Young, I., Mandel, J. L., Sassone-Corsi, P. & Hanauer, A. (1996) Mutations in the kinase Rsk-2 associated with Coffin-Lowry syndrome. *Nature.* 384 (6609), 567-570. Available from: doi: http://dx.doi.org/10.1038/384567a0.

Tsai, J. H., Donaher, J. L., Murphy, D. A., Chau, S. & Yang, J. (2012) Spatiotemporal regulation of epithelial-mesenchymal transition is essential for squamous cell carcinoma metastasis. *Cancer Cell.* 22 (6), 725-736. Available from: doi: https://dx.doi.org/10.1016/j.ccr.2012.09.022.

Tyanova, S., Temu, T., Sinitcyn, P., Carlson, A., Hein, M. Y., Geiger, T., Mann, M. & Cox, J. (2016) The Perseus computational platform for comprehensive analysis of (prote)omics data. *Nature Methods.* 13 (9), 731-740. Available from: doi: https://dx.doi.org/10.1038/nmeth.3901.

Tzatsos, A. (2009) Raptor binds the SAIN (Shc and IRS-1 NPXY binding) domain of insulin receptor substrate-1 (IRS-1) and regulates the phosphorylation of IRS-1 at Ser-636/639 by mTOR. *Journal of Biological Chemistry.* 284 (34), 22525-22534. Available from: doi: https://dx.doi.org/10.1074/jbc.M109.027748.

van der Bruggen, T., Nijenhuis, S., van Raaij, E., Verhoef, J. & van Asbeck, B. S. (1999) Lipopolysaccharide-induced tumor necrosis factor alpha production by human monocytes involves the raf-1/MEK1-MEK2/ERK1-ERK2 pathway. *Infection & Immunity.* 67 (8), 3824-3829. Available from: doi: https://www.ncbi.nlm.nih.gov/pubmed/10417144.

Vermeulen, L., Vanden Berghe, W., Beck, I. M. E., De Bosscher, K. & Haegeman, G. (2009) The versatile role of MSKs in transcriptional regulation. *Trends in Biochemical Sciences.* 34 (6), 311-318. Available from: doi: https://dx.doi.org/10.1016/j.tibs.2009.02.007.

Volarevic, S., Stewart, M. J., Ledermann, B., Zilberman, F., Terracciano, L., Montini, E., Grompe, M., Kozma, S. C. & Thomas, G. (2000) Proliferation, but not growth, blocked by conditional deletion of 40S ribosomal protein S6. *Science.* 288 (5473), 2045-2047. Available from: doi: http://dx.doi.org/10.1126/science.288.5473.2045.

Vyse, S., McCarthy, F., Broncel, M., Paul, A., Wong, J. P., Bhamra, A. & Huang, P. H. (2018) Quantitative phosphoproteomic analysis of acquired cancer drug resistance to pazopanib and dasatinib. *Journal of Proteomics.* 170 130-140. Available from: doi: https://dx.doi.org/10.1016/j.jprot.2017.08.015.

Wade, M., Li, Y. & Wahl, G. M. (2013) MDM2, MDMX and p53 in oncogenesis and cancer therapy. *Nature Reviews.Cancer.* 13 (2), 83-96. Available from: doi: https://dx.doi.org/10.1038/nrc3430.

Walker, K. K. & Levine, A. J. (1996) Identification of a novel p53 functional domain that is necessary for efficient growth suppression. *Proceedings of the National Academy of Sciences of the United States of America.* 93 (26), 15335-15340. Available from: doi: https://dx.doi.org/10.1073/pnas.93.26.15335.

Walsh, J. G., Cullen, S. P., Sheridan, C., Luthi, A. U., Gerner, C. & Martin, S. J. (2008) Executioner caspase-3 and caspase-7 are functionally distinct proteases. *Proceedings of the National Academy of Sciences of the United States of America.* 105 (35), 12815-12819. Available from: doi: https://dx.doi.org/10.1073/pnas.0707715105.

Wang, M. & Casey, P. J. (2016) Protein prenylation: unique fats make their mark on biology. *Nature Reviews Molecular Cell Biology.* 17 (2), 110-122. Available from: doi: https://dx.doi.org/10.1038/nrm.2015.11.

Wang, Q., Yang, S., Wang, K. & Sun, S. (2019) MET inhibitors for targeted therapy of EGFR TKI-resistant lung cancer. *Journal of Hematology & Oncology.* 12 (1), 63. Available from: doi: https://dx.doi.org/10.1186/s13045-019-0759-9.

Wang, S., Song, Y. & Liu, D. (2017) EAI045: The fourth-generation EGFR inhibitor overcoming T790M and C797S resistance. *Cancer Letters.* 385 51-54. Available from: doi: https://dx.doi.org/10.1016/j.canlet.2016.11.008.

Wang, Y., Law, W., Hu, J., Lin, H., Ip, T. & Wan, D. C. (2014) Discovery of FDA-approved drugs as inhibitors of fatty acid binding protein 4 using molecular docking screening. *Journal of Chemical Information & Modeling.* 54 (11), 3046-3050. Available from: doi: https://dx.doi.org/10.1021/ci500503b.

Weinstein, I. B. & Joe, A. (2008) Oncogene addiction. *Cancer Research.* 68 (9), 3077-3080. Available from: doi: https://dx.doi.org/10.1158/0008-5472.CAN-07-3293.

Weis, K. (2003) Regulating access to the genome: nucleocytoplasmic transport throughout the cell cycle. *Cell.* 112 (4), 441-451. Available from: doi: https://dx.doi.org/10.1016/S0092-8674(03)00082-5.

Weis, S. M. & Cheresh, D. A. (2011) Tumor angiogenesis: molecular pathways and therapeutic targets. *Nature Medicine.* 17 (11), 1359-1370. Available from: doi: https://dx.doi.org/10.1038/nm.2537.

Wellbrock, C., Karasarides, M. & Marais, R. (2004) The RAF proteins take centre stage. *Nature Reviews Molecular Cell Biology.* 5 (11), 875-885. Available from: doi: https://dx.doi.org/10.1038/nrm1498.

Werner, E., Kowalczyk, A. P. & Faundez, V. (2006) Anthrax toxin receptor 1/tumor endothelium marker 8 mediates cell spreading by coupling extracellular ligands to the actin cytoskeleton. *Journal of Biological Chemistry.* 281 (32), 23227-23236. Available from: doi: https://dx.doi.org/10.1074/jbc.M603676200.

Westermann, B. (2010) Mitochondrial fusion and fission in cell life and death. *Nature Reviews Molecular Cell Biology.* 11 (12), 872-884. Available from: doi: https://dx.doi.org/10.1038/nrm3013.

White-Gilbertson, S., Kurtz, D. T. & Voelkel-Johnson, C. (2009) The role of protein synthesis in cell cycling and cancer. *Molecular Oncology.* 3 (5-6), 402-408. Available from: doi: http://dx.doi.org/10.1016/j.molonc.2009.05.003.

Whyte, D. B., Kirschmeier, P., Hockenberry, T. N., Nunez-Oliva, I., James, L., Catino, J. J., Bishop, W. R. & Pai, J. K. (1997) K- and N-Ras are geranylgeranylated in cells treated with farnesyl protein transferase inhibitors. *Journal of Biological Chemistry.* 272 (22), 14459-14464. Available from: doi: https://dx.doi.org/10.1074/jbc.272.22.14459.

Wislez, M., Antoine, M., Baudrin, L., Poulot, V., Neuville, A., Pradere, M., Longchampt, E., Isaac-Sibille, S., Lebitasy, M. & Cadranel, J. (2010) Non-mucinous and mucinous subtypes of adenocarcinoma with bronchioloalveolar carcinoma features differ by biomarker expression and in the response to gefitinib. *Lung Cancer.* 68 (2), 185-191. Available from: doi: https://dx.doi.org/10.1016/j.lungcan.2009.05.021.

Woo, M. S., Ohta, Y., Rabinovitz, I., Stossel, T. P. & Blenis, J. (2004) Ribosomal S6 kinase (RSK) regulates phosphorylation of filamin A on an important regulatory site. *Molecular & Cellular Biology.* 24 (7), 3025-3035. Available from: doi: https://dx.doi.org/10.1128/MCB.24.7.3025-3035.2004.

Wu, G., Feng, X. & Stein, L. (2010) A human functional protein interaction network and its application to cancer data analysis. *Genome Biology.* 11 (5), R53. Available from: doi: https://dx.doi.org/10.1186/gb-2010-11-5-r53.

Xi, T. & Zhang, G. (2017) Epigenetic regulation on the gene expression signature in esophagus adenocarcinoma. *Pathology, Research & Practice.* 213 (2), 83-88. Available from: doi: https://dx.doi.org/10.1016/j.prp.2016.12.007.

Xing, J., Ginty, D. D. & Greenberg, M. E. (1996) Coupling of the RAS-MAPK pathway to gene activation by RSK2, a growth factor-regulated CREB kinase. *Science.* 273 (5277), 959-963. Available from: doi: https://www.ncbi.nlm.nih.gov/pubmed/8688081.

Xu, C., Buczkowski, K. A., Zhang, Y., Asahina, H., Beauchamp, E. M., Terai, H., Li, Y. Y., Meyerson, M., Wong, K. & Hammerman, P. S. (2015) NSCLC Driven by DDR2 Mutation Is Sensitive to Dasatinib and JQ1 Combination Therapy. *Molecular Cancer Therapeutics.* 14 (10), 2382-2389. Available from: doi: https://dx.doi.org/10.1158/1535-7163.MCT-15-0077.

Xu, S., Bayat, H., Hou, X. & Jiang, B. (2006) Ribosomal S6 kinase-1 modulates interleukin-1beta-induced persistent activation of NF-kappaB through phosphorylation of IkappaBbeta. *American Journal of Physiology - Cell Physiology.* 291 (6), 1336-1345. Available from: doi: https://dx.doi.org/10.1152/ajpcell.00552.2005.

Yan, C., Sever, Z. & Whitsett, J. A. (1995) Upstream enhancer activity in the human surfactant protein B gene is mediated by thyroid transcription factor 1. *Journal of Biological Chemistry.* 270 (42), 24852-24857. Available from: doi: https://dx.doi.org/10.1074/jbc.270.42.24852.

Yang, F., Sun, L., Li, Q., Han, X., Lei, L., Zhang, H. & Shang, Y. (2012a) SET8 promotes epithelial-mesenchymal transition and confers TWIST dual transcriptional activities. *EMBO Journal.* 31 (1), 110-123. Available from: doi: https://dx.doi.org/10.1038/emboj.2011.364.

Yang, H., Liu, J., Liao, D., Sun, Y., Chen, Z. & Zhang, X. (2012b) [Effects of breast cancer cells stably overexpressing RSK4 on growth of transplanted human breast cancer in severe combined immunodeficiency mice]. *Chung-Hua i Hsueh Tsa Chih [Chinese Medical Journal].* 92 (26), 1845-1848. Available from: doi: https://www.ncbi.nlm.nih.gov/pubmed/22944237.

Yang, Y., Fang, S., Jensen, J. P., Weissman, A. M. & Ashwell, J. D. (2000) Ubiquitin protein ligase activity of IAPs and their degradation in proteasomes in response to apoptotic stimuli. *Science.* 288 (5467), 874-877. Available from: doi: https://dx.doi.org/10.1126/science.288.5467.874.

Yatabe, Y., Mitsudomi, T. & Takahashi, T. (2002) TTF-1 expression in pulmonary adenocarcinomas. *American Journal of Surgical Pathology.* 26 (6), 767-773. Available from: doi: https://www.ncbi.nlm.nih.gov/pubmed/12023581.

Ye, J. Z., Donigian, J. R., van Overbeek, M., Loayza, D., Luo, Y., Krutchinsky, A. N., Chait, B. T. & de Lange, T. (2004a) TIN2 binds TRF1 and TRF2 simultaneously and stabilizes the TRF2 complex on telomeres. *Journal of Biological Chemistry.* 279 (45), 47264-47271. Available from: doi: https://dx.doi.org/10.1074/jbc.M409047200.

Ye, J. Z., Hockemeyer, D., Krutchinsky, A. N., Loayza, D., Hooper, S. M., Chait, B. T. & de Lange, T. (2004b) POT1-interacting protein PIP1: a telomere length regulator that recruits POT1 to the TIN2/TRF1 complex. *Genes & Development.* 18 (14), 1649-1654. Available from: doi: https://dx.doi.org/10.1101/gad.1215404.

Ye, Q., Wang, X., Jin, M., Wang, M., Hu, Y., Yu, S., Yang, Y., Yang, J. & Cai, J. (2018) Effect of RSK4 on biological characteristics of colorectal cancer. *World Journal of Surgical Oncology.* 16 (1), 240. Available from: doi: https://dx.doi.org/10.1186/s12957-018-1474-7.

Yntema, H. G., van den Helm, B., Kissing, J., van Duijnhoven, G., Poppelaars, F., Chelly, J., Moraine, C., Fryns, J. P., Hamel, B. C., Heilbronner, H., Pander, H. J., Brunner, H. G., Ropers, H. H., Cremers, F. P. & van Bokhoven, H. (1999) A novel ribosomal S6-kinase (RSK4; RPS6KA6) is commonly deleted in patients with complex X-linked mental retardation. *Genomics.* 62 (3), 332-343. Available from: doi: http://dx.doi.org/10.1006/geno.1999.6004.

Youle, R. J. & Strasser, A. (2008) The BCL-2 protein family: opposing activities that mediate cell death. *Nature Reviews Molecular Cell Biology.* 9 (1), 47-59. Available from: doi: https://dx.doi.org/10.1038/nrm2308.

Yu, H. A., Arcila, M. E., Rekhtman, N., Sima, C. S., Zakowski, M. F., Pao, W., Kris, M. G., Miller, V. A., Ladanyi, M. & Riely, G. J. (2013) Analysis of tumor specimens at the time of acquired resistance to EGFR-TKI therapy in 155 patients with EGFR-mutant lung cancers. *Clinical Cancer Research.* 19 (8), 2240-2247. Available from: doi: https://dx.doi.org/10.1158/1078-0432.CCR-12-2246.

Yu, J. & Zhang, L. (2008) PUMA, a potent killer with or without p53. *Oncogene.* 27 (Suppl 1), S71-83. Available from: doi: https://dx.doi.org/10.1038/onc.2009.45.

Yu, Q. & Stamenkovic, I. (2000) Cell surface-localized matrix metalloproteinase-9 proteolytically activates TGF-beta and promotes tumor invasion and angiogenesis. *Genes & Development.* 14 (2), 163-176. Available from: doi: https://www.ncbi.nlm.nih.gov/pmc/articles/PMC316345/.

Yu, Q. & Stamenkovic, I. (1999) Localization of matrix metalloproteinase 9 to the cell surface provides a mechanism for CD44-mediated tumor invasion. *Genes & Development.* 13 (1), 35-48. Available from: doi: https://www.ncbi.nlm.nih.gov/pmc/articles/PMC316376/.

Zaru, R., Ronkina, N., Gaestel, M., Arthur, J. S. C. & Watts, C. (2007) The MAPK-activated kinase Rsk controls an acute Toll-like receptor signaling response in dendritic cells and is activated through two distinct pathways. *Nature Immunology.* 8 (11), 1227-1235. Available from: doi: https://dx.doi.org/10.1038/ni1517.

Zeniou, M., Ding, T., Trivier, E. & Hanauer, A. (2002) Expression analysis of RSK gene family members: the RSK2 gene, mutated in Coffin-Lowry syndrome, is prominently expressed in brain structures essential for cognitive function and learning. *Human Molecular Genetics.* 11 (23), 2929-2940. Available from: doi: https://dx.doi.org/10.1093/hmg/11.23.2929.

Zerial, M. & McBride, H. (2001) Rab proteins as membrane organizers. *Nature Reviews Molecular Cell Biology.* 2 (2), 107-117. Available from: doi: https://dx.doi.org/10.1038/35052055.

Zhang, L., Whitsett, J. A. & Stripp, B. R. (1997) Regulation of Clara cell secretory protein gene transcription by thyroid transcription factor-1. *Biochimica Et Biophysica Acta.* 1350 (3), 359-367. Available from: doi: https://dx.doi.org/10.1016/S0167-4781(96)00180-7.

Zhang, X., Tee, L. Y., Wang, X., Huang, Q. & Yang, S. (2015) Off-target Effects in CRISPR/Cas9-mediated Genome Engineering. *Molecular Therapy.Nucleic Acids.* 4 e264. Available from: doi: https://dx.doi.org/10.1038/mtna.2015.37.

Zhao, Y., Xiong, X. & Sun, Y. (2011) DEPTOR, an mTOR inhibitor, is a physiological substrate of SCF(betaTrCP) E3 ubiquitin ligase and regulates survival and autophagy. *Molecular Cell.* 44 (2), 304-316. Available from: doi: http://dx.doi.org/10.1016/j.molcel.2011.08.029.

Zheng, G., Lyons, J. G., Tan, T. K., Wang, Y., Hsu, T., Min, D., Succar, L., Rangan, G. K., Hu, M., Henderson, B. R., Alexander, S. I. & Harris, D. C. H. (2009) Disruption of E-cadherin by matrix metalloproteinase directly mediates epithelial-mesenchymal transition downstream of transforming growth factor-beta1 in renal tubular epithelial cells. *American Journal of Pathology.* 175 (2), 580-591. Available from: doi: https://dx.doi.org/10.2353/ajpath.2009.080983.

Zheng, X., Carstens, J. L., Kim, J., Scheible, M., Kaye, J., Sugimoto, H., Wu, C., LeBleu, V. S. & Kalluri, R. (2015) Epithelial-to-mesenchymal transition is dispensable for metastasis but induces chemoresistance in pancreatic cancer. *Nature.* 527 (7579), 525-530. Available from: doi: https://dx.doi.org/10.1038/nature16064.

Zhou, Y., Yamada, N., Tanaka, T., Hori, T., Yokoyama, S., Hayakawa, Y., Yano, S., Fukuoka, J., Koizumi, K., Saiki, I. & Sakurai, H. (2015) Crucial roles of RSK in cell motility by catalysing serine phosphorylation of EphA2. *Nature Communications.* 6 7679. Available from: doi: https://dx.doi.org/10.1038/ncomms8679.

Zhu, J., Li, Q., Liu, J., Wei, W., Yang, H. & Tang, W. (2015) RSK4 knockdown promotes proliferation, migration and metastasis of human breast adenocarcinoma cells. *Oncology Reports.* 34 (6), 3156-3162. Available from: doi: http://dx.doi.org/10.3892/or.2015.4291.

Zimmermann, G., Papke, B., Ismail, S., Vartak, N., Chandra, A., Hoffmann, M., Hahn, S. A., Triola, G., Wittinghofer, A., Bastiaens, P. I. H. & Waldmann, H. (2013) Small molecule inhibition of the KRAS-PDEdelta interaction impairs oncogenic KRAS signalling. *Nature.* 497 (7451), 638-642. Available from: doi: https://dx.doi.org/10.1038/nature12205.

8. Supplementary Material

8.1 Chapter 2

Table S 1| Cell lines used in this study

ATCC® No.	Name	Tissue	Characteristics
CCL-185™	A549	Lung	Unmodified
-	cr421		RSK4 stable knockout (partial)
-	cr437		RSK4 stable knockout (complete)
CRL-1573™	HEK293A	Embryonic kidney	Unmodified
-	HEK293A-EV		Empty vector (EV) stable overexpression
-	HEK293A-RSK1		RSK1 stable overexpression
-	HEK293A-RSK4		RSK4 stable overexpression
HTB-4™	T24	Bladder	Unmodified
HTB-5™	TCCSUP		
HTB-1™	J82		
-	KP	Lung (mouse)	*Kras*$^{LSL\text{-}G12D/+}$;*p53*$^{flox/flox}$*

*LSL: loxP-stop-loxP cassette

Table S 2| Dharmacon siGENOME Human siRNAs

Target	siRNA Sequence	Targeted region: ORF*	Dharmacon siGENOME ID
RPS6KA1 (RSK1)	GAGAATGGGCTCCTCATGA	Exon 18 (1699-1717 bp**)	D-003025-**06**
	CAAGCGGGATCCTTCAGAA	Exon 16 (1356-1374 bp)	D-003025-**07**
	CCACCGGCCTGATGGAAGA	Exon 14 (1148-1166 bp)	D-003025-**08**
RPS6KA3 (RSK2)	GAAGGGAAGTTGTATCTTA	Exon 6 (418-436 bp)	D-003026-**05**
	GAAAGTATGTGTATGTAGT	Exon 17 (1457-1475 bp)	D-003026-**06**
	GGACAGCATCCAAACATTA	Exon 16 (1411-1429 bp)	D-003026-**07**
	GGAGGTGAATTGCTGGATA	Exon 17 (1492-1510 bp)	D-003026-**08**
RPS6KA2 (RSK3)	GATCGAAGATGGAGAGAGA	Exon 4 (314-332 bp)	D-004663-**02**
	TCAAGGATGTCTATGATGA	Exons 15/16 (1415-1433 bp)	D-004663-**04**
	GCAAGCGATGTGTGCATAA	Exon 14 (1286-1304 bp)	D-004663-**05**
	CGAATGAAATGCTCCGTAT	3 prime UTR	D-004663-**18**
RPS6KA6 (RSK4)	GCAAATGTATTACCAATTG	Exon 14 (1219-1237 bp)	D-004670-**01**
	GGACAACATCCCAACATTA	Exon 16 (1423-1441 bp)	D-004670-**02**
	GGTGGAAACTGGGACAATA	Exon 20 (1936-1954 bp)	D-004670-**03**
	GTAGATATGTTTACCTTGT	Exon 17 (1469-1487 bp)	D-004670-**04**
TP53 (p53)	GAGGTTGGCTCTGACTGTA	Exons 6/7 (670-688 bp)	D-003329-**05**
	GCACAGAGGAAGAGAATCT	Exon 8 (848-866 bp)	D-003329-**07**
	GAAGAAACCACTGGATGGA	Exon 9 (957-975 bp)	D-003329-**08**
	GCTTCGAGATGTTCCGAGA	3 prime UTR	D-003329-**26**

*ORF: Open reading frame (coding sequence)

**bp: Base pairs

Table S 3| Qiagen FlexiTube Human siRNAs

Target	siRNA Sequence	Targeted region: ORF	Qiagen FlexiTube ID
RPS6KA1 (RSK1)	CCCAACATCATCACTCTGAAA	Exon 16 (1408-1428 bp)	SI00046102 **(01)**
	TGCCACGTACTCCGCACTCAA	Exon 22 (2097-2117 bp)	SI04379480 **(14)**
	CAGGATATACTCCATTTGCCA	Exons 19/20 (1826-1846 bp)	SI02223060 **(09)**
	ACCATTGACTGGAATAAGCTA	Exons 12/13 (967-987 bp)	SI00046123 **(04)**
RPS6KA6 (RSK4)	TTGGATCATCTGCACCAATTA	Exon 7 (556-576 bp)	SI00106603 **(03)**
	CGGGAGGCTAGTGATATACTA	Exon 17 (1552-1572 bp)	SI00106610 **(04)**
	CAGCGGTATACTGCTGAACAA	Exon 21 (2008-2028 bp)	SI00287609 **(05)**
	GGCGAGGTAAATGGTCTTAAA	Exons 1/2 (76-96 bp)	SI02659748 **(06)**

Table S 4| RPS6KA1 and RPS6KA6 Variants - Annotations

Gene name		Ensembl	RefSeq	UCSC*	CCDS**	Protein name	Uniprot
RPS6KA1-204	Variant I	ENST00000374168.7	NM_002953.4	uc001bmr.2	CCDS284.1	p90 ribosomal S6 kinase alpha-1 (RSK1)	Q15418-1
RPS6KA1-220	Variant II	ENST00000531382.5	NM_001006665.2	uc001bms.2	CCDS30649.1		Q15418-2
RPS6KA6-201	Variant I	ENST00000262752.5	NM_014496.5	uc004eej.3	CCDS14451.1	p90 ribosomal S6 kinase alpha-6 (RSK4)	Q9UK32-1
RPS6KA6-204	Variant II	ENST00000620340.4	NM_001330512.1	uc011mqt.2	CCDS83480.1		Q9UK32-2

*UCSC: University of California Santa Cruz genome browser

**CCDS: Consensus Coding Sequence project

Table S 5| RPS6KA1 and RPS6KA6 Variants - Characteristics

Gene name		mRNA (bp*)	ORF (bp)	Protein (aa**)
RPS6KA1-204	Variant I	3192	2208	735
RPS6KA1-220	Variant II	3118	2235	744
RPS6KA6-201	Variant I	8465	2238	745
RPS6KA6-204	Variant II	8427	2238	745

*bp: Base pairs

**aa: Amino acids

Table S 6| PCR cloning primers

Gene	Primer sequence (5'-3')
RPS6KA1-204 (RSK1) transcript variant I	**For**: CCCTCGAGCCGCTCGCCCAGCTCAAGGAG
	Rev: GAGAATTCCCAGGGTGGTGGATGGCAACTT
RPS6KA6-201 (RSK4) transcript variant I	**For**: CCCTCGAGCTACCATTCGCTCCT CAGGAC
	Rev: GAGAATTCCCAGGCCAGTTGATGTTCGCTT
RPS6KA6-204 (RSK4) transcript variant II	**For**: CCCTCGAGGGTCTCTCTACCTCAGCAATT
	Rev: GAGAATTCCCAGGCCAGTTGATGTTCGCTT

Gene-specific sequence

XhoI site

EcoRI site

Table S 7| Mutagenesis primers

Gene	Mutation	WT codon (5'-3')	Primer sequence (5'-3')
RPS6KA1-204 (RSK1) transcript variant I	S221E	**TCT** **AGA**	**For**: ACCACGAGAAGAAGGCCTAT**GAA**TTCTGCGGGACAGTGGAGTA **Rev**: TACTCCACTGTCCCGCAGAA**TTC**ATAGGCCTTCTTCTCGTGGT
	S221A	**TCT** **AGA**	**For**: ACCACGAGAAGAAGGCCTAT**GCT**TTCTGCGGGACAGTGGAGTA **Rev**: TACTCCACTGTCCCGCAGAA**AGC**ATAGGCCTTCTTCTCGTGGT
RPS6KA6-201 (RSK4) transcript variant I	S232E	**TCA** **TGA**	**For**: ATCAAGAAAAGAAGGCTTAC**GAA**TTTTGTGGTACAGTAGAGTA **Rev**: TACTCTACTGTACCACAAAA**TTC**GTAAGCCTTCTTTTCTTGAT
	S232A	**TCA** **TGA**	**For**: ATCAAGAAAAGAAGGCTTAC**GCA**TTTTGTGGTACAGTAGAGTA **Rev**: TACTCTACTGTACCACAAAA**TGC**GTAAGCCTTCTTTTCTTGAT

Table S 8| Western blotting primary antibodies

Protein	Species (moAb)	MW (kDa)	Dilution	Company	Cat. No.	Clone	Tested applications/Notes
RSK1/2/3	Rabbit (poly)	90	1:1000	Cell Signalling	9347	-	WB
Phospho-RSK1/2/4 (Ser363)	Rabbit (poly)	90	1:500	Santa Cruz	sc-17033	-	WB
RSK4 (1-100aa)	Rabbit	90	1:500 (WB) 1:100 (IF)	Abcam	ab76117	EP1982Y	WB IF (A549: non-specific nuclear signal)
RSK4 (346-462aa)	Rabbit (poly)	90	1:500 (WB) 1:50 (IHC)	Sigma Prestige	HPA002852	-	WB (good) IF (good) IHC (good) *this Ab picks 'RSK4' signal in cr437: WB, IF, IHC
Phospho-RSK4 (Ser232)	Rabbit	90	1:1000	Abcam	ab81290	EP1524Y	WB (species reactivity: human & mouse)
RSK1	Rabbit	90	1:1000	Cell Signalling	8408	D6D5	WB/IF (species reactivity: human & mouse)
RSK2	Rabbit	90	1:1000	Cell Signalling	5528	D21B2	WB
S6K1	Mouse	70	1:1000	Santa Cruz	sc-100423	S-04	WB
S6K2	Goat	70	1:1000	Santa Cruz	sc-9381	C-19	WB
KRAS	Mouse	21	1:1000	Santa Cruz	sc-30	F234	WB
HRAS	Rabbit (poly)	21	1:1000	Santa Cruz	sc-520	C-20	WB
rpS6	Mouse	32	1:1000	Cell Signalling	2317	54D2	WB
Phospho-rpS6 (Ser235/236)	Rabbit	32	1:1000	Cell Signalling	2211	-	WB
p44/42 MAPK (ERK1/2)	Mouse	44-42	1:1000	EMD Millipore	05-1152	MK12	WB
Phospho-p44/42 MAPK (ERK1/2) (Thr202/Tyr204)	Rabbit	p44-42	1:1000	Cell Signalling	9101	-	WB
Akt1	Rabbit	60	1:1000	Cell Signalling	2938	C73H10	WB
Phospho-Akt (Ser473)	Rabbit	60	1:1000	Cell Signalling	9271	-	WB
FGFR1	Mouse	145	1:1000	Abcam	ab824	M5G10	WB

Phospho-FGFR1 (Tyr653/654)	Mouse	145	1:1000	Cell Signalling	3476	55H2	WB
MDM2	Mouse	90	1:1000	Abcam	ab16895	2A10	WB
Phospho-MDM2 (Ser166)	Rabbit	90	1:1000	Cell Signalling	3521	-	WB
p53	Mouse	53	1:1000	Santa Cruz	sc-126	DO-1	WB
PUMA	Rabbit	23	1:1000	Cell Signalling	12450	D30C10	WB
$p21^{Cip1/WAF1}$	Mouse	21	1:1000	Santa Cruz	sc-817	187	WB
Rb	Mouse	110	1:1000	Cell Signalling	9309	4H1	WB
Phospho-Rb (Ser780)	Rabbit	110	1:1000	Cell Signalling	9307	-	WB
c-Myc	Rabbit	57-70	1:1000	Cell Signalling	9402	-	WB
c-IAP2 (BIRC3)	Rabbit	70	1:1000	Cell Signalling	3130	58C7	WB
c-IAP2 (BIRC3)	Rabbit	70	1:1000	Sigma	HPA002317	-	WB (species reactivity: human & mouse)
c-IAP1 (BIRC2)	Rabbit	70	1:1000	Abcam	ab108361	EPR4673	WB
Bcl-2	Mouse	25	1:500	Santa Cruz	sc-509	100	WB
Mcl-1	Rabbit (poly)	40	1:1000	Santa Cruz	sc-819	S-19	WB
BID	Rabbit (poly)	15,22	1:1000	Cell Signalling	2002	-	WB
Apaf-1	Rabbit (poly)	135	1:1000	Cell Signalling	5088	R205	WB
PDCD4	Rabbit	60	1:1000	Cell Signalling	9535	D29C6	WB
PARP	Rabbit	89,116	1:1000	Cell Signalling	9542	-	WB
Cleaved Caspase-3 (Asp175)	Rabbit	17,19	1:1000	Cell Signalling	9661	-	WB (species reactivity: human & mouse)
Caspase-7	Rabbit	20,35	1:1000	Cell Signalling	9492	-	WB
Caspase-8	Rabbit	10,57	1:1000	Cell Signalling	4790	D35G2	WB
Caspase-9	Rabbit	35,37,47	1:1000	Cell Signalling	9502	-	WB
Caspase-10	Rabbit	63 to 66	1:1000	Cell Signalling	9752	-	WB
E-Cadherin	Rabbit	135	1:1000	Cell Signalling	3195	24E10	WB
N-Cadherin	Mouse	135	1:1000	Cell Signalling	14215	13A9	WB
Vimentin	Rabbit	57	1:1000	Cell Signalling	5741	D21H3	WB
β-Catenin	Rabbit	92	1:1000	Cell Signalling	8480	D10A8	WB
Slug	Rabbit	30	1:1000	Cell Signalling	9585	C19G7	WB

Snail	Rabbit	29	1:1000	Cell Signalling	3879	C15D3	WB
CD44	Mouse	85-130	1:1000	Cell Signalling	3570	156-3C11	WB
HCAM (CD44)	Mouse	85-130	1:1000	Santa Cruz	sc-7297	DF1485	WB
NF-κB1 p105/p50	Rabbit	105, 50	1:1000	Cell Signalling	12540	D7H5M	WB
NF-κB2 p100/p52	Rabbit	100, 52	1:1000	Cell Signalling	4882	-	WB
NF-κB p65	Mouse	65	1:1000	Cell Signalling	6956	L8F6	WB
Phospho-NF-κB p65 (Ser536)	Rabbit	65	1:1000	Cell Signalling	3031	-	WB
mTOR	Rabbit	289	1:1000	Cell Signalling	2983	7C10	WB
Phospho-mTOR (Ser2481)	Rabbit	289	1:1000	Cell Signalling	2974	-	WB
Phospho-mTOR (Ser2448)	Rabbit	289	1:1000	Cell Signalling	2971	-	WB
GFP	Mouse	27	1:1000	Santa Cruz	sc-9996	B-2	WB/IF
FLAG®	Rabbit	1012.9 Da	1:1000	Sigma	F7425	-	WB/IF
FLAG®	Mouse	1012.9 Da	1:1000	Sigma	F1804	M2	WB/IF
HA	Mouse	1102.1 Da	1:1000	Sigma	H3663	HA-7	WB/IF
Vinculin	Mouse	130	1:10000	Sigma	V9131	hVIN-1	WB (species reactivity: human & mouse)
α-Tubulin	Mouse	52	1:10000	Sigma	T5168	B-5-1-2	WB
β-Actin	Mouse	42	1:10000	Sigma	A2228	AC-74	WB
Lamin B1	Mouse	70	1:10000	Santa Cruz	sc-374015	B-10	WB

Table S 9| Western blotting secondary antibodies

Species	Dilution	Company	Cat. No.
Polyclonal Swine a-Rabbit Ig/HRP	1:10000	Agilent: Dako	P0399
Polyclonal Goat a-Mouse Ig/HRP	1:5000	Agilent: Dako	P0447
Polyclonal Rabbit a-Goat Ig/HRP	1:2000 (1:5000 for loading controls)	Sigma	A5420

Table S 10| Lung cancer cell line panel

ATCC® No.	Name	Tissue	Histology	Tumour source	TP53 status	KRAS status	NRAS status
CCL-185™	A549	Lung	Adenocarcinoma (non-small cell)	Primary	WT	p.G12S	WT
CRL-5803™	H1299	Lung	Carcinoma (large cell)	Metastasis (lymph node)	NULL	WT	p.Q61K
-	EKVX	Lung	Adenocarcinoma (non-small cell)	Primary	p.E204X	WT	WT
-	HOP-62	Lung	Adenocarcinoma (non-small cell)	Primary	c.G673-2A>G	p.G12C	WT
CRL-5800™	H23	Lung	Adenocarcinoma (non-small cell)	Primary	p.M246I	p.G12C	WT
-	H322M	Lung	Bronchoalveolar Adenocarcinoma (non-small cell)	Primary	p.R248L	WT	WT
-	HOP-92	Lung	Carcinoma (large cell)	Primary	p.R175L	WT	WT
HTB-177™	H460	Lung	Carcinoma (large cell)	Metastasis (pleural effusion)	WT	p.Q61H	WT
CRL-5826™	H226	Lung	Mesothelioma (squamous cell)	Metastasis (pleural effusion)	WT	WT	WT
CRL-2503™	NL20	Lung	Bronchial epithelium	Non-tumourigenic	WT	WT	WT
-	ATII (Alveolar type II pneumocytes)	Lung	Alveolar epithelium	Non-tumourigenic	WT	WT	WT

Table S 11| NCI-60 human cancer cell line panel

ATCC® No.	Name	Cancer/Tissue	Disease/Histology	Tumour source
CCL-185™	A549	Lung	Adenocarcinoma (non-small cell)	Primary
HTB-22™	MCF7	Mammary gland;	ER+, PR-, HER2- Adenocarcinoma **(TP53 WT)**	Metastasis (pleural effusion)
HTB-133™	T-47D	Breast	ER+, PR+, HER2- Ductal carcinoma	Metastasis (pleural effusion)
HTB-26™	MDA-MB-231		ER-, PR-, HER2- Adenocarcinoma	Metastasis (pleural effusion)
HTB-126™	Hs 578T		ER-, PR-, HER2- Carcinoma	Primary
HTB-122™	BT-549		ER-, PR-, HER2- Ductal carcinoma	Primary
CRL-1740™	LNCaP	Prostate	AR+ (androgen-sensitive) Carcinoma	Metastasis (lymph node)
CRL-3314™	C4-2		AR+ (androgen-insensitive) Carcinoma	LNCaP-derived (xenograft tumour; castrated mouse)
HTB-81™	DU-145		AR- (androgen-insensitive) Carcinoma	Metastasis (brain)
CRL-1435™	PC-3		AR- (androgen-insensitive) Adenocarcinoma	Metastasis (bone)
HTB-44™	A-498	Kidney	Carcinoma	Primary
-	RXF 393		Carcinoma	NS*
-	SN12C		Carcinoma	Primary
-	TK-10		Clear cell carcinoma	NS*
-	UO-31		Carcinoma	NS*
HTB-46™	Caki-1		Clear cell carcinoma	Metastasis (skin)
-	LOX-IMVI	Melanoma	Malignant melanoma	Metastasis (lymph node)
HTB-68™	SK-MEL-2		Malignant melanoma	Metastasis (thigh skin)
HTB-70™	SK-MEL-5		Malignant melanoma	Metastasis (axillary node)
HTB-72™	SK-MEL-28		Malignant melanoma	NS*
-	OVCAR-8	Ovarian	Serous adenocarcinoma	Primary
HTB-77™	SK-OV-3		Serous cystadenocarcinoma	NS*
-	NCI-ADR-RES		Serous adenocarcinoma	Primary
CCL-247™	HCT-116	Colon	Colorectal carcinoma	NS*
-	KM-12		Colorectal carcinoma	Primary
HTB-38™	HT-29		Colorectal adenocarcinoma	Primary
-	HCC-2998		Colorectal carcinoma	Primary
CCL-227™	SW-620		Dukes' type C, colorectal adenocarcinoma	Metastasis (lymph node)
CCL-225™	HCT-15		Dukes' type C, colorectal adenocarcinoma	NS*

CCL-222™	COLO 205		Dukes' type C, colorectal adenocarcinoma	Metastasis (ascites)
-	SF-268	CNS; Brain (glioma)	Astrocytoma	NS*
-	SF-295		Glioblastoma	NS*
-	SF-539		Gliosarcoma	NS*
CCL-243™	K-562	Bone marrow	Chronic myelogenous leukemia (CML)	Primary
CCL-155™	RPM1 8226	Peripheral blood	Plasmacytoma; myeloma	Primary

*NS: Not specified

Table S 12| qRT-PCR primers

Gene	Primer sequence (5'-3')	Targeted region: ORF
RPS6KA6 (RSK4)	**For**: TGCTCAAGGTTCTTGGTCAG	Exon 3
	Rev: TTTGTCCGAACTCTGTCTCG	Exon 5
RPS6KA1 (RSK1)	**For**: CGGAAGGAGACCATGACACTGA	Exon 10
	Rev: GTTGGCAGGATTCCGCTTGAAC	Exon 11
MDM2	**For**: TGTTTGGCGTGCCAAGCTTCTC	Exon 4
	Rev: CACAGATGTACCTGAGTCCGATG	Exon 6
TP53	**For**: TAACAGTTCCTGCATGGGCGGC	Exon 7
	Rev: AGGACAGGCACAAACACGCACC	Exon 8
BBC3 (PUMA)	**For**: CCCTGGAGGGTCCTGTACAATC	Exon 4
	Rev: CTAATTGGGCTCCATCTCGGGG	Exon 4
CDKN1A (p21)	**For**: TGGAGACTCTCAGGGTCGAAA	Exon 2
	Rev: GGCGTTTGGAGTGGTAGAAATC	Exon 3
BIRC2 (c-IAP1)	**For**: AGCTAGTCTGGGATCCACCTC	Exon 2
	Rev: GGGGTTAGTCCTCGATGAAG	Exon 2
BIRC3 (c-IAP2)	**For**: TGGAAGCTACCTCTCAGCCTAC	Exon 2
	Rev: GGAACTTCTCATCAAGGCAGA	Exon 2
BCL2	**For**: TTTGAGTTCGGTGGGGTCAT	Exon 1
	Rev: TGACTTCACTTG TGGCCCAG	Exon 2
PDCD4	**For**: GCAGAAAATGCTGGGACTGAG	Exon 4
	Rev: TGTACCCCAGACACCTTTGC	Exon 5
CDH1 (E-Cadherin)	**For**: CCCGCCTTATGATTCTCTGCTCGTG	Exon 16
	Rev: TCCGTACATGTCAGCCAGCTTCTTG	Exon 16
CDH2 (N-Cadherin)	**For**: GACGGTTCGCCATCCAGAC	Exon 9
	Rev: TCGATTGGTTTGACCACGG	Exon 10
VIM (Vimentin)	**For**: TGTCCAAATCGATGTGGATGTTTC	Exon 5
	Rev: TTGTACCATTCTTCTGCCTCCTG	Exon 5
HPRT1	**For**: TGACCTTGATTTATTTTGCATACC	Exon 2
	Rev: CGAGCAAGACGTTCAGTCCT	Exon 3

Table S 13| Immunofluorescence primary antibodies

Protein	Species (moAb)	Dilution	Company	Cat. No.	Clone
RSK4 (346-462aa)	Rabbit (poly)	1:500	Sigma Prestige	HPA002852	-
RSK1	Rabbit	1:1000	Cell Signalling	8408	D6D5
FLAG®	Rabbit	1:1000	Sigma	F7425	-
Alexa Fluor™ 488® Phalloidin	-	1X (165 nM) final conc.	Thermo Fisher	A12379	-
MitoTracker® Red CMXRos	-	250 nM final conc.	Thermo Fisher	M7512	-

Table S 14| Immunofluorescence secondary antibodies

Species	Wavelength (nm)	Dilution	Company	Cat. No.
Goat anti-Ms Goat anti-Rb	488	1:1000	Thermo Fisher	A-11001 A-11008
Goat anti-Ms Goat anti-Rb	555	1:1000	Thermo Fisher	A32727 A32732

8.2 Chapter 3

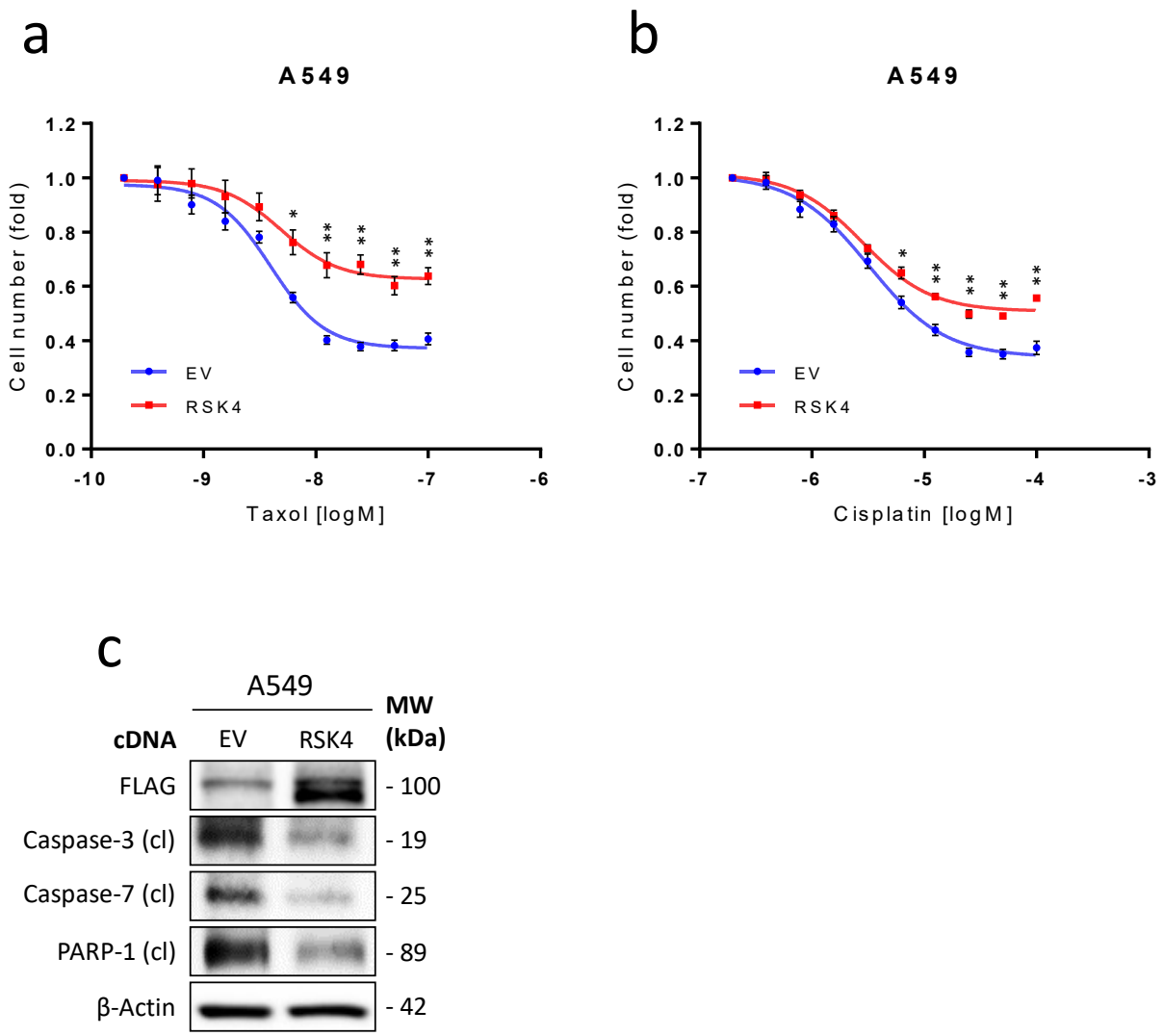

Figure S 1| RSK4 emerges as a potent regulator of chemo-sensitivity in lung cancer cells. **(a, b)** RSK4 cDNA expression increases resistance of A549 cells to paclitaxel (taxol) and cisplatin. Cell viability was determined by crystal violet staining of A549 cells transfected (24-48 h) with a final concentration of 2.5 µg EV (empty vector) or RSK4 cDNAs, before treated with 2-fold serially diluted **(a)** paclitaxel (taxol) (0-100 nM) or **(b)** cisplatin (0-100 µM) for 48-72 h. Data plotted as a fold change relative to the untreated EV condition and represent mean ± SEM of three independent biological replicates performed in quadruplicates. **(c)** RSK4 cDNA expression decreases the cleavage of Caspase-3, Caspase-7 and PARP-1. Immunoblotting of FLAG (RSK4), cleaved (cl) Caspase-3, Caspase-7 and PARP-1 in whole cell A549 extracts transfected (24-48 h) with a final concentration of 2.5 µg EV (empty vector) or RSK4 cDNAs. β-Actin was used as a loading control. Data are representative of two independent biological replicates. Statistical significance was assessed by an unpaired Student's *t*-test in GraphPad Prism. *; $P \leq 0.05$, **; $P \leq 0.01$. cl; cleaved.

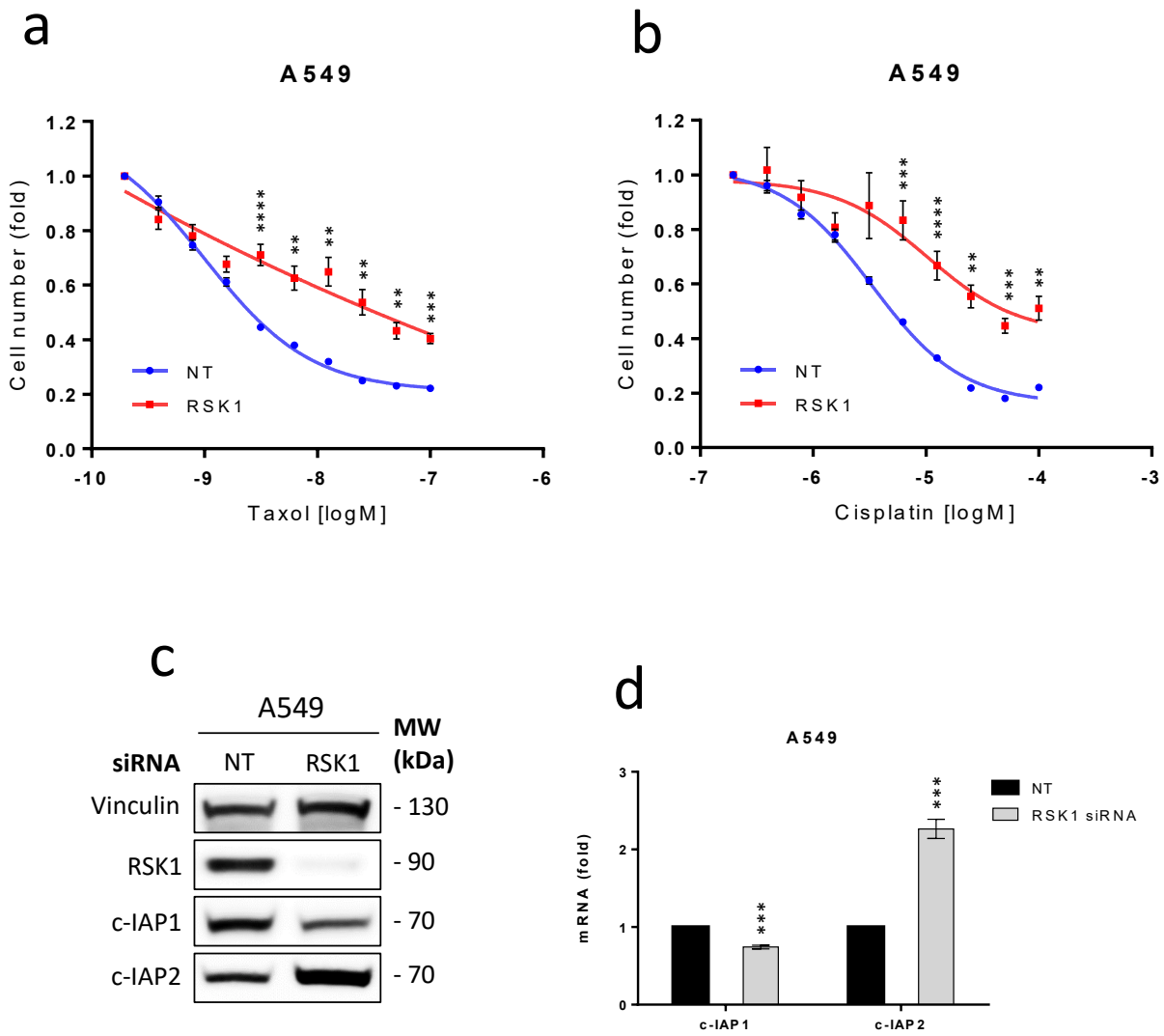

Figure S 2| RSK1 opposes RSK4 chemo-sensitivity effects in lung cancer cells. (a, b) RSK1 silencing increases resistance of A549 cells to paclitaxel (taxol) and cisplatin. Cell viability was determined by crystal violet staining of A549 cells transfected (24-48 h) with a final concentration of 20 nM NT (non-targeting) or RSK1 siRNAs, before treated with 2-fold serially diluted **(a)** paclitaxel (taxol) (0-100 nM) or **(b)** cisplatin (0-100 µM) for 48-72 h. Data plotted as a fold change relative to the untreated NT condition and represent mean ± SEM of three independent biological replicates performed in quadruplicates. **(c)** Immunoblotting of RSK1, c-IAP1 and c-IAP2 in whole cell A549 extracts transfected (48-72 h) with a final concentration of 20 nM NT (non-targeting) or RSK1 siRNAs. Vinculin was used as a loading control. Data are representative of three independent biological replicates. **(d)** qRT-PCR analysis of c-IAP1 (BIRC2) and c-IAP2 (BIRC3) mRNAs in A549 cells transfected (48-72 h) with a final concentration of 20 nM NT (non-targeting) or RSK1 siRNAs. *Ct* values were normalised to HPRT housekeeping gene and shown as a fold change relative to NT control condition. Data represent mean ± SEM of three independent biological replicates performed in triplicates. Statistical significance was assessed by an unpaired Student's *t*-test in GraphPad Prism. **; $P \leq 0.01$, ***; $P \leq 0.001$, ****; $P \leq 0.0001$.

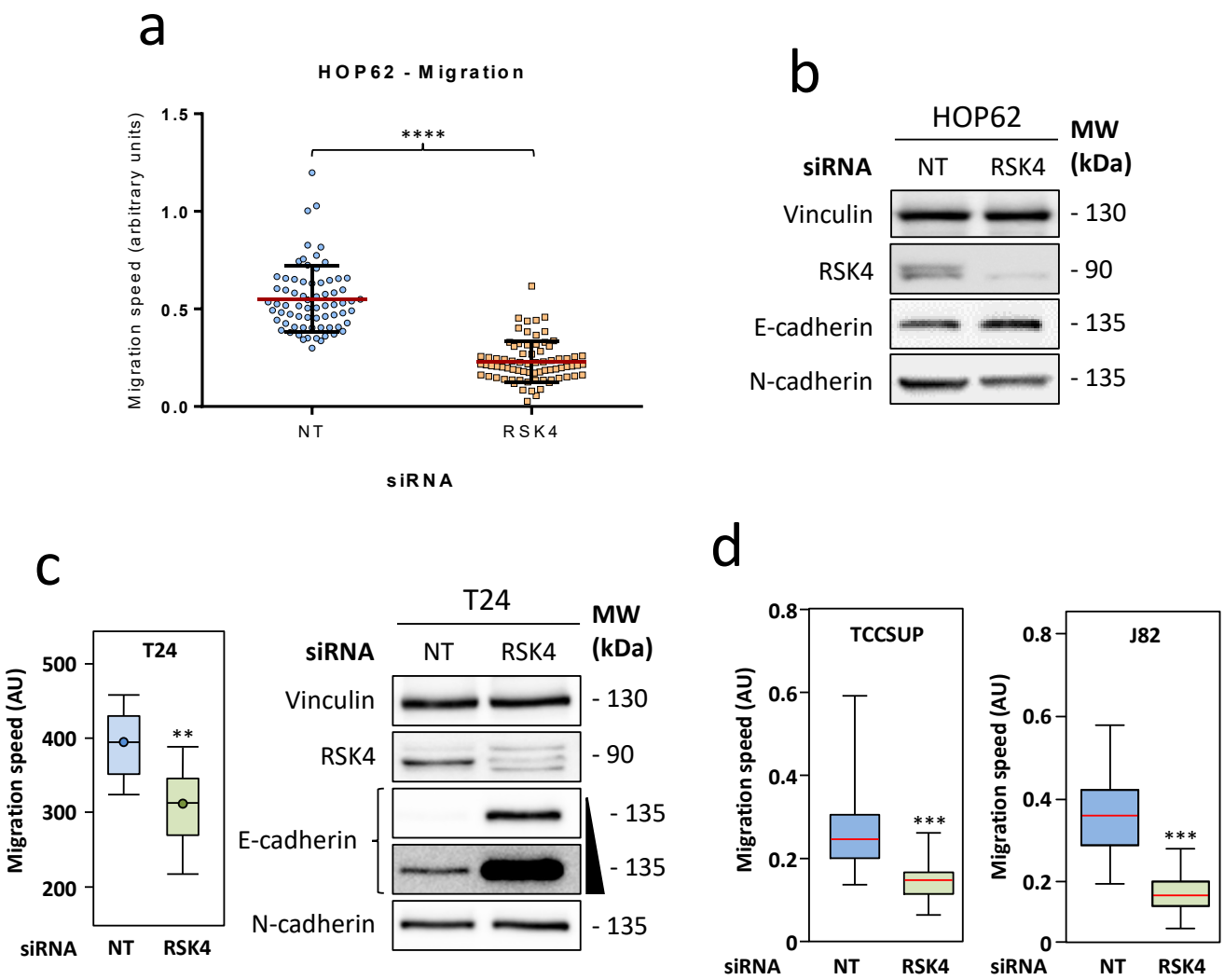

e

Number of colonies																						
Section		#1	#2	#3	#4	#5	#6	#7	#8	#9	#10	Section		#1	#2	#3	#4	#5	#6	#7	#8	#9	#10
A549 mice	#1	>10	>10	>10	>10	>10	>10	>10	>10	>10	>10	cr437 mice	#1	4	4	4	4	4	5	5	5	5	5
	#2	>10	>10	>10	>10	>10	>10	>10	>10	>10	>10		#2	1	1	1	1	1	1	0	0	0	0
	#3	>10	>10	>10	>10	>10	>10	>10	>10	>10	>10		#3	1	1	1	1	0	0	0	1	1	1
	#4	>10	>10	>10	>10	>10	>10	>10	>10	>10	>10		#4	4	4	4	4	5	6	7	6	5	5
	#5	0	0	0	0	0	0	0	0	0	0		#5	1	1	1	1	1	1	1	1	1	1
	#6	>10	>10	>10	>10	>10	>10	>10	>10	>10	>10		#6	2	2	2	2	0	0	0	0	0	0
	#7	>10	>10	>10	>10	>10	>10	>10	>10	>10	>10		#7	1	2	2	2	4	4	4	3	3	3
	#8	0	0	0	0	0	0	0	0	0	0		#8	1	1	1	1	0	0	0	0	1	0

Figure S 3| RSK4 downregulation inhibits lung and bladder cancer cell migration *in vitro*. **(a, c, d)** Migration speed of **(a)** HOP62 (lung), **(c)** T24 (bladder), **(d)** TCCSUP (bladder) and J82 (bladder) cells transfected (24-48 h) with a final concentration of 20 nM NT (non-targeting) or RSK4 siRNAs. Time-lapse brightfield imaging was performed for 18 h (1 image/10 min) (Zeiss Axiovert 100 Inverted Widefield Microscope, MRC, Imperial College London) and migrating cells were tracked manually in FIJI Image-J. Migration speed was analysed using "Cell Migration analysis.R" script written in RStudio 0.99.89 by Dr Olivier Pardo (Division of Cancer, Imperial College London, London, UK; o.pardo@imperial.ac.uk). Data are presented as a **(a)** scatter plot showing migration speed (arbitrary units) of

individual cells or **(c, d)** box plot, and the mean ± SD of three independent biological replicates performed in quintuplicates. **(b & c, right)** Immunoblotting of RSK4, E-cadherin and N-cadherin in whole cell **(b)** HOP62 and **(c, right)** T24 extracts transfected (48-72 h) with a final concentration of 20 nM NT (non-targeting) or RSK4 siRNAs. Vinculin was used as a loading control. Data are representative of three independent biological replicates. **(e)** CRISPR/Cas9-mediated knockout of RSK4 inhibits metastatic dissemination *in vivo* (See **Figure 13**). Table showing the number of tumour nodules (colonies) in each microtome slice/section (N=10) between each A549 (control) or cr437 mouse lung (N=8). Statistical significance was assessed by an unpaired Student's *t*-test in GraphPad Prism. **; $P \leq 0.01$, ***; $P \leq 0.001$, ****; $P \leq 0.0001$.

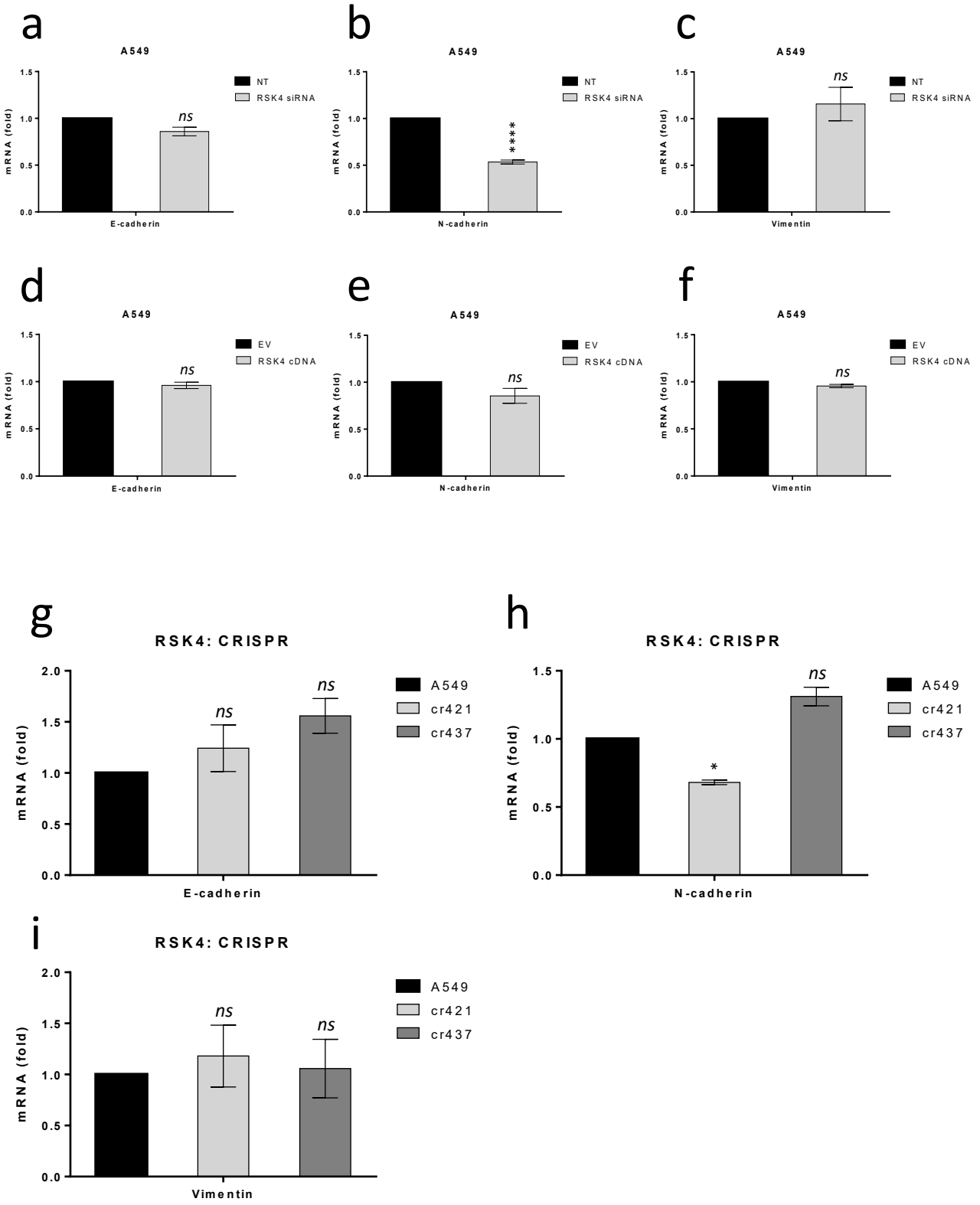

Figure S 4| mRNA expression of EMT markers downstream of RSK4 siRNA knockdown or CRISPR/Cas9 knockout. **(a-i)** qRT-PCR analysis of E-cadherin (CDH1), N-cadherin (CDH2) and Vimentin (VIM) mRNAs in **(a-f)** A549 cells transfected (48-72 h) with **(a-c)** a final concentration of 20 nM NT (non-targeting) or RSK4 siRNAs, **(d-f)** transfected (24-48 h) with a final concentration of 2.5 µg EV (empty vector) or RSK4 cDNAs or in **(g-i)** A549 (control), cr421 (partial RSK4 KO) and cr437 (complete RSK4 KO) cells. *Ct* values were normalised to HPRT housekeeping gene and shown as a fold change relative to NT, EV or A549 control conditions. Data represent mean ± SEM of

three independent biological replicates performed in triplicates. Statistical significance was assessed by an unpaired Student's *t*-test in GraphPad Prism. *ns*; non-significant ($P > 0.05$), *; $P \leq 0.05$, ****; $P \leq 0.0001$.

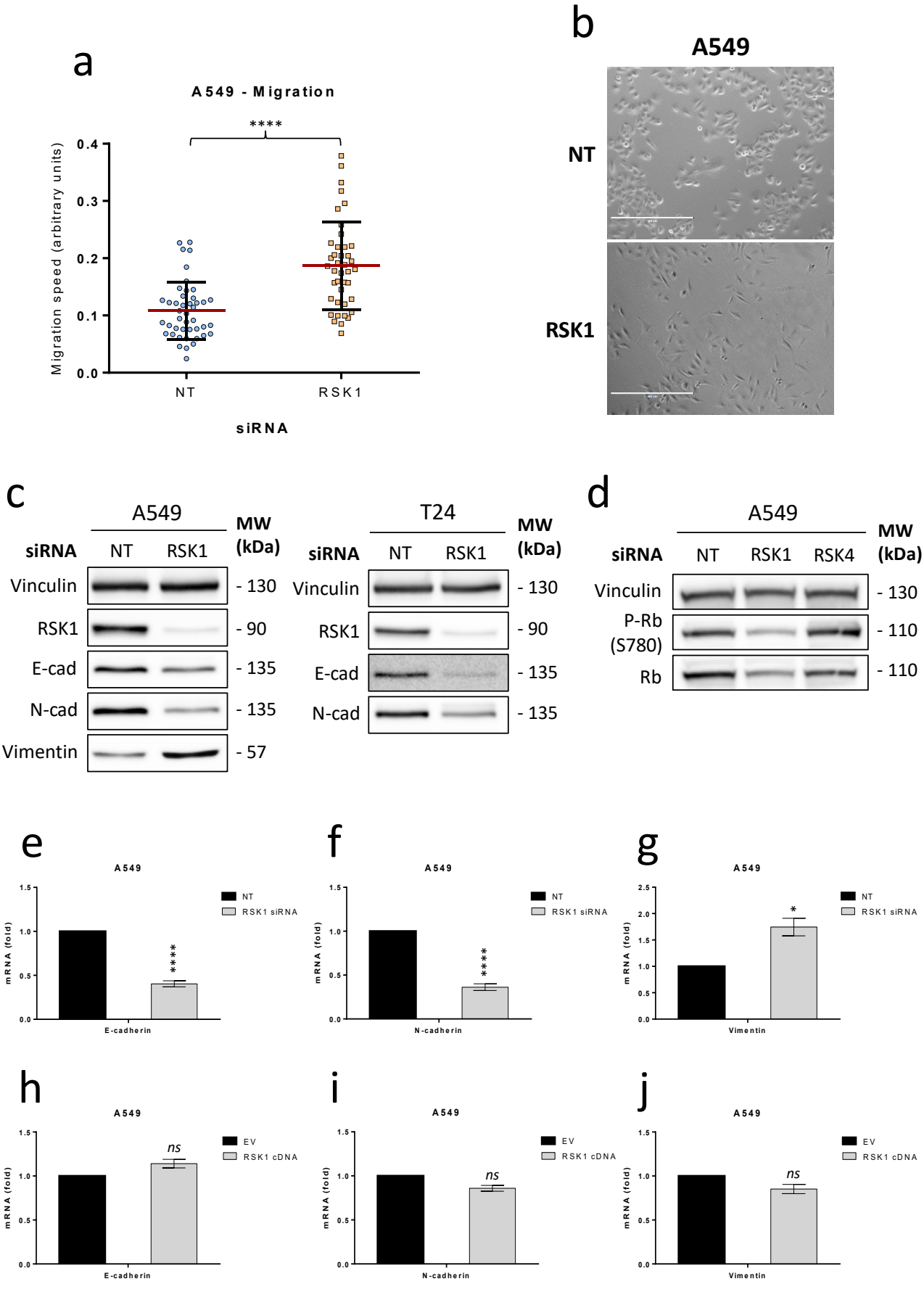
a
A549 - Migration
****
Migration speed (arbitrary units)
0.4
0.3
0.2
0.1
0.0
NT
RSK1
siRNA
b
A549
NT
RSK1
c
A549
siRNA
NT
RSK1
MW (kDa)
Vinculin
- 130
RSK1
- 90
E-cad
- 135
N-cad
- 135
Vimentin
- 57
T24
siRNA
NT
RSK1
MW (kDa)
Vinculin
- 130
RSK1
- 90
E-cad
- 135
N-cad
- 135
d
A549
siRNA
NT
RSK1
RSK4
MW (kDa)
Vinculin
- 130
P-Rb (S780)
- 110
Rb
- 110
e
A549
mRNA (fold)
NT
RSK1 siRNA
****
E-cadherin
f
A549
mRNA (fold)
NT
RSK1 siRNA
****
N-cadherin
g
A549
mRNA (fold)
NT
RSK1 siRNA
*
Vimentin
h
A549
mRNA (fold)
EV
RSK1 cDNA
ns
E-cadherin
i
A549
mRNA (fold)
EV
RSK1 cDNA
ns
N-cadherin
j
A549
mRNA (fold)
EV
RSK1 cDNA
ns
Vimentin

Figure S 5| RSK1 downregulation enhances A549 cell migration *in vitro*. (a) Migration speed of A549 cells transfected (24-48 h) with a final concentration of 20 nM NT (non-targeting) or RSK1 siRNAs. Time-lapse brightfield imaging was performed for 18 h (1 image/10 min) (Zeiss Axiovert 100 Inverted Widefield Microscope, MRC, Imperial College London) and migrating cells were tracked manually in FIJI Image-J. Migration speed was analysed using "Cell Migration analysis.R" script written in RStudio 0.99.89 by Dr Olivier Pardo (Division of Cancer, Imperial College London, London, UK; o.pardo@imperial.ac.uk). Data are presented as a scatter plot showing migration speed (arbitrary units) of individual cells and the mean ± SD of three independent biological replicates performed in quintuplicates. **(b)** Brightfield images of NT (non-targeting) or RSK1 siRNA-transfected A549 cells. (scale bars: 400 µm). **(c)** Immunoblotting of RSK1, E-cadherin, N-cadherin and Vimentin in whole cell A549 (left) or T24 (right) extracts transfected (48-72 h) with a final concentration of 20 nM NT (non-targeting) or RSK1 siRNAs. Vinculin was used as a loading control. Data are representative of three independent biological replicates. **(d)** Immunoblotting of Phospho-Rb (Ser780) and Rb in whole cell A549 extracts transfected (48-72 h) with a final concentration of 20 nM NT (non-targeting), RSK1 or RSK4 siRNAs. Vinculin was used as a loading control. Data are representative of three independent biological replicates. **(e-j)** qRT-PCR analysis of E-cadherin (CDH1), N-cadherin (CDH2) and Vimentin (VIM) mRNAs in A549 cells transfected (48-72 h) with **(e-g)** a final concentration of 20 nM NT (non-targeting) or RSK1 siRNAs, **(h-j)** transfected (24-48 h) with a final concentration of 2.5 µg EV (empty vector) or RSK1 cDNAs. *Ct* values were normalised to HPRT housekeeping gene and shown as a fold change relative to NT or EV control conditions. Data represent mean ± SEM of three independent biological replicates performed in triplicates. Statistical significance was assessed by an unpaired Student's *t*-test in GraphPad Prism. *ns*; non-significant ($P > 0.05$), *; $P \leq 0.05$, ****; $P \leq 0.0001$.

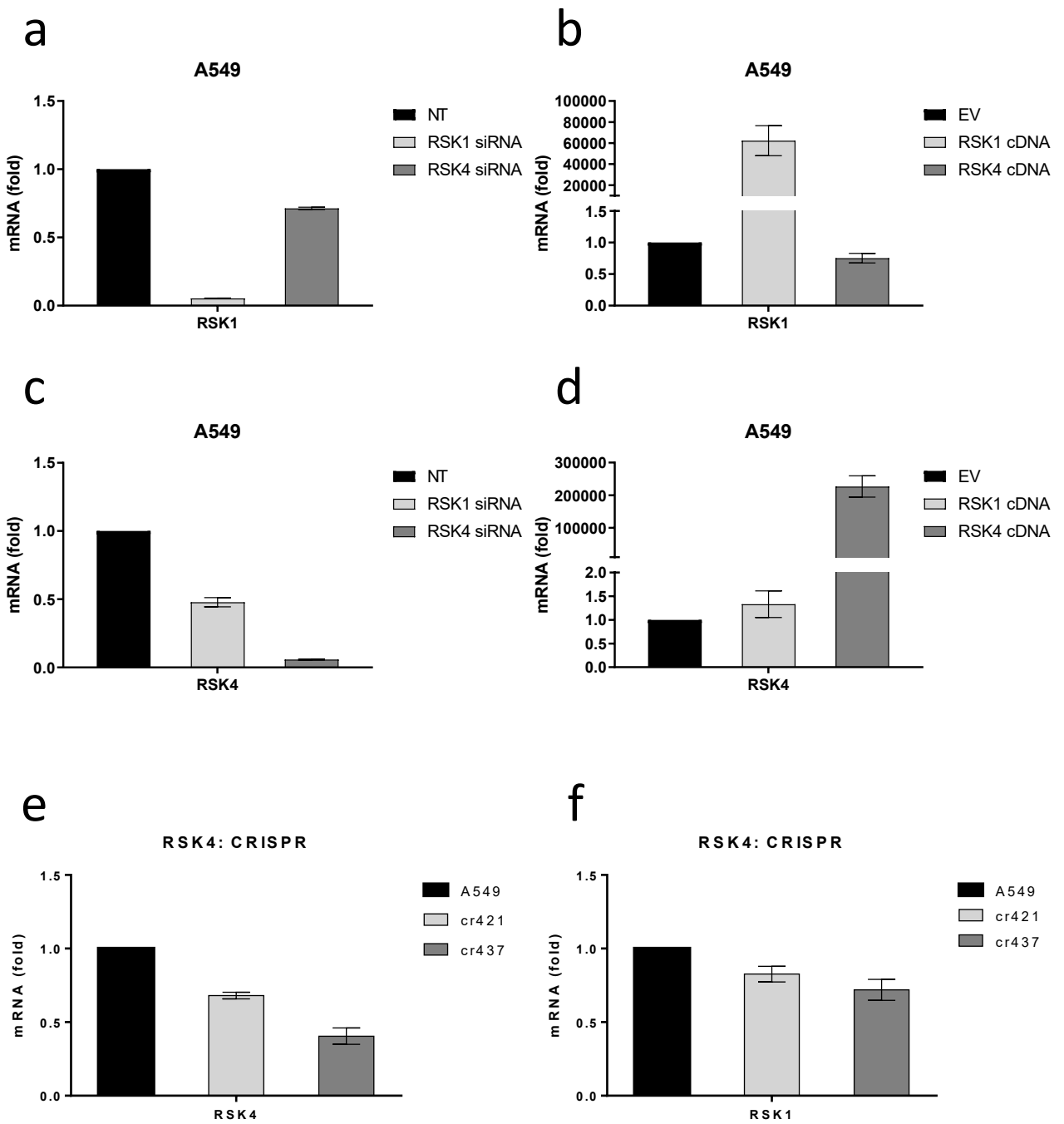

Figure S 6| RSK1 or RSK4 knockdown or overexpression. **(a, b)** qRT-PCR analysis of RSK1 mRNA in A549 cells **(a)** transfected (48-72 h) with a final concentration of 20 nM NT (non-targeting), RSK1 or RSK4 siRNAs or **(b)** transfected (24-48 h) with a final concentration of 2.5 µg EV (empty vector), RSK1 or RSK4 cDNAs. **(c, d)** qRT-PCR analysis of RSK4 mRNA in A549 cells **(c)** transfected (48-72 h) with a final concentration of 20 nM NT (non-targeting), RSK1 or RSK4 siRNAs or **(d)** transfected (24-48 h) with a final concentration of 2.5 µg EV (empty vector), RSK1 or RSK4 cDNAs. **(e, f)** qRT-PCR analysis of **(e)** RSK4 **(f)** RSK1 mRNAs in A549 (control), cr421 (partial RSK4 KO) and cr437 (complete RSK4 KO) cells. *Ct* values were normalised to HPRT housekeeping gene and shown as a fold change relative to NT or EV control conditions. Data represent mean ± SEM of three independent biological replicates performed in triplicates.

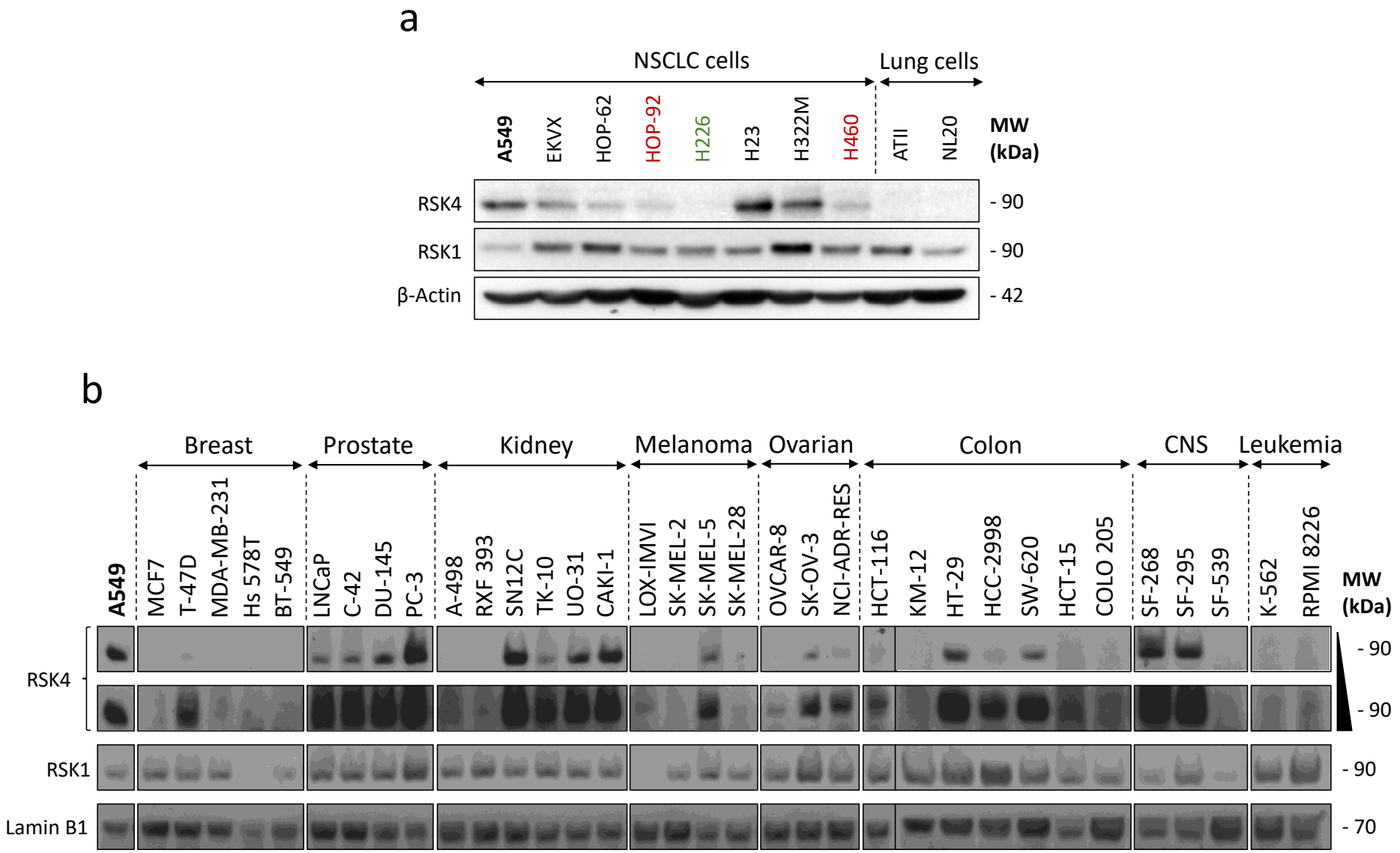
a
NSCLC cells
Lung cells
A549
EKVX
HOP-62
HOP-92
H226
H23
H322M
H460
ATII
NL20
MW (kDa)
RSK4
RSK1
β-Actin
- 90
- 90
- 42
b
Breast
Prostate
Kidney
Melanoma
Ovarian
Colon
CNS
Leukemia
A549
MCF7
T-47D
MDA-MB-231
Hs 578T
BT-549
LNCaP
C-42
DU-145
PC-3
A-498
RXF 393
SN12C
TK-10
UO-31
CAKI-1
LOX-IMVI
SK-MEL-2
SK-MEL-5
SK-MEL-28
OVCAR-8
SK-OV-3
NCI-ADR-RES
HCT-116
KM-12
HT-29
HCC-2998
SW-620
HCT-15
COLO 205
SF-268
SF-295
SF-539
K-562
RPMI 8226
MW (kDa)
RSK4
RSK1
Lamin B1
- 90
- 90
- 90
- 70

Figure S 7| RSK1 and RSK4 expression in a panel of NCI-60 human tumour cell lines. (a) RSK4 is overexpressed in lung cancer cell lines compared to normal lung cells. Immunoblotting of RSK1 and RSK4 in a panel of non-small cell lung cancer (NSCLC) cell lines versus normal lung cells. Lung adenocarcinoma (LUAD) cells: A549, EKVX, HOP-62, H23 and H322M; large cell carcinoma (LCC) cells: HOP-92 and H460; lung squamous cell carcinoma (LUSC) cells: H226; normal lung cells: ATII (alveolar type II pneumocytes) and NL20 (bronchial epithelium). β-Actin was used as a loading control (See **Table S 10**). **(b)** Immunoblotting of RSK1 and RSK4 in a panel of NCI-60 cancer cell lines. Lysates were run on the E-PAGE™ 48 Protein Electrophoresis System (Invitrogen™). Lamin B1 was used as a loading control (See **Table S 11**). The work presented here was performed by Devmini Moonamale (personal communication).

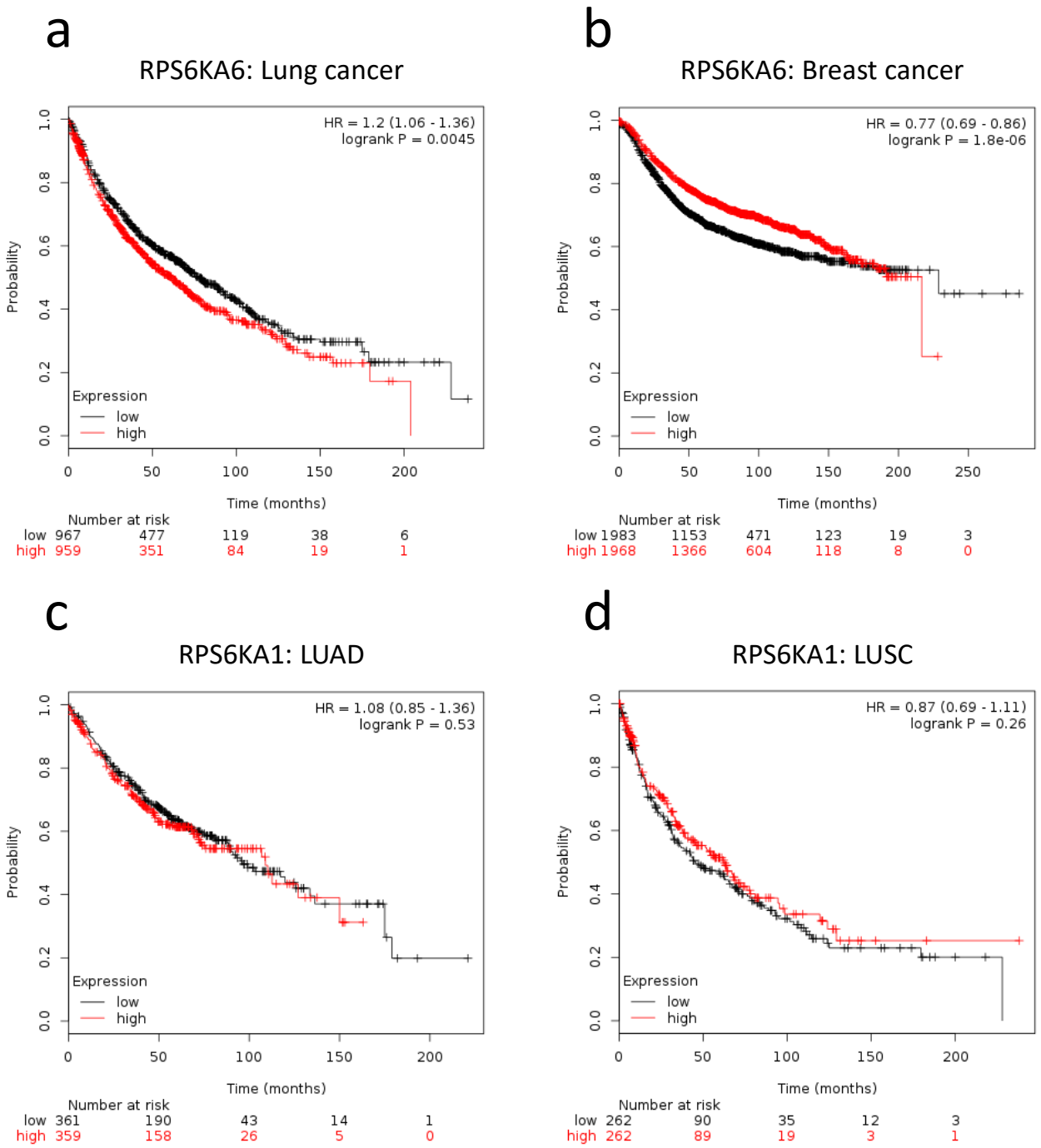

Figure S 8| Kaplan-Meier survival analysis of RSK1 and RSK4. **(a, b)** Kaplan-Meier plot of *RPS6KA6* (RSK4) mRNA expression (gene chip) in **(a)** lung cancer (P=4.5×10^{-3}) and **(b)** breast cancer (P=1.8×10^{-6}) patients. **(c, d)** Kaplan-Meier plot of *RPS6KA1* (RSK1) mRNA expression (gene chip) in **(c)** lung adenocarcinoma (LUAD) (non-significant) and **(d)** lung squamous cell carcinoma (LUSC) (non-significant) patients (Nagy et al., 2018).

8.3 Chapter 4

8.3.1 Supplementary Figures

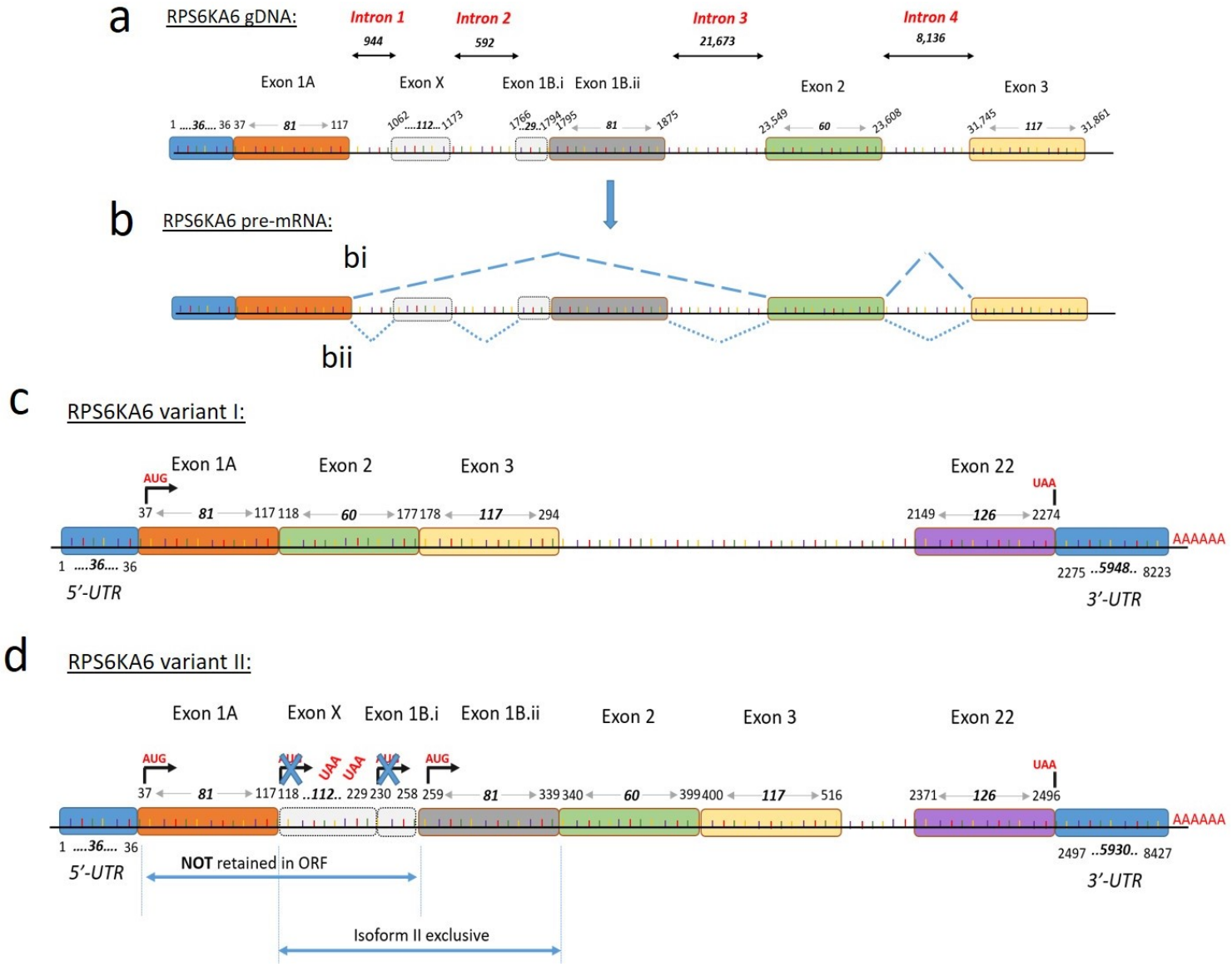
a
RPS6KA6 gDNA:
Intron 1
944
Intron 2
592
Intron 3
21,673
Intron 4
8,136
Exon 1A
Exon X
Exon 1B.i
Exon 1B.ii
Exon 2
Exon 3
b
RPS6KA6 pre-mRNA:
bi
bii
c
RPS6KA6 variant I:
Exon 1A
Exon 2
Exon 3
Exon 22
AUG
UAA
AAAAAA
5'-UTR
3'-UTR
d
RPS6KA6 variant II:
Exon 1A
Exon X
Exon 1B.i
Exon 1B.ii
Exon 2
Exon 3
Exon 22
NOT retained in ORF
Isoform II exclusive

Figure S 9| Mapping RSK4 transcript variants based on NCBI RefSeq data. **(a)** Part of *RPS6KA6* (RSK4) genomic DNA (gDNA) illustrating the exons involved in the alternative splicing: Exon X, Exon 1B.i and Exon 1B.ii. **(b)** RSK4 pre-mRNA undergoes alternative splicing and either **(bi)** skips Exon X, Exon 1B.i and Exon 1B.ii and gives rise to **(c)** RSK4 variant I, or **(bii)** not, to give rise to **(d)** RSK4 variant II. **(c)** RSK4 variant I represents the 'canonical' isoform where protein translation starts from Exon 1A. **(d)** Due to the presence of two stop codons (UAA) in Exon X and the absence of start codons (AUG) in Exon X or Exon 1B.i, translation starts from Exon 1B.ii in RSK4 variant II.

→ Therefore, at the protein level, these variants differ only in the first exon (i.e. 81 bp; coding for the first 27 aa).

→ RSK4 variant II was PCR-cloned with a forward primer starting from Exon 1B.ii.

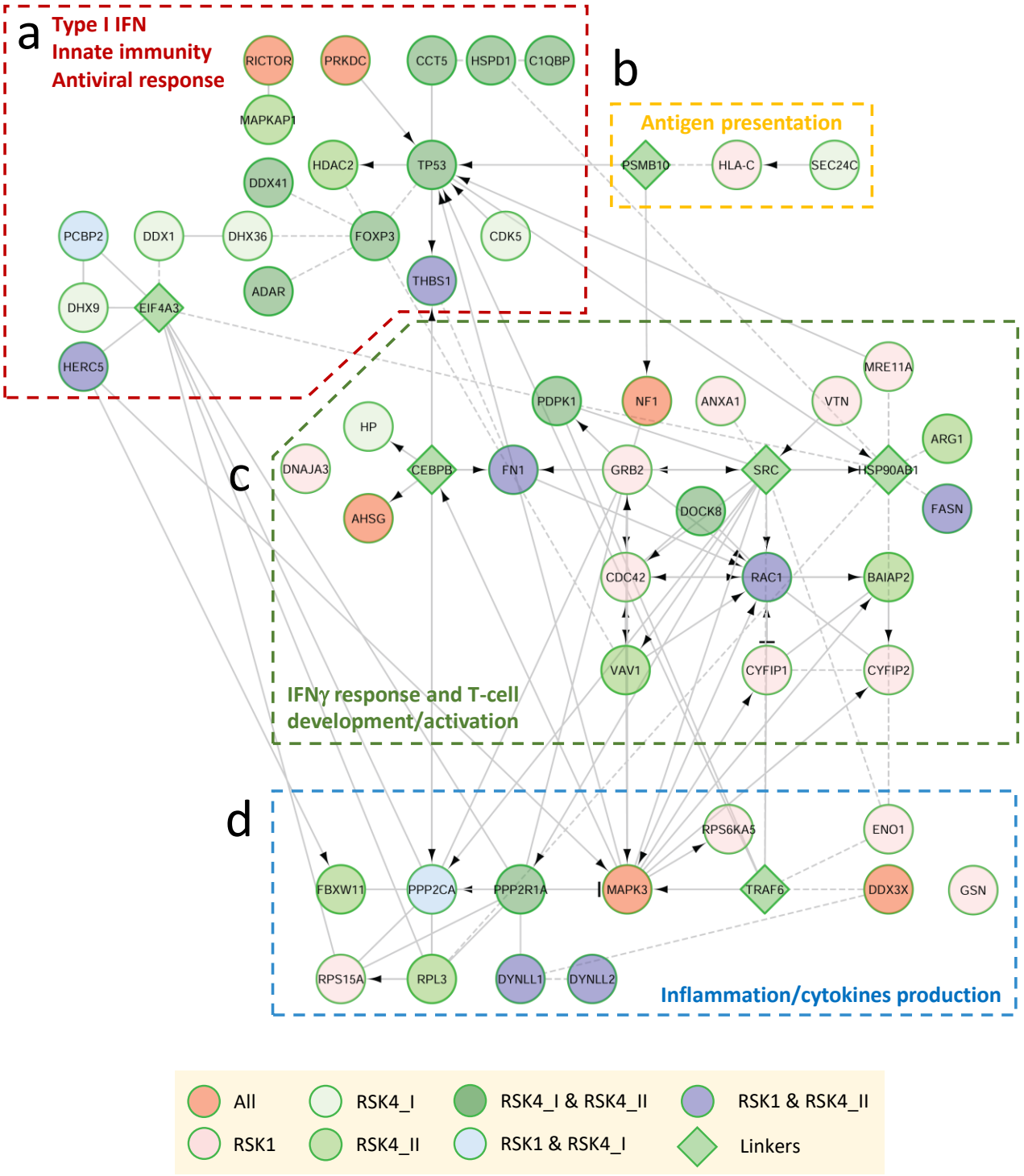

Figure S 10| RSK1 and RSK4 interact with proteins involved in immune response. RSK1, RSK4 variant I and RSK4 variant II were affinity purified from HEK293A cells and complexes were analysed by LC-MS/MS. LC-MS/MS data were searched against the human protein database UniProtKB/Swiss-Prot and integrated into signalling networks following Cytoscape analysis: **(a)** Type I IFN, Innate immunity and Antiviral response, **(b)** Antigen presentation, **(c)** IFNγ response and T-cell development/activation, **(d)** Inflammation and cytokines production. Arrows indicate positive regulation whereas blunt arrows indicate negative regulation. LC-MS/MS was performed by Mark Skehel (collaboration) and pathway analysis by Olivier Pardo (personal communication).

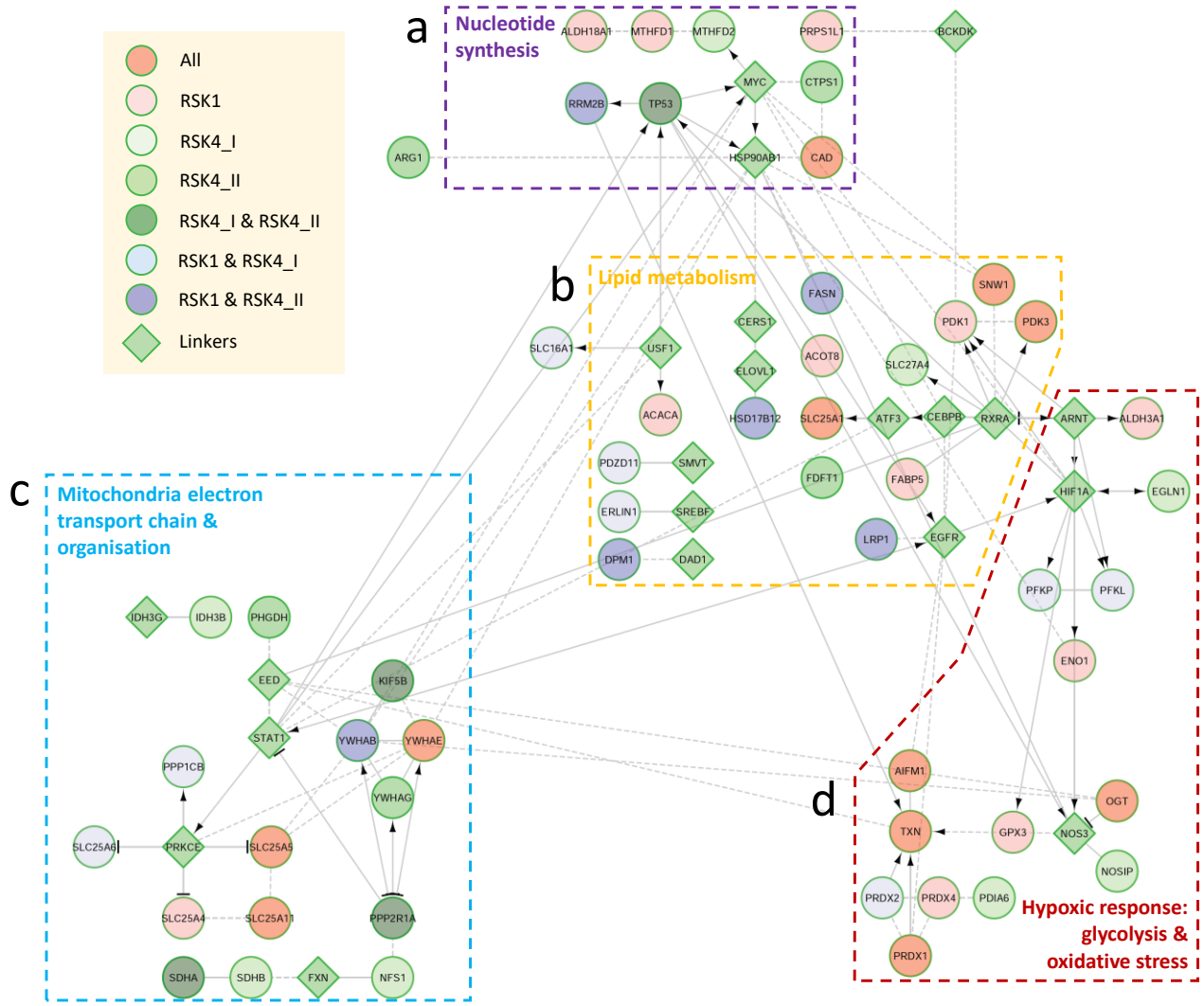

Figure S 11| RSK1 and RSK4 interact with proteins involved in metabolic pathways. RSK1, RSK4 variant I and RSK4 variant II were affinity purified from HEK293A cells and complexes were analysed by LC-MS/MS. LC-MS/MS data were searched against the human protein database UniProtKB/Swiss-Prot and integrated into signalling networks following Cytoscape analysis: **(a)** Nucleotide synthesis, **(b)** Lipid metabolism, **(c)** Mitochondria electron transport chain & organisation, **(d)** Hypoxic response: glycolysis & oxidative stress. Arrows indicate positive regulation whereas blunt arrows indicate negative regulation. LC-MS/MS was performed by Mark Skehel (collaboration) and pathway analysis by Olivier Pardo (personal communication).

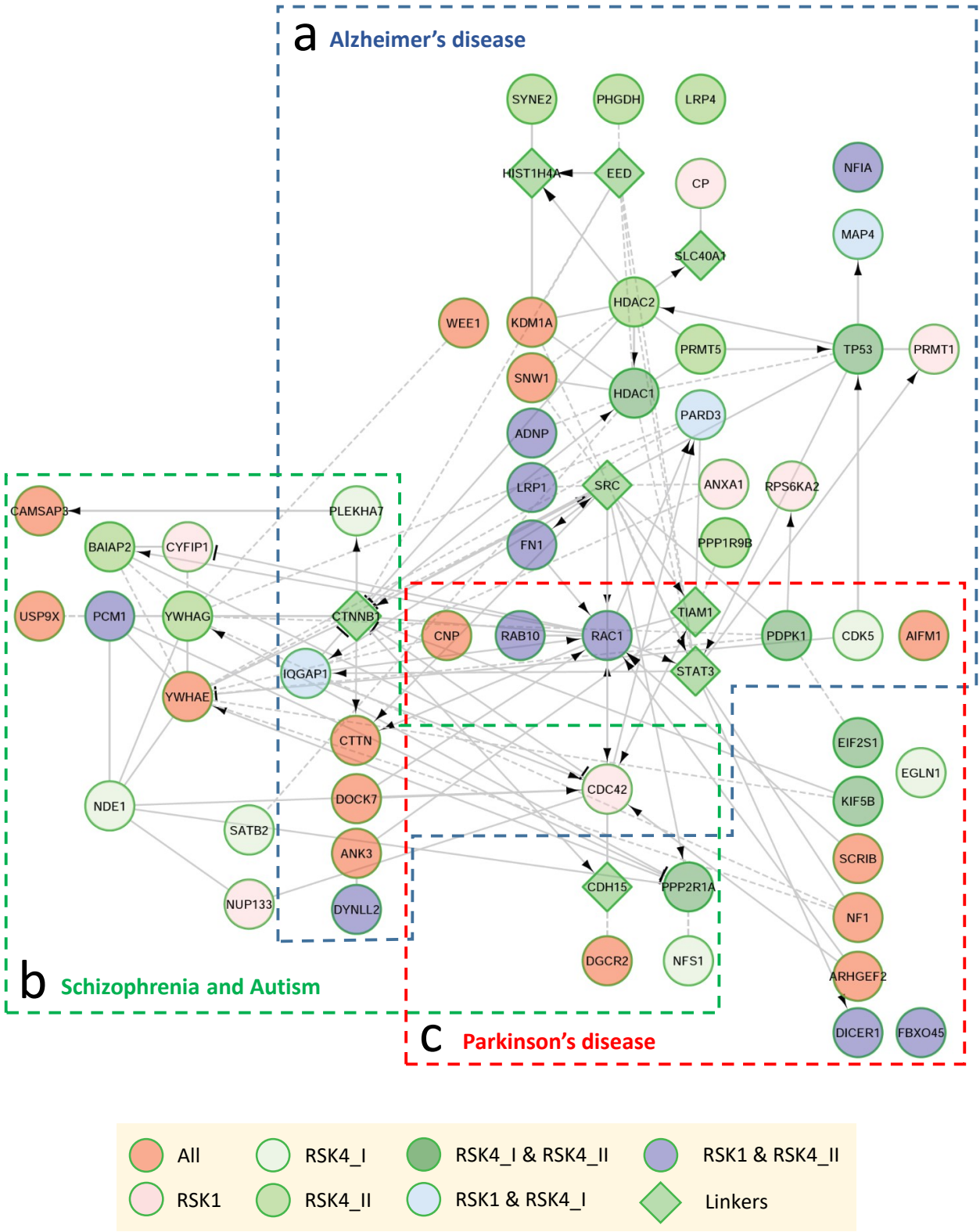

Figure S 12| RSK1 and RSK4 interact with proteins involved in neurodegeneration pathways. RSK1, RSK4 variant I and RSK4 variant II were affinity purified from HEK293A cells and complexes were analysed by LC-MS/MS. LC-MS/MS data were searched against the human protein database UniProtKB/Swiss-Prot and integrated into signalling networks following Cytoscape analysis: **(a)** Alzheimer's disease, **(b)** Schizophrenia and Autism, **(c)** Parkinson's disease. Arrows indicate positive regulation whereas blunt arrows indicate negative regulation. LC-MS/MS was performed by Mark Skehel (collaboration) and pathway analysis by Olivier Pardo (personal communication).

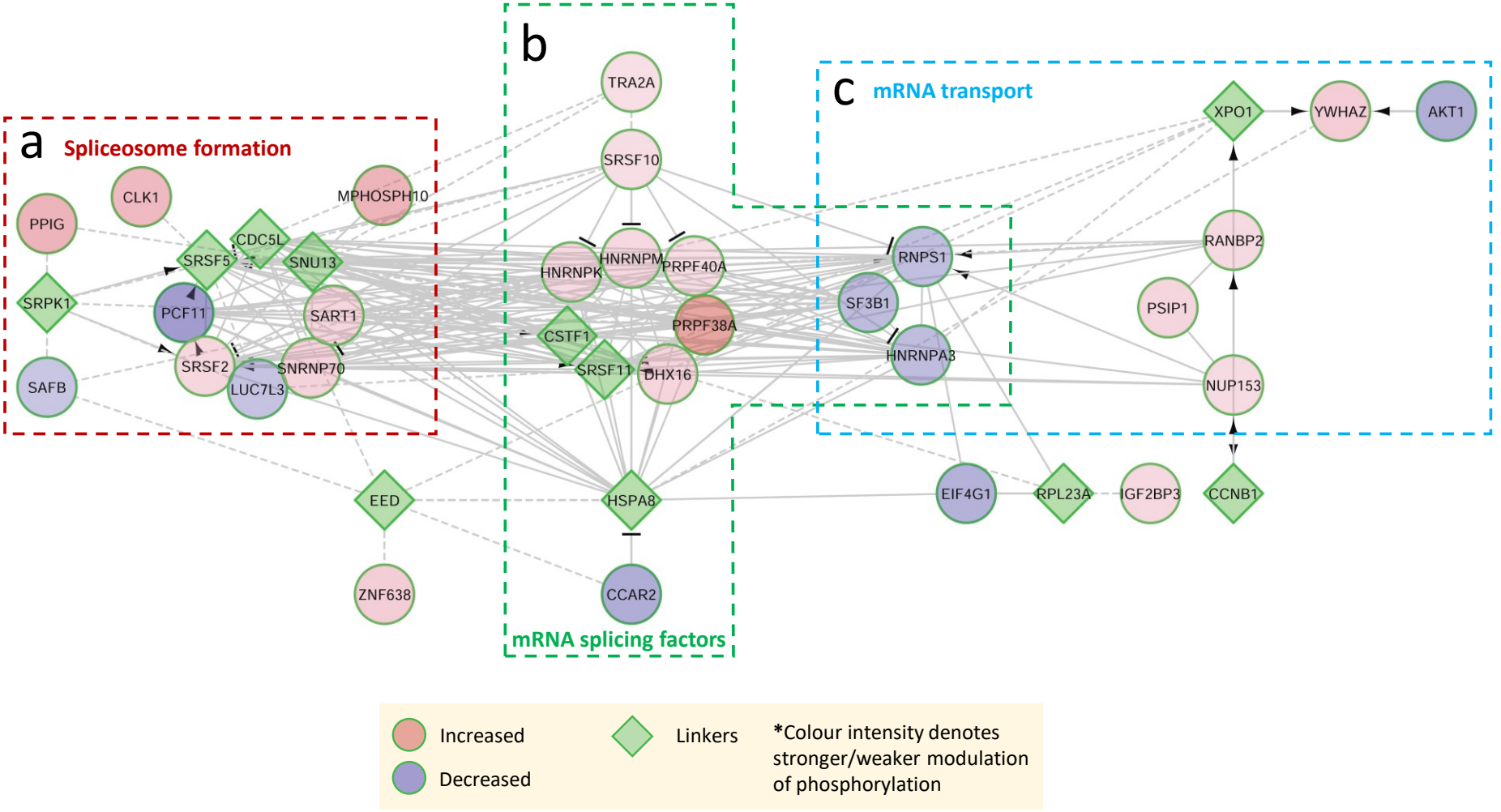

Figure S 13| RSK4 modulates the phosphorylation of proteins involved in mRNA splicing and transport. RSK4 was transiently downregulated in A549 cells, lysates were trypsin digested and labelled with tandem mass tag (TMT) isobaric labelling reagents. Pooled and labelled samples (80%) were subjected to IMAC phosphopeptide enrichment and analysed by LC-MS/MS. LC-MS/MS data were searched against the human protein database UniProtKB/Swiss-Prot and integrated into signalling networks following Cytoscape analysis: **(a)** Spliceosome formation, **(b)** mRNA splicing factors, **(c)** mRNA transport. Arrows indicate positive regulation whereas blunt arrows indicate negative regulation. LC-MS/MS was performed by Howard Desmond and Paul Huang (collaboration) and pathway analysis by Olivier Pardo (personal communication).

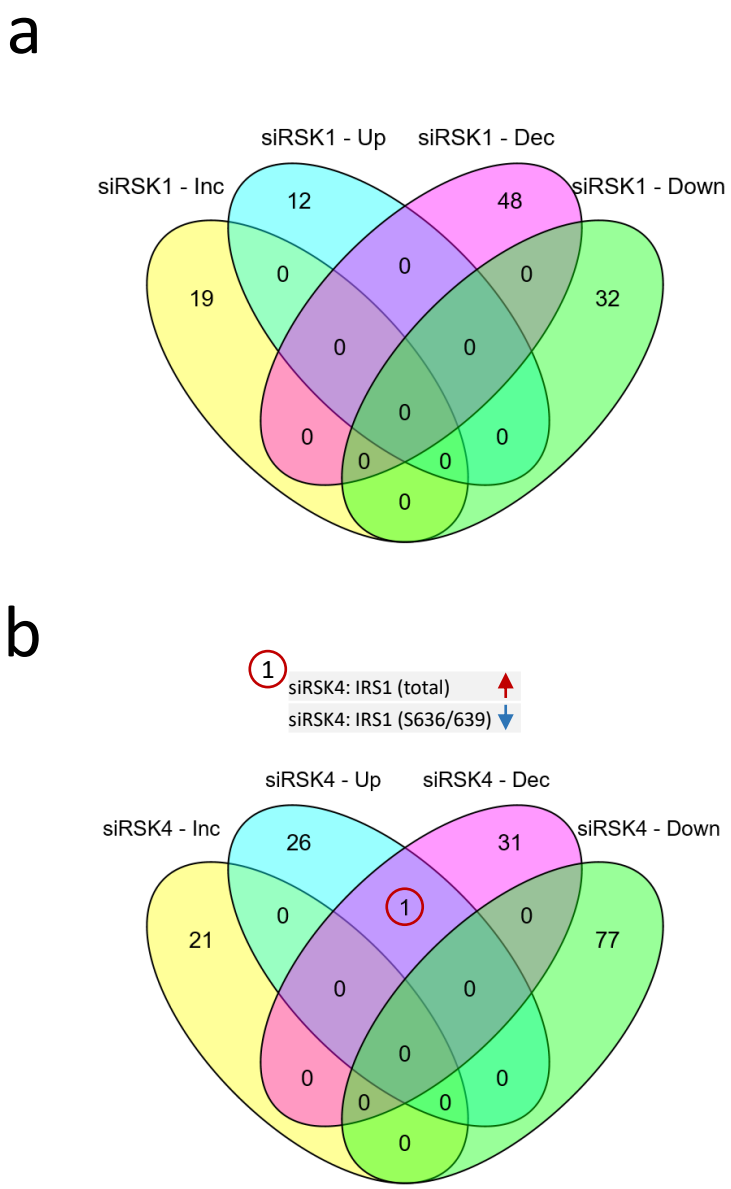

Figure S 14| Identification of common phosphoproteomics and total proteomics hits. **(a)** Venn diagram of RSK1 increased phosphorylation (siRSK1 - Inc), upregulated (siRSK1 - Up), decreased phosphorylation (siRSK1 - Dec) and downregulated (siRSK1 - Down) hits. **(b)** Venn diagram of RSK4 increased phosphorylation (siRSK4 - Inc), upregulated (siRSK4 - Up), decreased phosphorylation (siRSK4 - Dec) and downregulated (siRSK4 - Down) hits: Insulin receptor substrate 1 (IRS1: Ser636/639).

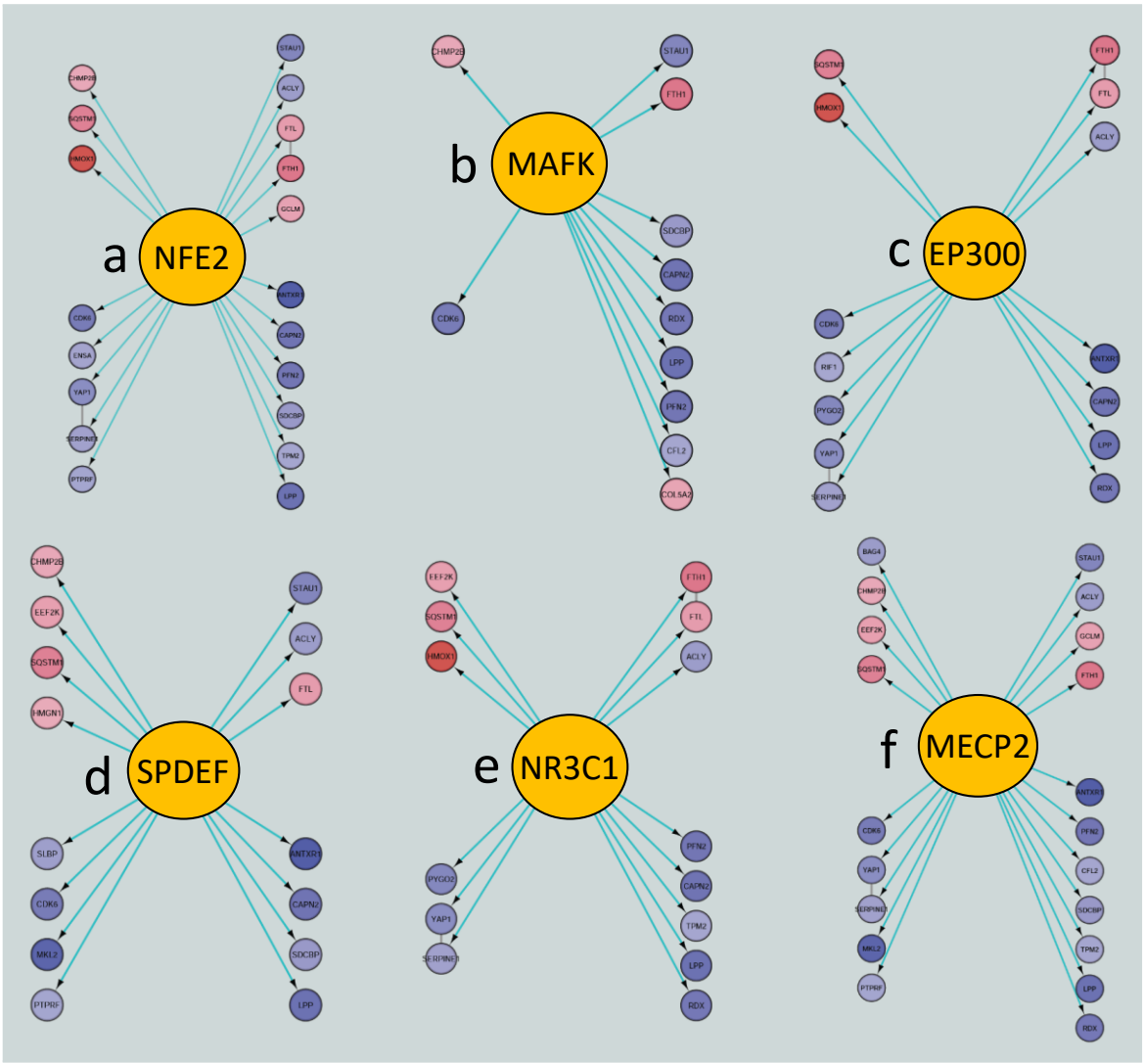

Figure S 15| Transcription factor analysis of RSK4 total proteomics hits. RSK4 was transiently downregulated in A549 cells, lysates were trypsin digested and labelled with tandem mass tag (TMT) isobaric labelling reagents. Pooled and labelled samples (20%) were fractionated by strong cation-exchange (SCX) chromatography and analysed by LC-MS/MS. LC-MS/MS data were searched against the human protein database UniProtKB/Swiss-Prot followed by transcription factor analysis using the iRegulon plugin of Cytoscape. Predicted transcription factors that could explain most changes are: **(a)** NFE2, **(b)** MAFK, **(c)** Histone acetyltransferase EP300, **(d)** SPDEF, **(e)** Glucocorticoid receptor NR3C1 and **(f)** MECP2. Red colour denotes upregulation and blue colour denote downregulation, while colour intensity indicates stronger/weaker upregulation or downregulation. The work presented here was performed by Olivier Pardo (personal communication).

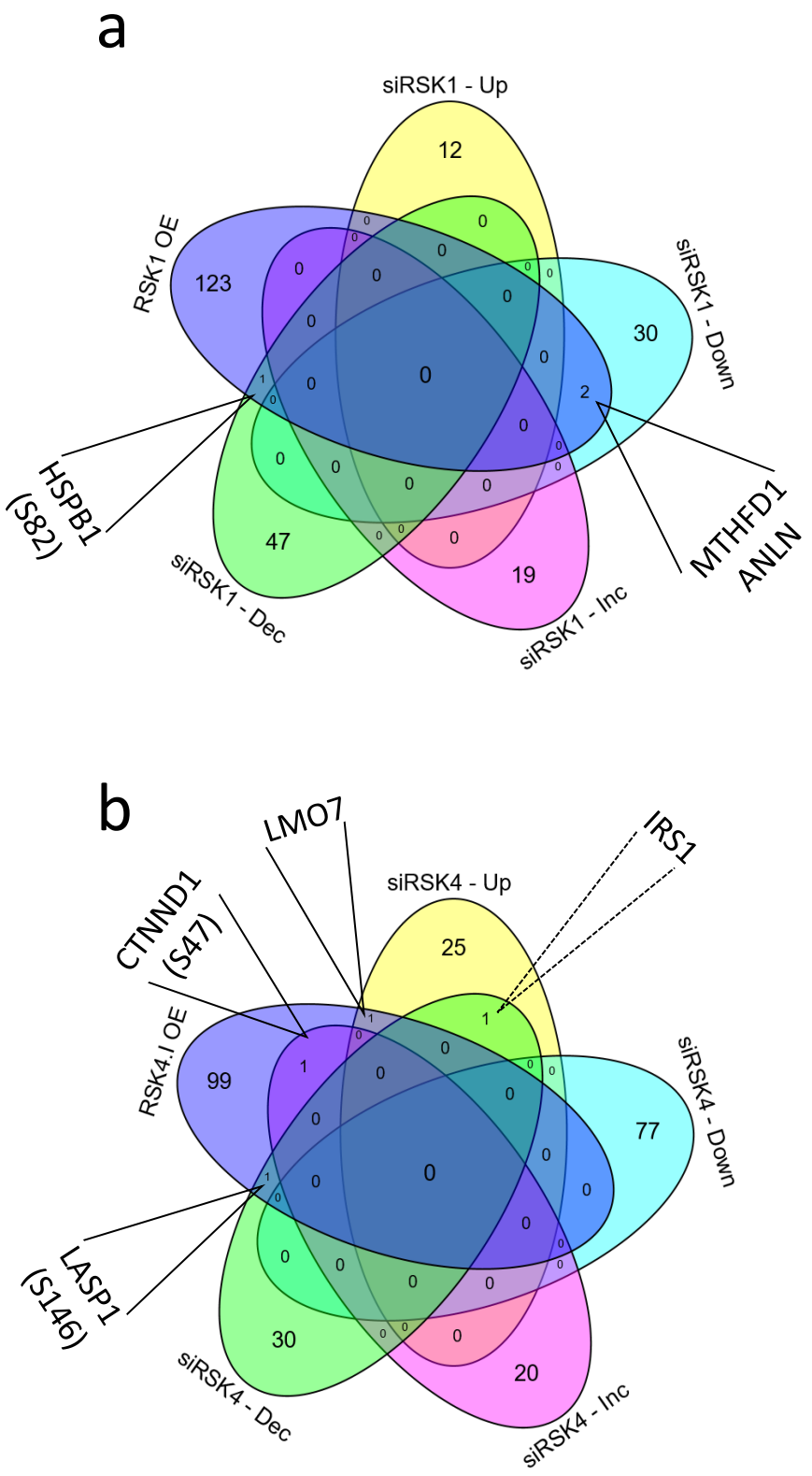

Figure S 16| Identification of shared hits between tandem affinity purification and phosphoproteomics/proteomics screens. **(a)** Venn diagram of RSK1 interacting partners (RSK1 OE [overexpression] & affinity purification) integrated with RSK1 upregulated (siRSK1 - Up), downregulated (siRSK1 - Down), increased phosphorylation (siRSK1 - Inc) and decreased phosphorylation (siRSK1 - Dec) hits: Heat shock protein 27 (HSP27 or HSPB1: Ser82); C-1-tetrahydrofolate synthase (MTHFD1); Anillin (ANLN). **(b)** Venn diagram of RSK4 interacting partners (RSK4 OE [overexpression] & affinity purification) integrated with RSK4 upregulated (siRSK4 - Up), downregulated (siRSK4 - Down), increased phosphorylation (siRSK4 - Inc) and decreased phosphorylation (siRSK4 - Dec) hits: LIM and SH3 protein 1 (LASP1: Ser146); catenin delta-1 (CTNND1 or p120-catenin: Ser47); LIM domain only protein 7 (LMO7); Insulin receptor substrate 1 (IRS1).

8.3 Chapter 4

8.3.2 Supplementary Tables

Table S 15| RSK1 exclusive tandem affinity purification hits – LC-MS/MS

RSK1 affinity purification									
ABHD12	BAT3	CSNK2A2	FIBP	HNRNPA2B1	MYO1B	PSMA7	RPS5	SPRR3	TUBA1A
ACOT8	BRD2	CSNK2B	FYCO1	HSP40: DNAJA3	MYO6	PSMB2	RPS6KA1	SRP14	U2AF1
ACTA1	C18orf24	CYFIP1	GANAB	HSP40: DNAJB1	NDUFA10	PSMD1	RPS6KA2	SRPRB	UPF1
AHNAK2	CCAR2	CYFIP2	GPRASP2	HSP40: DNAJC19	NDUFA3	PSMD6	RPS6KA3	STRAP	VPS29
AHSA1	CDC42	DHX15	GPX3	HSPA6 (HSP70)	NEURL4	PSMD7	RPS6KA5	SUPT16H	VTN
AIP	CENPF	DHX9	GRAMD1B	HSPB1 (HSP27)	NUP133	PTPMT1	RPS6KA6	TAF4	WAPAL
ALDH18A1	CMTR1	DMXL2	GRB2	ILF2	NUP155	RAP1B	SAR1A	TCAF1	WDR11
ALDH3A1	COA7	DNAH8	GSN	KDR	NUP205	RPL10	SFXN4	TCEB2	WDR6
ANLN	COPA	EHBP1	GTF3C3	KIAA1542	PDK1	RPL27	SLC25A4	THBS2	WDR7
ANXA1	CP	EIF3G	HIC2	MAP2K6	PPL	RPS14	SMC1A	TRAPPC10	ZNF90
AZI1	CRNN	EIF3S9	HLA-C	MIC13	PRDX4	RPS15A	SMC2L1	TRAPPC3	ZSWIM4
BABAM1	CSDE1	ENO1	HNRNPA0	MRE11A	PRMT1	RPS18	SNRPD2	TRAPPC9	
BAG2	CSNK2A1	FABP5	HNRNPA1	MTHFD1	PRPS1L1	RPS23	SNRPD3	TTF2	

→ Colour coding system groups proteins that belong to the same family

Table S 16| RSK4 variant I exclusive tandem affinity purification hits – LC-MS/MS

RSK4 variant I affinity purification							
ABCB5	CTNND1	EIF4G3	HP	MAP7	PLEKHA1	SDHB	TRIM33
ABL2	CYTH3	ELAVL1	HSDL2	MAP7D2	PLEKHA6	SEC24C	TTK
ACTR10	DCTN5	EPRS	IDH3B	MAP7D3	PLEKHA7	SFXN2	UQCRC2
ACTR1B	DDX1	ERC1	IGSF10	MARK3	PLS3	SLC27A4	VPS4A
ATAD3A	DDX39A	FAM179B	IPO5	NDE1	PTPN23	SLFN11	WDFY3
ATAD5	DECR2	FAM83B	ITIH6	NEDD4L	RCN1	SLFN5	XPO1
C14orf166	DHX34	FAM98B	KDM3B	NFS1	RFC3	SPRED2	YTHDF2
C1orf22	DHX36	FUS	KIF16B	NOSIP	RNASEN	SPTLC1	ZBTB40
CCDC168	DNAJA1 (HSP40)	GALK1	KIF7	NUP153	RPS2	SRSF3	ZC3H7B
CDK12	EDRF1	HNRNPC	KIFC1	PALLD	RPS6KA1	STPG2	ZCCHC11
CDK5	EGLN1	HOMER2	LASP1	PARS2	RPS6KA6	STUB1	ZMYM5
CSE1L	EIF3F	HOMER3	LIMK2	PDCD2L	RRBP1	THSD4	ZNF598
CSNK1A1	EIF3I	HOOK2	LMO7	PDIA6	SATB2	TRIB3	

→ Colour coding system groups proteins that belong to the same family

Table S 17| RSK4 variant II exclusive tandem affinity purification hits – LC-MS/MS

RSK4 variant II affinity purification								
ABCF2	C1R	DNAJC7 (HSP40)	HUWE1	MTPAP	PPP1R9B	RNGTT	SLC25A12	VPS13A
ABI2	C2orf44	DNASE1L3	HYI	MUC19	PPP6R1	RPL13A	SNRPE	XRN2
AK6	CAMK2D	DOCK4	IQCB1	NEXN	PPP6R3	RPL19	SNRPF	YWHAG
AKNAD1	CBX3	EDC3	KANK2	NKTR	PRC1	RPL3	STAU1	ZNF639
ANKRD26	CEP250	EIF3D	LACRT	NUP214	PRMT5	RPL4	STK38	
ARG1	CHD5	FBXW11	LCN1	NXF1	PRPF19	RPL8	SYNE1	
ASCC3	CHID1	FXR1	LMNA	OBSL1	PRPF3	RPS29	SYNE2	
ATAD3B	CPSF7	G3BP2	LRP4	PABPC1	PRPF31	RPS6KA1	TCP1	
ATP5A1	CSTA	GTF3C5	MAPKAP1	PACSIN2	PTBP1	RPS6KA6	TMPO	
ATP5J2-PTCD1	CTPS1	GTPBP2	MATR3	PHF5A	RCC2	RYR2	TOMM20	
BAIAP2	DNAH1	HDAC2	MCMBP	PHGDH	RFC5	SF1	UBE3C	
BAIAP2L1	DNAJB4	HNRNPK	MRS2	POLD2	RHBDF2	SF3B2	UTP15	
BSN	DNAJC11 (HSP40)	HTATSF1	MTMR4	POLDIP3	RIF1	SKIV2L2	VAV1	

→ Colour coding system groups proteins that belong to the same family

Table S 18| RSK1/RSK4 variant I/RSK4 variant II shared tandem affinity purification hits – LC-MS/MS

RSK1/RSK4.I/RSK4.II affinity purification							
ACOT9	CAMSAP3	DDX3X	KDM1A	PGAM5	SCRIB	TUBB2A	ZNF318
AHNAK	CAPZA1	DDX5	KIAA0528	PHLDB2	SEC16A	TUBB2C	
AHSG	CAPZA2	DGCR2	KIF1A	PLEKHA5	SERBP1	TUFM	
AIFM1	CAPZB	DOCK7	MAPK3/ERK1	POLD1	SETX	TXN	
ANK3	CC2D1A	FLG2	MIBP1	POLD3	SFPQ	USP9X	
ARAF	CDC2	FLNA	MLLT4	PPP6R2	SHROOM3	WEE1	
ARHGAP21	CDC37	GCDH	MYCBP2	PRDX1	SLC25A1	WWP2	
ARHGEF2	CEP170	GTSE1	NEK1	PRKDC	SLC25A11	XRN1	
ATAD3A	CKAP4	HNRNPH1	NF1	PRRC2A	SLC25A13	YWHAE	
BUB1B	CNP	HNRNPU	NUMA1	RICTOR	SLC25A3	YWHAZ	
BUB3	CTBP2	HNRNPF	OGT	ROCK2	SLC25A5	ZBTB21	
C21orf2	DDB1	HRNR	PCBP1	RPS11	SNW1	ZFYVE16	
CAD	DDX17	HSPA9 (HSP70)	PDK3	RPS3A	TTN	ZNF198	

→ Colour coding system groups proteins that belong to the same family

Table S 19| RSK1/RSK4 variant II shared tandem affinity purification hits – LC-MS/MS

RSK1/RSK4.II affinity purification					
ADNP	FAM193A	ISOC1	PRPF8	RPS7	TPR
ANKRD28	FAM21A	KIAA0196	RAB10	RRM2B	TRIM28
ANKRD52	FAM21C	KIAA1033	RAC1	RUVBL1	TRIM41
ATG2B	FASN	LRP1	RCOR1	RUVBL2	UBR5
CCDC53	FAT1	MTBP	RCOR2	SEC61A1	WASH
DICER1	FBXO45	MYO10	RCOR3	SEC61B	WASH2P
DPM1	FGFR3	NCKAP1	RPL10A	SHROOM1	YWHAB
DST	FN1	NDUFA4	RPL26L1	SKA2	
DYNLL1	GTF2I	NHSL2	RPL31	SKA3	
DYNLL2	GTF3C1	PCM1	RPL35A	SNRNP200	
EMD	GTF3C2	PHB2	RPL38	SSBP1	
EPS15	HERC5	PML-RAR	RPS2	THBS1	
EPS15L1	HSD17B12	PPP6C	RPS27	TICRR	

→ Colour coding system groups proteins that belong to the same family

Table S 20| RSK1/RSK4 variant I shared tandem affinity purification hits – LC-MS/MS

RSK1/RSK4.I affinity purification		
ACP1	MCM5	SLC25A6
ARL1	MSH6	SMC4
ATP5C1	NSUN2	TIMM50
CAND1	PARD3	TRRAP
CLTC	PCBP2	UTRN
EIF4A1	PDZD11	XP32
ERBB2IP	PFKL	YTHDC2
ERLIN1	PFKP	
FECH	PPP1CB	
HOMER1	PRDX2	
HSPH1 (HSP110)	PSMC6	
KLHL8	RAD50	
MAP4	RHBDF1	

→ Colour coding system groups proteins that belong to the same family

Table S 21| RSK4 variant I/RSK4 variant II shared tandem affinity purification hits – LC-MS/MS

RSK4.I/RSK4.II affinity purification			
C1QBP	FLNC	MTCL1	SDHA
CCT5	FOXP3	MYH9	SF3B3
CKAP5	GGA2	NONO	SLC25A22
CNOT1	HACD3	PDPK1 (PDK1)	SOGA1
DDX41	HDAC1	PKP2	SRRT
DNAJA2 (HSP40)	HNRNPM	PPIL1	TARDBP
DOCK6	HSPD1 (HSP60)	PPIP5K2	TBC1D2B
DOCK8	ICT1	PPP2R1A	TP53
EIF2S1	IGF2R	PRPF4B	TRIM68
FAM120A	KHDRBS1	PRSS3	TTC28
FAM193B	KIF5B	RBM14	UBE1
FKBP8	LGALS3BP	RTCB	VDAC2
FLJ10842	LRCH2	SAMHD1	ZNF703

→ Colour coding system groups proteins that belong to the same family

Table S 22| RSK1 and RSK4 (increased) phosphoproteomics hits – LC-MS/MS

siRSK1 - Increased		siRSK4 - Increased		siRSK1/4 - Increased
AKAP10 (S187)	PSIP1	ABCC1	MNX1	ARID1A (S702)
BAG3	RANBP10	ACBD5	NKTR	GIGYF1 (S148)
BCR	RNF113A	ATF7IP	PGM1	
CCT2	SRSF7	BRCA1	PPIG	
CTPS1	STMN1;STMN2	CAD (S1038)	PRKAR2B	
(HSPC) HSP90AB1	WASL	CDC20 (S41)	RHBDF2	
MAK		CDC42EP1	SLC6A11	
MTFR1		CTNND1 (S47)	U2SURP	
NCL		DAB2		
NELFE		EIF5		
NOMO1;NOMO2;NOMO3		GTPBP1		
PPP1R18		KMT2A		
PRRC2A (S1085)		MAGI3		

Table S 23| RSK1 and RSK4 (decreased) phosphoproteomics hits – LC-MS/MS

siRSK1 - Decreased				siRSK4 - Decreased			siRSK1/4 - Decreased
ADAR	HSP90AA1	NRD1	SON;ADAMTS7	ABLIM1	KHNYN	RPL18A	siRSK1: NES (S459)
ANKRD17	HSPB1 (S82)	PCM1	SORBS3	AHNAK (S220)	LASP1 (S146)	SIPA1L1	siRSK4: NES (S768)
ARHGEF10	KRT18	PHLDB2 (S387)	SPP1	AP3B1	MCM2	STK4	MGRN1 (S523/524)
ATN1	LARP1	PRKAB2	SPTBN1	ARHGAP11A	MICALL1	SVIL	BYSL (S98)
BCL3	LARP7	PRKDC (S3205)	TMEM238	CCDC6	MLLT4 (S1736)	TSC2	
BRD4	LMNB1	PRPF4B	ULK1	CDK13	MPRIP	WDHD1	
C1orf52	LPHN2	RPL23A (S43)	WBP4	CXorf23	NAA10		
CD3EAP	LRRFIP1	RPS3A (Y256, S263)	ZC3H13	DARS2	NEMF		
CIT	MAP1B	RPS6	ZNF185	DNAH14	NOP14		
DENR	MAP3K7	RRAS2		DNTTIP2	ORC2		
EPB41L2	MATR3	RRP1B		EIF4G1	RAB13		
ETV3	MICALL2	SAP30		G3BP1	REV3L		
FAM134A	NPM1	SCRIB (S504)		IRS1 (S636/639)	RNF4		

→ Colour coding system groups proteins that belong to the same family

Table S 24| RSK1 and RSK4 (upregulated) total proteomics hits – LC-MS/MS

siRSK1 - Upregulated	siRSK4 - Upregulated			siRSK1/4 - Upregulated
CD63	BCL2L13	IRS1	VPS37B	CFDP1
CDR2L	CDC42EP3	LMO7		CROT
FAM114A1	CDH1/E-cadherin	MID1		GFER
GNPNAT1	CHMP2B	NRCAM		STOM
HMGB3	CTSC	OCLN		UBE2G2
NEDD4	F11R	PEG10		XIAP
NPEPL1	FTH1	PKP3		
RBKS	GCLM	POF1B		
SETD7	GRB2	RAB27B		
SLC7A11	H1F0	RP2		
SULT1A3	HKDC1	SPINT2		
TXNRD1	HMGN1	SQSTM1		
	HMOX1	ST13P5;ST13;ST13P4		

Table S 25| RSK1 and RSK4 (downregulated) total proteomics hits – LC-MS/MS

siRSK1 - Downregulated			siRSK4 - Downregulated						siRSK1/4 - Downregulated
ALDOC	HN1L	SMAD4	ACLY	CAPNS1	GPATCH1	PDIA3	RDX	STAG1	CDK6
ANLN	HSDL1	SYNE1	AKAP8	CFL2	GPRIN3	PEA15	REPS1	STAU1	NDRG3
C11orf85	IKBIP	TBC1D13	ANKFY1	CKS1B	GRB10	PFN2	RHPN2	STRA6	SMG9
CHD8;CHD7	KIAA0101	TNS4	ANTXR1	CLGN	HPGD	PIK3C2A	RIF1	TAGLN	TNPO2
CISD3	MTHFD1	TWF1	ARF4	CTDSPL2	IDI1	PIP4K2B	RPS6KA3	TGFB1I1	TPM2
CPNE3	MTR	TYMS	ASPH	CYP24A1	ITGA2	POFUT1	SART3	THUMPD3	
DNMBP	PLK1		ATL3	DCBLD2	LPP	PPIL3	SCPEP1	TRUB1	
DOCK10	PM20D2		AXL	DPYD	MAD2L1	PPT1	SDCBP	TSNAX	
ERCC6L	PRCP		BAG4	DSN1	MKL2	PRKCA	SEC24D	YAP1	
FADS1	RPL14		C17orf75	ENSA	MOB1A	PTBP3	SERPINE1	YTHDF3	
FADS2	RPL22L1		C1orf52	EXOC5	NCEH1	PTPRF	SLBP	ZC3HAV1L	
FAM160B1	RPS6KA1		C5orf51	FAM91A1	NTHL1	QKI	SLC38A2		
HELLS	RRM1		CAPN2	GFPT1	PBK	RCN2	SMCHD1		

→ Colour coding system groups proteins that belong to the same family

8.4 Chapter 5

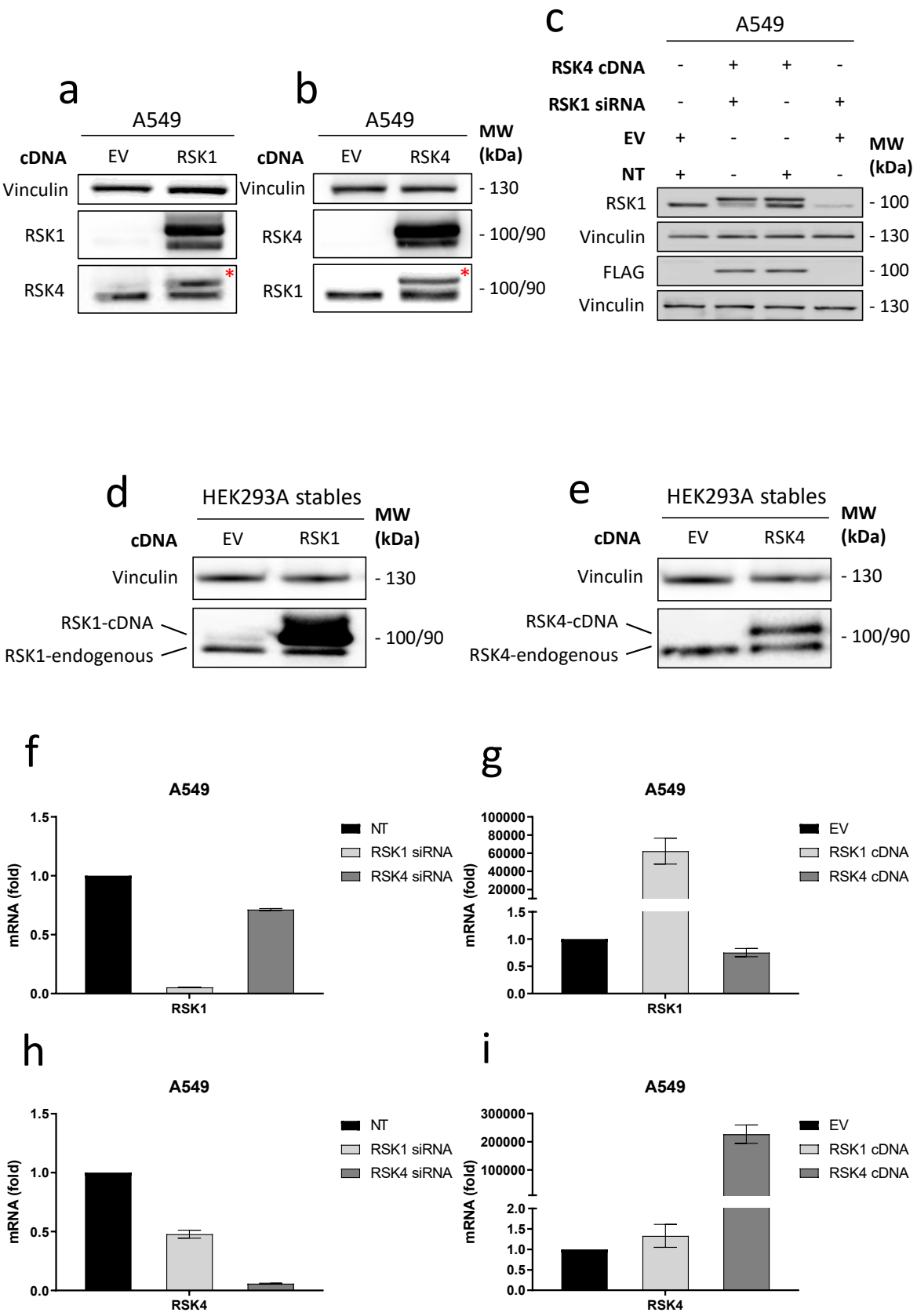

Figure S 17| RSK1 and RSK4 antibody cross-reactivity, HEK293A stable cell lines and confirmation of transient knockdown and overexpression. **(a, b)** RSK4 and RSK1 antibodies detect a second band (red asterisk) following RSK1 and RSK4 overexpression, respectively. Immunoblotting of RSK1 and RSK4 in A549 whole cell extracts transfected (24-48 h) with a final concentration of 2.5 µg EV (empty vector), RSK1 or RSK4 cDNAs. Vinculin was used as a loading control. **(c)** Concurrent RSK4

overexpression and RSK1 silencing indicates that RSK1 cross-reacts with overexpressed RSK4. Immunoblotting of RSK1 and FLAG in A549 whole cell extracts double transfected with a final concentration of 2.5 µg EV (empty vector) or RSK4 cDNAs (24-48 h) and with a final concentration of 20 nM NT (non-targeting) or RSK1 siRNAs (48-72 h). Vinculin was used as a loading control. Immunoblotting of **(d)** RSK1 and **(e)** RSK4 in whole cell HEK293A extracts previously transfected with dual-tagged (FLAG-HA) EV (empty vector), RSK1 or RSK4 cDNAs and selected following puromycin treatment. Vinculin was used as a loading control. **(f, g)** qRT-PCR analysis of RSK1 mRNA in A549 cells **(f)** transfected (48-72 h) with a final concentration of 20 nM NT (non-targeting), RSK1 or RSK4 siRNAs or **(g)** transfected (24-48 h) with a final concentration of 2.5 µg EV (empty vector), RSK1 or RSK4 cDNAs. **(h, i)** qRT-PCR analysis of RSK4 mRNA in A549 cells **(h)** transfected (48-72 h) with a final concentration of 20 nM NT (non-targeting), RSK1 or RSK4 siRNAs or **(i)** transfected (24-48 h) with a final concentration of 2.5 µg EV (empty vector), RSK1 or RSK4 cDNAs. *Ct* values were normalised to HPRT housekeeping gene and shown as a fold change relative to NT or EV control conditions. Data represent mean ± SEM of three independent biological replicates performed in triplicates. The work presented in **c** was performed by Thanasis Tsalikis (personal communication). The overexpression of RSK1 and RSK4 (including loading controls) in **a, b** are shown again in **Figure 29c** at higher exposure (same lysate).

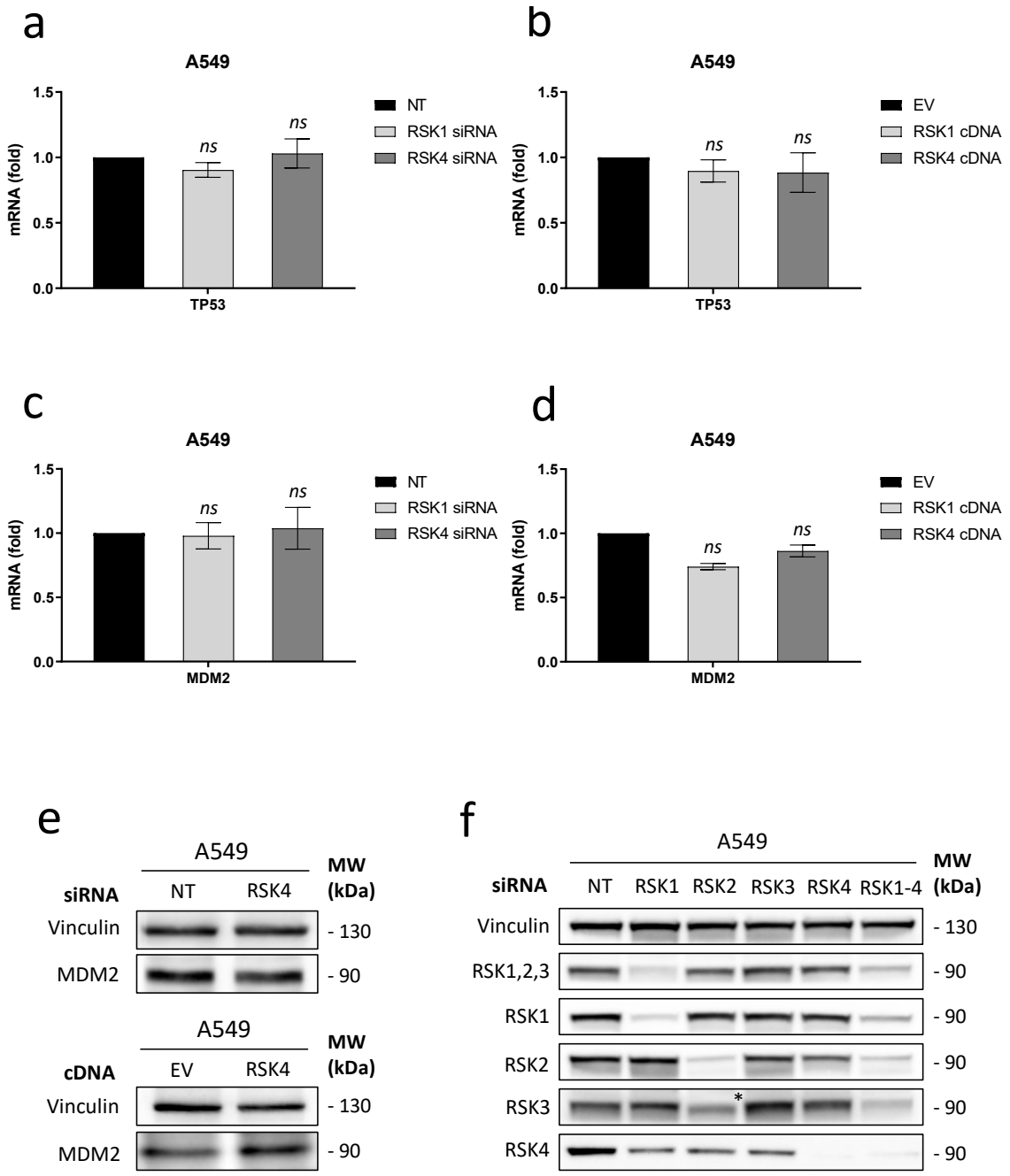

Figure S 18| RSK1 and RSK4 do not regulate p53 and MDM2 at the mRNA level. **(a, b)** qRT-PCR analysis of TP53 mRNA in A549 cells **(a)** transfected (48-72 h) with a final concentration of 20 nM NT (non-targeting), RSK1 or RSK4 siRNAs or **(b)** transfected (24-48 h) with a final concentration of 2.5 µg EV (empty vector), RSK1 or RSK4 cDNAs. **(c, d)** qRT-PCR analysis of MDM2 mRNA in A549 cells **(c)** transfected (48-72 h) with a final concentration of 20 nM NT (non-targeting), RSK1 or RSK4 siRNAs or **(d)** transfected (24-48 h) with a final concentration of 2.5 µg EV (empty vector), RSK1 or RSK4 cDNAs. *Ct* values were normalised to HPRT housekeeping gene and shown as a fold change relative to NT or EV control conditions. Data represent mean ± SEM of three independent biological replicates performed in triplicates. Statistical significance was assessed by an unpaired Student's *t*-test in GraphPad Prism. *ns*; non-significant ($P > 0.05$). **(e)** Immunoblotting of MDM2 in whole cell A549 extracts transfected (48-72 h) with a final concentration of 20 nM NT (non-targeting) or RSK4 siRNAs (top) or transfected (24-48 h) with a final concentration of 2.5 µg EV (empty vector) or RSK4 cDNAs (bottom). **(f)** Immunoblotting for the indicated proteins in whole cell A549 extracts transfected (48-72 h) with a final concentration of 20 nM NT (non-targeting), RSK1, RSK2, RSK3, RSK4 or RSK1-4 siRNAs. Vinculin was used as a loading control. Data are representative of two independent biological replicates.*RSK3 antibody detects RSK2 protein as verified by RSK2 and RSK3 siRNA oligo deconvolution (data not shown). RSK3 knockdown was confirmed by qRT-PCR analysis with RSK3 specific primers (data not shown). Experiment **f** is shown again in **Figure S 24b**.

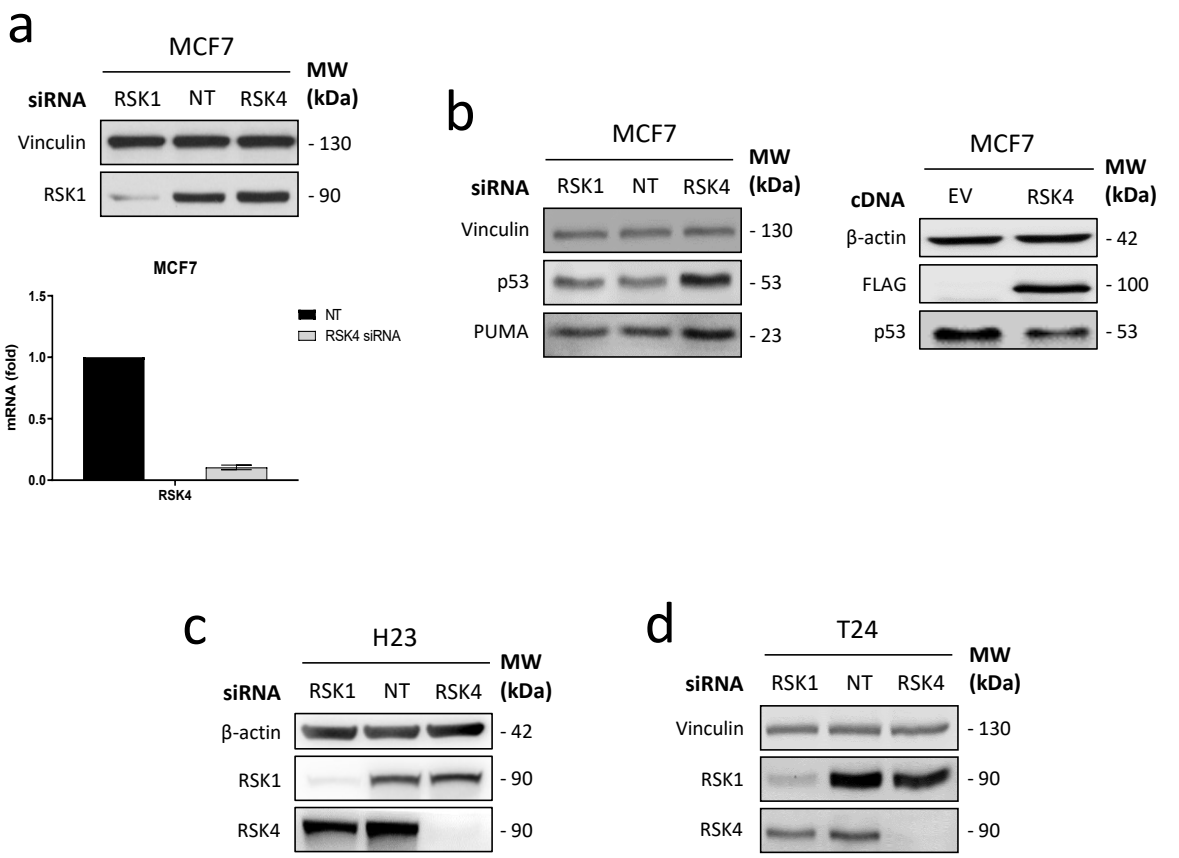

Figure S 19| Confirmation of RSK1 and RSK4 silencing in MCF7, H23 and T24 cell lines. **(a)** Confirmation of RSK1 (top) and RSK4 (bottom) knockdown in whole cell MCF7 extracts by immunoblotting and qRT-PCR analysis, respectively (RSK4 protein levels are almost undetectable in MCF7 cells). **(b)** Immunoblotting of p53 and PUMA in whole cell MCF7 extracts transfected (48-72 h) with a final concentration of 20 nM NT (non-targeting), RSK1 or RSK4 siRNAs (left) or transfected (24-48 h) with a final concentration of 2.5 μg EV (empty vector) or RSK4 cDNAs (right). **(c, d)** Confirmation of RSK1 and RSK4 knockdown in whole cell **(c)** H23 and **(d)** T24 extracts by immunoblotting. Data are representative of three independent biological replicates. The work presented in **a-b** was performed by Thanasis Tsalikis (personal communication).

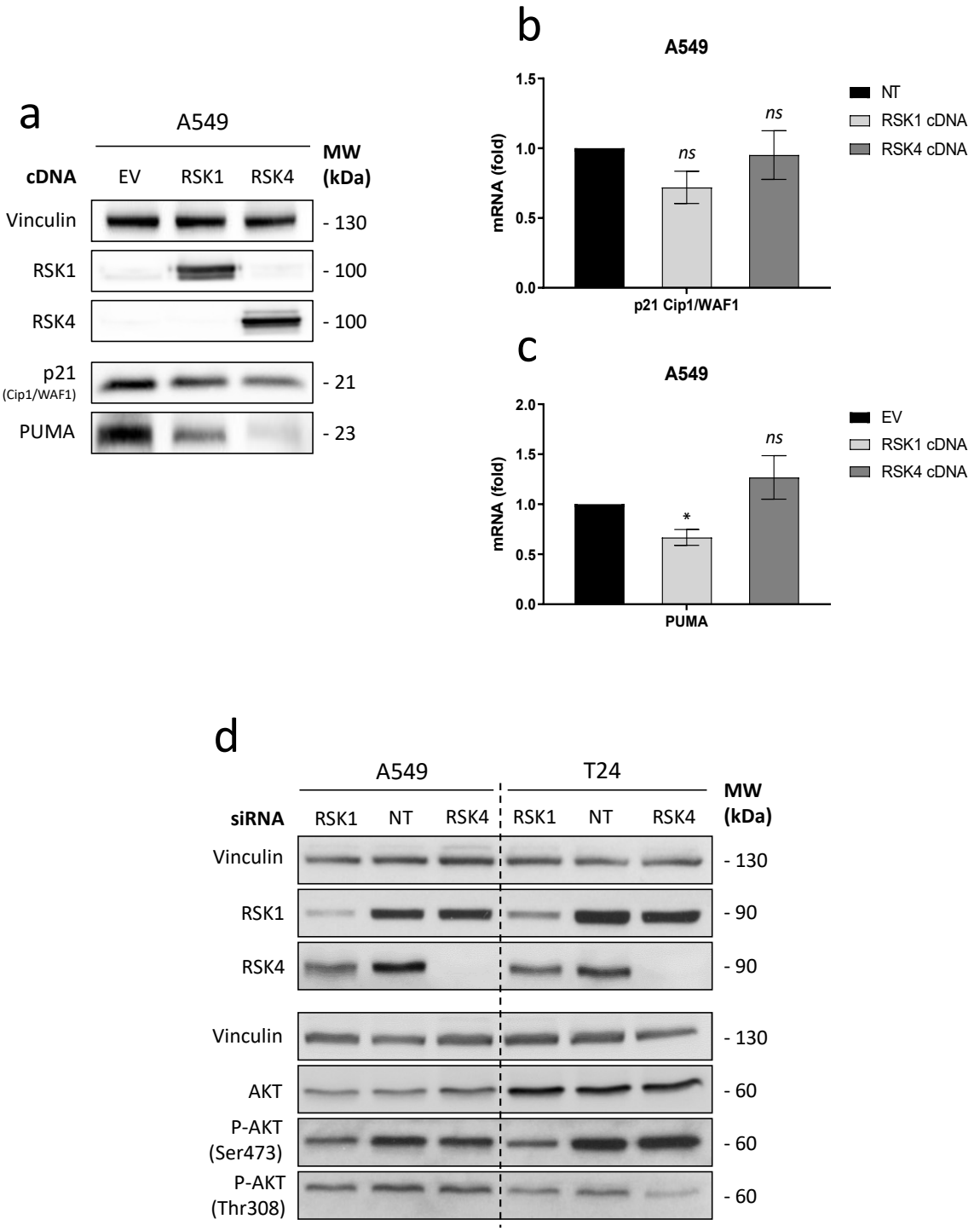

Figure S 20| RSK1 and RSK4 manipulation – effects on p21, PUMA, AKT and Caspase-7. **(a)** Immunoblotting of RSK1, RSK4, $p21^{Cip1/WAF1}$ and PUMA in whole cell A549 extracts transfected (24-48 h) with a final concentration of 2.5 µg EV (empty vector), RSK1 or RSK4 cDNAs. Vinculin was used as a loading control. Data are representative of three independent biological replicates. **(b, c)** qRT-PCR analysis of **(b)** $p21^{Cip1/WAF1}$ (CDKN1A) and **(c)** PUMA (BBC3) mRNAs in A549 cells transfected (24-48 h) with a final concentration of 2.5 µg EV (empty vector), RSK1 or RSK4 cDNAs. *Ct* values were normalised to HPRT housekeeping gene and shown as a fold change relative to EV control condition. Data represent mean ± SEM of three independent biological replicates performed in triplicates. Statistical significance was assessed by an unpaired Student's *t*-test in GraphPad Prism. *ns*; non-significant ($P > 0.05$), *; $P \leq 0.05$. **(d)** Immunoblotting of RSK1, RSK4, AKT, Phospho-AKT (Ser473) and Phospho-AKT (Thr308) in whole cell A549 (left) and T24 (right) extracts transfected (48-72 h) with a final concentration of 20 nM NT (non-targeting) RSK1 or RSK4 siRNAs. Vinculin was used as a loading control. Data are representative of three independent biological replicates. The work presented in **d** was performed by Thanasis Tsalikis (personal communication).

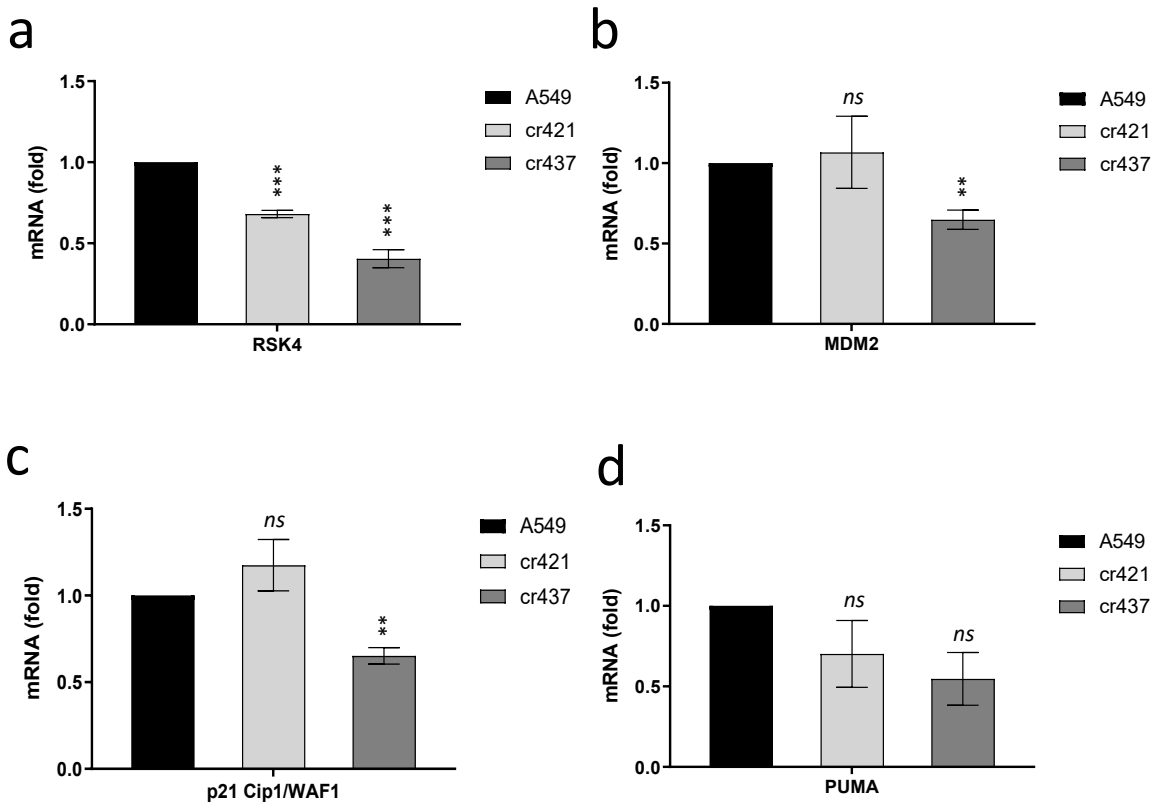

Figure S 21| RSK4 CRISPR/Cas9-mediated knockout effects on MDM2, p21 and PUMA mRNAs. qRT-PCR analysis of **(a)** RSK4, **(b)** MDM2, **(c)** $p21^{Cip1/WAF1}$ (CDKN1A) and **(d)** PUMA (BBC3) mRNAs in A549 (control), cr421 (partial RSK4 KO) and cr437 (complete RSK4 KO) cells. *Ct* values were normalised to HPRT housekeeping gene and shown as a fold change relative to A549 control condition. Data represent mean ± SEM of three independent biological replicates performed in triplicates. Statistical significance was assessed by an unpaired Student's *t*-test in GraphPad Prism. *ns*; non-significant ($P > 0.05$), **; $P \leq 0.01$, ***; $P \leq 0.001$. (See **Figure 35** for Immunoblotting analysis).

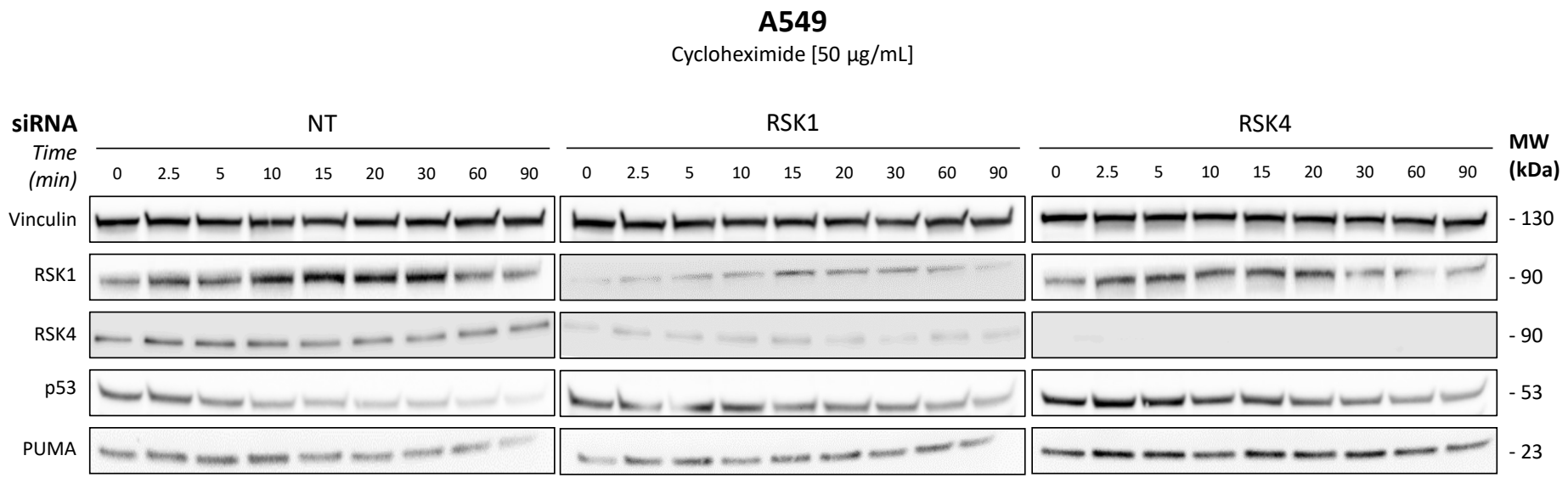

Figure S 22| RSK1 and RSK4 downregulation stabilises p53. Immunoblotting of RSK1, RSK4, p53 and PUMA in whole cell A549 extracts transfected (48-72 h) with a final concentration of 20 nM NT (non-targeting), RSK1 or RSK4 siRNAs and treated with 50 µg/mL cycloheximide for the indicated time points. Vinculin was used as a loading control. Data are representative of two independent biological replicates (See **Figure 32a** for quantification). The work presented here was performed by Alex Power (personal communication).

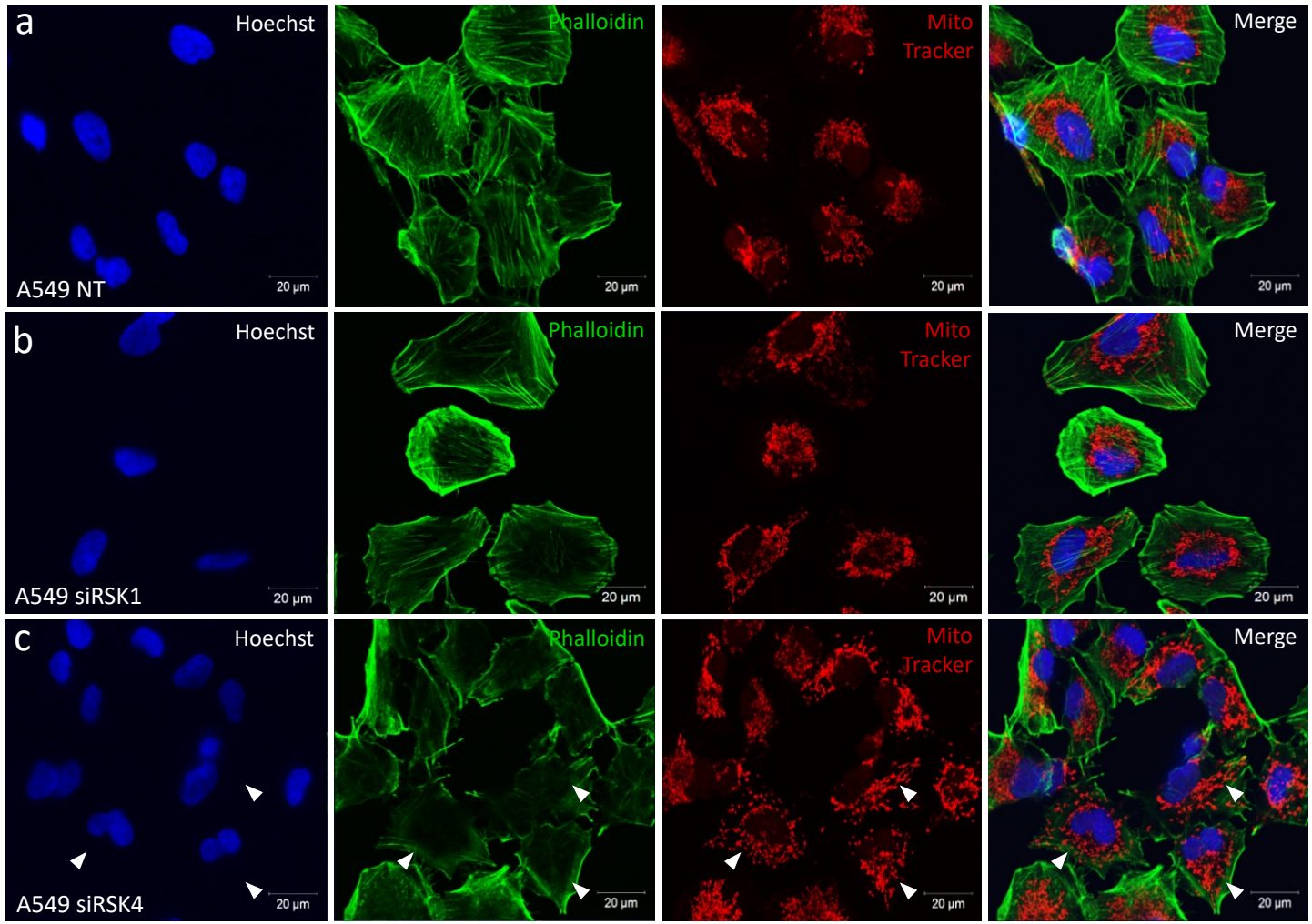

Figure S 23| RSK4 downregulation alters the mitochondrial network. Confocal microscopy of A549 cells grown on 12 mm coverslips, transfected (48-72 h) with a final concentration of 20 nM **(a)** NT (non-targeting), **(b)** RSK1 or **(c)** RSK4 siRNAs, dual-stained with Phalloidin and MitoTracker, and counterstained with Hoechst. Confocal images were captured on an inverted Zeiss LSM-780 (FILM, Imperial College London, UK). White arrows indicate affected cells (scale bars: 20 µm). Data are representative of two independent biological replicates.

8.5 General

This section includes preliminary data.

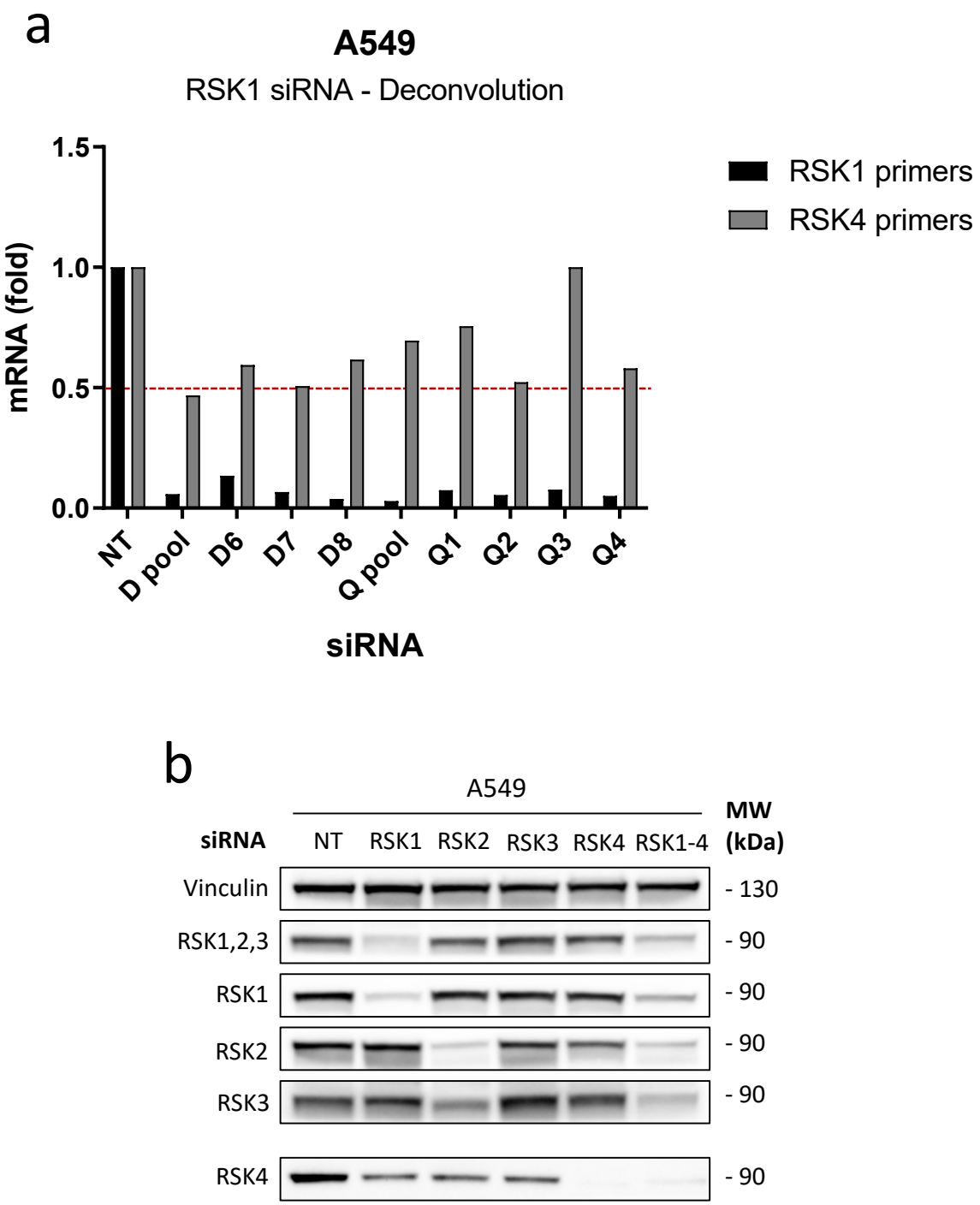

Figure S 24| RSK1-3 could be implicated in the regulation of RSK4 expression. **(a)** RSK1 siRNA deconvolution indicates reduction of RSK4 mRNA levels by 30%-50%. qRT-PCR analysis of RSK1 and RSK4 mRNAs in A549 cells transfected (48-72 h) with a final concentration of 20 nM NT (non-targeting), Dharmacon (D) pool (i.e. D6, D7 and D8), D6, D7, D8, Qiagen (Q) pool (i.e. Q1, Q2, Q3, Q4), Q1, Q2, Q3 or Q4 siRNAs. *Ct* values were normalised to HPRT housekeeping gene and shown as a fold change relative to NT control condition. Data represent the mean of technical triplicates. **(b)** RSK1-3 silencing decrease RSK4 protein levels. Immunoblotting for the indicated proteins in whole cell A549 extracts transfected (48-72 h) with a final concentration of 20 nM NT (non-targeting), RSK1, RSK2, RSK3, RSK4 or RSK1-4 siRNAs. Vinculin was used as a loading control. Data are representative of two independent biological replicates. Experiment **b** is shown again in **Figure S 18f**.

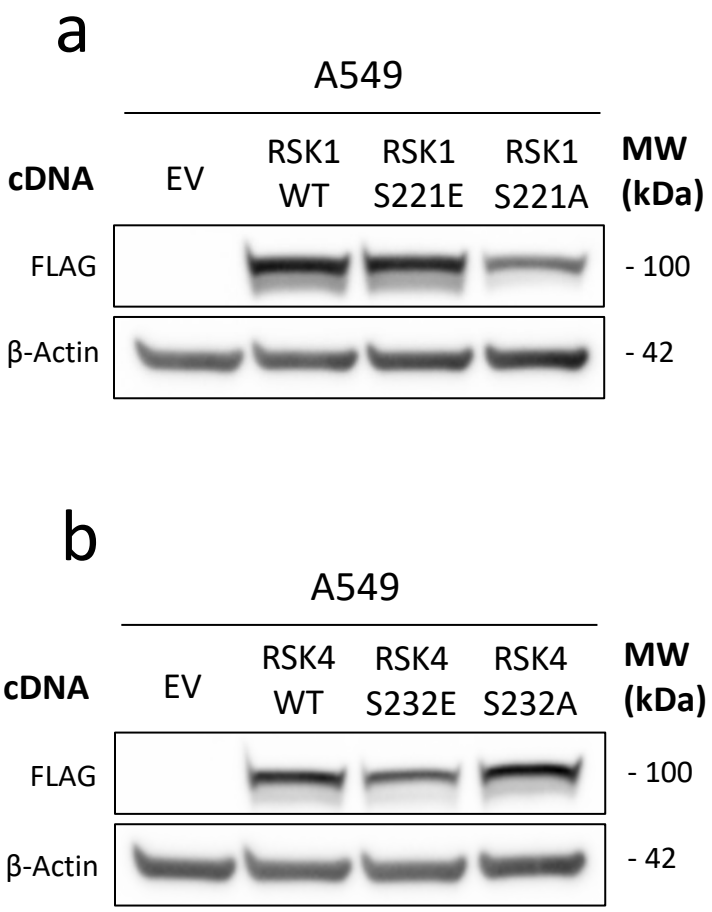

Figure S 25| RSK1 and RSK4 kinase active and dead mutants. (a, b) RSK1 and RSK4 kinase active (RSK1: S221E; RSK4: S232E) and dead (RSK1: S221A; RSK4: S232A) mutants expressed in A549 cells. Immunoblotting of FLAG in whole cell A549 extracts transfected (24-48 h) with a final concentration of **(a)** 2.5 µg EV (empty vector), RSK1 WT, RSK1 S221E, RSK1 S221A cDNAs or **(b)** 2.5 µg EV, RSK4 WT, RSK4 S232E, RSK4 S232A cDNAs. β-Actin was used as a loading control.

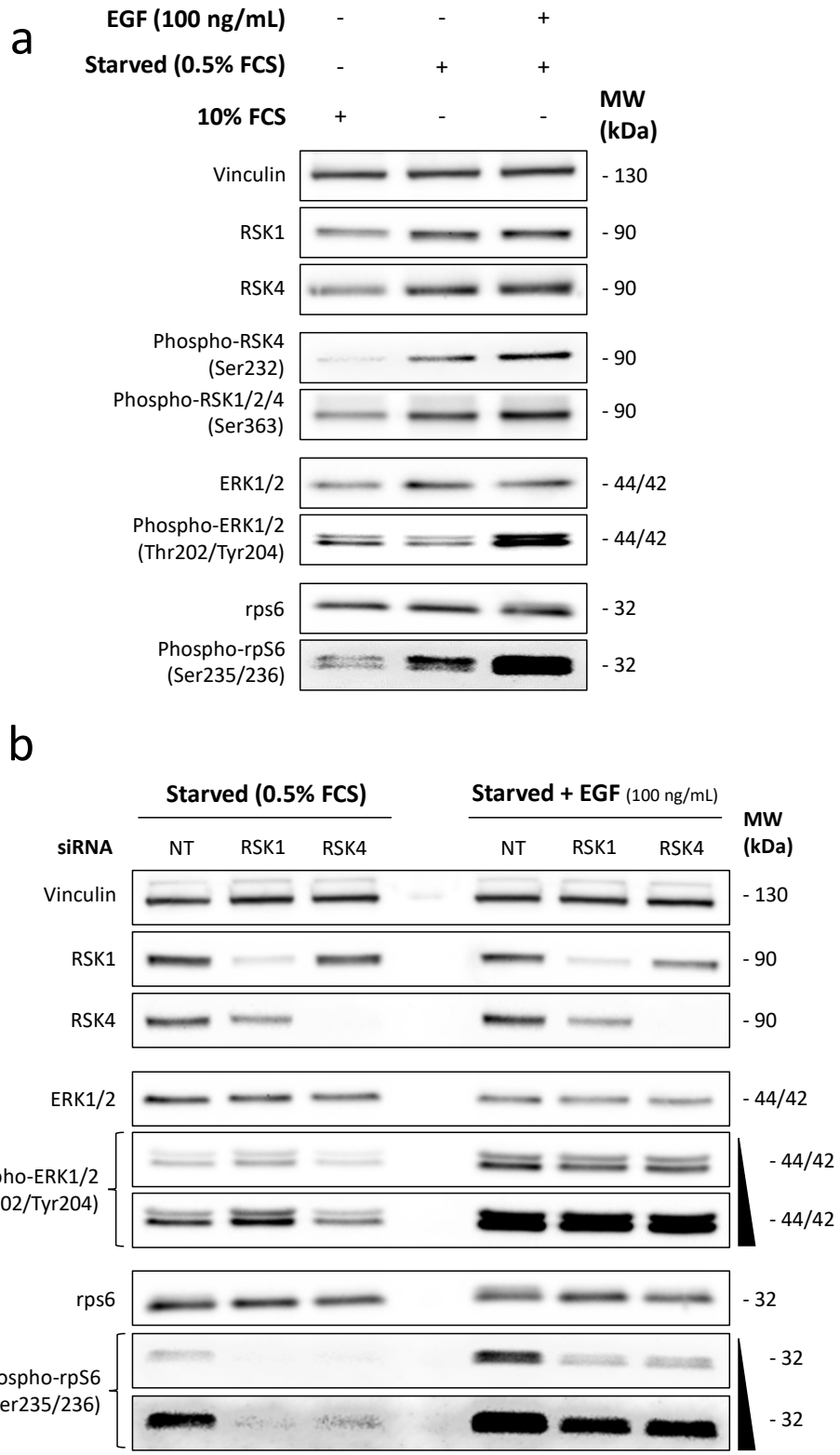

Figure S 26| EGF stimulation increases phosphorylation of RSK1 and RSK4. **(a)** Immunoblotting for the indicated proteins in whole cell A549 extracts serum-starved (or not: 10% FCS) overnight with 0.5% FCS and stimulated with/without 100 ng/mL EGF (epidermal growth factor) for 15 min. Vinculin was used as a loading control. Data are representative of three biological replicates. **(b)** Immunoblotting for the indicated proteins in whole cell A549 extracts transfected (48-72 h) with a final concentration of 20 nM NT (non-targeting), RSK1 or RSK4 siRNAs, serum-starved overnight with 0.5% FCS and stimulated with/without 100 ng/mL EGF for 15 min. Vinculin was used as a loading control. Data are representative of three independent biological replicates.

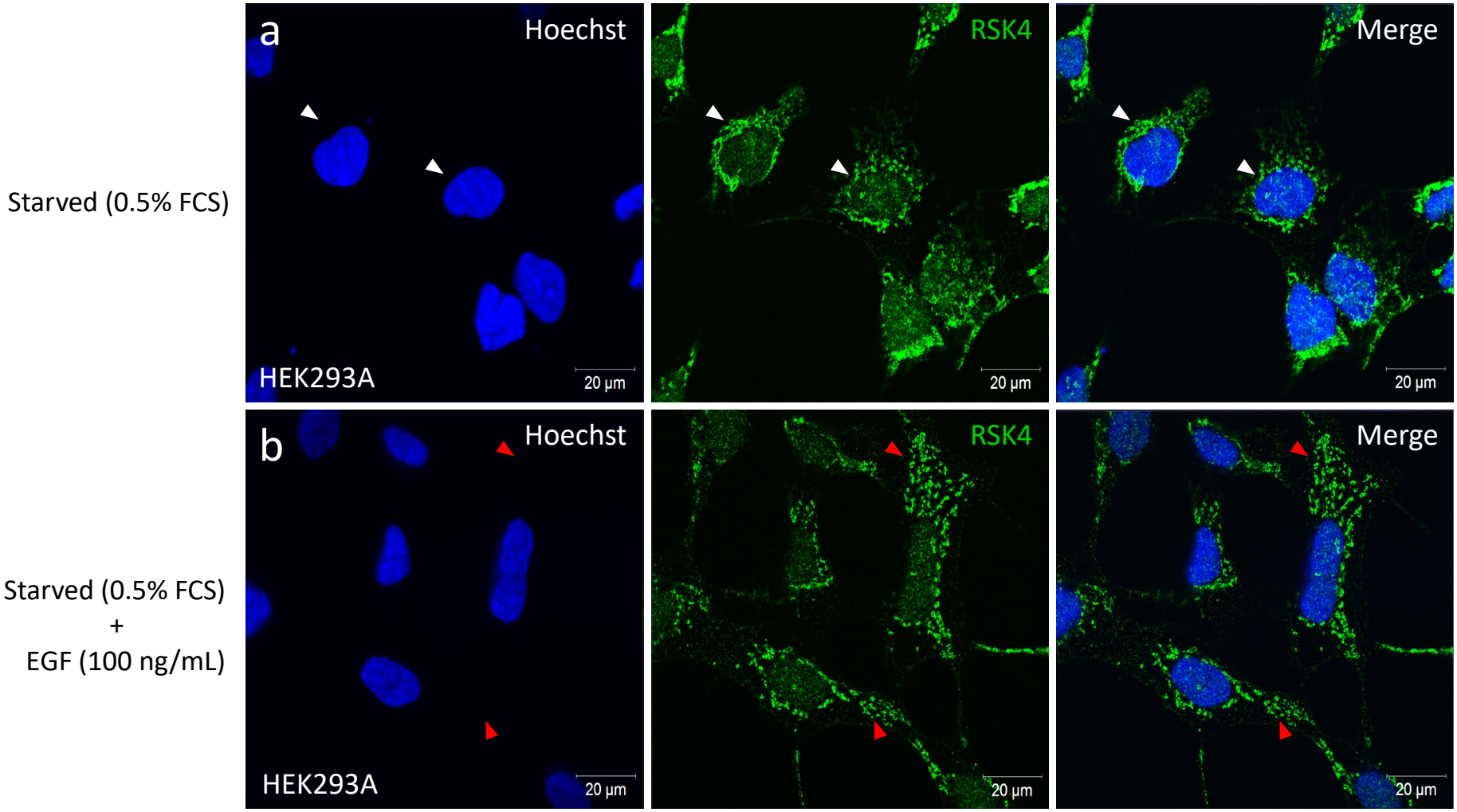

Figure S 27| EGF stimulation causes RSK4 spreading in the cytoplasm. Confocal microscopy of HEK293A cells grown on 12 mm coverslips **(a)** serum-starved overnight with 0.5% FCS or **(b)** serum-starved overnight with 0.5% FCS and then stimulated with 100 ng/mL EGF (epidermal growth factor) for 15 min, stained with RSK4 (green) and counterstained with Hoechst. Confocal images were captured on an inverted Zeiss LSM-780 (FILM, Imperial College London, UK). White arrows indicate RSK4 perinuclear localisation and red arrows indicate RSK4 spreading in the cytoplasm (scale bars: 20 µm). Data are representative of two independent biological replicates.